SHEAR STRENGTH CHARACTERISTICS OF SAND

by

NABIL FAHIM MASSOUD

A Thesis

in

The Faculty

of

Engineering

Presented in Partial Fulfillment of the Requirements

for the degree of Master of Engineering at

Concordia University

Montréal, Québec, Canada

November 1981

ABSTRACT

SHEAR STRENGTH CHARACTERISTICS OF SAND

NABIL FAHIM MASSOUD

Knowledge of strength properties and deformational behaviour of soils, under different stress conditions is necessary in the analysis of most field problems in geotechnical engineering. Due to the complex nature of the soil material and the wide variation in its response, several techniques have been developed to determine the shear strength of the soil.

The purpose of this investigation is to present the results of an experimental study on the shear strength of dry sands. The shear strengths were presented as a function of the confining pressure acting on the sample, relative density of the material tested and the testing technique. The results were analyzed to determine the components of the shear strength and energy losses.

ACKNOWLEDGEMENTS

I wish to express my sincere gratitude to Dr. A.M. Hanna, under whose direct supervision and able guidance the present investigation has been carried out. The amount of consistent enthusiasm and constant encouragement received is gratefully acknowledged.

I am thankful to the Department of Civil Engineering at the Technical University of Nova Scotia for lending the plane-strain apparatus.

Thanks to my colleague Mr. Harold Leroux, for his assistance to set-up the equipment.

I am deeply indebted to Mr. N. Shenouda, for his assistance in preparation of the drawings.

Thanks to Ms. M. Pierotti for patiently typing the thesis.

Thanks are due to the National Research Council of Canada for the principal assistance during the time of this work.

Finally, I am indebted to my wife, Nelly, for her constant encouragement throughout my studies.

TABLE OF CONTENTS

LIST OF SYMBOLS

SYMBOL	REPRESENTS
ε_f	Axial strain at failure.
ε_1	Major principal strain.
ε_2	Intermediate principal strain.
ε_3	Minor principal strain.
$\Delta\varepsilon_1$	Increment of major principal strain.
$\Delta\varepsilon_3$	Increment of minor principal strain.
σ_1	Major principal stress.
σ_2	Intermediate principal stress.
σ_3	Minor principal stress.
σ_n	Normal stress in direct shear.
τ_d	Shear stress required to provide energy for dilation.
τ	Shear Stress.
τ_r	Residual shear stress.
δv	Volume expansion.
Δx	Transverse displacement in horizontal direction.
Δy	Transverse displacement in vertical dicrection.
ϕ	Angle of shearing resistance.
ϕ_u	Angle of friction between the particles.
ϕ_f	Corrected angle of friction (Rowe).
ϕ_{cv}	Value of angles ϕ, or ϕ_f or ϕ_r at critical void ratio.
ϕ_r	Corrected angle of friction (Bishop).
ϕ_d	Angle of friction determined from drained tests.

SYMBOL	REPRESENTS
ϕ_f	Angle of friction at the residual condition in direct shear.
ϕ_{dr}	Angle of friction after dilatancy effect is deducted.
ϕ_{ds}.	Angle of friction in direct shear.
ϕ_{ps}	Angle of friction in plane strain.

LIST OF FIGURES

LIST OF TABLES

CHAPTER I

INTRODUCTION

1.1 General

Usually the shear strength parameter of the soil can be determined from the results of triaxial, plane-strain compression and direct shear box tests.

The conventional triaxial compression test ($\sigma_1 > \sigma_2 = \sigma_3$) simulates the three dimensional case, such as circular footings, cofferdams, ... etc., while the plane-strain compression ($\sigma_1 > \sigma_2 > \sigma_3$) simulates the two dimensional case, such as retaining walls, embankments, earth dams, tunnels, strip footings, foundations and excavations, where the intermediate principal stresses acting along the axis of zero deformation. The shear box test simulates the condition of one dimensional case, where the failure plane is forced to occur at a predetermined location.

1.2 Outline of the Thesis

In chapter one, a general introduction to the present work is given. Chapter two presents the previous work. Laboratory test techniques and properties of the materials used are discussed in chapter three. The experimental results are presented in chapter four. In chapter five, analysis and discussion of test results are presented. The conclusion is given in chapter six.

CHAPTER II

PREVIOUS WORK

2.1 General

Cohesionless soils are defined as those in which interparticle forces or bonds make a negligible contribution to the mechanical behaviour of the soil.

The crushing strength of soil particles is generally large compared with the normal stress in the soil mass. Changes in normal stress, therefore, cause only limited volume changes due to rearrangement of the particles. However, very large deformations may result from sliding at the particle surfaces, as a result of applied shear stresses which exceed the shearing resistance on these surfaces. The shear strength of a soil is the resistance to such shear stresses, at failure, on a rupture surface within the soil mass.

The relative sliding between particles is the most important mechanism of deformation within a soil mass. Hence, the resistance of soil to deformation is influenced strongly by the shear resistance at contacts between particles. A knowledge of the magnitude of this shear resistance, and of the factors that influence this resistance, is basic to the mastery of soil mechanics problems. If the shear strength of the soil is greater or equal than the shear stress at any given plane, then the soil mass is safe against failure, otherwise the failure will occur.

The shear strength of granular material is affected largely by the

void ratio, the confining stresses, the rate of loading, and to a lesser extent by the particle shape, the surface roughness, and the grain-size distribution.

2.2 Factors Contributing to Shearing Strength in Sands.

2.2.1 General

The shear resistance between particles is made of two components:

(a) One whose magnitude is controlled by the sliding or rolling friction (there is no significant volume change associated with this type of action).

(b) A second component whose magnitude is related to the degree of interlocking.

2.2.2 Interparticle Friction

Terzaghi (1925) suggested that the frictional resistance was caused by physical - chemical molecular bonds formed at the contacts between surfaces. The contacts form a very small proportion of the total area of solids, and the contact pressures are high.

Amonton's law (1699) states that the frictional resistance at each contact point of the particles is proportional to the normal force at that contact, and hence the overall resistance increases as the confining stress increases. The maximum shearing Force at the point of contact can be expressed in terms of frictional angle "ϕ_u" as following, and in reference to figure 2.1.

$$T_{max.} = N.f = N.\tan \phi_u \qquad (2.1)$$

where

$T_{max.}$: the maximum shear on the surface.

N : the normal Force across this surface.

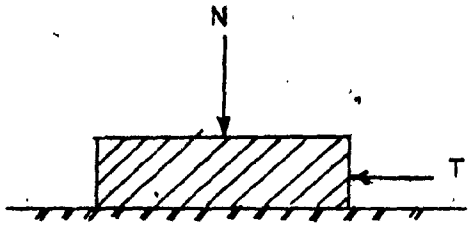

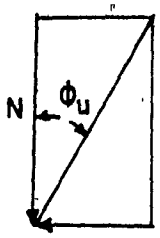

$T_{max} = N \tan \phi_u$

FIG. 2.1 DEFINITION OF FRICTION ANGLE "ϕ_u"

f : the coefficient of friction.

ϕ_u : the frictional angle.

Rowe (1962) showed that the friction angle ϕ_u is affected by the size of the particles as shown in figure 2.2. Since an increase in particle size decreases the number of particles subjected to a given pressure, and therefore, increases the load per contact, the value of ϕ_u decreases with both pressure increase and particle size increase.

2.2.3 Interlocking

In actual soil the particles are in contact with the others, and the planes of sliding through the contact points are inclined to the direction of the shear stress, as shown in figure 2.3.a. In order to bring about a shear failure between particles, it is not only necessary to overcome the frictional resistance, but it is in addition necessary to make particles move up or down and over one another, as shown in figure 2.3.b.

The phenomenon of interlocking is the resistance offered by the soil to volume change during shear. In case of dense sand there is considerable degree of interlocking between the particles and before complete shear failure can take place, this interlocking must be overcome in addition to the frictional resistance at the point of contact. After a peak stress is reached at failure, the degree of interlocking decrease and produces an increase in the volume of the specimen. In loose sand there is no initial particle interlocking to be overcome, and the soil will exhibit a low strength.

The energy required by the particles to ride one over the other and to expand against the confining stress will be the greatest in cases

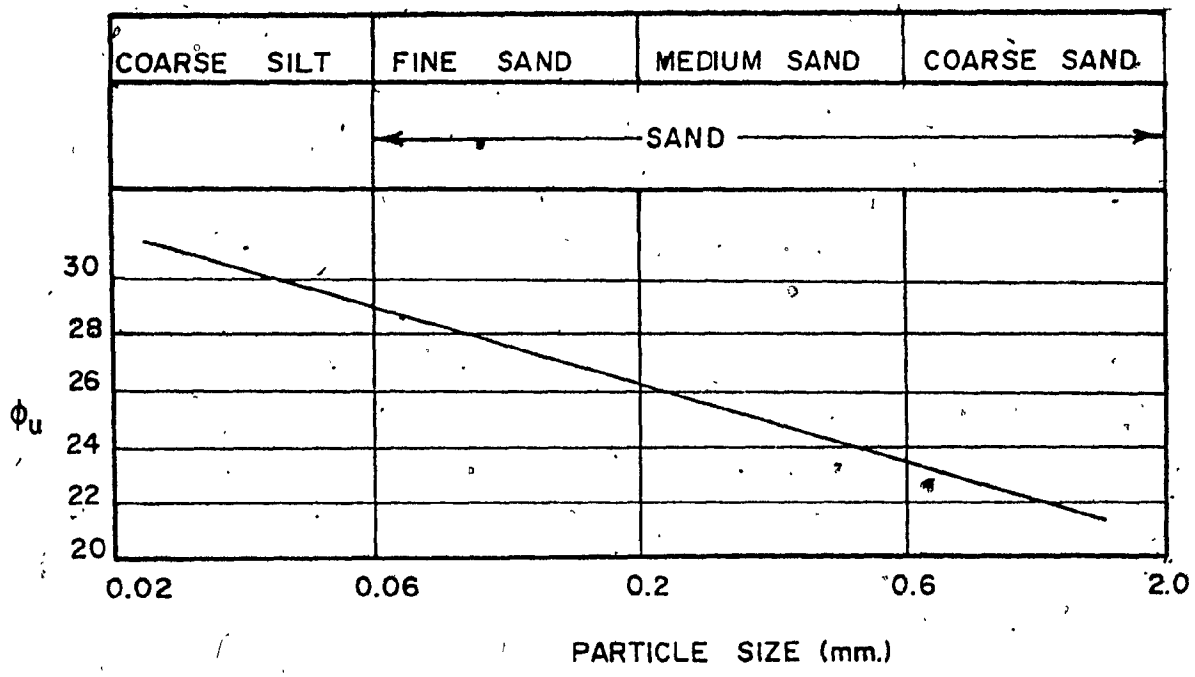

FIG. 2. 2. FRICTION ANGLE OF QUARTZ SAND AS A FUNCTION OF GRAIN SIZE (AFTER ROWE, 1962)

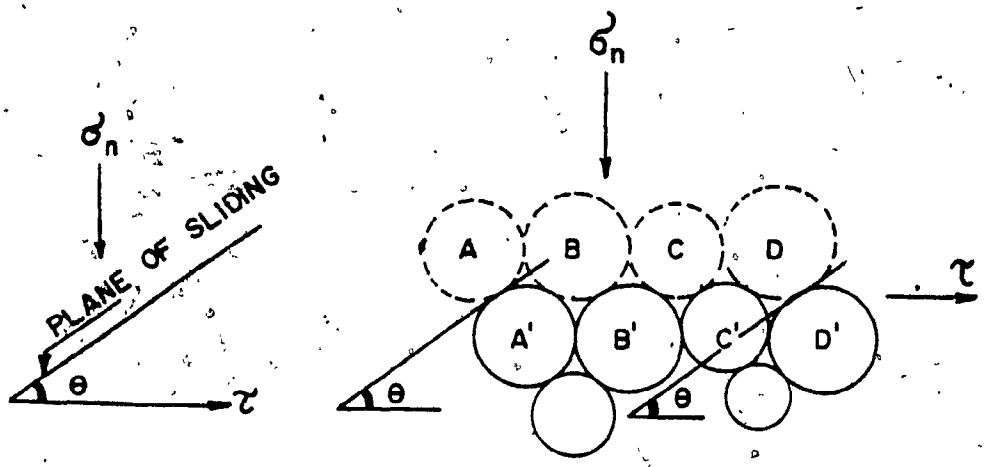

FIG. 2.3.a SLIDING OF PARTICLES

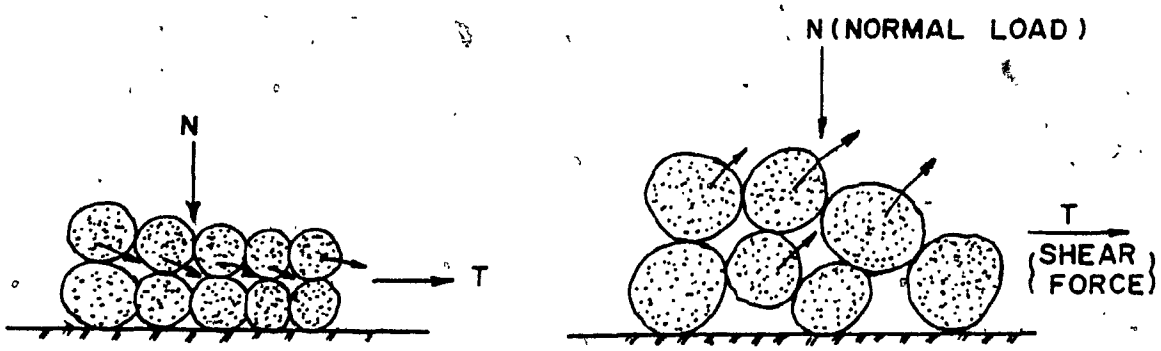

FIG. 2.3.b VOLUME CHANGE IN COHESIONLESS SOILS DURING SHEAR

where the degree of interlocking between the particles is the highest.

The shear strength of sand along any plane, according to Mohr-Coulomb failure theory was found to be a function of the normal stress on that plane, as

$$S = f(\sigma) \qquad (2.1)$$

Coulomb (1776) defined the function f as a linear function of the normal stress, with no account of the volume changes accompanying shear strain,

then

$$S = \sigma_n \tan \phi \qquad (2.2)$$

where

S = shear strength of sand

σ_n = normal stress

ϕ = angle of shearing resistance.

Casagrande (1940) attributed the volume expansion of sand to the necessity for interlocked particles to slide up and over each other to allow deformation to occur. He found the full extent of the dependence of the angle of shearing resistance "ϕ" on the void ratio, and the associated volume change during shear.

Casagrande in his paper (1940), had presented the original concepts of critical void ratio "$e_{cv.}$" in triaxial compression test, to describe the particular state of density at which the sand will shear with no volume changes. He defined the angle of shearing resistance at constant volume or resedual condition as "$\phi_{cv.}$", which reflect the combined effect of the frictional angle "ϕ_u" and the degree of interlocking that can

occur with zero overall volume change during continued straining. He derived an expression for the angle of shearing resistance at constant volumne as:

$$\text{Sin } \phi_{cv.} = \left(\frac{\sigma_1-\sigma_3}{\sigma_1+\sigma_3}\right)_{cv.} \qquad (2.3)$$

where

σ_1 = major principal stress

σ_3 = minor principal stress

$\phi_{cv.}$ = angle of shearing resistance at constant volume.

Taylor (1948) drew an attention to the contribution made by particles interlocking, which involved volume increase on shear, to the strength of dense sand. For dense sand samples tested in direct shear tests, he suggested that part of shear stress required to cause failure, was used up in providing the energy required to permit the sand to expand against the normal stress. The shear strength was therefore, the combined result of two factors - sliding friction and dilatancy or volume change components. Taylor derived an expression, to determine the shear stress component due to dilatancy as follows:

$$\delta W = T_d . \Delta X = \sigma_n . \Delta H$$

or

$$\tau_d = \sigma_n . \frac{\Delta H}{\Delta X} \qquad (2.4)$$

where

δW = the work done against the normal stress

τ_d = the shear stress required to provide engergy for expansion.

σ_n = applied normal stress

ΔX = incremental horizontal displacement

ΔH = increment in thickness of the sample

Bishop (1950), had independently derived an expression for the separation of the frictional and dilatancy components of dense sand samples tested in direct shear box, as shown in figure (2.4), and presented test results which 'indicated that the increase in shear strength (as measured by ϕ) with density was due primarily to the increased tendency of the sample to dilate, and that the work done in overcoming frictional forces (measured by ϕ_u) was almost unchanged',

therefore

The total work done = work done against the normal stress + work done to shear the sample against frictional resistance,

then

$$\tau.A.\Delta X = (\tau-\tau_d).A.\Delta X + \sigma_n.A.\Delta H$$

or

$$\frac{\tau-\tau_d}{\sigma_n} = \frac{\tau}{\sigma_n} - \frac{\Delta H}{\Delta X} \qquad (2.5)$$

where

σ_n = normal stress.

τ = shear stress.

τ_d = shear stress necessary to cause the sample to dilate against normal stress.

$\tau-\tau_d$ = shear stress required to shear the sample against frictional resistance only.

ΔX = increment of the horizontal displacement.

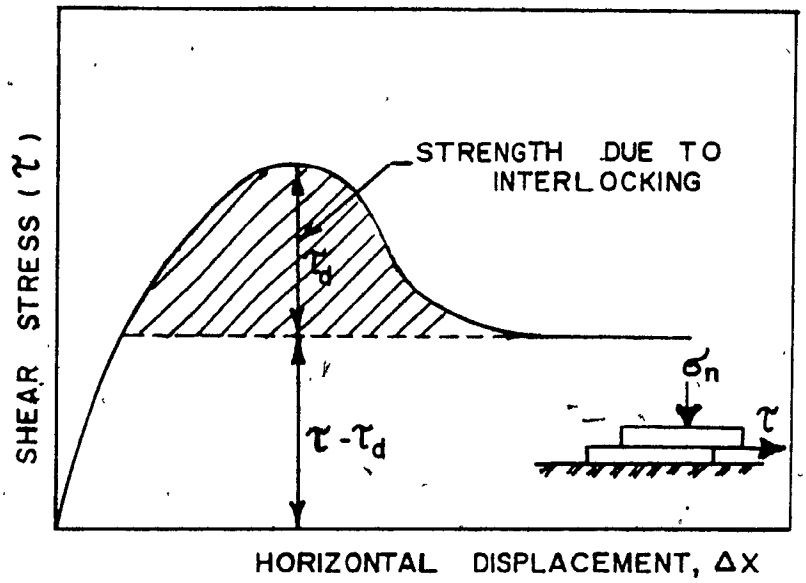

FIG. 2.4 STRENGTH COMPONENTS OF DENSE SAND SAMPLES IN SHEAR BOX (BISHOP, 1950)

ΔH = increment of the vertical displacement.

then equation (2.5) may be written as:

$$\tan \phi_u = \tan \phi - \frac{\Delta V}{A.\Delta X} \qquad (2.6)$$

where

ΔV = the volume expansion in the vertical direction.

A = cross-sectional area of the sample.

In triaxial compression test, Bishop and Eldin (1953), and Bishop (1954) formulated an expression to determine the protion of the deviator stress which must be applied to provide the sample with the energy required to expand against the confining stress, as:

$$(\Delta\sigma)_e = \sigma_3 \cdot \frac{\Delta V}{V.\varepsilon_1} \qquad (2.7)$$

where

σ_3 = minor principal stress.

ε_1 = incremental increase in axial strain.

$\frac{\Delta V}{V}$ = volumetric strain

$\sigma_3.\frac{\Delta V}{V}$ = work done by the specimen

$\Delta\sigma.\varepsilon_1$ = work put into the specimen

$(\Delta\sigma)_e$ = deviator stress required to provide the energy for expansion.

If the angle of shearing resistance of a sand determined from the total applied stresses at failure in a drained triaxial compression test is designated as ϕ_d, and the angle of friction computed after the deduction of dilatancy component is termed ϕ_{dr}, then

$$\tan^2 (45° + \frac{\phi d}{2}) = (\frac{\sigma 1}{\sigma_2}) \quad \text{failure} \qquad (2.8)$$

and, by using equation (2.7), then:

$$\tan^2 (45° + \frac{\phi dr}{2}) = (\frac{\sigma 1}{\sigma_3} - \frac{\Delta V}{V.\varepsilon_1}) \quad \text{failure} \qquad (2.9)$$

In (1957) Newland and Allely derived an expression to determine the shear stress required to mobilize the resistance to dilation of dense sand samples tested in direct shear box and triaxial compression.

In direct shear test, when sliding just begins as shown in figure (2.5), the shear stress and rate of volume expansion reach maximum values $\tau_{max.}$ and $(\frac{\delta V}{\delta \Delta})_{max.}$, since at this stage the angle of sliding (β) is at its maximum value

then

$$\frac{T}{N} = \tan (\phi_u + B) = \frac{\tan \phi_u + \tan \beta}{1 - \tan \phi_u . \tan \beta}$$

$$\tau_{max} = \sigma_n \tan \phi_u + \sigma_n . \tan \beta + \tau_{max.} \tan \phi_u . \tan \beta$$

or

$$\tau_{max.} = \tau_R + (\sigma_n . \frac{\delta V}{\delta \Delta} + \tau_{max} . \tan \phi_u . \tan \beta) \qquad (2.10)$$

where.

$\tau_{max.}$ = maximum shear stress at failure.

σ_n = normal stress

τ_R = shear stress required to overcome frictional forces, or the residual stress (β=0).

ϕ_u = angle of sliding friction

β = angle of sliding.

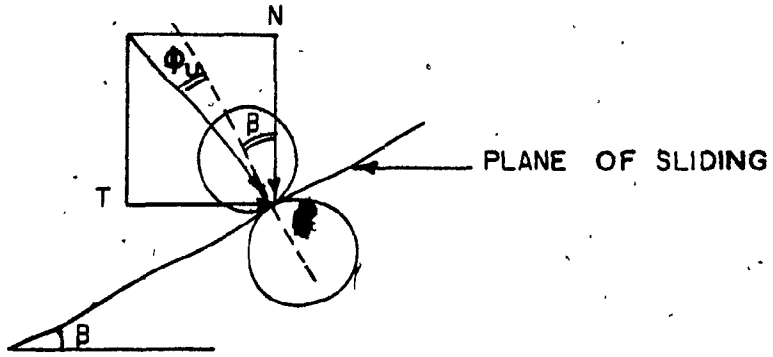

FIG. 2.5 INTERPARTICLE SLIDING

δV = volume expansion in vertical direction.

$\delta \Delta$ = volume expansion in horizontal direction.

$\sigma_n \frac{\delta V}{\delta \Delta}$ = component of "τ" due to the external work done against the normal stress "σ_n".

$\tau_{max.} \tan. \phi_u \therefore \tan \beta$ = component of "τ" due to the additional work done against friction on account of the inclination of the slip plane ($\beta > 0$).

In case of triaxial compression test, they suggested that the difference between the peak and residual stresses could be accounted for by considering the energy required to cause expansion against the confining stress, as

$$(\sigma_1)_{max.} - \sigma_R = \sigma_3 \left(\frac{\Delta V}{V \varepsilon_1}\right)_{max.} \qquad (2.11)$$

where

$(\sigma_1)_{max.}$ = major principal stress at failure.

σ_3 = minor principal stress.

σ_R = residual stress.

V = total volume of the sample.

ΔV = volume change.

ε_1 = axial strain.

After applying Taylor-Bishop expression (1954), which has been given in equation (2.9), Rowe (1962) found that the corrected angle of friction "ϕ_{dr}" computed after the dilatancy component is deducted, still greater than the angle of friction between the particles "ϕ_u". He therefore derived an alternate expression for determining the angle of friction of a granular material after dilatancy effects were deducted, ϕ_f as follows

$$\tan^2 \left(45° + \frac{\phi_f}{2}\right) = \frac{\sigma_1}{\sigma_3} \cdot \frac{1}{1 + \frac{dV}{V \varepsilon_1}} \qquad (2.12)$$

where

ϕ_f = Rowe's frictional angle.

ε_1 = axial strain.

σ_1 = major principal stress.

σ_3 = minor principal stress.

$\frac{dv}{V}$ = volumetric strain.

2.3 Stress Dilatancy Theory

The stress-dilatancy theory as proposed by Rowe (1962), gives a relationship between stress ratio and dilatancy expressed as $1 - \frac{dv}{Vd\varepsilon_1}$, where dv is the unit volumetric strain, and $d\varepsilon_1$ is the axial strain in the direction of major principal stress.

Rowe neglected the elastic strains and examined the static and geometry of an ideal system of spheres and rods, in which a mechanism of deformation was assumed. He considered, for example, the case of uniform rods arranged in dense packing under triaxial compression, as shown in figure (2.6.a). If the forces on the rod are P_1 and P_3 along the major and minor principal directions respectively. There relationship when sliding occurs as shown in figure (2.6.b), is

$$P_1 = P_3 \tan(\phi_u + \beta) \qquad (2.13)$$

where

β = the angle between the major principal stress direction and the sliding plane.

ϕ_u = the angle of friction of the material.

If L_1 and L_3 are the distances between alternate rows in the major and minor principal stress directions, then

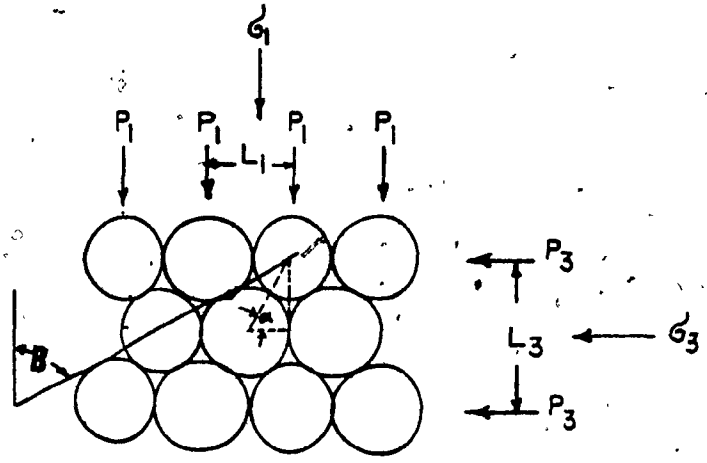

FIG. 2.6. a UNIFORM RODS, DENSE PACKING (AFTER ROWE, 1962)

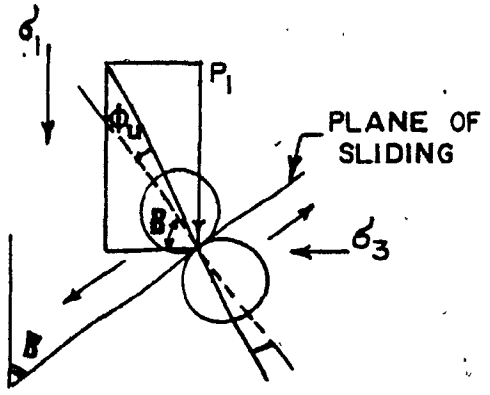

FIG. 2.6. b INTERPARTICLE SLIP

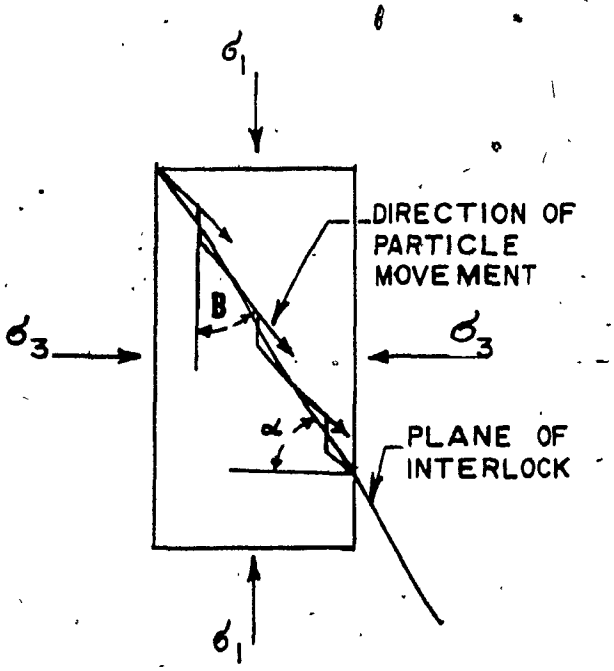

FIG. 2.6 .c. IDEALIZED RELATIONSHIPS BETWEEN DIRECTION OF PARTICLE MOVEMENT & PLANE OF INTERLOCK

$$\sigma_1 = \frac{P_1}{L_1} \quad \text{and} \quad \sigma_3 = \frac{P_3}{L_3}$$

Substituting this into equation (2.13) we have:

$$\frac{\sigma_1}{\sigma_3} = \frac{P_1 . L_3}{L_1 . P_3} = \frac{L_3}{L_1} . \tan (\phi_u + \beta)$$

or

$$\frac{\sigma_1}{\sigma_3} = \tan \alpha . \tan(\phi_u + \beta) \qquad (2.14)$$

where

α = the angle between an imaginary plane of particle interlock and the minor principal stress direction, as shown in figure (2.6.c).

σ_1 = major principal stress.

σ_3 = minor principal stress.

The strain increments, $\delta\varepsilon_1$ and $\delta\varepsilon_3$ are related by the deformation mechanism, and this is expressed as:

$$\frac{\delta\varepsilon_3}{\delta\varepsilon_1} = \frac{1}{2} \tan \alpha . \tan \beta$$

$$= \frac{1}{2} (1 - \frac{dv}{d\varepsilon}) \qquad (2.15)$$

The energy ratio is the "ratio of work done per unit volume on the assembly by the major principal stress to the work done by the assembly against the minor principal stress during an increment of expansion"

$$E = \frac{\text{WORK IN}}{\text{WORK OUT}} = \frac{\sigma_1 . \delta\varepsilon_1}{2\sigma_3 . \delta\varepsilon_3}$$

$$= \frac{\tan \alpha . \tan(\phi_u + \beta)}{\tan \alpha . \tan \beta}$$

$$= \frac{\tan (\phi_u + \beta)}{\tan \beta} \qquad (2.16)$$

$$= \frac{\sigma_1}{\sigma_3(1 - \frac{dv}{d\varepsilon_1})} \qquad (2.17)$$

Rowe suggested that in real soil, a minimum - energy ratio state will be developed when $\beta = \beta_{critical} = (45° - \frac{\phi_u}{2})$

Differentiating equation (2.16) with respect to β.

$$\frac{dE}{d\beta} = \frac{d}{d\beta}\left[\frac{\tan(\phi_u + \beta)}{\tan\beta}\right]$$

$$= \frac{\sec^2(\phi_u + \beta)}{\tan\beta} - \frac{\tan(\phi_u + \beta)}{\sin^2\beta} \qquad (2.18)$$

$$\frac{dE}{d\beta} = 0 \qquad \text{when } \beta = \beta_c$$

then

$$\sin 2\beta_c = \sin 2(\phi_u + \beta_c)$$

either

$$\phi_u = 0$$

or $$\beta_c = 45° - \frac{\phi_u}{2}$$

and substitution into equations (2.16) and (2.17) give:

$$\frac{\sigma_1}{\sigma_3} \cdot \frac{1}{(1 - \frac{dv}{d\varepsilon_1})} = E_{min.} = \tan^2(45° + \frac{\phi_u}{2}) \qquad (2.19)$$

Equation (2.19), can be written as

$$\frac{\sigma_1}{\sigma_3} = (1 - \frac{dv}{d\varepsilon_1}) \cdot \tan^2(45° + \frac{\phi_u}{2}) \qquad (2.20)$$

where

σ_1 = the major principal stress.

σ_3 = the minor principal stress.

ϕ_u = frictional angle between particles.

dv = unit volumetric strain.

$d\varepsilon_1$ = the axial strain.

The corrected angle of friction "ϕ_f" has been used in place of "ϕ_u" to fit the stress-dilatancy theory, and equation (2.20) becomes

$$\frac{\sigma_1}{\sigma_3} = (1 - \frac{dv}{d\varepsilon_1}) \cdot \tan^2 (45° - \frac{\phi_f}{2}) \qquad (2.21)$$

The smallest possible value of ϕ_f is ϕ_u when only a few particles contacts are sliding, and the largest possible value of $\phi_f = \phi_{cv.}$, where $\phi_{cv.}$ is the coulomb angle of shearing resistance at the critical state, occurs when all possible contacts are sliding at large strains. Consequently, ϕ_f lies in the range

$$\phi_u \leq \phi_f \leq \phi_{cv.} \qquad (2.22)$$

Application of the expression given in equation (2.21) to a series of strength tests conducted on cohesionless soil at different void ratios, led Rowe to the following observations:

For dense sands the dilatancy effects reduced the angle of friction "ϕ_f" to a value equal to that for frictional sliding "ϕ_u". For higher void ratios, the angle of friction after deduction of the dilatancy effects still higher than "ϕ_u".

Accordingly Rowe concluded that throughout most of the range of void ratios there were three strength components of the granular materials, as shown in figure (2.7)

1 - The strength mobilized by frictional resistance (F).

2 - The strength developed by energy required to rearrange soil particles (R).

3 - The strength developed by energy required to cause expansion or dilation against the confining stress.

In a detailed analysis of the factors contributing to the strength of granular materials, Rowe, Barden and Lee (1964) proposed that the energy required to cause dilation can be subdivided into:

a - Energy required to do external work during volume change (ED).

b - Energy absorbed in friction as the mass dilate (ID).

Lee (1968), formulated an expression for the strength components of granular soils tested in direct shear box, as:

$$\tan \phi_r = \tan \phi_d + \frac{\Delta V}{A.\Delta X} \qquad (2.23)$$

or

$$\tan \phi_r = \tan \phi_d + \frac{V_o.\Delta v}{A.\Delta X} \qquad (2.24)$$

where

ϕ_r = corrected angle of shearing resistance in drained test taking into account external work done due to dilatancy.

ϕ_d = measured drained ϕ.

ΔV = change in volume of the sample.

Δv = change in volume per unit volume (negative for all increasing volumetric strain).

V_o = original volume of the sample.

A = cross-sectional area.

ΔX = horizontal displacement in direction of shearing force.

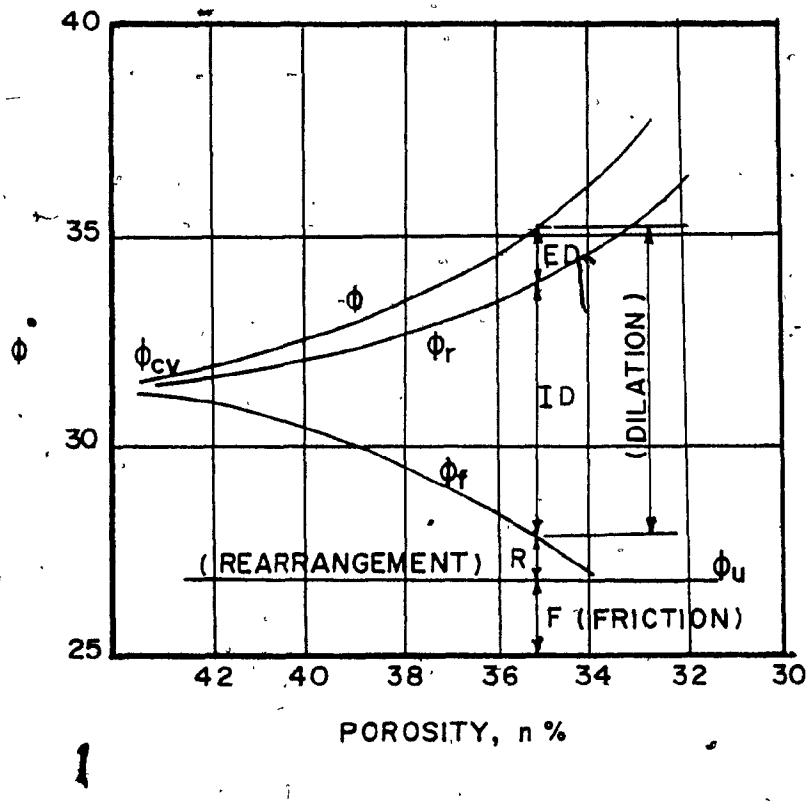

FIG. 2.7 RELATIONSHIPS BETWEEN VARIOUS FRICTION ANGLES & POROSITY OF A GRANULAR MATERIALS (AFTER ROWE, BARDEN AND LEE, 1964)

In triaxial compression tests, on granular soils, Lee (1968), derived an expression for the angle of shearing resistance corrected for dilatancy, which has been defined by Taylor-Bishop (1954), as:

$$\tan^2 (45° + \frac{\phi_r}{2}) = \frac{\sigma_1}{\sigma_3} + \frac{\Delta V}{V.\varepsilon_1} \qquad (2.25)$$

where

σ_1 = the major principal stress.

σ_3 = the minor principal stress.

$\frac{\Delta V}{V}$ = volumetric strain (negative if dilating).

ε_1 = axial strain in direction of major principal stress.

The corresponding expression by Rowe was given as

$$\tan^2 (45° + \frac{\phi_f}{2}) = \frac{\sigma_1}{\sigma_3} \cdot [\frac{1}{(1 - \frac{\Delta V}{V\varepsilon_1})}] \qquad (2.26)$$

the difference between equation (2.25) and (2.26) gives the energy absorbed within the sample as a result of the rearrangement of the particles.

2.4 Energy Components During Shear Tests.

General

The total work done during the application of a principal stress system and as a result of the associated volume change may be divided into three principal components, as

1 - Internal energy absorbed in friction, if no volume change takes place. This is subdivided into two components:

(i) Energy absorbed due to the true interparticle friction angle "ϕ_u".

(ii) Additional energy absorbed and required to rearrange soil particles.

2 - Internal energy absorbed in friction as the mass dilate.

3 - External work done during volume changes.

The components of energy loss during a direct shear test were examined by using a model as shown in figure 2.8. The plane of sliding is at angle of θ to the direction of the external shearing force S, so that the gross work done due to displacement ΔX is $S.\Delta X$. However, some of the input energy is used to let the sample to expand against the external load "N", then

The net work done on the sample =

$$S.\Delta X - N.\Delta X.\tan\theta \qquad (2.27)$$

Taylor (1948), defined an equivalent shearing force, S_r, which was associated with the energy dissipated within the sample, then

$$S_r.\Delta X = S.\Delta X - N.\Delta X.\tan\theta \qquad (2.28)$$

or

$$\tan\phi_r = \tan\phi_d - \frac{\Delta V}{A.\Delta X} \qquad (2.29)$$

where

ϕ_r = corrected angle of shearing resistance taking into account the external work due to dilation.

ϕ_d = measured drained angle of shearing resistance.

ΔV = the incremental increase or decrease in volume ($\Delta V = A.\Delta y$).

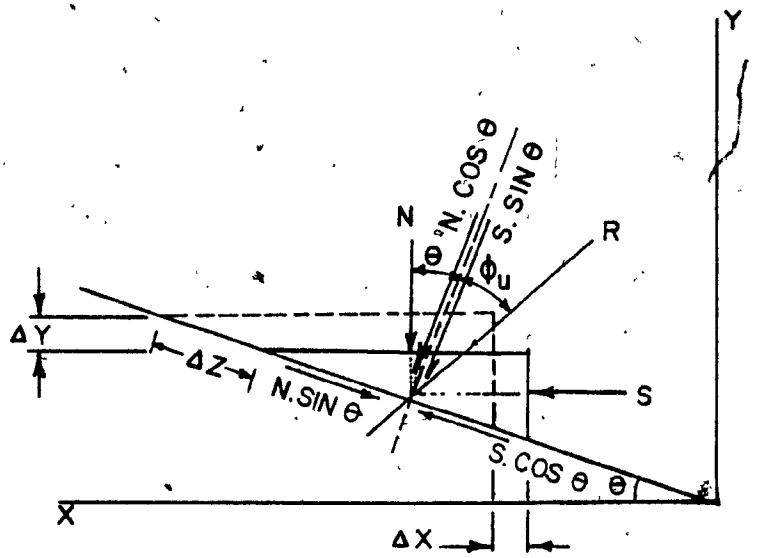

FIG. 2.8 SLIDING WEDGE (AFTER ROWE, 1962)

A = cross-sectional area of the sample.

ΔX = the incremental displacement in direction of S.

ΔY = the incremental vertical displacement in direction of N.

The work equation in the direction of plane of sliding is:

$$S.\cos\theta.\Delta Z = N.\sin\theta.\Delta Z + (S.\sin\theta+N.\cos\theta)\Delta Z.\tan\phi_u \qquad (2.30)$$

where

ϕ_u = true angle of friction.

ΔZ = the incremental displacement along the place of sliding.

The volumetric strain $= \frac{\Delta V}{V} = \frac{A.\Delta Z.\sin\theta}{V}$

$$= \frac{A.\sin\theta}{V} \cdot \frac{\Delta X}{\cos\theta} = \frac{A.\Delta X}{V} \cdot \tan\theta$$

then

$$\tan\theta = \frac{\Delta V}{A\Delta X} \qquad (2.31)$$

substituting (2.31) into (2.30)

then

$$\frac{S}{N} = \frac{\Delta V}{A.\Delta X} + \left(\frac{S}{N} \cdot \tan\phi_u \cdot \frac{\Delta V}{A.\Delta X} + \tan\phi_u\right) \qquad (2.32)$$

and using equation (2.29), then

$$\tan\phi_r = \tan\phi_d \cdot \tan\phi_u \cdot \frac{\Delta V}{A.\Delta X} + \tan\phi_u \qquad (2.33)$$

From equation (2.33), it can be seen that there is a strength term associated with dilatancy which is within the sample, as well as an external energy related to dilatancy.

Rowe (1957), found that, there is an additional energy component absorbed within the sample because slides in a natural soil do not necessarily occur in directions associated with a minimum energy state. This condition can be expressed by replacing ϕ_u with ϕ_f then

$$\tan \bar{\phi_r} = \tan \phi_d \cdot \tan \phi_f \cdot \frac{\Delta V}{A \cdot \Delta X} + \tan \phi_f \qquad (2.34)$$

where

ϕ_f = Rowe's frictional angle.

Bishop (1954), followed the same approach as taylor (1948), to derive an energy correction for triaxial compression test. When a triaxial sample is subjected to increments in axial and radial strains of $\Delta\varepsilon_1$ and $\Delta\varepsilon_3$ respectively.

The total energy change per unit volume transmitted to the element δE is divided into two components namely the internal stored and elastic energy, δU and the energy dissipated in shear or frictional heat loss, δW. thus

$$\delta E = \delta W + \delta U \quad ..... \qquad (2.35)$$

Bishop (1954) and Rowe (1962) working with sand, neglected the elastic component δU which is small for dense sands.

then

$$\delta E = \delta W = \sigma_1 \cdot \Delta\varepsilon_1 - (-2\sigma_3 \cdot \Delta\varepsilon_3)$$

$$= \sigma_1 \cdot \Delta\varepsilon_1 + 2\sigma_3 \cdot \Delta\varepsilon_3 \qquad (2.36)$$

$$= \sigma_1 \cdot \Delta\varepsilon_1 + \sigma_3 (\delta V - \Delta\varepsilon_1) \qquad (2.37)$$

Setting

$$q = \sigma_1 \cdot \sigma_3 \quad ; \quad \delta V = \Delta\varepsilon_1 + 2\Delta\varepsilon_3 ;$$

$$P = \frac{1}{3}(\sigma_1 + 2\sigma_3) = \frac{q}{3} + \sigma_3$$

the following forms of equation (2.37) are obtained

$$\delta E = \delta W = \Delta\varepsilon_1 [\sigma_1 - \sigma_3 (1 - \frac{\delta V}{\Delta\varepsilon_1})] \qquad (2.38)$$

$$= \Delta\varepsilon_1 [q + \sigma_3 \frac{\delta V}{\Delta\varepsilon_1}] \qquad (2.39)$$

$$= q\,\Delta\varepsilon_1 + \sigma_3\,\delta V$$

$$= q\,\Delta\varepsilon_1 + \delta V\left(P - \frac{q}{3}\right)$$

$$= q\left(\Delta\varepsilon_1 - \frac{\delta V}{3}\right) + P.\delta V \qquad (2.40)$$

$$= (q.\Delta\varepsilon) + (P.\delta V) \qquad (2.41)$$

where,

q = $(\sigma_1 - \sigma_3)$ = deviator stress.

P = mean stress.

σ_1 = major principal stress.

σ_3 = minor principal stress.

$\Delta\varepsilon_1$ = increment of major principal strain.

$\Delta\varepsilon_3$ = increment of minor principal strain.

δV = $(\Delta\varepsilon_1 + 2\Delta\varepsilon_3)$ increment of volumetric strain.

δE = increment of energy per unit volume transmitted to the element.

δW = increment of energy dissipated per unit volume in shear or frictional heat loss.

δU = increment in internal stored and elastic energy per unit volume.

$\Delta\varepsilon$ = $\left(\Delta\varepsilon_1 - \frac{\delta V}{3}\right)$

Bishop defined a "corrected" deviator stress $(\sigma_1 - \sigma_3)_r$, which does work (δW) in moving through $(\Delta\varepsilon_1)$, and all of which is absorbed internally in frictional heat.

then

$$\delta W = (\sigma_1 - \sigma_3)_r . (\Delta\varepsilon_1) \qquad (2.42)$$

equating (2.42) and (2.38):

$$(\sigma_1 - \sigma_3)_r = (\sigma_1 - \sigma_3) + \sigma_3 . \delta V/\Delta\varepsilon_1 \qquad (2.43)$$

where $\sigma_3 \frac{\delta V}{\Delta\varepsilon_1}$ is the correction which must be applied to the observed deviator stress $(\sigma_1 - \sigma_3)$ in order to obtain the so called "corrected" deviator stress.

The Coulomb ϕ_{r_1} associated with this corrected deviator and the actual principal stresses was given by Bishop and Eldin (1953) in the form

$$\sin \phi_{r_1} = \frac{(\sigma_1 - \sigma_3)_r}{\sigma_1 + \sigma_3}$$

$$= \frac{(\sigma_1 - \sigma_3) + \sigma_3 \frac{\delta V}{\Delta\varepsilon_1}}{\sigma_1 + \sigma_3} \qquad (2.44)$$

An alternative "corrected" ϕ, which corresponds to the total work absorbed internally after elimination of all external work done by dilation, was defined as

$$\tan^2 (45° + \frac{\phi_r}{2}) = \frac{(\sigma_1 - \sigma_3)_r + \sigma_3}{\sigma_3} \qquad (2.45)$$

or

$$\tan^2 (45 + \frac{\phi_r}{2}) = (\frac{\sigma_1}{\sigma_3}) + (\frac{\delta V}{\Delta\varepsilon_1}) \qquad (2.46)$$

From equation (2.43), we might observe that the effect of dilation is to modify the cell pressure by the factor

$$[1 - (\frac{\delta V}{\Delta\varepsilon_1})]$$

Rowe (1962), derived an expression for the "corrected ϕ" as

$$\tan^2 (45° + \frac{\phi_f}{2}) = \frac{(\sigma_1 - \sigma_3)_r}{\sigma_3[1 - \frac{\delta V}{\Delta \varepsilon_1})]} + 1 \qquad (2.47)$$

or

$$\tan^2 (45° + \frac{\phi_f}{2}) = \frac{(\sigma_1 - \sigma_3) + \sigma_3 (\frac{\delta V}{\Delta \varepsilon_1})}{\sigma_3 [1 - \frac{\delta V}{\Delta \varepsilon_1}]} + 1 \qquad (2.48)$$

2.5 Strength Limits in Triaxial and Plane Strain Compression Tests.

Rowe (1969) expressed the stress dilatancy equation as:

$$R = DK \qquad (2.49)$$

where

R = stress ratio = $\sigma_1 | \sigma_3$.

D = dilatancy rate = $1 - \frac{dv}{d\varepsilon_1}$.

$K = \tan^2 (45° + \frac{\phi_f}{2})$.

the value of ϕ_f range between ϕ_u and ϕ_{cv}.

Rowe suggested that if the dilatancy rate of D = 2, then the stress ratio of a sand in the densest state is given by

$$\sigma_1 | \sigma_3 = 2 \tan^2 (45° + \frac{\phi_u}{2}) \qquad (2.50)$$

Taking D = 1 and the relationship $\phi_f = \phi_{cv}$ for the loosest state, then

$$\sigma_1 | \sigma_3 = \tan^2 (45° + \frac{\phi_{cv}}{2}) \qquad (2.51)$$

In plane strain compression for any packing $\phi_f = \phi_{cv}$.

Therefore, for the densest state

$$\sigma_1 | \sigma_3 = 2 \tan^2 (45° + \frac{\phi_{cv}}{2}) \qquad (2.52)$$

and for the loosest state

$$\sigma_1/\sigma_3 = \tan^2 (45° + \frac{\phi_{cv}}{2}) \qquad (2.53)$$

The maximum dilatancy rate of 2 is not necessarily reached by dense packings. An increase of mean principal stress, for example, leads to crushing and a reduction of the dilatancy rate to such an extent that at very high pressures the dilatancy rate is unity.

Bishop (1954), derived an expression for the relationship between ϕ_{cv} and ϕ_u as follows

$$\text{Sin } \phi_{cv} = \frac{15 \tan \phi_u}{10 + 3 \tan \phi_u} \qquad (2.54)$$

2.6 Relationship between Plane-strain and Direct Shear Test

As reported by Rowe (1969) several researchers have reported direct measurements of normal and shear stresses on the boundary of an element of sand in the centre of the Cambridge simple shear apparatus MK6. Assuming uniformity of strain throughout the element; it has been shown that the direction of principal stress and strain coincide during small incremental stress relations.

Based on the above observation Rowe derived the following expression

$$\tan \phi_{ds} = \tan \phi_{ps} \cdot \text{Cos } \phi_{cv} \qquad (2.55)$$

where

ϕ_{ds} : the value of ϕ for direct shear tests.

ϕ_{ps} : the value of ϕ for plane strain tests.

2.7 Comparison Between Triaxial, Plane-Strain Compression and Direct Shear Tests

The failure characteristics of the plane-strain and triaxial compression test series, conducted on Brasted sand have been analysed by Cornforth, 1964. He came to a conclusion as shown in figure 2.9, that the strength of the sand samples tested in plane-strain was always greater than the strength of the corresponding triaxial sand samples tested at the same placement density. The difference varies from $\frac{1}{2}°$ at the lowest densities to more than 4° for the dense samples.

The strength results, obtained by Nash (1953), from the triaxial compression and direct shear tests series, conducted on a fine sand, are shown in figure 2.10. He concluded that the strength obtained from the direct shear tests were greater by 10% than the strength obtained from the triaxial tests at the smallest porosities. At higher porosities, the strength values from the triaxial tests were greater by 5% than the strength values of the corresponding direct shear tests.

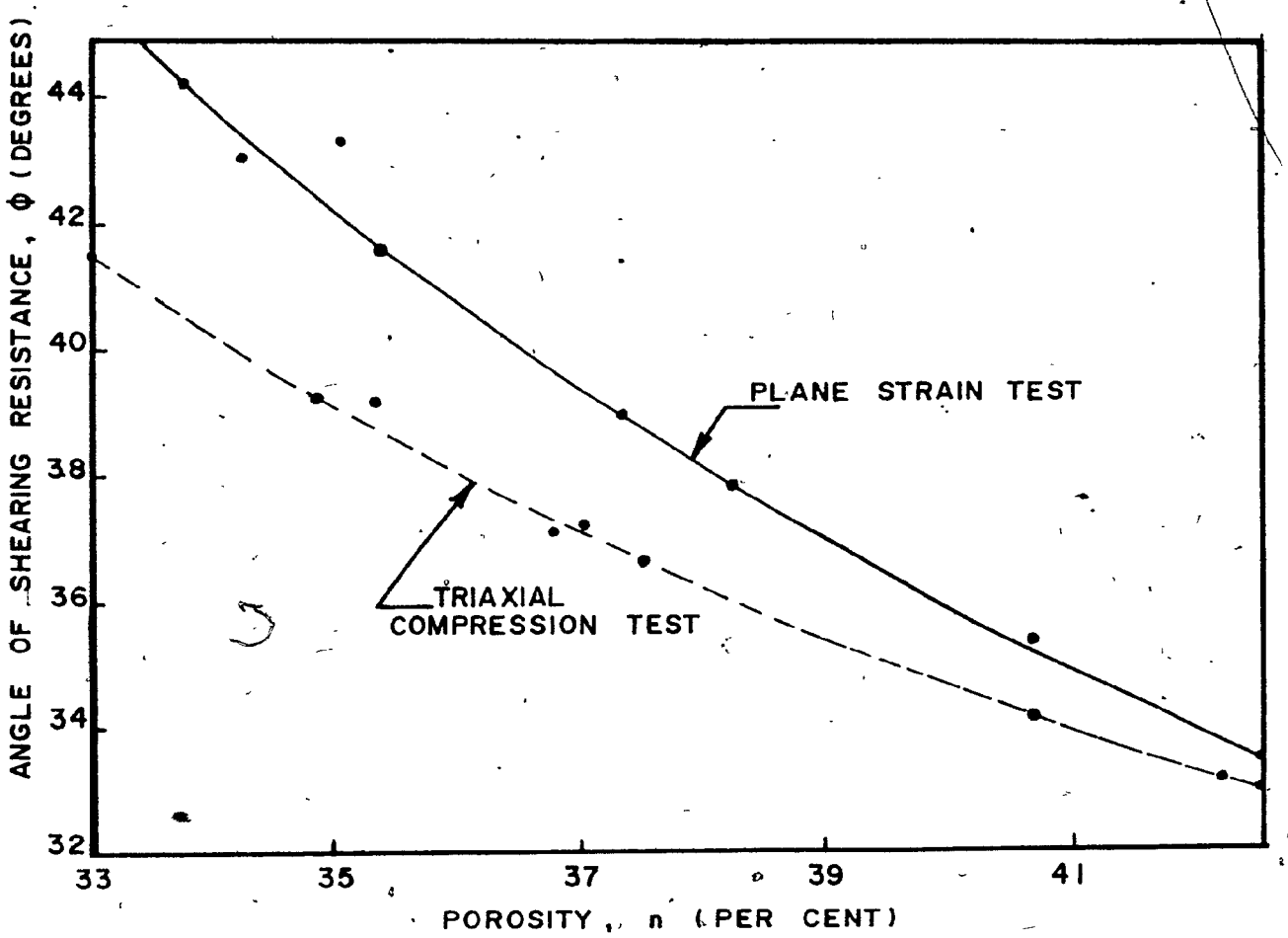

FIG. 2.9 COMPARISON OF PLANE STRAIN & TRIAXIAL COMPRESSION TESTS AT CELL PRESSURE OF 40 PSI (AFTER DEREK H. CORNFORTH, 1964)

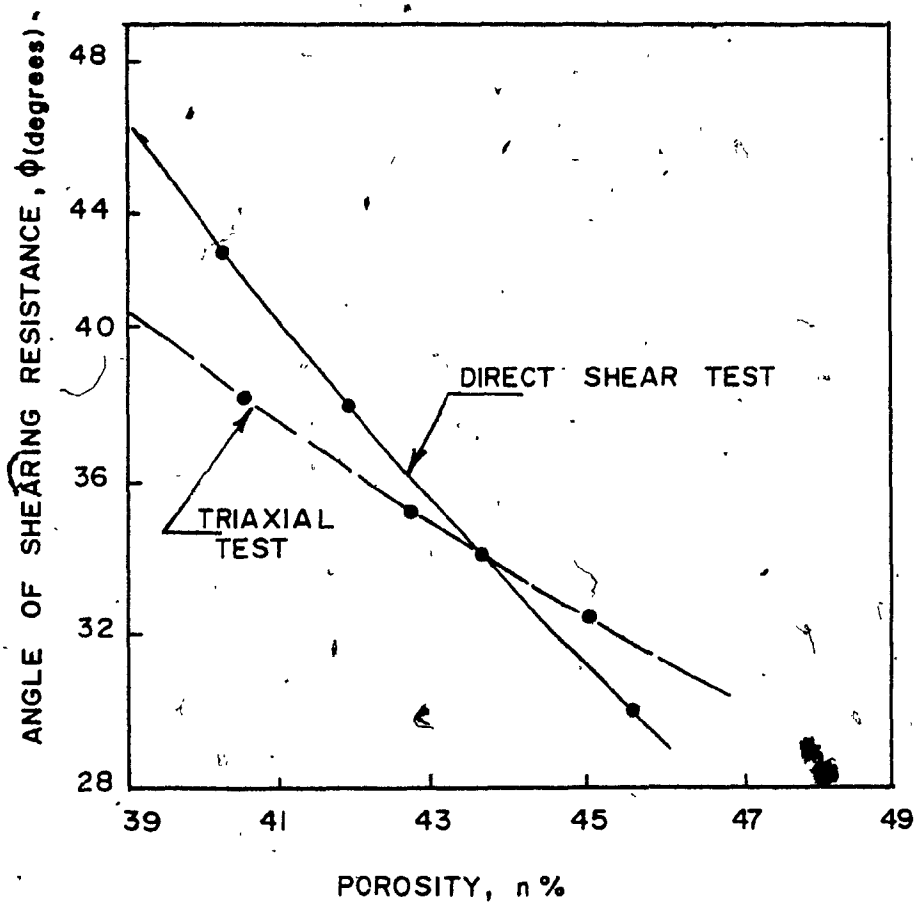

FIG 2·10 COMPARISON OF DIRECT SHEAR & TRIAXIAL COMPRESSION TESTS (AFTER NASH, 1953)

CHAPTER III

TEST TECHNIQUE AND MATERIALS

3.1 General

In this investigation tests are conducted using triaxial, shear box, and plane-strain apparatus. In this chapter the description of the equipment, materials and test procedure are given.

3.2 Materials

The materials used in this investigation were air-dry sand. The chemical analysis indicated that the sand used designated as silica (99.9% silica). From the grain size distribution curves, figure 3.1, it would appear that each one of the sand grains used was: medium to fine sand for sand A, and coarse to medium sand for sand B, and C respectively. The description of the sand tested is given in table 3.1.

3.3 Triaxial Compression Test

3.3.1 Apparatus

The tests were carried out in a triaxial cell as shown in figure 3.2, which consists of a prespex cylinder fitted between a base and a top cap. Through the base there is a pressure connection to fill the cell with water. In the top cap there is an air release valve, which is kept open during the filling of the cell of water. A stainless steel piston running through the centre of the top cap applies the vertical compressive load on the specimen under test. Another inlet is often

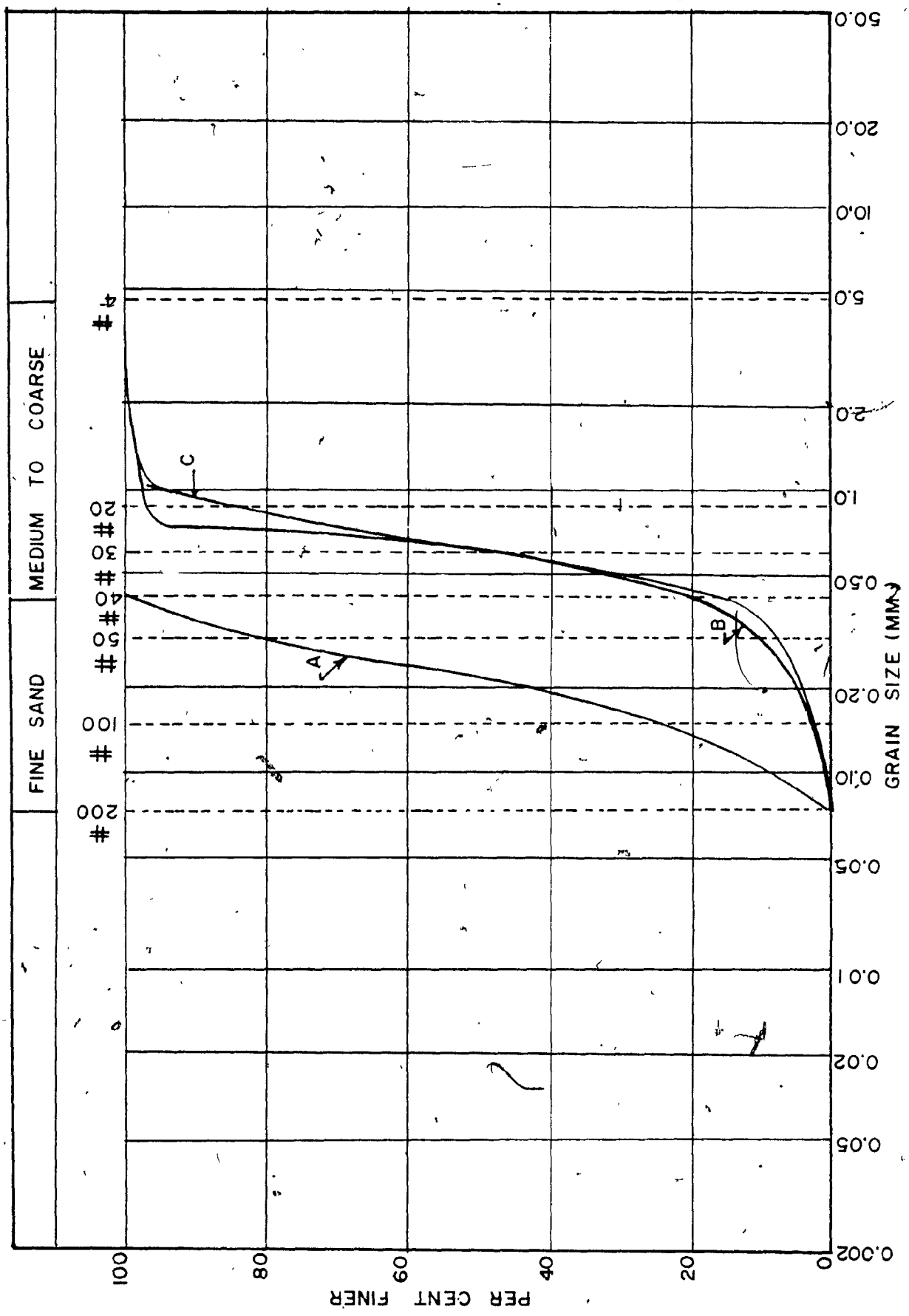

FIG. 3.1 GRAIN SIZE DISTRIBUTION

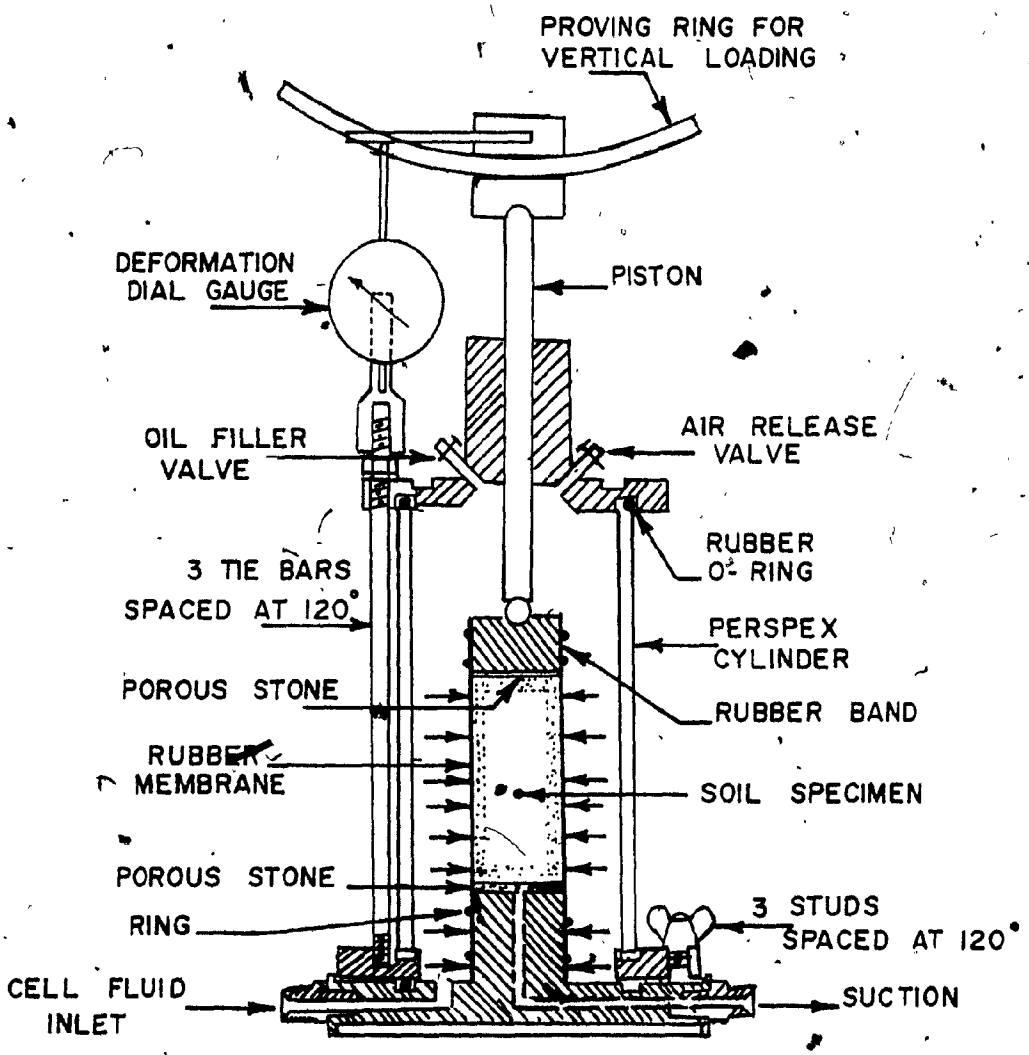

FIG. 3.2 THE TRIAXIAL CELL

provided in the top cap for filling some light machine oil in the cell above the water to prevent any leakage. The vertical strain of the speciman is measured from the downward movement of the piston as indicated by the dial guage fixed to the top cap of the triaxial cell.

3.3.2 Sample Preparation

A cylindercal specimens generally having a length: diameter ratio of 2, were used in the tests. The circular base has a central pedestal on which the specimen was placed. The specimen was prepared in a rubber membrane about 0.20 mm thickness, inside a rigid former which fits around the pedestal. The diameter of the specimen was measured by a micrometer at the mid height, one inch below the top and one inch above the bottom, then the specimen was turned 90 degrees and the other three readings were taken. The average was the required diameter.

A small negative pressure was applied by mouth to maintain the stability of the specimen, while the former was removed and prior to the application of the cell pressure.

3.3.3 Test Procedures

After the sample was prepared, the cell assembled on the triaxial machine. The cell was filled nearly to the top with distilled water. The top 0.2 inch was filled with paraffin oil to prevent any leakage during the test. The cell pressure was applied for about one hour before starting shearing of the sample. At the application of the cell pressure by using the mercury control system, the initial volume change reading was taken by using the volume measuring device. The loading ram was lowered to be in contact with the bearing ball of the platen. The axial stress was applied to the sample at a machine rate of 0.015 inch

per minute after one hour from the application of the cell pressure. Sets of readings of the axial stress, the volume change and the vertical deformation were taken up to failure and continued until the ultimate condition.

The self compensating mercury control system used in these tests, was originally developed at the Imperial College, London. This system develops a pressure in the cell water equal to the difference in levels between the mercury surfaces in the two limbs. Any leakage from the cell or volume change in the specimen is automatically compensated by the movement of the upper cylinder under the action of a spring of an appropriate stiffness. The volume change measuring was based on the volume of water entering or leaving the cell to compensate for the change in volume of the sample, and then corrected for cell expansion and the movement of the loading ram. The correction due to the movement of the ram was added to the observed decrease in the volume by an amount of $a_r \cdot \Delta L$, where a_r is the cross-sectional area of the ram and ΔL, the vertical movement. Also the correction due to expansion of the cell was subtracted from the increase of the volume recorded.

Figure 3.3 shows the volume change device, used with samples 1.5 inch diameter.

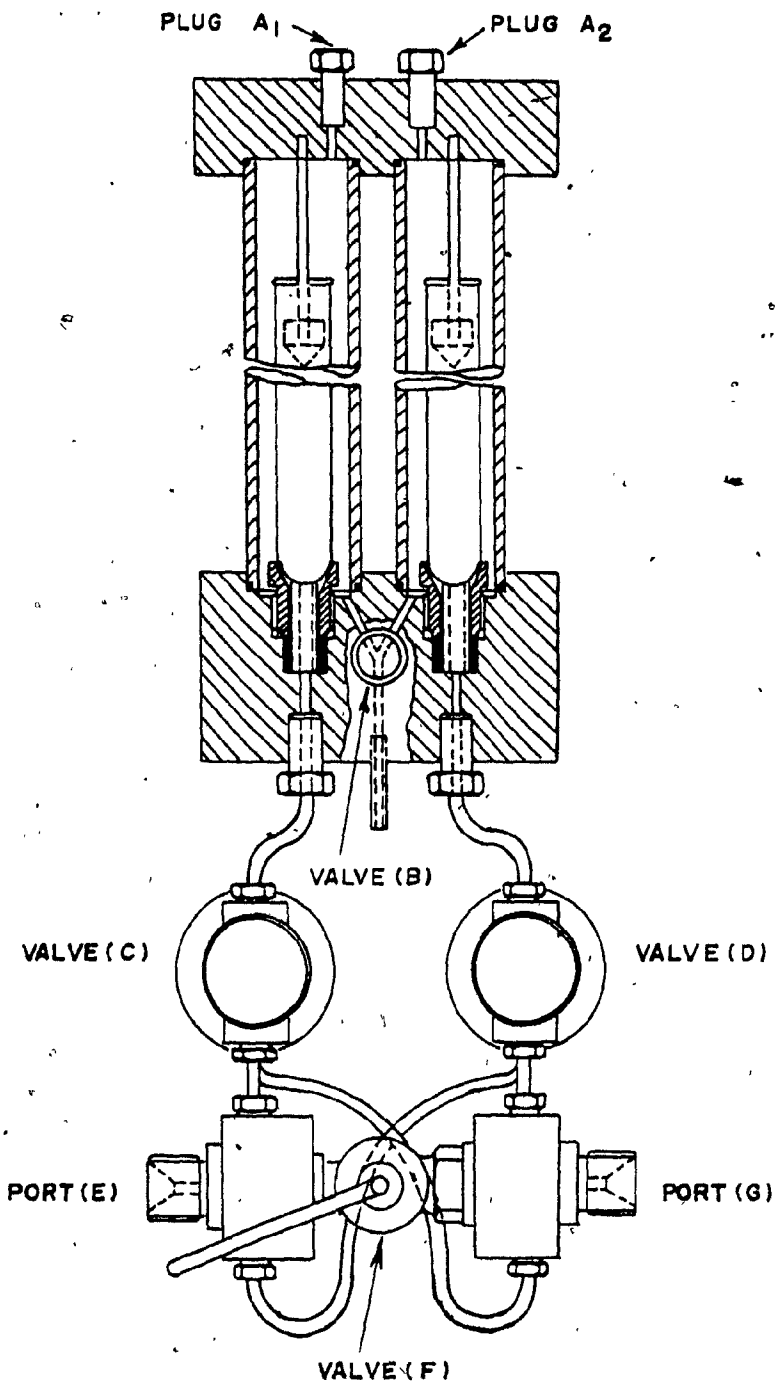

FIG. 3.3 VOLUME CHANGE TWIN BURETTE TYPE FOR USE WITH SAMPLES $1\frac{1}{2}$" - 4" DIA.

Table 3.1

Sand Properties

Determination Number	Sand A	Sand B	Sand C
Specific gravity (G_s)	2.65	2.63	2.64
maximum density $(\gamma_d)_{max.}$	115 lbs./ cft.	109 lbs./ cft.	106 lbs./ cft.
minimum density $(\gamma_d)_{min.}$	97 lbs./ cft.	95 lbs./ cft.	88 lbs./ cft.
minimum void ratio $(e)_{min.}$	0.40	0.50	0.40
maximum void ratio $(e)_{max.}$	0.80	0.90	0.95

3.4 Direct Shear Box Test

3.4.1 Apparatus

The test was carried out in a box split in two halves. The box is square in section and it is split horizontally at the level of the centre of the soil specimen. The lower half of the box is rigidly held in position in a container. The container itself rests over slides or rollers and can be pushed forward at a constant rate by a jack, driven by electric motor. The upper half of the box bears against a calibrated steel proving ring. The movement of the lower part of the box is transmitted through the specimen to the upper part and hence on the proving ring, the reading of which indicates the shear force. Normal load was applied on the specimen from a loading yoke bearing upon a

metal pressure pad through a steel ball. The pressure pad fits into the box over the upper serrated plate. Figure 3.4 shows a diagramatic representation of the shear box test.

3.4.2 Sample Preparation

The direct shear box tests were performed on samples having dimensions of 2.40, 2.40, and 0.80 inch (width, length and thickness respectively). The samples were prepared by depositing the sand into the box by using a spoon or small funnel. Care was taken to be sure that the thickness of the bed produced was uniform and also the sample thickness was sufficient. The top surface of the sample was leveled before placing the serrated plate into place.

A loading block was placed on the serrated plate. Dial gauge was fixed at the end of horizontal bar connected with another one in the vertical position.

3.4.3 Test Procedures

After preparing the samples, the ball bearing and the hanger were placed on the loading block. The dial gauges which shows vertical and horizontal strain of the sample were adjusted. The normal loads were placed on the load hanger, with the lever loading arm in horizontal position. When the machine rate was selected (0.048 inch per minute), the beam jack was turned to apply the load on the sample. The two parts of the box were separated by removing the vertical lock screws, and then the upper frame was raised by turning the spacing screws to give a spacing of 1/16 of an inch. The loading bar was adjusted to be in contact with shear box, and then the dial gauges were adjusted to zero.

The test then was ready to begin. Sets of readings of the proving

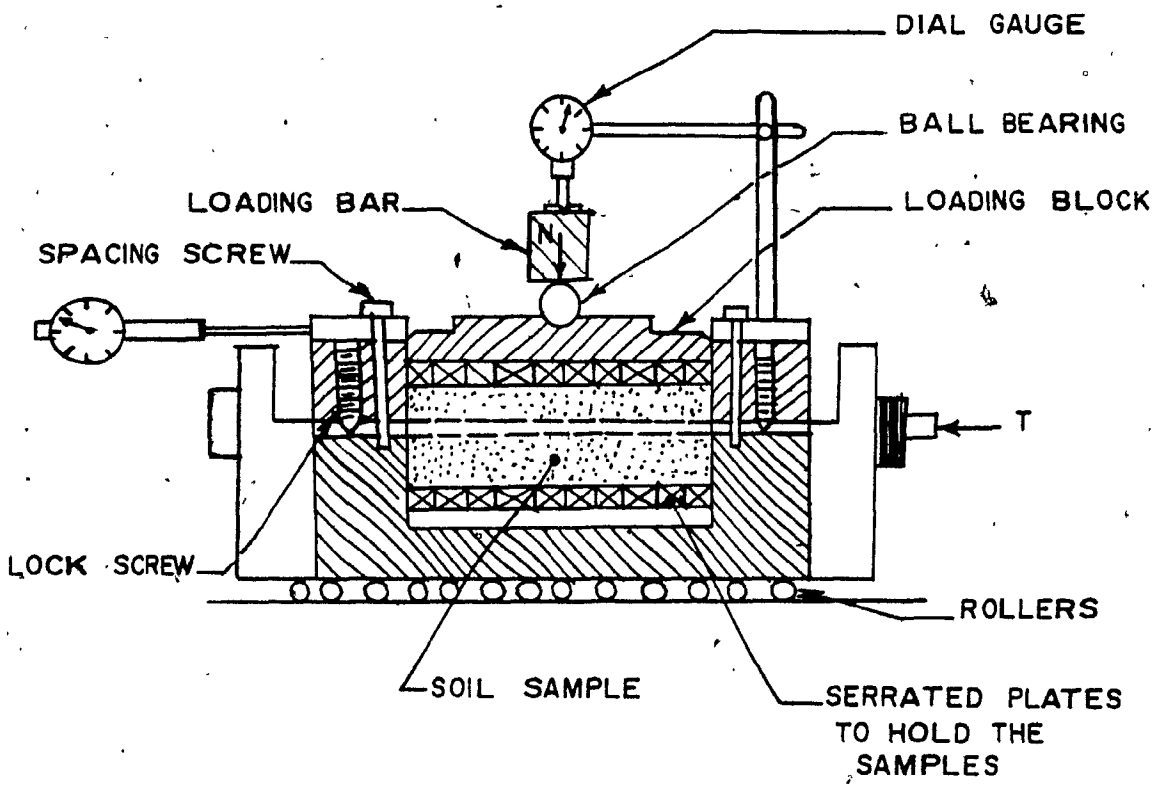

FIG. 3.4 DIAGRAMATIC REPRESENTATION OF THE SHEAR BOX

ring and dial gauges were taken every 15 seconds for the first two minutes, and then every 30 seconds until the peak load on the proving ring has been passed and the readings have decreased to a constant value. The stress-strain curve was plotted for each test.

3.5 Plane Strain Compression Test

3.5.1 Apparatus

This test was carried out in a stainless steel cell, having a rectangular cross-section. Two side plates were used to prevent any change in the length of the sample, and to maintain the plane strain condition during the test. The water cells were made of two rubber membranes with thickness of 0.20 mm, and two prespex plates. In the top frame of the stainless steel cell, there is an air release valve which is kept open during the filling of the cell with water. A stainless steel loading bar having a square cross-section running through the centre of the top cap which was placed on the top of the sample. Also a dial gauge was used to measure the vertical deformation. Figures 3.5.a and 3.5.b show two different sections of the apparatus.

3.5.2 Sample Preparation

The nominal dimensions of the samples used were chosen as 3.62, 1.50 and 2.95 inch (width, length and height). The specimen was prepared in a rubber membrane of 0.02 inch thickness, placed inside a rigid former which fits around the pedestal. After the form was full of sand, the raining of the sand was stopped; the sides of the former were cleaned gently with a small hair brush. A small negative pressure was applied to maintain the stability of the specimen while the former was removed. Then with using an accurate scale, the dimensions of the sample were measured.

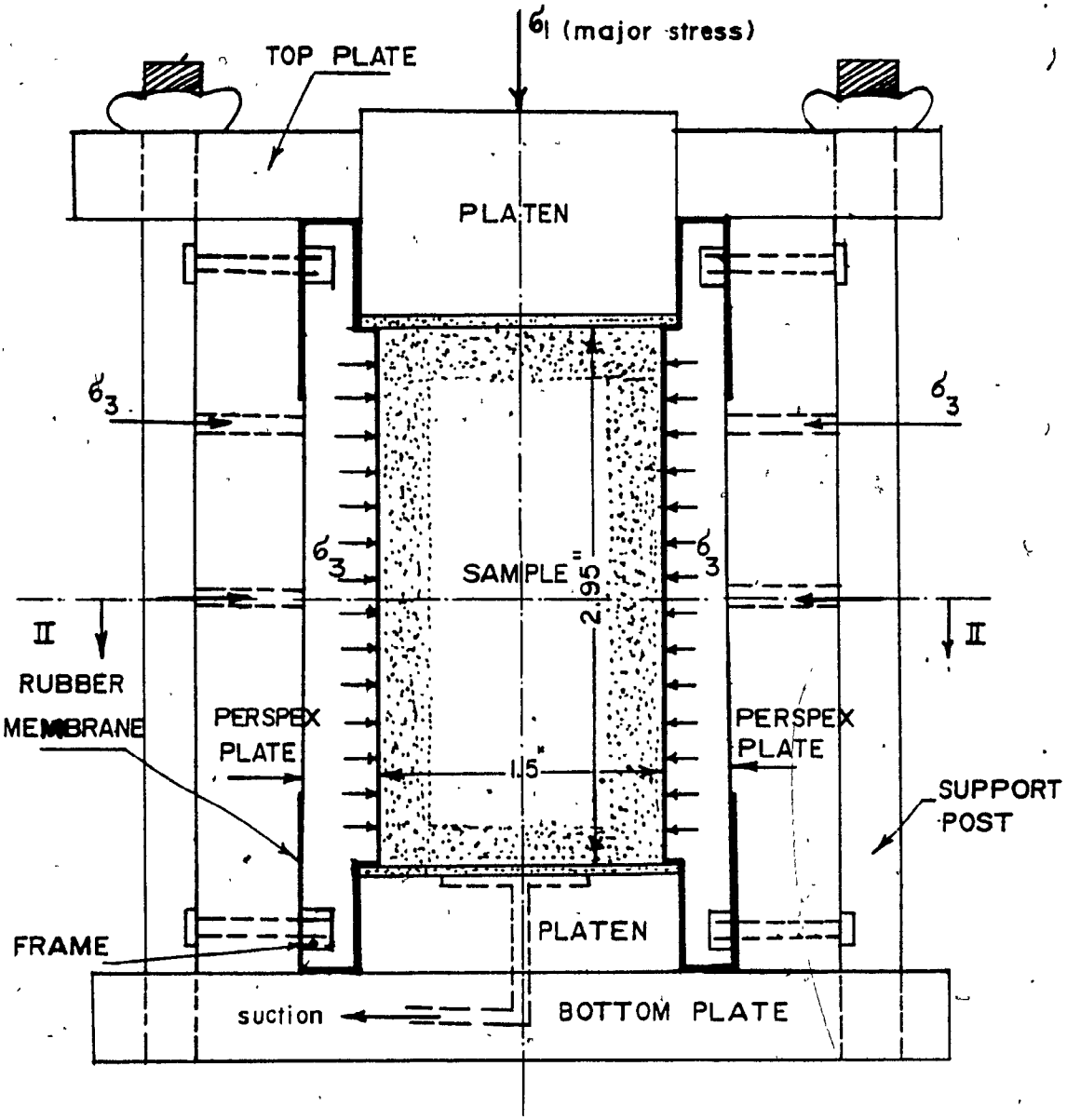

FIG. 3.5 a VERTICAL SECTION OF PLANE-STRAIN
(SEC. I-I SEE FIG. 3-5-b)

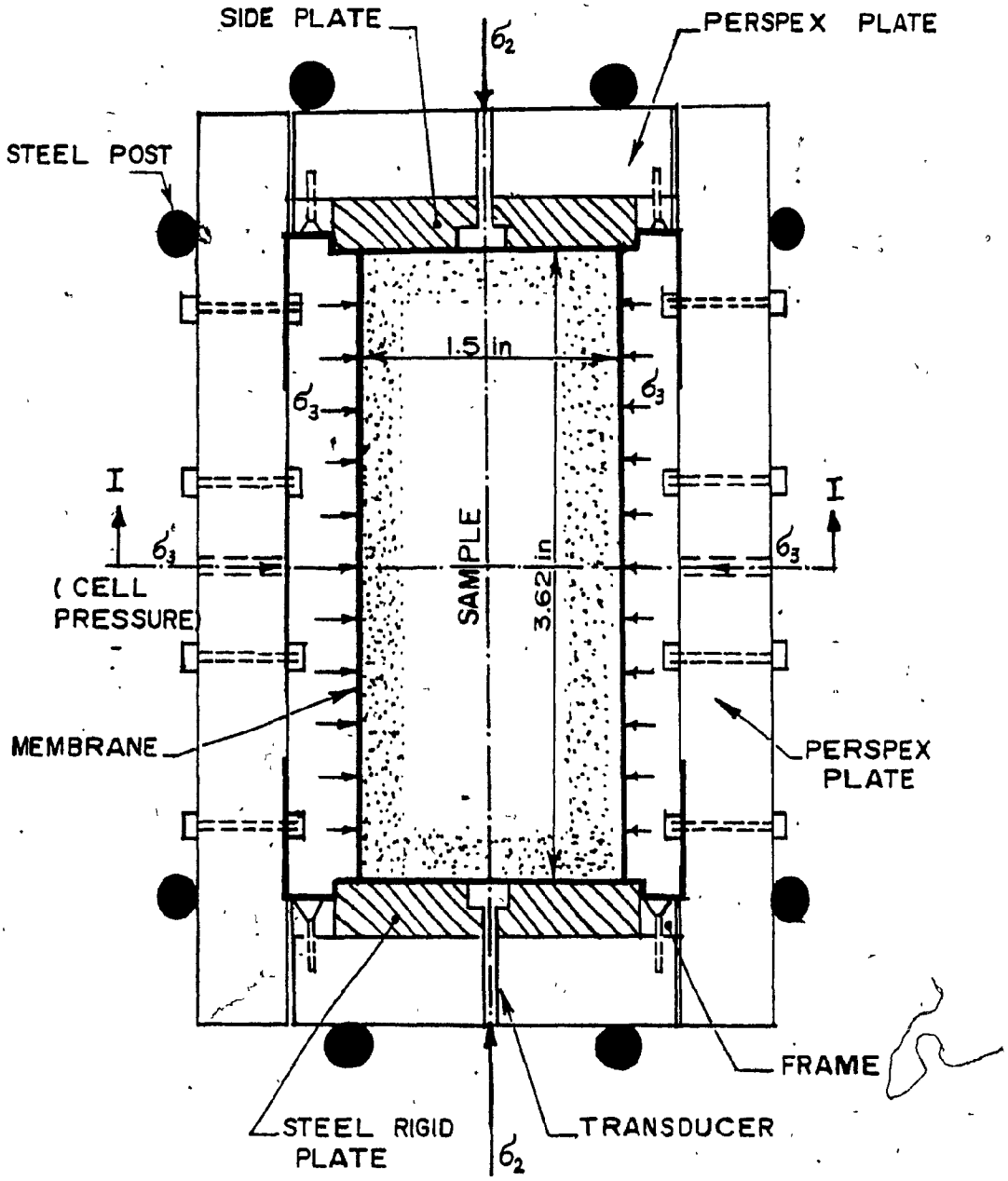

FIG. 3.5.b HORIZONTAL SECTION OF PLANE STRAIN (SEC. II-II)

3.5.3 Test Procedures

After the sample was prepared, the apparatus was assembled on the triaxial machine. The cell was filled with water nearly to the top. The cell pressure was applied for about one hour before starting to shear the sample. Two pressure transducers were placed in the centre of the side plates, to measure the intermediate principal stress. The sample was loaded via the loading bar, at a machine rate of 0.016 inch/minute.

Sets of readings of the intermediate principal stress, vertical deformation, and volume change were taken at intervals of 0.25% up to failure and continued until the ultimate condition.

Figure 3.6, shows the details of the experimental set up for the drained plane strain compression test.

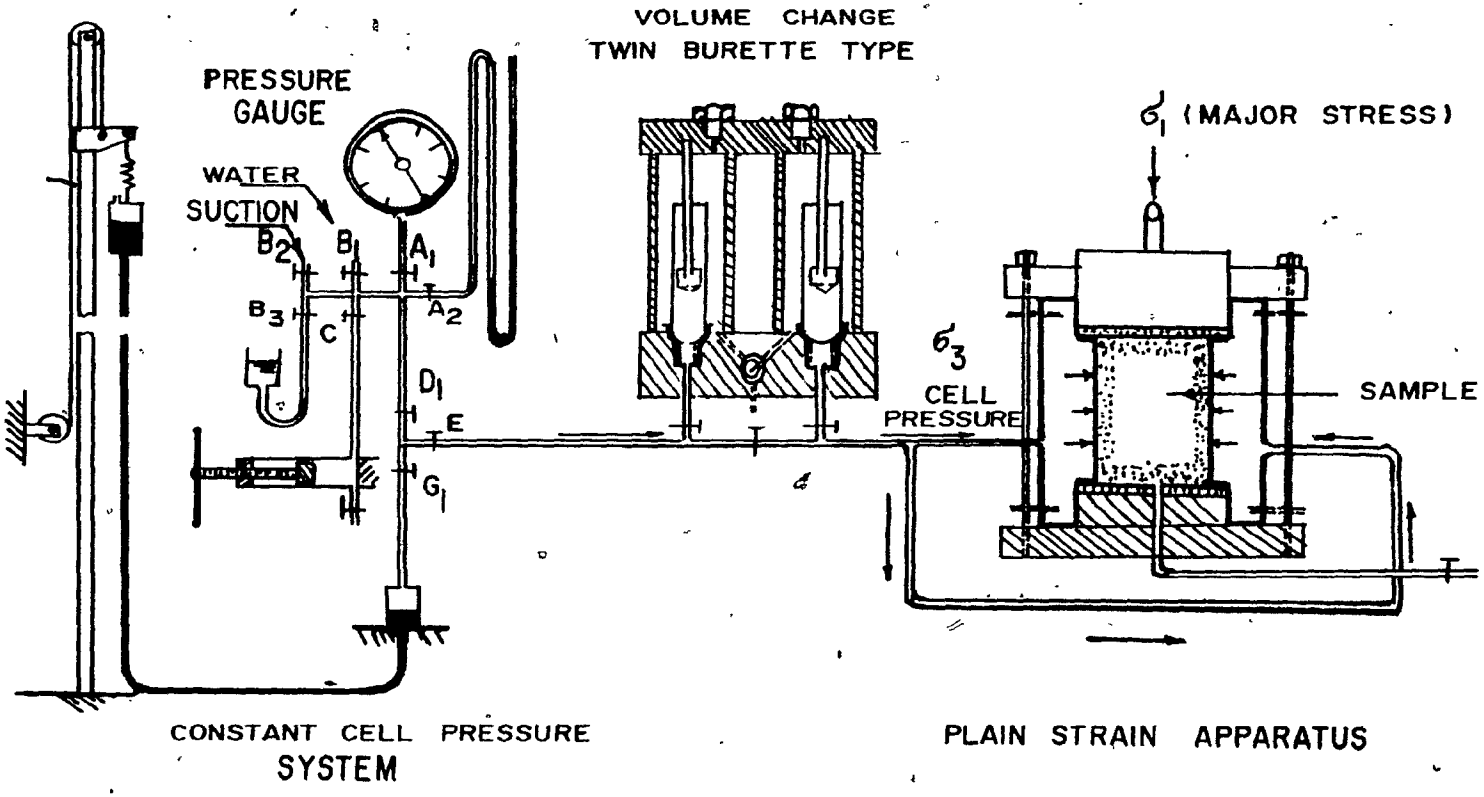

FIG. 3.6 DIAGRAMATIC LAYOUT OF PLANE STRAIN TEST SET UP

CHAPTER IV

TEST RESULTS

4.1 General

In this chapter, the experimental results for triaxial compression, direct shear box and plane strain compression tests are summarized in tables and presented in graphic form.

4.2 Consolidated - Drained Triaxial Compression Tests

These tests were conducted on samples istropically consolidated at the required confining pressure. The axial stress increased at a constant machine rate of 0.015 inches per minute, one hour after the application of the confining pressure. This allows time for the cell to expand and reach a state where further expansion was negligable.

Sets of readings were generally taken at intervals of 0.30% axial strain up to failure, and continued until the ultimate condition had been reached.

The test results are summarized in tables 4.1 to 4.3 and presented in graphical form in figures 4.1 to 4.9.

The shear strength parameter, (ϕ), was computed for each individual test, based on the assumption that the failure envelope was a straight line passing through the origin.

From Mohr-Coulomb failure criterion:

$$\tan^2 (45° + \phi/2) = \sigma_1/\sigma_3$$

or

Table No. 4-1

Summary of Test Results in Triaxial Compression Tests on Sand "A"

Test * Number	Unit Weight γ_d (Lbs./ft.^{3})	Void Ratio e	Porosity n %	Relative Density D_r %	Cell Pressure σ_3 (Lbs./in.^{2})	Deviator Stress $(\sigma_1-\sigma_3)$ (Lbs./in.^{2}) at failure	Volumatric Strain $\frac{\Delta V}{V}$ % at failure	Axial Strain ε_1 % at failure	Angle of Shearing Resistance ϕ (degrees)	Remarks
A-M-1	104.20	0.61	37.88	48	25	66.50	+ 1.0	3.20	35	Medium Dense
A-M-2	106.00	0.58	37	55	50	130.34	+ 0.80	4	34.50	" "
A-M-3	104.50	0.605	38	49	65	161	+ 0.50	5	33.50	" "
A-M-4	108.90	0.54	35	65	25	72	+ 1.60	2.95	36	" "
A-M-5	108.90	0.54	35	65	50	133	+ 1.30	3.85	35	" "
A-M-6	108.90	0.54	35	65	65	159	+ 1.20	4.50	33.50	" "
A-D-1	113.30	0.48	32	80	25	85	+ 2.10	2.80	39	Dense Sand
A-D-2	113.30	0.48	32	80	50	150	+ 1.92	3.20	37	" "
A-D-3	113.30	0.48	32	80	65	185.50	+ 1.71	3.80	36	" "

* A: Sand type

M: Medium-dense sand

D: Dense sand

Table No. 4-2

Summary of Test Results in Triaxial Compression Tests on Sand "B"

Test * Number	Unit Weight γ_d (Lbs./ft.^{3})	Void Ratio e	Porosity n %	Relative Density D_r %	Cell Pressure σ_3 (Lbs./in.^{2})	Deviator Stress $(\sigma_1 - \sigma_3)$ (Lbs./in.^{2}) at failure	Volumetric Strain $\frac{\Delta V}{V}$ % at failure	Axial Strain ε_1 % at failure	Angle of Shearing Resistance ϕ (degrees)	Remarks
B-M-1	105.40	0.59	37	77.50	25	83.50	+ 1.20	3.70	37.50	Medium-dense
B-M-2	102.88	0.63	39	68	50	149.40	+ 1.10	4.40	36	" "
B-M-3	104.80	0.60	37.50	75	65	185.0	+ 1.00	4.80	34	" "
B-M-4	103.64	0.618	38.50	70.50	25	100	+ 0.65	6.40	36.80	" "
B-M-5	97.50	0.72	42	45	50	127	+ 0.40	8.0	34	" "
B-D-1	109.70	0.53	35	92.50	25	76.80	+ 1.50	3.25	39.50	Dense-sand
B-D-2	109.60	0.53	35	92.0	50	162.35	+ 1.30	3.50	38.20	" "
B-D-3	108.20	0.55	35.50	88	65	200.66	+ 1.25	3.60	37.50	" "
B-D-4	104.10	0.612	38	72.50	50	150	+ 1.20	2.95	36.90	" "
B-D-5	109.90	0.526	34.50	93	65	212.63	+ 1.35	3.50	38.50	" "

* B: Sand type

M: Medium-dense sand

D: Dense sand

Table No. 4-3

Summary of Test Results in Triaxial Compression Tests on Sand "C"

Test * Number	Unit Weight γ_d (Lbs./ft.^{3})	Void Ratio e	Porosity n %	Relative Density D_r %	Cell Pressure σ_3 (Lbs./in.^{2})	Deviator Stress $(\sigma_1-\sigma_3)$ (Lbs./in.^{2}) at failure	Volumetric Strain $\frac{\Delta V}{V}$ % at failure	Axial Strain ε_1 % at failure	Angle of Shearing Resistance ϕ (degrees)	Remarks
C-M-1	94.11	0.70	41	45	25	72.91	+ 1.80	6	40	Medium-dense
C-M-2	92.50	0.73	42	40	50	135.42	+ 1.60	9	36	" "
C-M-3	92.40	0.73	42	40	65	177	+ 1.40	10	35	" "
C-M-4	95.50	0.675	40	50	25	92	+ 2.75	5.50	40.50	" "
C-M-5	94.11	0.70	41	45	50	155	+ 1.70	8.40	37	" "
C-M-6	92.50	0.73	42	40	50	156	+ 1.75	8.65	37.50	" "
C-D-1	101.90	0.57	36	69	25	114	+ 3.25	5.00	44	Dense sand
C-D-2	102.23	0.567	36.50	68	50	170	+ 3.00	5.50	40.55	" "
C-D-3	101.26	0.58	36.70	67.50	65	234	+ 2.95	7	40	" "
C-D-4	105.60	0.54	35	74.50	25	120.50	+ 3.50	4.50	45	" "
C-D-5	102.43	0.56	36	70.50	50	191	+ 3.00	5	41	" "
C-D-6	105.60	0.515	34	79	65	251	+ 4.94	5.20	41.10	" "

* C: Sand type
M: Medium-dense sand
D: Dense sand

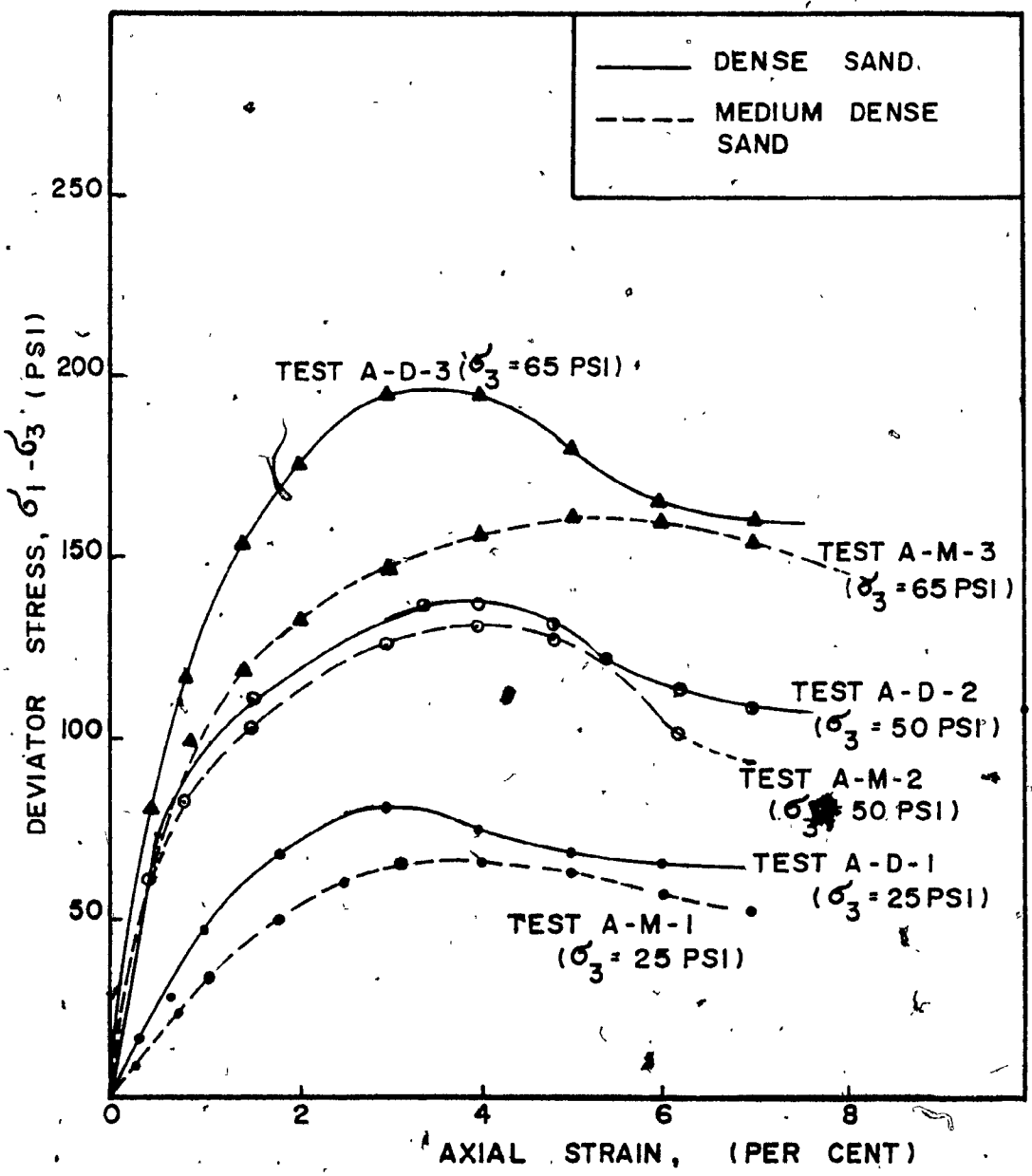

FIG. 4.1 STRESS - STRAIN RELATIONSHIP IN TRIAXIAL COMPRESSION TESTS FOR SAND "A"

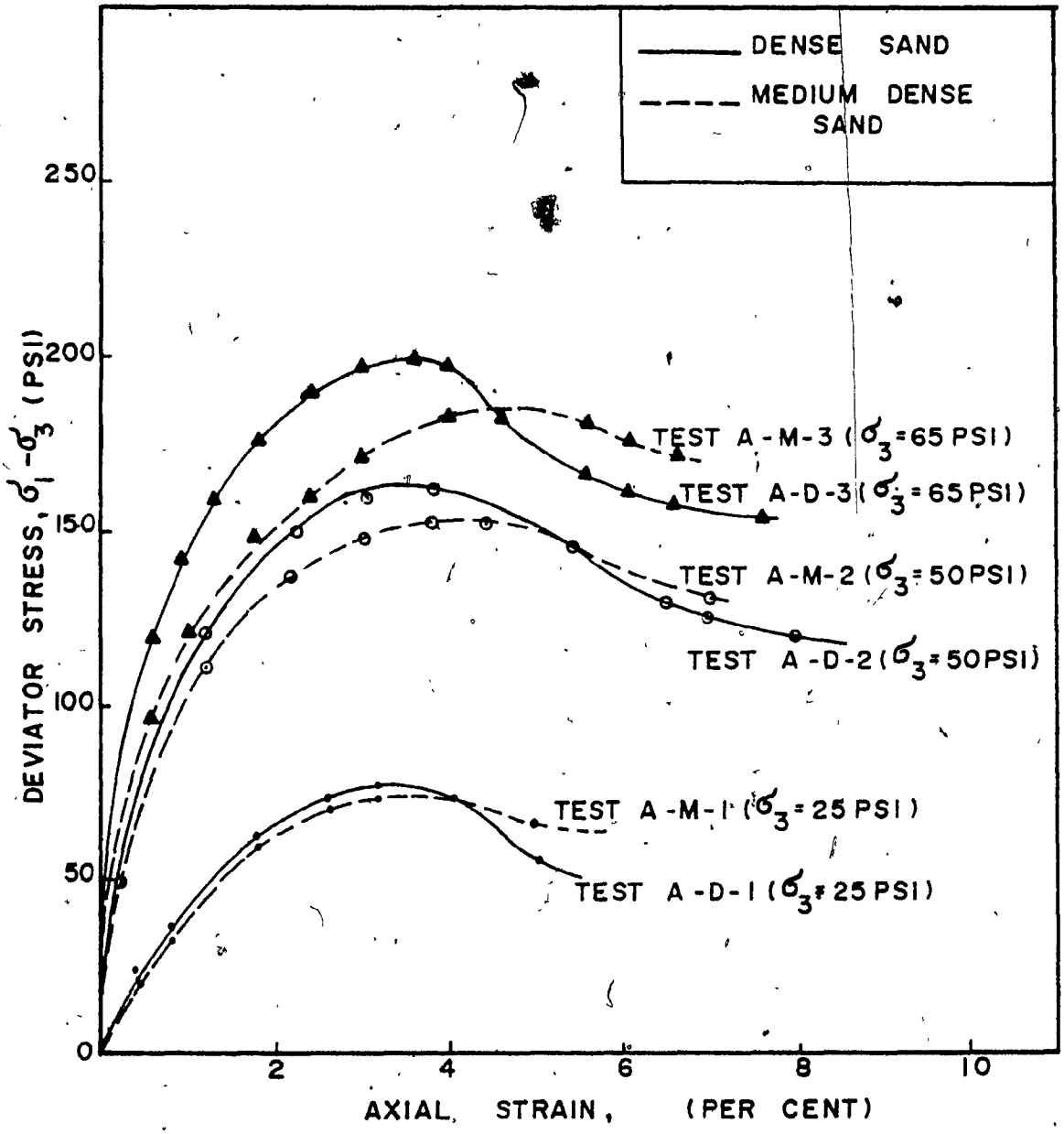

FIG. 4.2 STRESS-STRAIN RELATIONSHIP IN TRIAXIAL COMPRESSION TESTS FOR SAND "B"

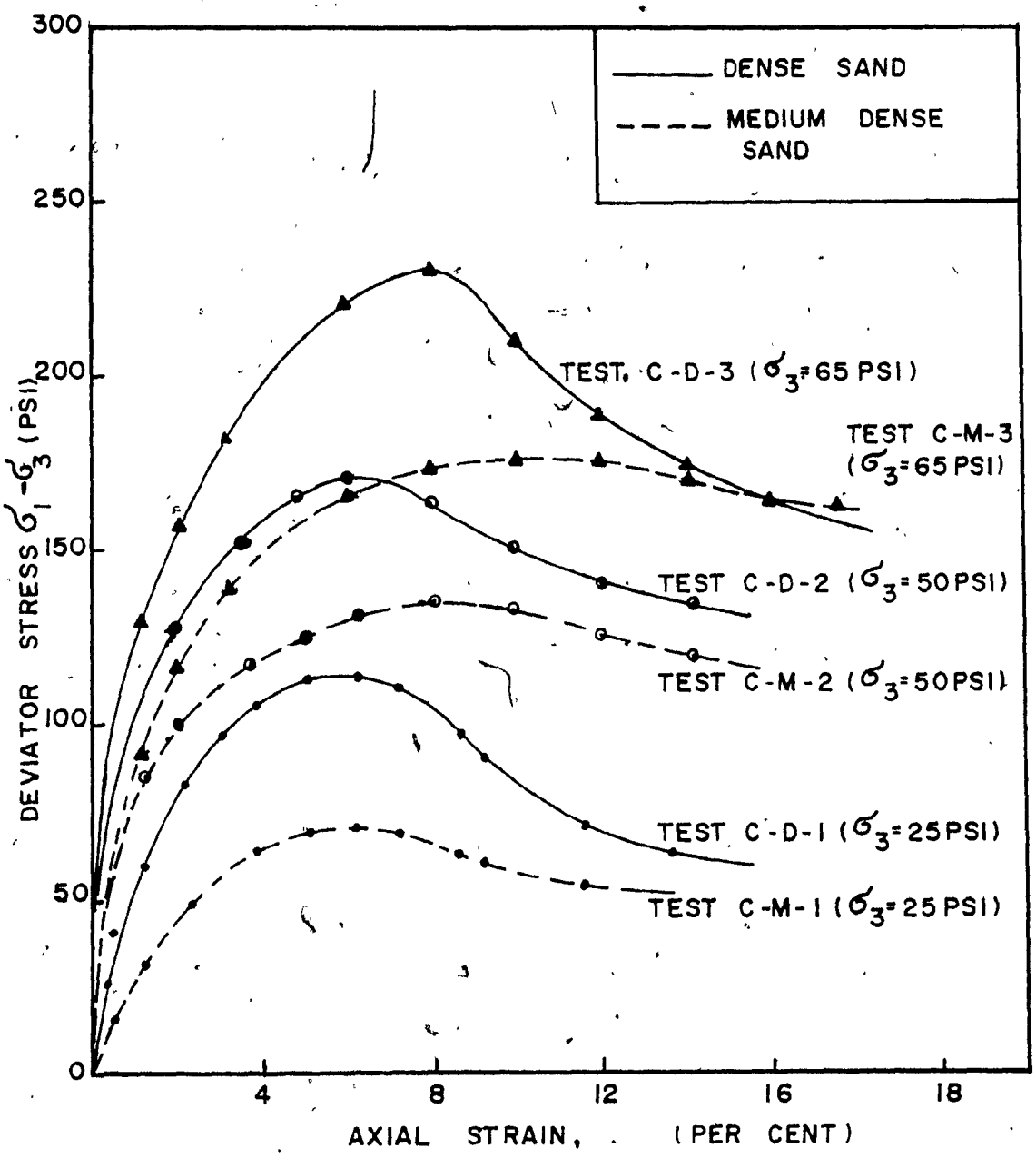

FIG. 4.3 STRESS - STRAIN RELATIONSHIP IN TRIAXIAL COMPRESSION TESTS FOR SAND "C"

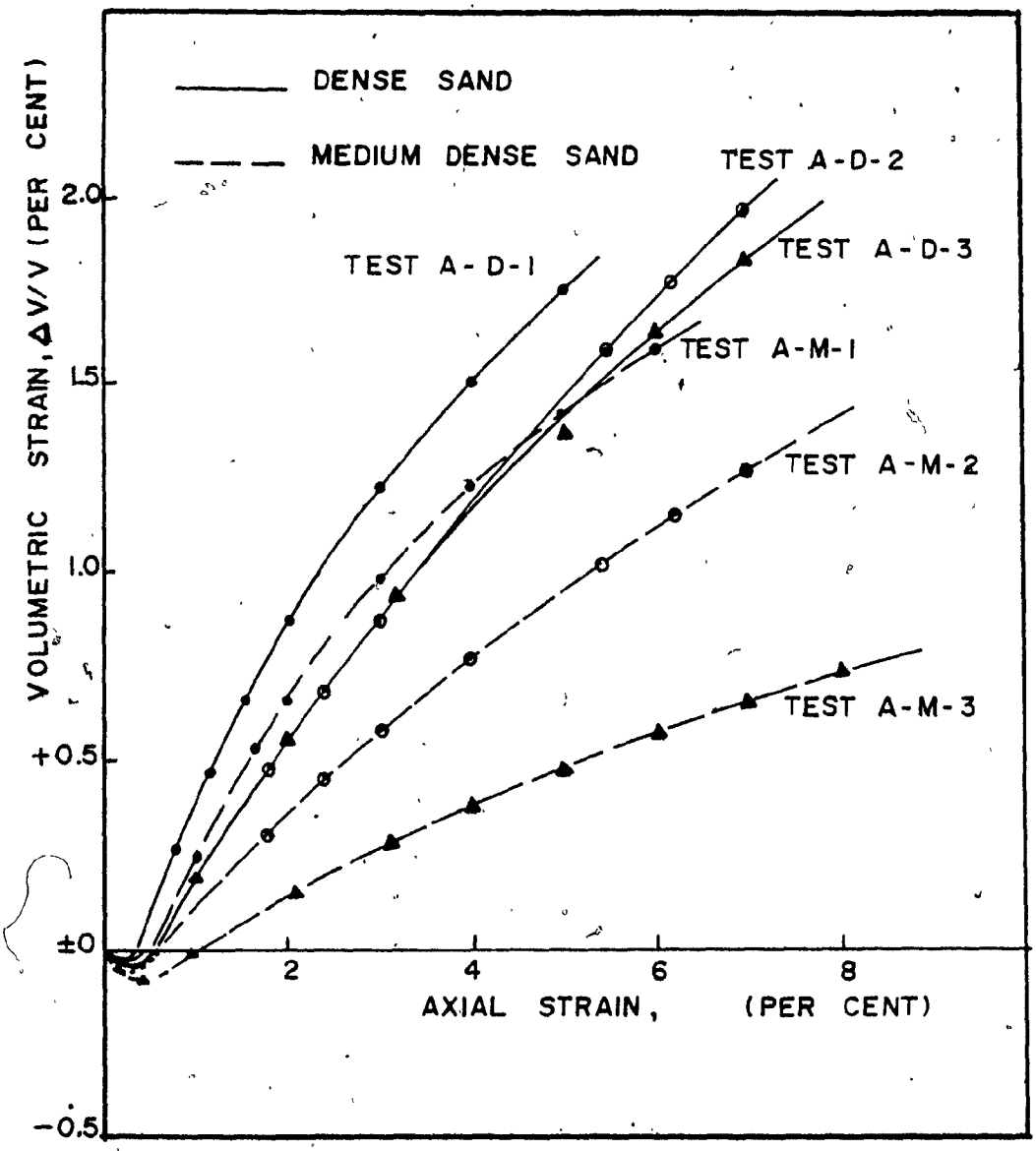

FIG. 4. 4 VOLUMETRIC STRAIN IN TRIAXIAL COMPRESSION TESTS FOR SAND "A"

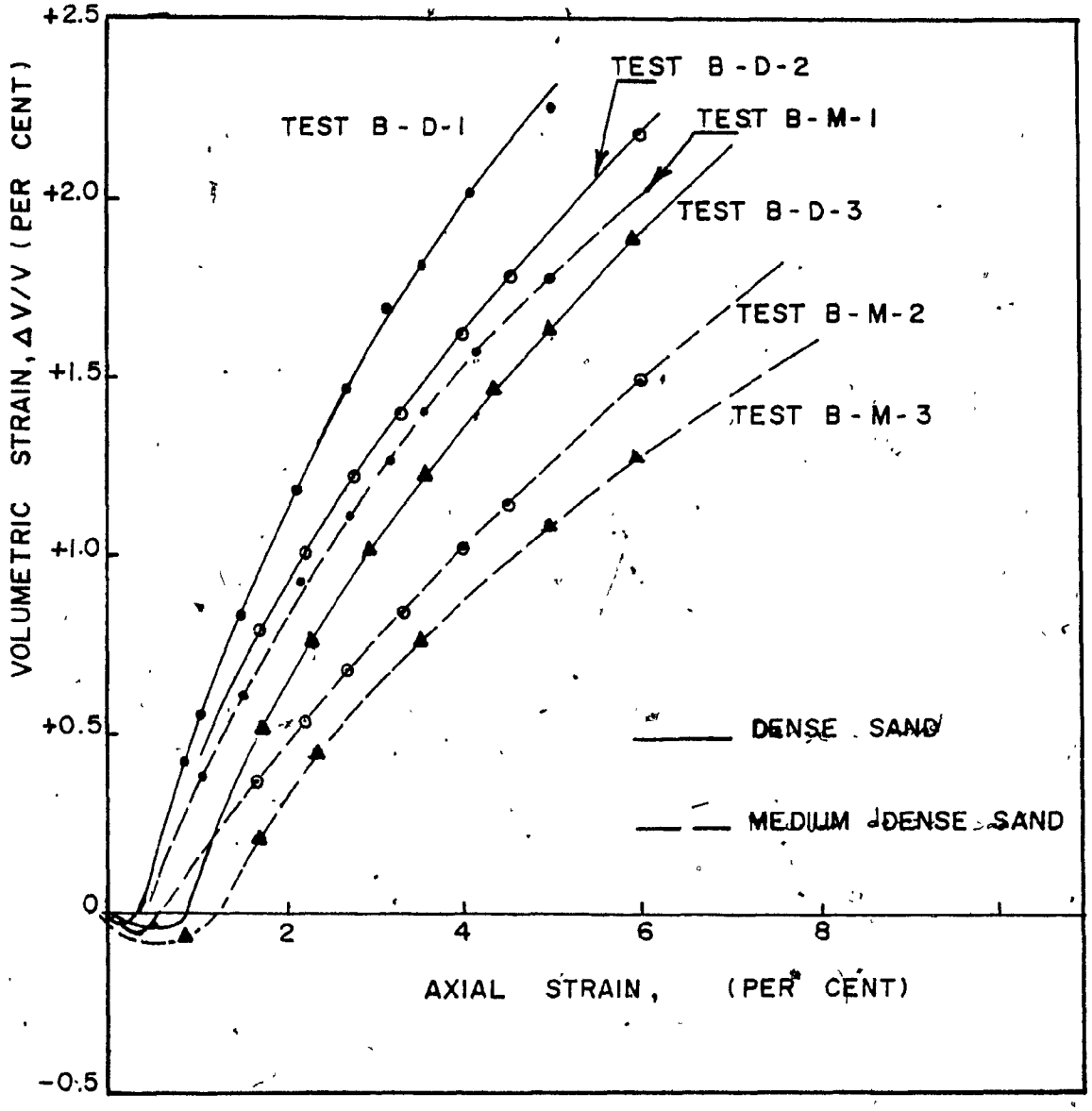

FIG. 4.5 VOLUMETRIC STRAIN IN TRIAXIAL COMPRESSION TESTS FOR SAND "B"

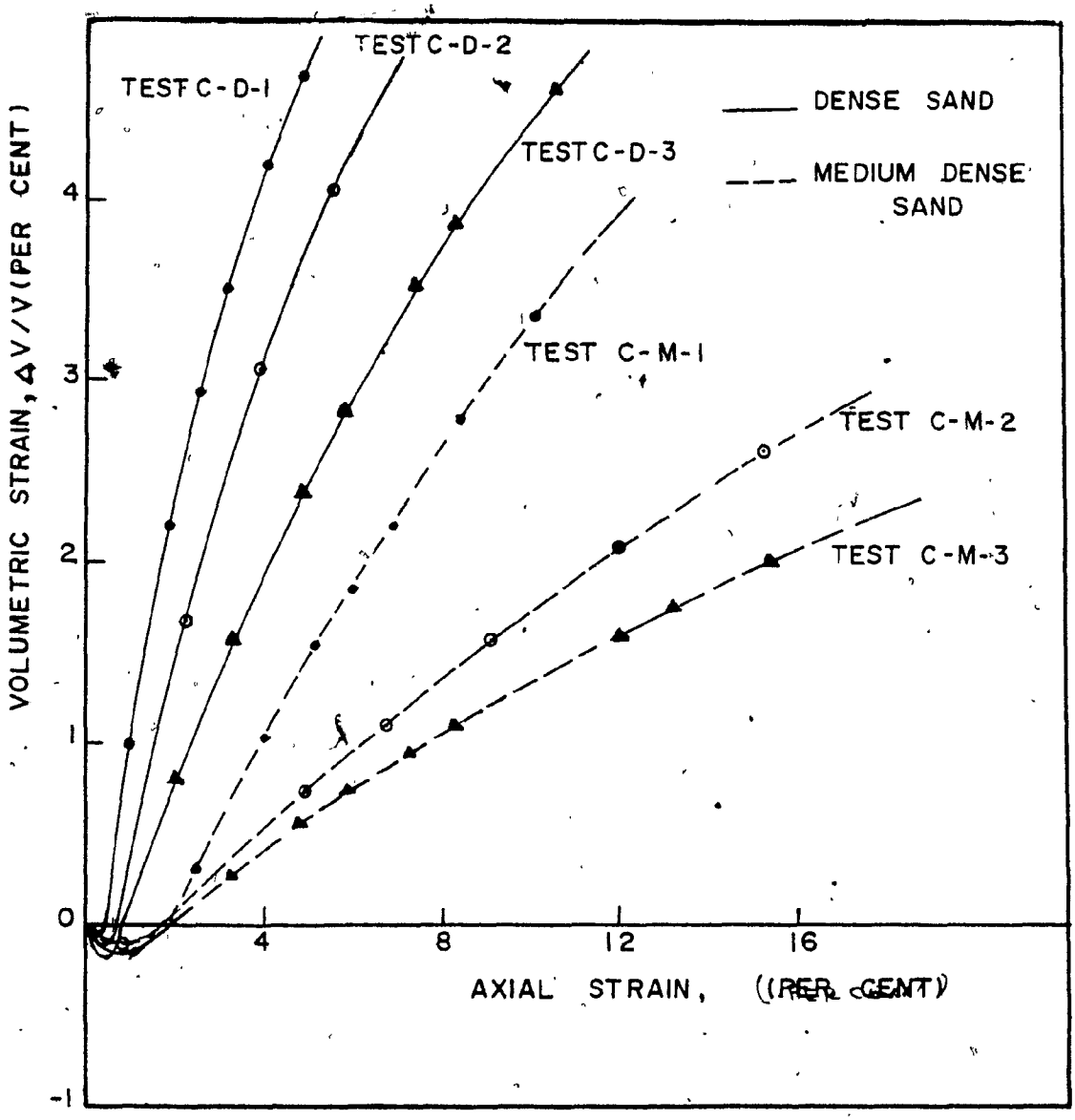

FIG. 4. 6 VOLUMETRIC STRAIN IN TRIAXIAL COMPRESSION TESTS FOR SAND "C"

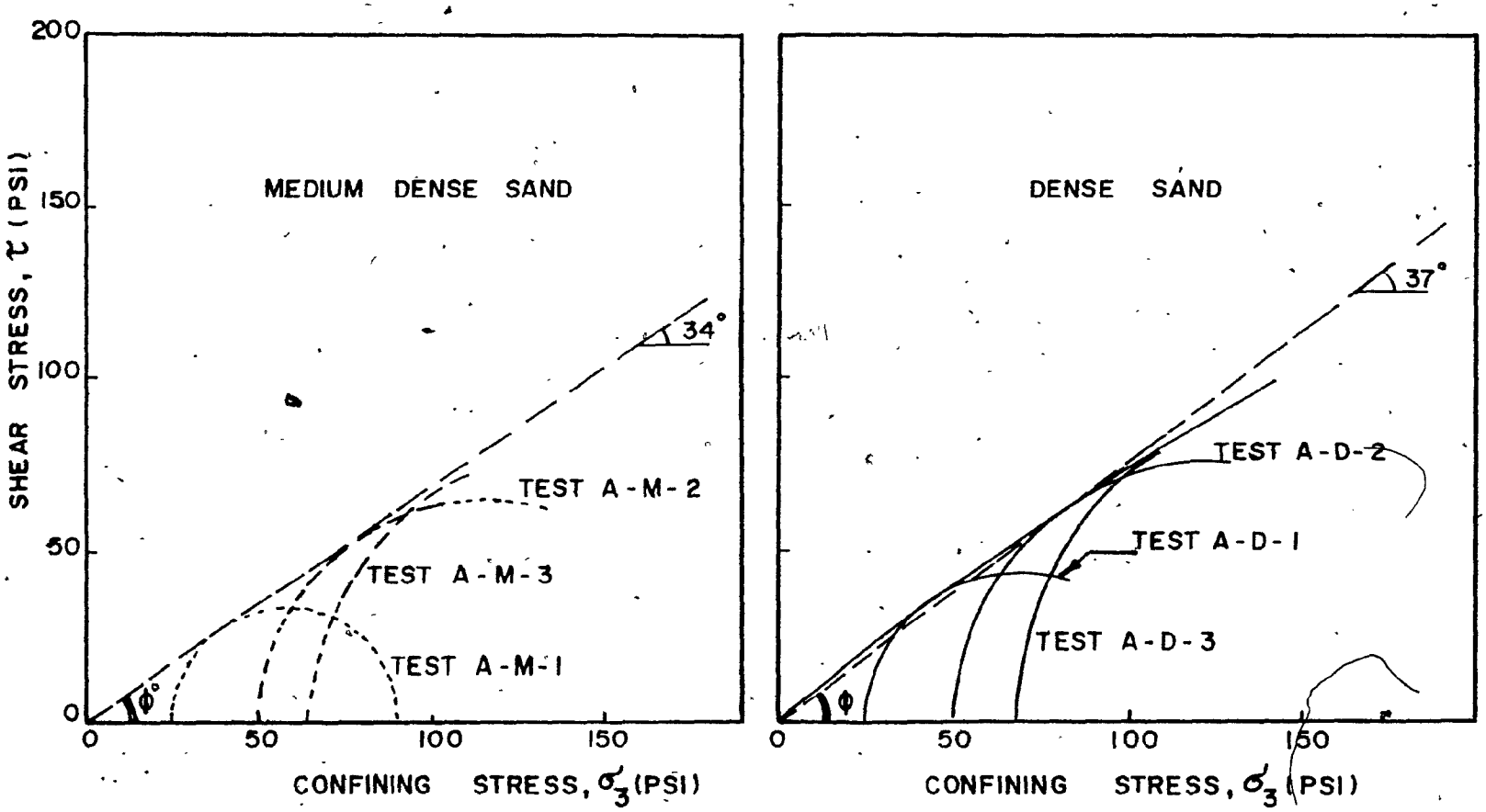

FIG. 4.7 MOHR COULOMB ENVELOPE IN TRIAXIAL COMPRESSION TESTS FOR SAND "A"

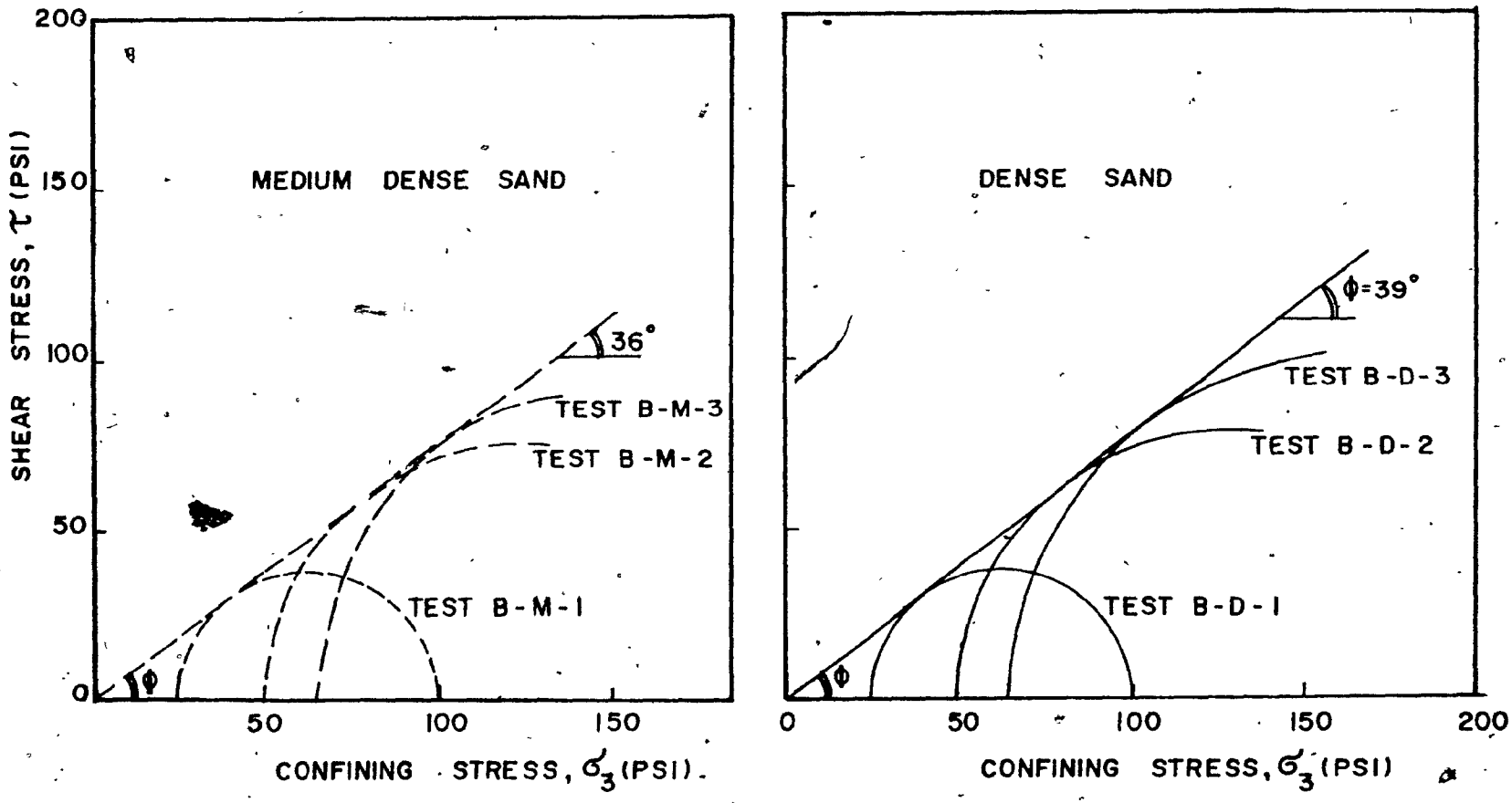

FIG. 4.8 MOHR COULOMB ENVELOPE IN TRIAXIAL COMPRESSION TESTS FOR SAND "B"

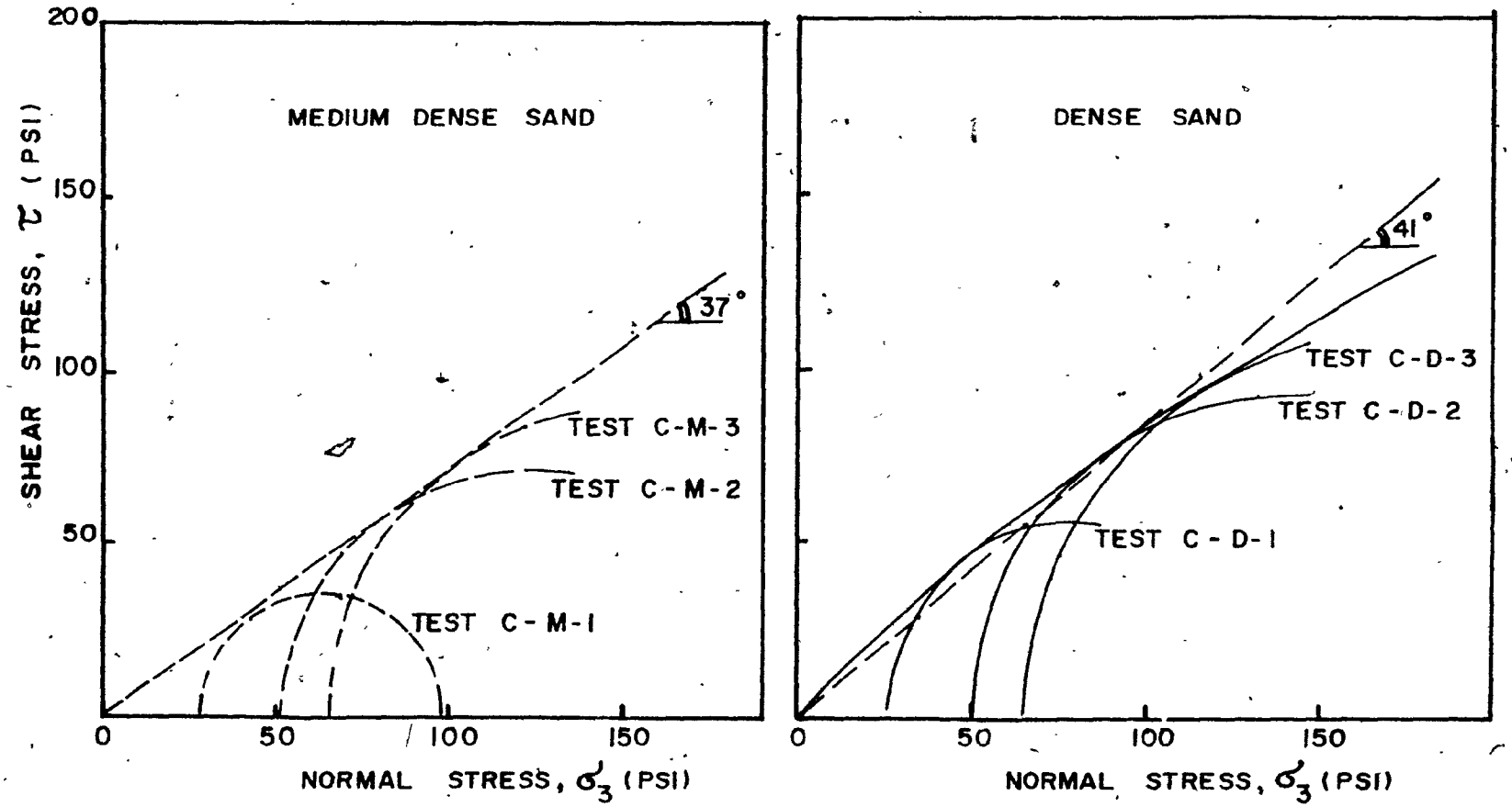

FIG. 4.9 MOHR COULOMB ENVELOPE IN TRIAXIAL COMPRESSION TESTS FOR SAND "C"

$$\sin \phi = \frac{\sigma_1 - \sigma_3}{\sigma_1 + \sigma_3}$$

where σ_1 and σ_3 are the major and minor principal stresses respectively. Either the maximum deviator stress or the maximum stress ratio could be considered as the failure criterion because both yielded the same results for drained tests on sand.

In the analysis of test results, the maximum deviator stress was used as the failure criterion because this yielded a more pronounced peak value.

Figures 4.1 to 4.3 show the stress strain curves for dense and medium dense sand samples, of sand A, B and C respectively. The tests were run at 25, 50 and 65 psi confining pressure.

Certain trends are immediately noticeable from the plots. As the strain increased, the stress also increased and generally reached a clearly defined peak for dense sand samples. The stresses then decreased with the strain increase.

Also, with an increase in confining pressure the axial strain and the deviator stress at failure were increased.

For medium-dense sand samples, it may be noted from the stress-strain curves that at failure the axial strains were larger, and the deviator stresses were lower, compared to the corresponding values for the dense sand samples.

Figure 4.4 to 4.6 show the variation of the volumetric strain for the three types of sand A, B and C respectively. From these figures, it can be noted that the volumetric strain at failure decreased as the confining stress was increased, while the relative density was decreased.

Figures 4.7 to 4.9 show the Mohr-Coulomb plots for sand A, B and C respectively. It can be observed from these figures that the failure envelope for dense sand samples was almost a straight line, up to a certain value of confining stress, which was less than the corresponding value, as the case of medium-dense sand samples.

4.3 Direct Shear Box Tests

The direct shear box tests were conducted on 2.4 inch by 2.40 inch by 0.80 inch high samples. The rate of shear displacement was chosen as 0.048 inch per minute.

These tests were carried out on medium-dense and dense sand samples, and at normal stresses of 25, 50 and 62 psi.

The shear strength parameter (ϕ) of the sand tested was obtained from the stress ratio at failure, and based on the Mohr-Coulomb failure criterion as

$$\tau_f = \sigma_n \cdot \tan \phi$$

where τ_f and σ_n are, respectively the shear and normal stress on the plane of failure.

The test results are summarized in tables 4.4 to 4.6 and presented in graphical form in figures 4.10 to 4.15.

From the stress-shear displacement curves, plotted in figures 4.10 to 4.12, for sand A, B and C respectively, it may be noted that the shear-displacement at failure increased with an increase of the normal stress and a decrease of the relative density. Also, the ratio of shear to normal stress, at failure, increased with a decrease of the normal stress and an increase of the density.

Table No. 4-4

Summary of Test Results in Direct Shear Tests on Sand "A"

Test * Number	Unit Weight γ_d (Lbs./ft.^{3})	Void Ratio e	Porosity n %	Relative Density D_r %	Normal Stress σ_n (Lbs./in.^{2})	Shear Stress τ (Lbs./in.^{2}) at failure	Stress Ratio τ/σ_n at failure	Change of Thickness Δy (inch) at failure	Angle of Shearing Resistance ϕ (degrees)	Remarks
A-M-1	105.40	0.56	36	60	25	18.16	0.726	+ 0.0016	36	Medium dense
A-M-2	105.40	0.56	36	60	50	33.72	0.674	+ 0.00144	34	" "
A-M-3	100.60	0.64	39	40	62	39.60	0.637	+ 0.0008	32.50	" "
A-M-4	102.40	0.61	38	47.50	25	17.50	0.700	+ 0.00144	35	" "
A-M-5	102.40	0.61	38	47.50	50	33.22	0.664	+ 0.0011	33.60	" "
A-M-6	105.40	0.56	36	60	62	40.30	0.650	+ 0.0008	33	" "
A-D-1	113.00	0.48	32.50	80	25	19.71	0.788	+ 0.0018	38.25	Dense sand
A-D-2	113.00	0.46	31.50	85	50	35.66	0.713	+ 0.0016	35.50	" "
A-D-3	113.00	0.46	31.50	85	62	41.80	0.674	+ 0.0014	34	" "
A-D-4	113.00	0.46	31.50	85	25	20.98	0.839	+ 0.0024	40	" "
A-D-5	110.00	0.50	33	75	50	36.50	0.730	+ 0.0008	36	" "
A-D-6	111.50	0.48	32.50	80	62	41.04	0.662	+ 0.0010	33.50	" "

* A: Sand type
M: Medium dense sand
D: Dense sand

Table No. 4-5

Summary of Test Results in Direct Shear Tests on Sand "B"

Test * Number	Unit Weight γ_d (Lbs./ft.^{3})	Void Ratio e	Porosity n %	Relative Density D_r %	Normal Stress σ_n (Lbs./in.^{2})	Shear Stress τ (Lbs./in.^{2}) at failure	Stress Ratio τ/σ_n at failure	Change of Thickness Δy (inch) at failure	Angle of Shearing Resistance ϕ (degrees)	Remarks
B-M-1	101.60	0.64	39	65	25	20.98	0.839	+ 0.0024	40	Medium-dense
B-M-2	102.15	0.63	38.60	67.50	50	35.01	0.700	+ 0.0020	35	" "
B-M-3	102.15	0.63	38.60	67.50	62	40.26	0.649	+ 0.0018	33	" "
B-M-4	96.80	0.72	42	47.50	25	17.50	0.700	+ 0.002	35	" "
B-M-5	96.80	0.72	42	47.50	50	32.47	0.649	+ 0.0016	33	" "
B-M-6	96.80	0.72	42	47.50	62	38.74	0.625	+ 0.0014	32	" "
B-D-1	108	0.54	35	90	25	22.50	0.900	+ 0.0032	42	Dense sand
B-D-2	108	0.54	35	90	50	39.77	0.795	+ 0.0024	38.50	" "
B-D-3	108	0.54	35	90	62	45	0.726	+ 0.0020	36	" "

* B: Sand type

M: Medium dense sand

D: Dense sand

Table No. 4-6

Summary of Test Results in Direct Shear Tests on Sand "C"

Test * Number	Unit Weight γ_d (Lbs./ft.^{3})	Void Ratio e	Porosity n %	Relative Density D_r %	Normal Stress σ_n (Lbs./in.^{2})	Shear Stress τ (Lbs./in.^{2}) at failure	Stress Ratio τ/σ_n at failure	Change of Thickness Δy (inch) at failure	Angle of Shearing Resistance ϕ (degrees)	Remarks
C-M-1	95.90	0.65	39.40	54	25	23.97	0.959	+ 0.002	43.80	Medium dense
C-M-2	96.93	0.63	39	58	50	41.95	0.839	+ 0.0016	40	" "
C-M-3	95.20	0.66	40	53	62	54.85	0.885	+ 0.0010	41.50	" "
C-M-4	91.30	0.73	42	50	25	20.98	0.839	+ 0.0016	40	" "
C-M-5	91.30	0.73	42	50	50	40.50	0.810	+ 0.0014	39	" "
C-M-6	91.30	0.73	42	50	62	49.85	0.804	+ 0.0010	38.80	" "
C-D-1	102.70	0.49	33	84	25	26.25	1.050	+ 0.0023	46.40	Dense sand
C-D-2	101.32	0.51	37	80	50	48.28	0.966	+ 0.002	44	" "
C-D-3	100	0.53	35	76	62	56.81	0.916	+ 0.0011	42.50	" "
C-D-4	102.70	0.49	33	84	50	50	1.00	+ 0.0024	45	" "

* C: Sand type

M: Medium dense sand

D: Dense sand

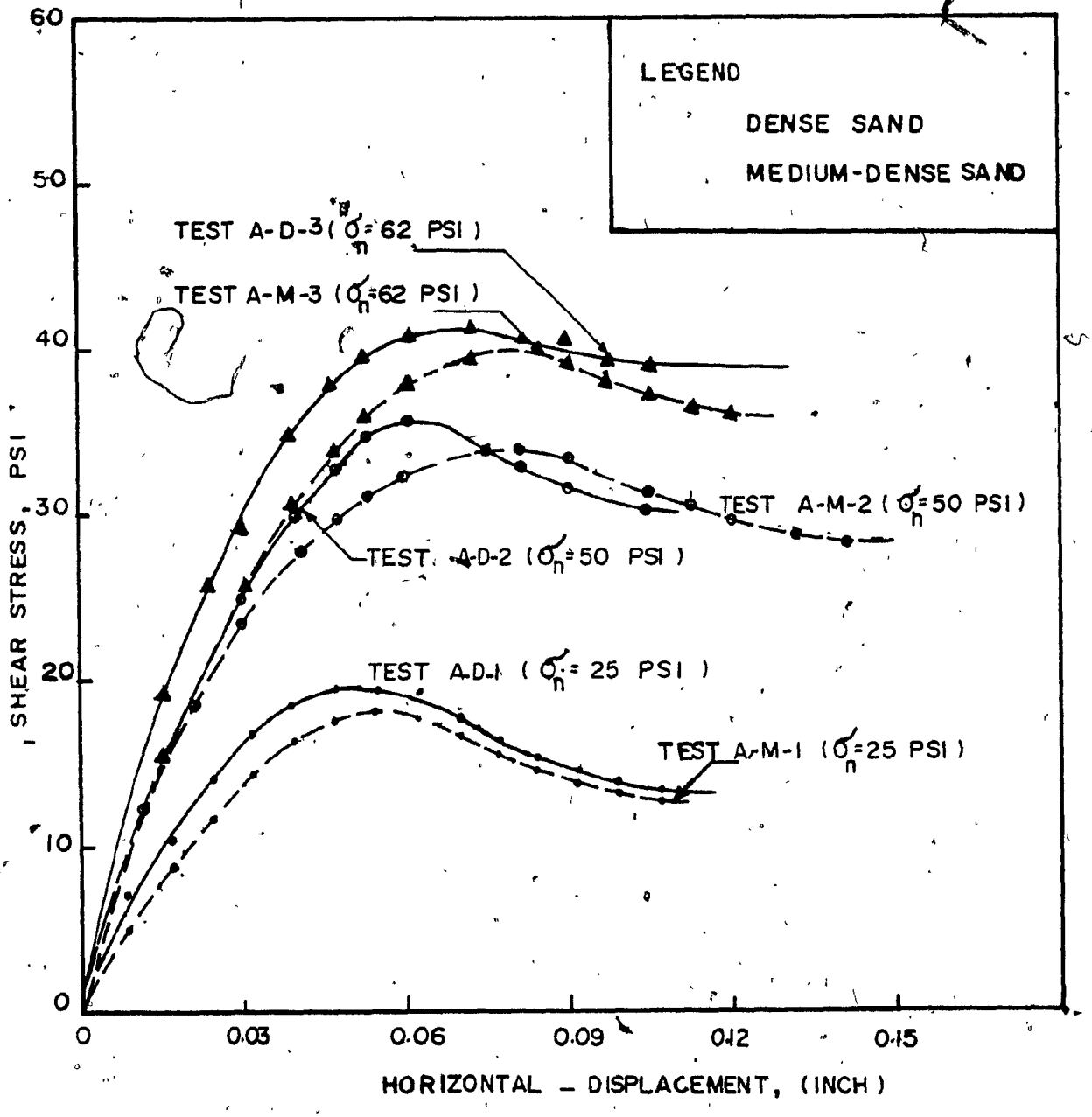

FIG 4-10 STRESS DISPLACEMENT CURVE IN DIRECT SHEAR TESTS FOR SAND "A"

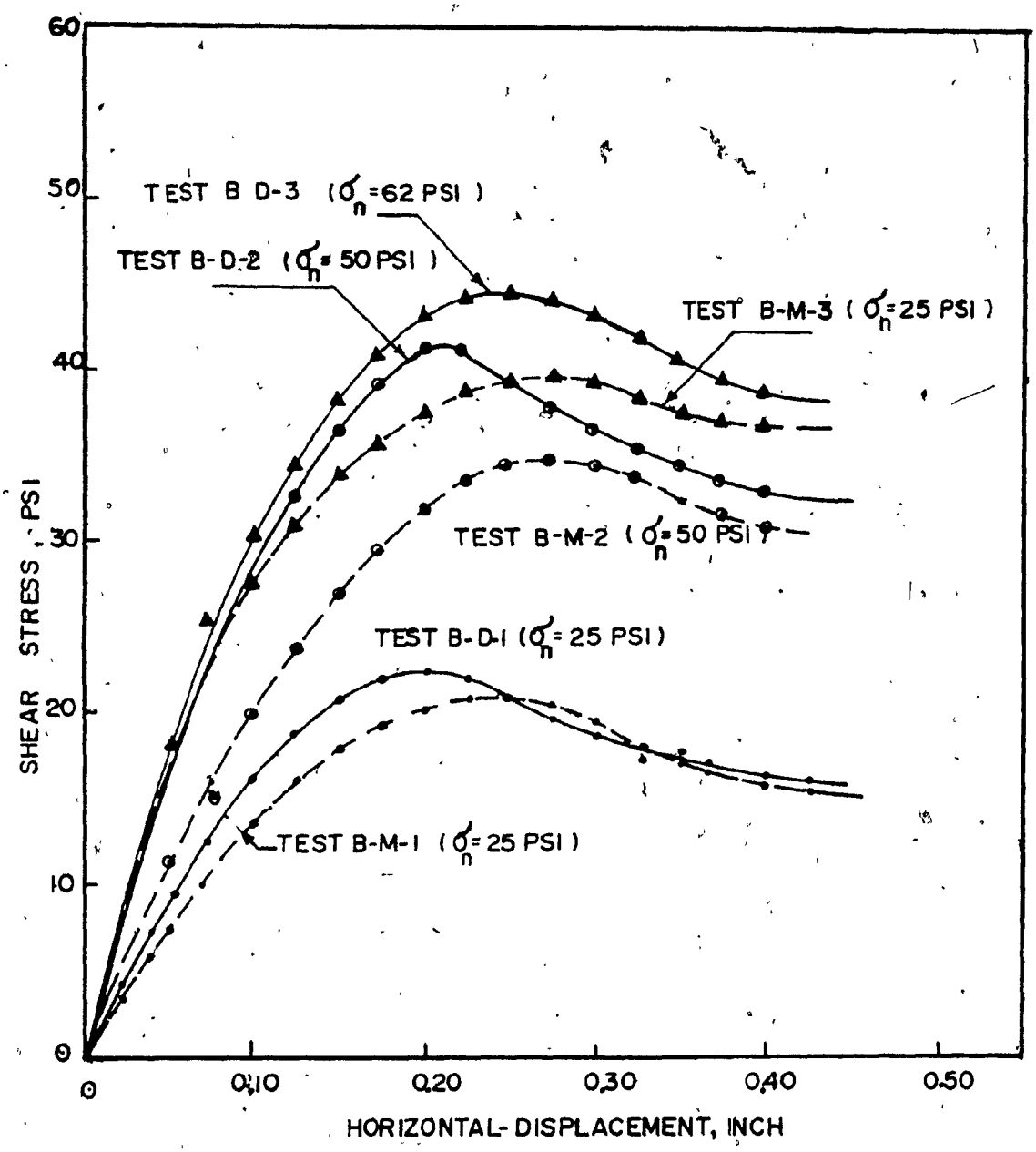

FIG. 4-11 STRESS DISPLACEMENT CURVE IN DIRECT SHEAR TESTS FOR SAND "B"

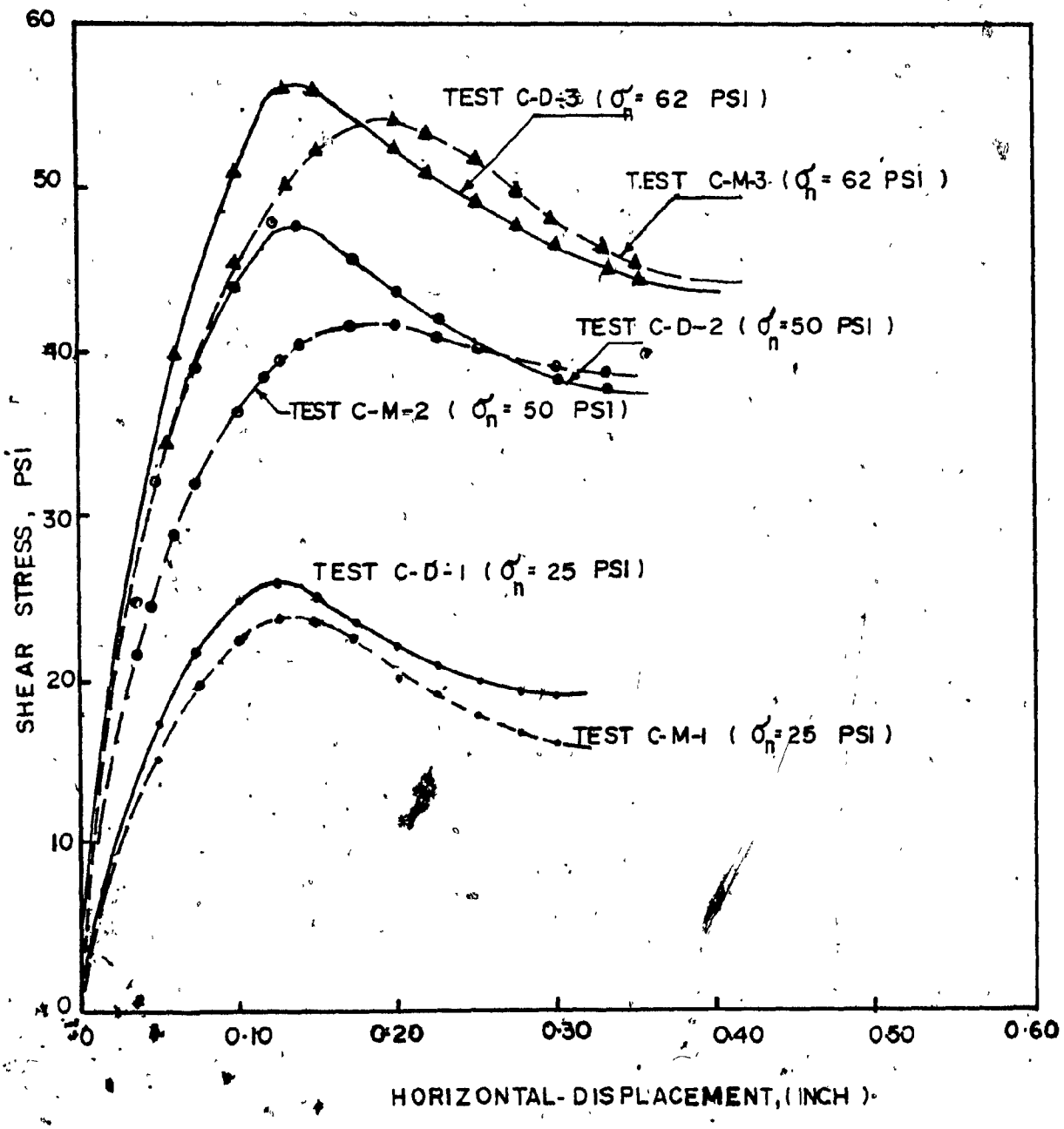

FIG. 4-12 STRESS DISPLACEMENT CURVE IN DIRECT SHEAR TESTS FOR SAND "C"

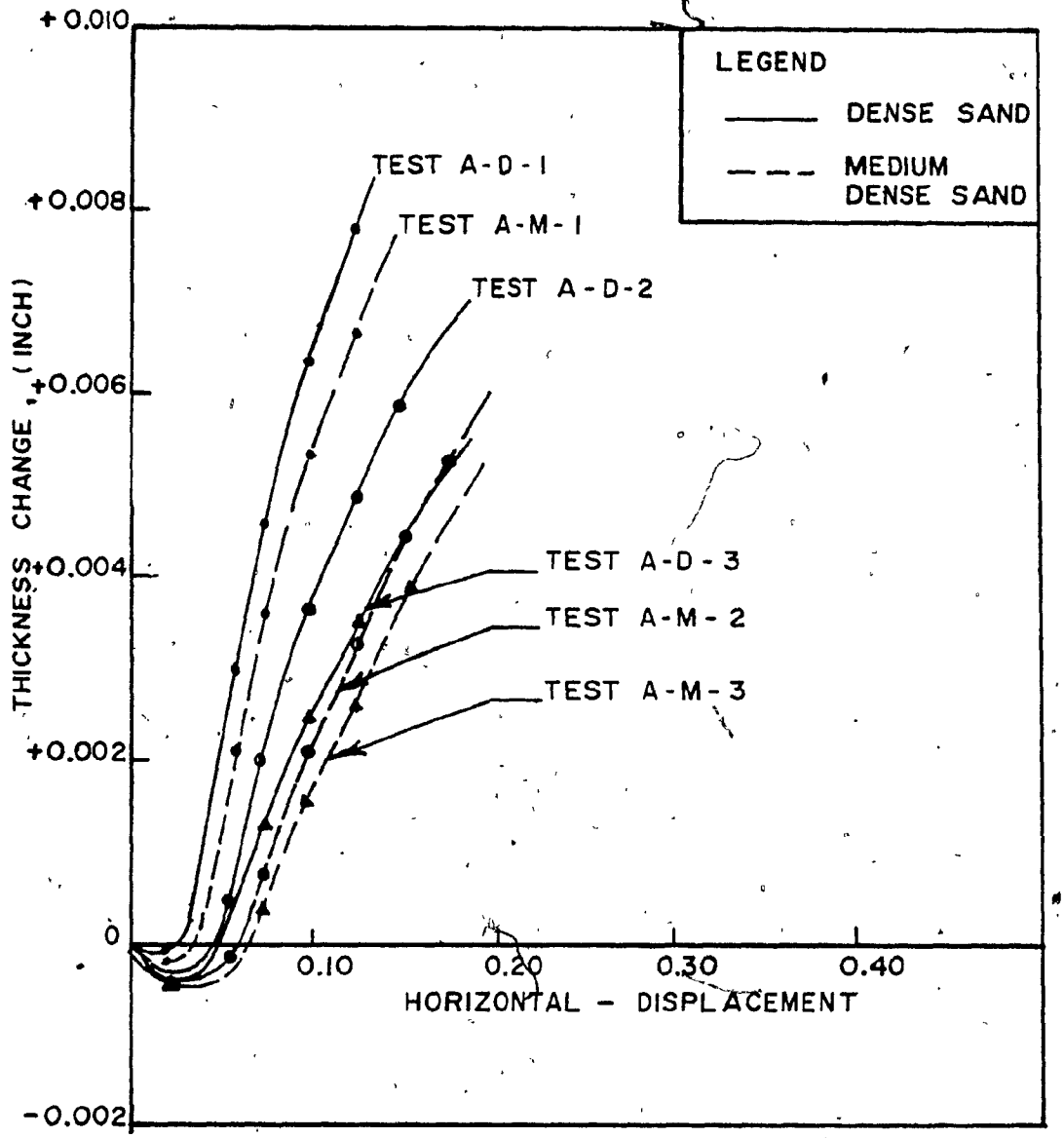

FIG. 4.13 HORIZONTAL DISPLACEMENT VS THICKNESS CHANGE IN DIRECT SHEAR TESTS. FOR SAND "A".

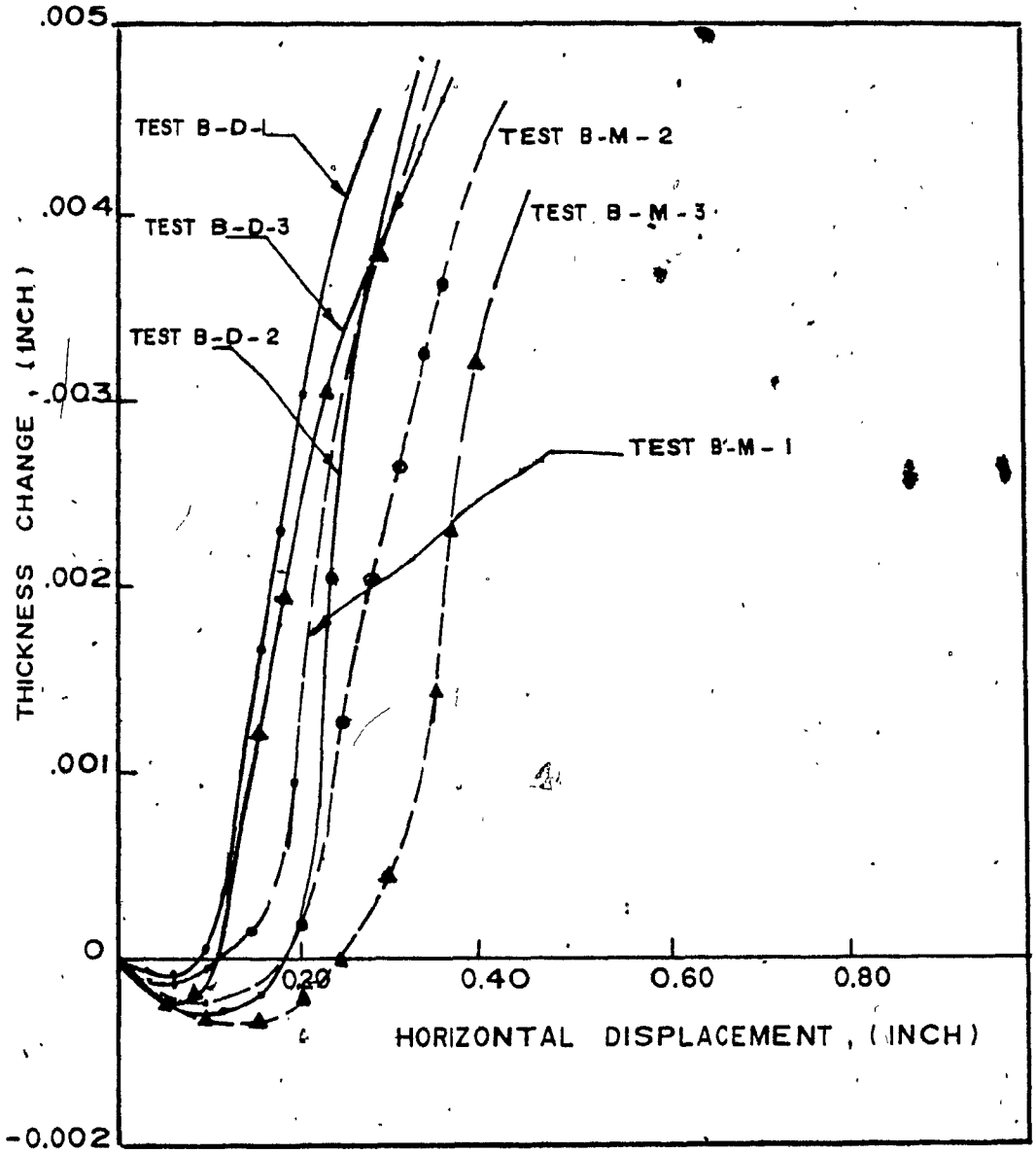

FIG. 4.14 HORIZONTAL DISPLACEMENT VS THICKNESS CHANGE IN DIRECT SHEAR TESTS FOR SAND "B"

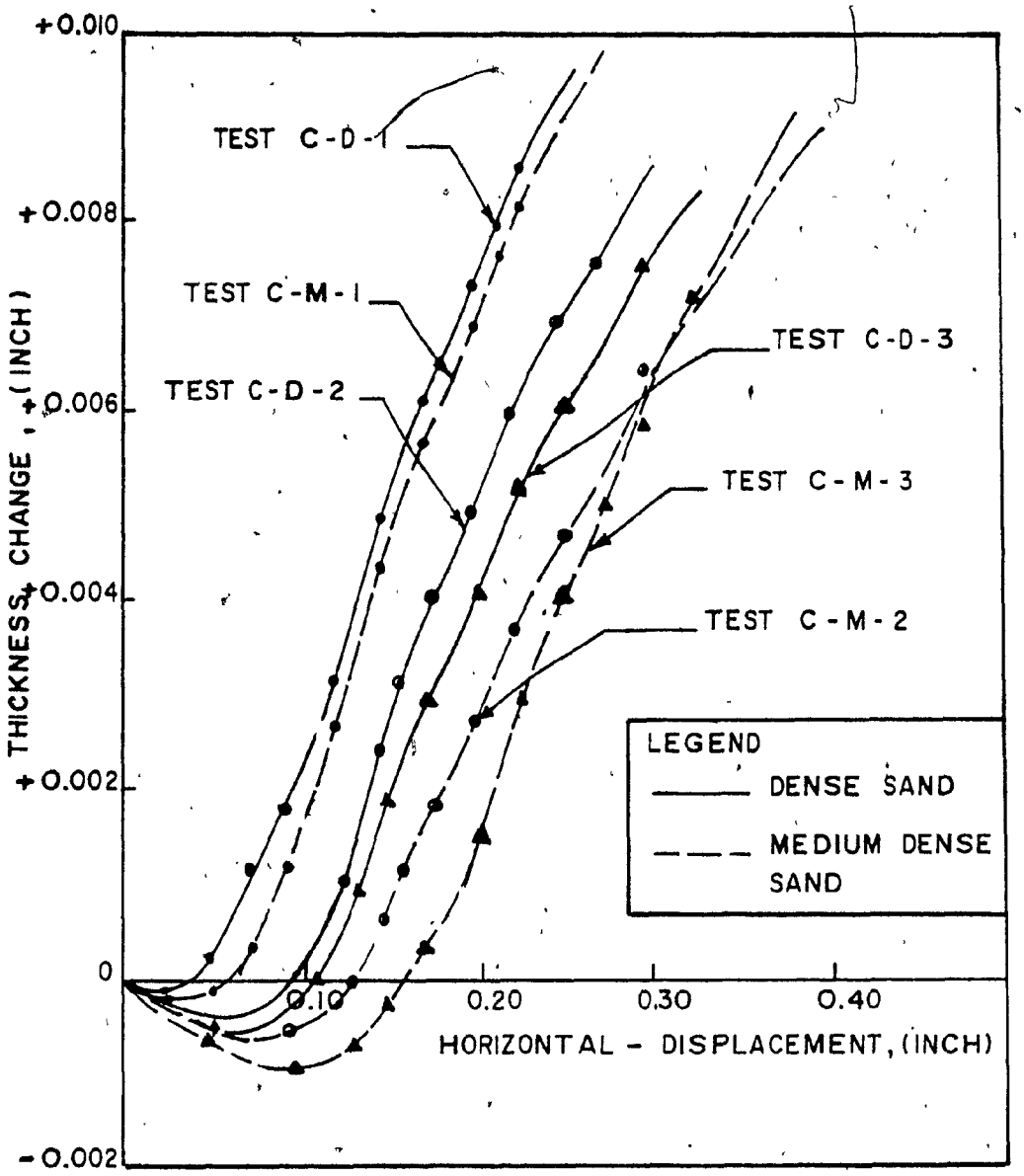

FIG. 4.15 HORIZONTAL DISPLACEMENT VS THICKNESS CHANGE IN DIRECT SHEAR TESTS FOR SAND "C"

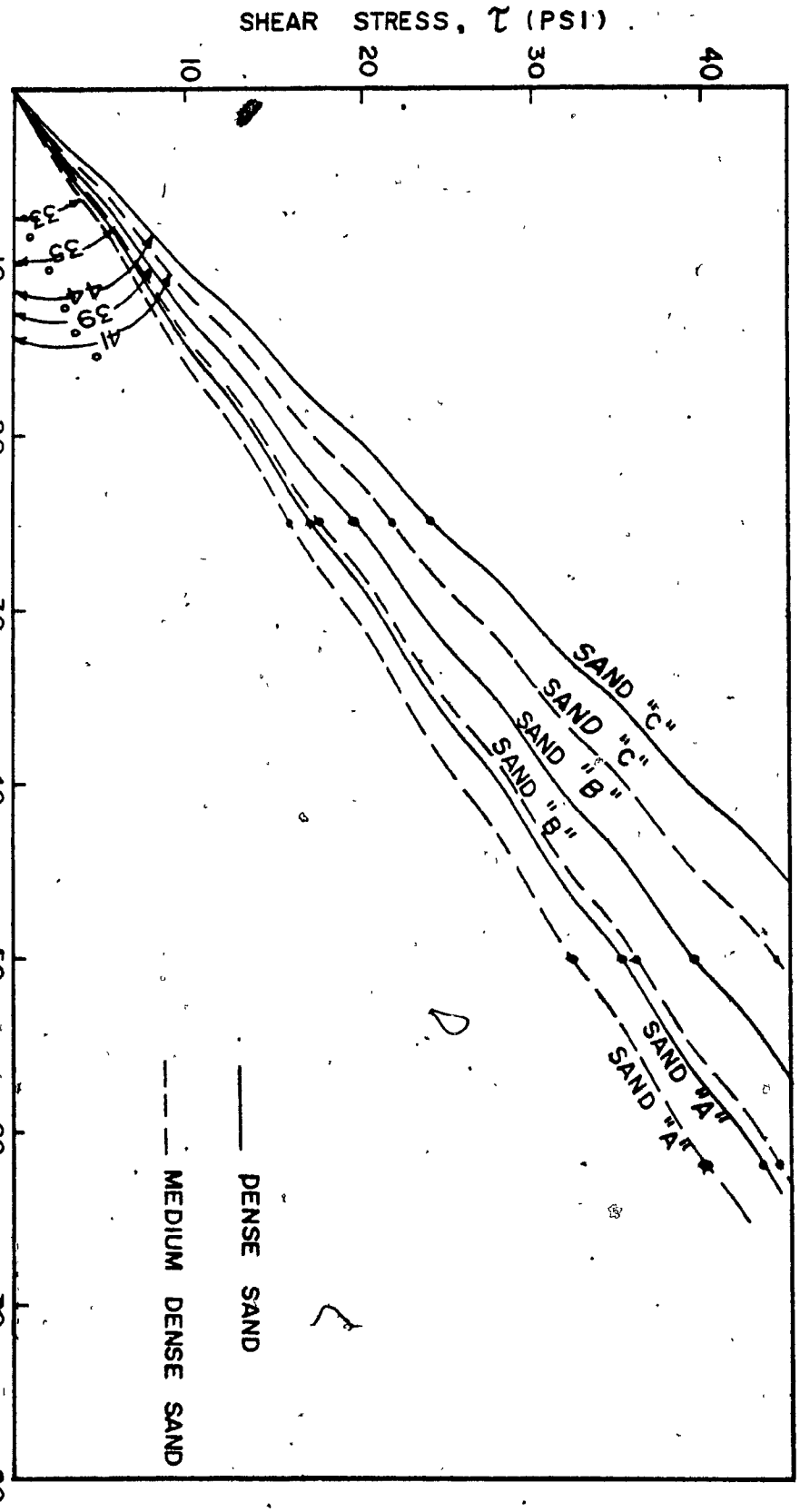

FIG. 4. 16. NORMAL STRESS VS SHEAR STRESS IN DIRECT SHEAR TESTS FOR SAND "A", "B", "C"

The change of thickness against the horizontal displacement of the three kinds of sand, tested at different relative density and normal stress, is plotted in figures 4.13 to 4.15. From these graphs, it can be observed that the vertical displacement at failure increased with a decrease of the normal stress and an increase of the density. Also, at very small shear displacements, there was a decrease in the thickness of the samples. This decrease was the smallest for the samples tested at the lowest normal stress and at the same state of density.

4.4 Plane Strain Tests

These tests were conducted on samples with nominal dimensions of 3.63, 2.95 and 1.5 inches in respective width, height and length. The axial stress (σ_1) increased at a constant machine rate of 0.016 inch per minute, while the cell pressure (σ_3) was held constant.

Throughout a shear test, readings were taken of the axial deformation dial gauge, the proving ring, the volume change burette and the pressure transducers. Sets of readings were generally taken at intervals of 0.25% axial strain up to failure. Some tests were terminated at failure, but the majority were continued until the ultimate condition had been reached.

The shear strength parameter (ϕ) for the sand tested was determined from the principal failure criterion of plane strain condition, developed by Bishop, (1966), where ϕ is calculated as

$$\frac{1}{2}\,\mathrm{Cos}^2\,\phi = \frac{\sigma_2}{\sigma_1 + \sigma_3}\ ,$$

where σ_1, σ_2 and σ_3 are the respective major, intermediate and minor principal stresses.

This equation, was derived according to the following:

Wood, (1958) carried out series of tests on sand by using the plane strain apparatus, and he noted that the relationship between σ_2 and σ_1 at failure approximated to the expression:

$$\sigma_2 = K_o \sigma_1 \qquad (4.1)$$

where K_o is the coefficient of earth pressure at rest with zero strain in the direction of the intermediate principal stress. Also, tests reported by Bishop (1958) and Simons (1958) has shown that there was an imperical relationship between K_o and ϕ, which could be represented by an expression due to Jaky (1944 and 1948); as

$$K_o = 1 - \text{Sin}\ \phi \qquad (4.2)$$

combining these two expressions (4.1 and 4.2) and putting

$$\text{Sin}\ \phi = \frac{\sigma_1 - \sigma_3}{\sigma_1 + \sigma_3}$$

then

$$\frac{\sigma_2}{\sigma_1 + \sigma_3} = \frac{1}{2}\ \text{Cos}^2\ \phi$$

The test results are summarized in tables 4.7 to 4.9, and presented in graphical form in figures 4.17 to 4.22.

From the stress-strain curves plotted in figures 4.17 to 4.19, for sands A, B and C, which were tested at cell pressures of 5, 25 and 50 psi and at different densities, it should be noted that there was a similarity in the shape of the major and intermediate stress-strain curves.

Certain trends are immediately noticeable from the stress-strain curves. With an increase in cell pressure, the axial strain in failure

increased, while both the major and intermediate principal stresses were increased. The corresponding value of the frictional angle decreased.

From the variation of volumetric strain plotted in figures 4.20 to 4.22, it is clear that the volume change at failure increased with an increase in the relative density and a decrease of the cell pressure.

Table No. 4-7

Summary of Test Results in Plane-Strain Compression Tests on Sand "A"

Test * Number	Unit Weight γ_d (Lbs./ft.^{3})	Void Ratio e	Porosity n %	Relative Density D_r %	Cell Pressure σ_3 (Lbs./in.^{2})	Intermediate Stress σ_2 (Lbs./in.^{2}) at failure	Major Stress σ_1 (Lbs./in.^{2}) failure	Volumetric Strain $\Delta V/V$ % at failure	Axial Strain ε_1 % at failure	Angle of Shearing Resistance ϕ (degrees)	Remarks
A-M-1	104.65	0.60	37.50	50	5	12	37	+ 0.32	2	40.89	Medium dense
A-M-2	103.715	0.615	38	46	25	50.50	137.75	+ 0.25	3	38	" "
A-M-3	105.70	0.58	37	55	50	102	262	+ 0.10	3.50	36	" "
A-M-4	105.70	0.58	37	55	5	10	31	+ 0.32	1.85	41.81	" "
A-M-5	100.30	0.67	40	32.5	5	11	30	+ 0.25	3.65	37.55	" "
A-M-6	104.65	0.60	37.50	50	25	51	144	+ 0.28	2.90	39	" "
A-D-1	113.18	0.48	32.40	82.50	5	13.50	45.70	+ 0.35	0.60	43.20	Dense sand
A-D-2	113.18	0.47	32	83	25	52	168	+ 0.30	0.60	43	" "
A-D-3	111.60	0.50	33	75	50	104	290	+ 0.27	1.60	40.30	" "
A-D-4	113.95	0.47	32	83	50	100	307	+ 0.29	0.83	42	" "

*-A: Sand type

M: Medium dense sand

D: Dense sand

Table No. 4-8

Summary of Test Results in Plane-Strain Compression Tests on Sand "B"

Test * Number	Unit Weight γ_d (Lbs/.ft.^{3})	Porosity n %	Void Ratio e	Relative Density D_r %	Cell Pressure σ_3 (Lbs./in.^{2})	Intermediate Stress σ_2 (Lbs./in.^{2}) at failure	Major Stress σ_3 (Lbs./in.^{2}) at failure	Volumetric Strain $\Delta V/V$ % at failure	Axial Strain ε_1 % at failure	Angle of Shearing Resistance ϕ (degrees)	Remarks
B-M-1	102	38.70	0.63	67.50	5	15	49.50	+ 0.54	2.4	42	Medium dense
B-M-2	100.60	39	0.64	65	25	53	161	+ 0.28	2.75	40.98	" "
B-M-3	102	38.70	0.63	67.50	50	101	284.50	+ 0.10	3.25	39	" "
B-M-4	95.93	42	0.72	47.50	5	12	34	+ 0.415	2.6	38	" "
B-M-5	95.93	42	0.72	47.50	25	50.50	133	+ 0.20	2.95	36.90	" "
B-M-6	103.77	37	0.59	77.50	50	103	302	+ 0.30	2.95	40	" "
B-D-1	108.12	34.50	0.526	93	5	14.50	51	+ 0.66	0.85	44	Dense sand
B-D-2	107.80	35	0.53	92.50	25	54	177	+ 0.38	1.10	43	" "
B-D-3	108.12	34.50	0.526	93.50	50	104	315	+ 0.22	1.0	40.98	" "
B-D-4	105.60	36	0.564	84	50	102	301	+ 0.14	1.45	40.30	" "

* B: Sand type

M: Medium dense sand

D: Dense sand

Table No. 4-9

Summary of Test Results in Plane-Strain Compression Tests on Sand "C"

Test * Number	Unit Weight γ_d (Lbs./ft.^{3})	Void Ratio e	Porosity n %	Relative Density D_r %	Cell Pressure σ_3 (Lbs./in.^{2})	Intermediate Stress σ_2 (Lbs./in.^{2}) at failure	Major Stress σ_1 (Lbs./in.^{2}) at failure	Volumetric Strain $\Delta V/V$ % at failure	Axial Strain ε_1 % at failure	Angle of Shearing Resistance ϕ (degrees)	Remarks
C-M-1	93	0.70	41	45	5	12.50	42.50	+ 0.20	4	43.50	Medium dense
C-M-2	92.40	0.71	41.50	44	25	50	159.78	+ 0.18	4.50	42.60	" "
C-M-3	91.86	0.72	42	42	50	102	298	+ 0.15	6	40	" "
C-D-1	102.60	0.54	35	74.50	5	15	62	+ 0.70	1.5	48	Dense sand
C-D-2	101.28	0.56	36	71	25	50.50	192	+ 0.68	1.65	47	" "
C-D-3	101.28	0.56	36	71	50	105.20	346	+ 0.65	1.86	43	" "
C-D-4	103.27	0.53	34.60	76	5	10	41.50	+ 0.75	1.30	49	" "
C-D-5	103.27	0.53	34.60	76	25	52	211	+ 0.70	1.40	48	" "
C-D-6	102.60	0.54	35	74.50	50	101	354	+ 0.62	1.48	44.50	" "
C-D-7	100.80	0.567	36.50	68	25	50	183	+ 0.60	2.0	46	" "

* C : Sand type

M : Medium dense sand

D : Dense sand.

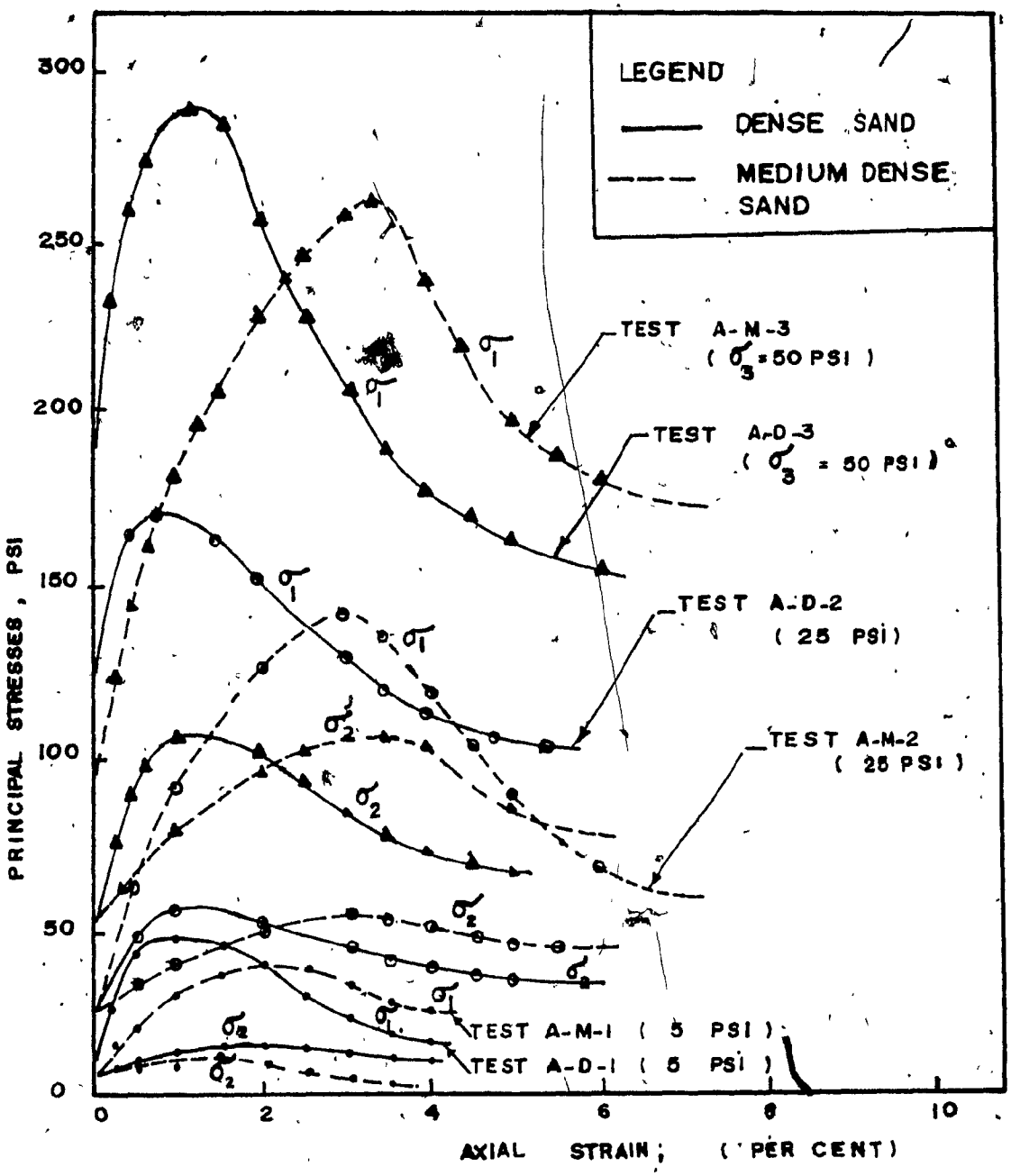

FIG. 4-17 STRESS - STRAIN RELATIONSHIP IN PLANE - STRAIN TESTS (SAND "A")

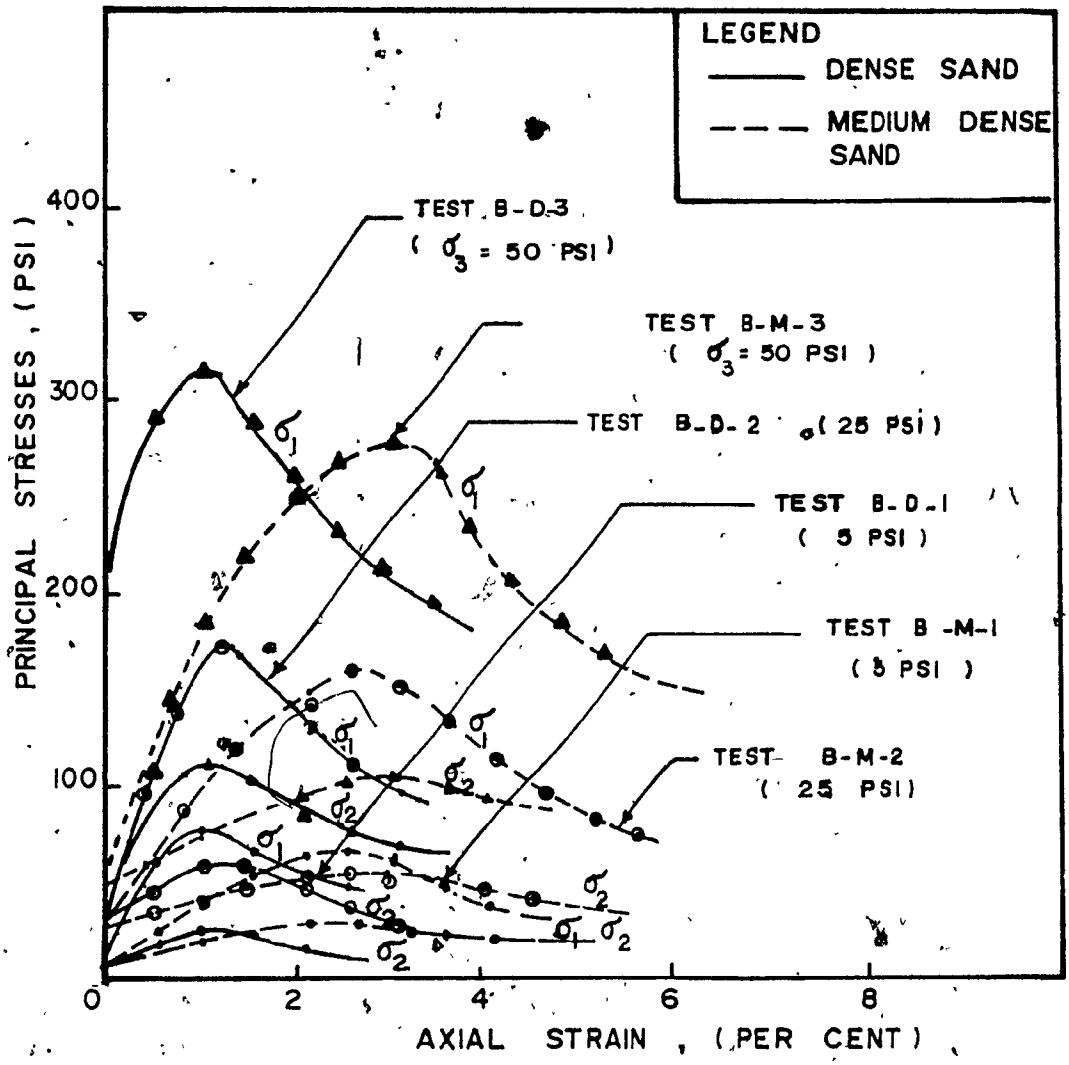

FIG. 4.18 STRESS-STRAIN RELATIONSHIP IN PLANE STRAIN TESTS FOR SAND "B"

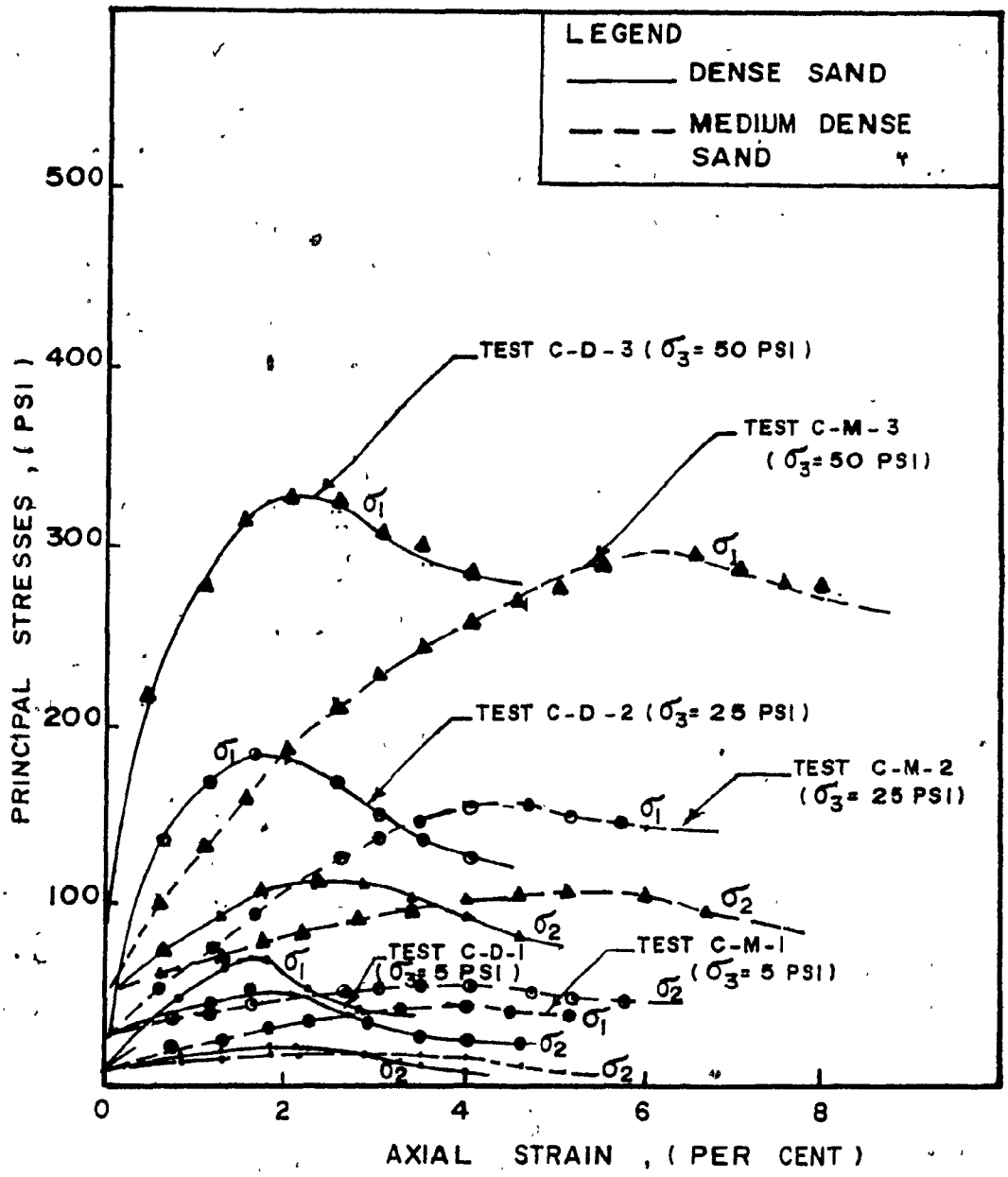

FIG. 4.19 STRESS - STRAIN RELATIONSHIP IN PLANE - STRAIN COMPRESSION TESTS FOR (SAND "C")

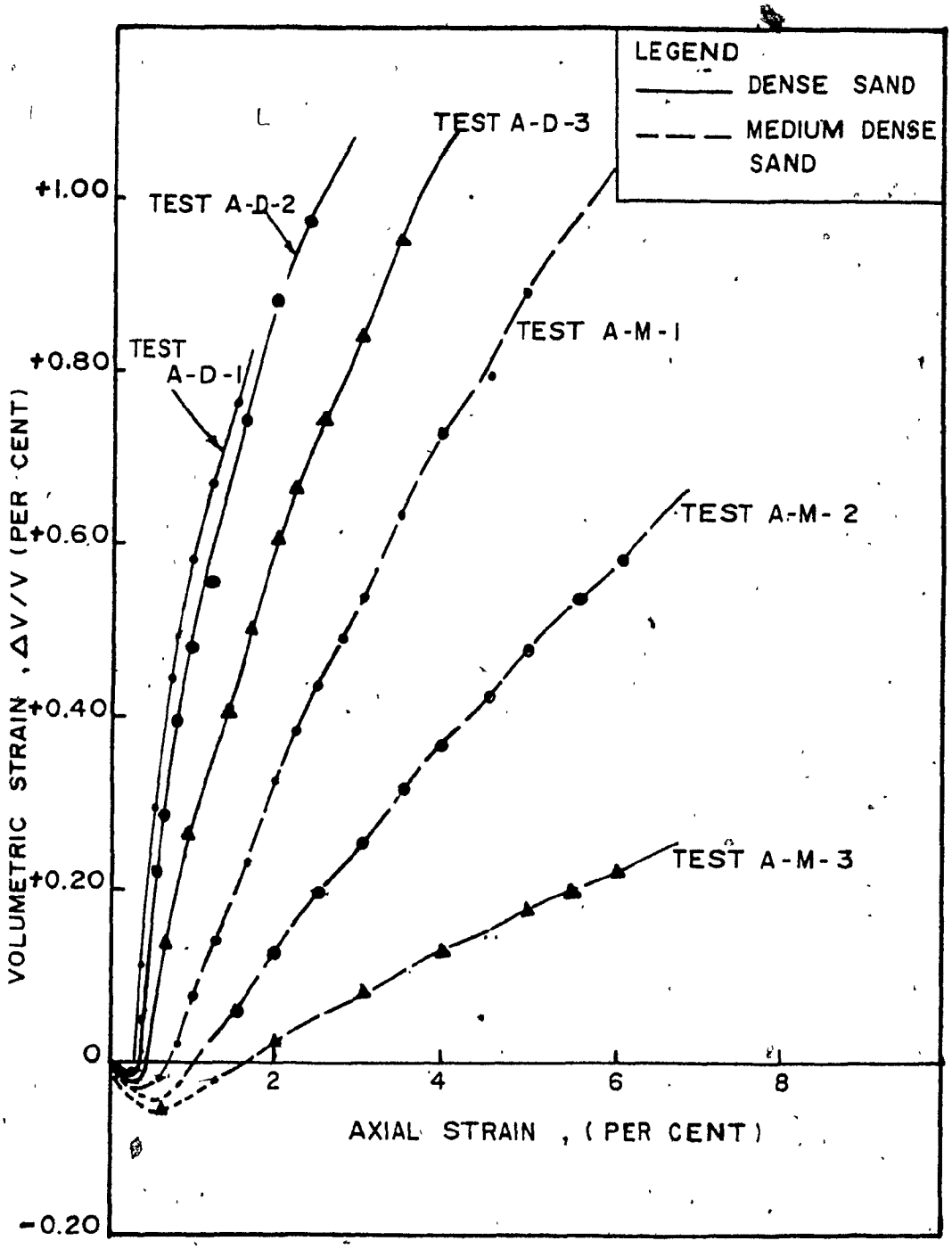

FIG. 4.20 VOLUMETRIC STRAIN IN PLANE STRAIN COMPRESSION TESTS FOR SAND "A"

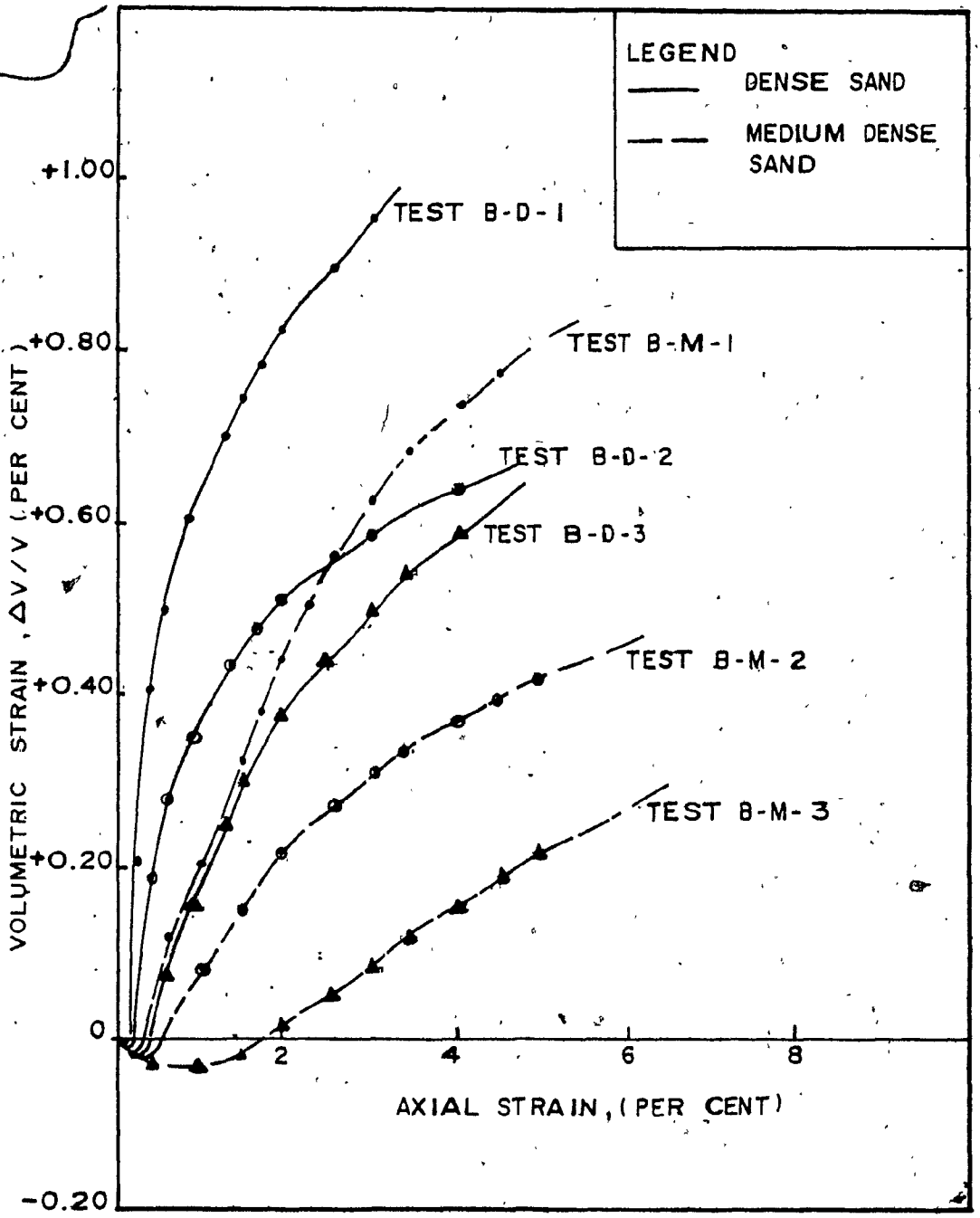

FIG. 4.21 VOLUMETRIC STRAIN IN PLANE STRAIN COMPRESSION TESTS FOR SAND "B"

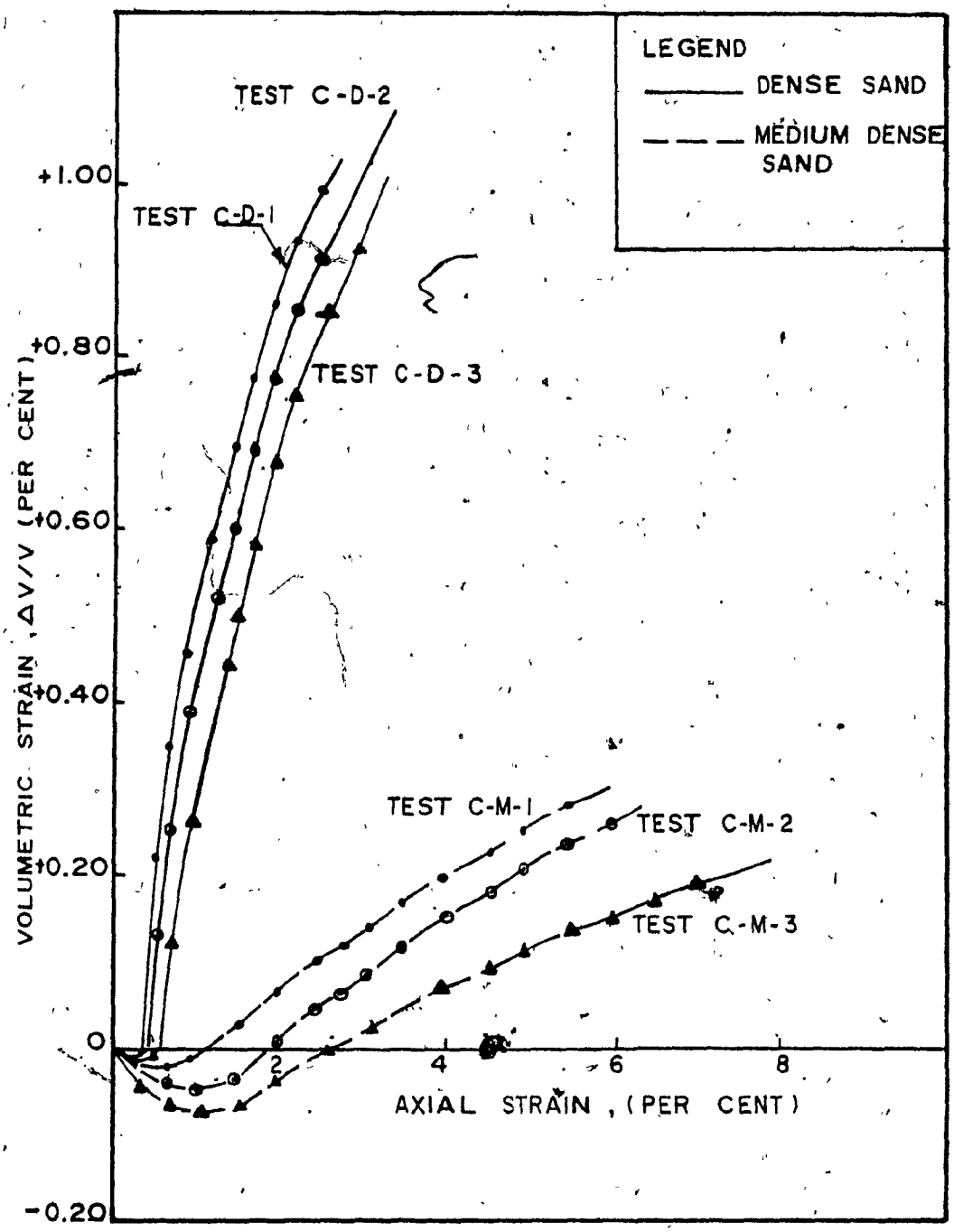

FIG. 4.22. VOLUMETRIC STRAIN IN PLANE STRAIN COMPRESSION TESTS FOR SAND "C"

CHAPTER V

ANALYSIS AND DISCUSSION OF TEST RESULTS

In this chapter, the experimental results from triaxial, plane-strain compression and direct shear tests are discussed in detail. The data was analysed to evaluate the factors affecting on the strength of the sands. The test data is analysed to determine the shear displacement and shear strength components for the sand tested.

Comparison of the strength parameter (ϕ) for the sand tested in plane-strain, triaxial compression and direct shear tests are made.

5.1 Consolidated-Drained Triaxial Compression Tests.

5.1.1 General Discussion

The test results are summarized in tables 4.1 to 4.3 and presented in graphical form in figures 4.1 to 4.9. In this chapter, these test results are represented in figures 5.1 to 5.6.

Figure 5.1 shows the variation of the deviator stress at failure with the confining stress. From this figure, it can be seen that the deviator stress increased with an increase of the confining stress and the relative density.

Figure 5.2 shows a plot of the volumetric strain against the confining pressure. It can be observed that the volumetric strain at failure was decreasing with the increase of the confining pressure. Also, the volumetric strain at failure for sand C was greater than those of sand A and B, tested at the same conditions. This is due to the high degree of interlocking between the particles, in case of sand C due to the effect of

grading and angularity of the soil particles.

Figure 5.3 and 5.4, show the variation of the angle of shearing resistance with the confining pressure and porosity respectively. It can be seen from these figures that the angle of shearing resistance decreases as the confining pressure increases and the initial porosity increases. That can be explained by the phenomenon of interlocking, where an increase of the confining pressure decreases the interlocking, because the particles become flattened at the points of contact, sharp corners are crushed, and particles break. Also, for dense sand samples, the degree of interlocking is the highest where the energy required by the particles to ride one over the other and to expand or dilate against the confining pressure will be the greatest.

Figure 5.5 presents the volumetric strain at failure versus the intial porosity of the sand samples. From this figure, it can be observed that the volumetric strain at failure increased with the decrease of the initial porosity. That, is to say that the high degree of interlocking for the case of dense sand samples, should be overcome by the expansion which tends to take place during shear.

Figure 5.6 shows the axial strain at failure versus the initial porosity. From this figure, it can be seen that the axial strain at failure is increasing with an increase of the initial porosity.

5.1.2 Analysis of Triaxial Test Data

5.1.2.1 Shear-Displacement

In the triaxial tests, the shear displacement takes place along a plane inclined at an angle of $(45° + \frac{\Phi}{2})$ with the plane of the major

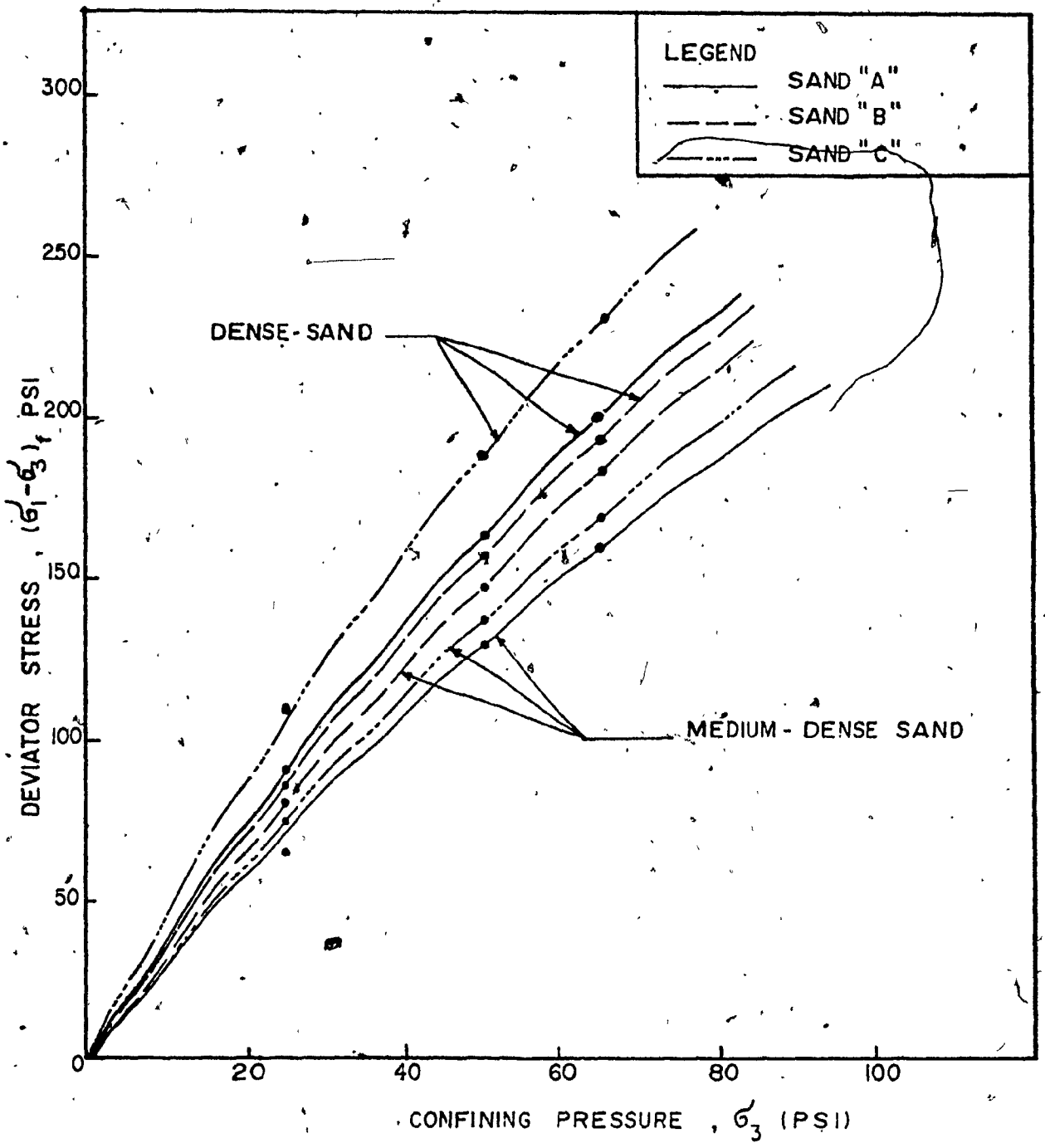

FIG. 5.1 CONDITION OF FAILURE IN TRIAXIAL COMPRESSION TESTS

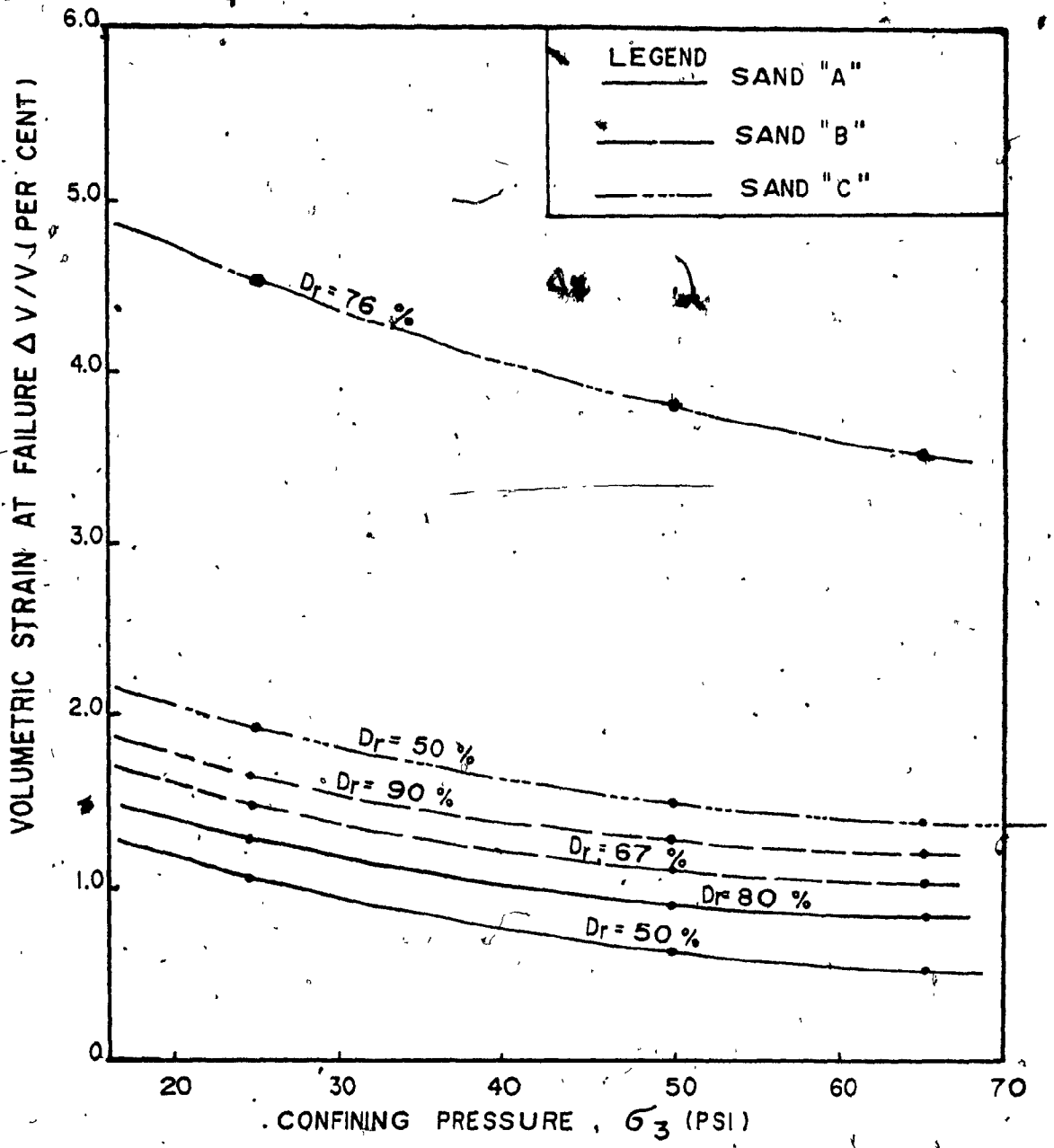

FIG. 5. 2 VOLUMETRIC STRAIN IN TRIAXIAL COMPRESSION TESTS VS CONFINING PRESSURE

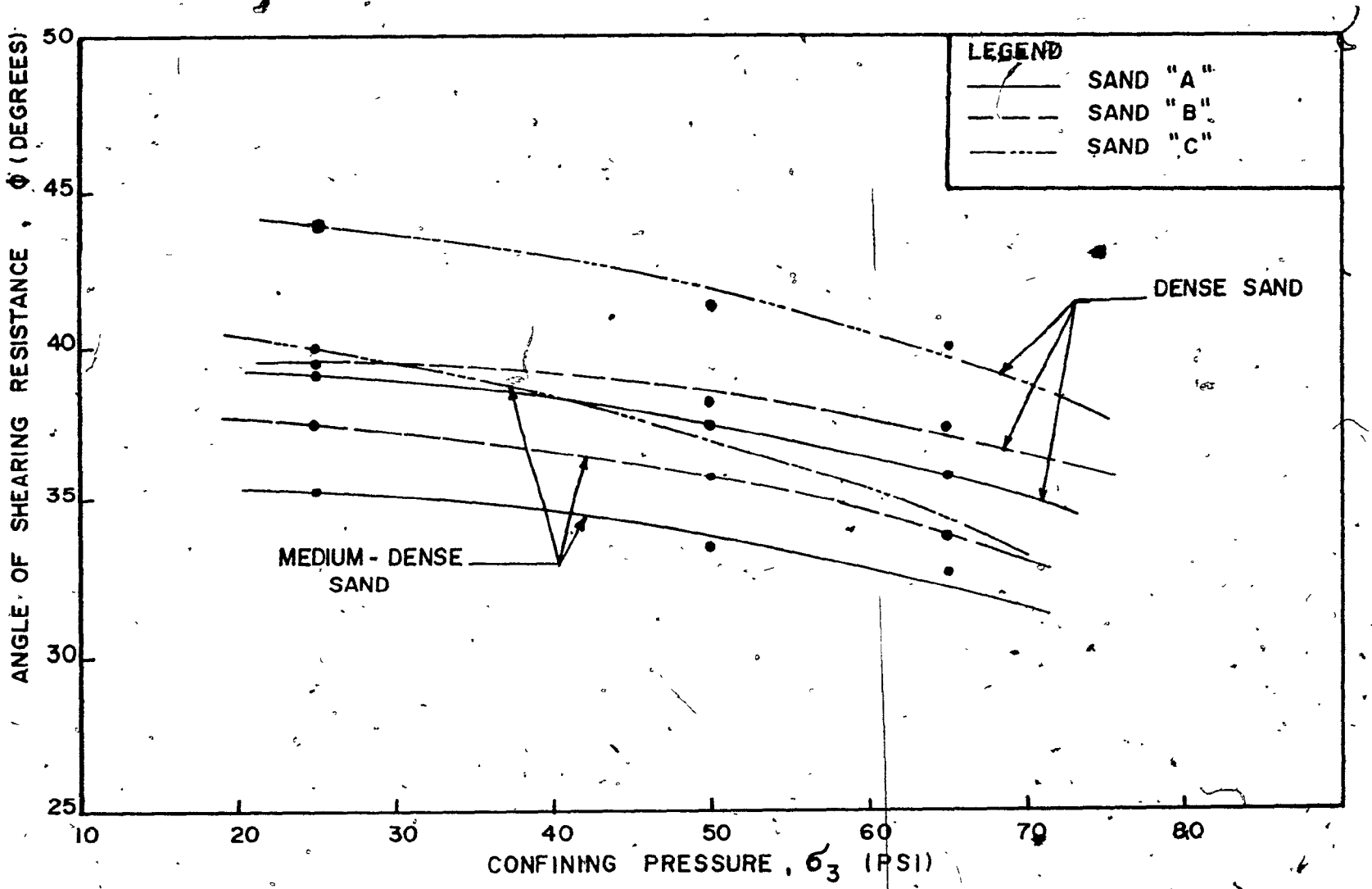

FIG. 5. 3 ANGLE OF SHEARING RESISTANCE IN TRIAXIAL COMPRESSION TESTS VS CONFINING PRESSURE

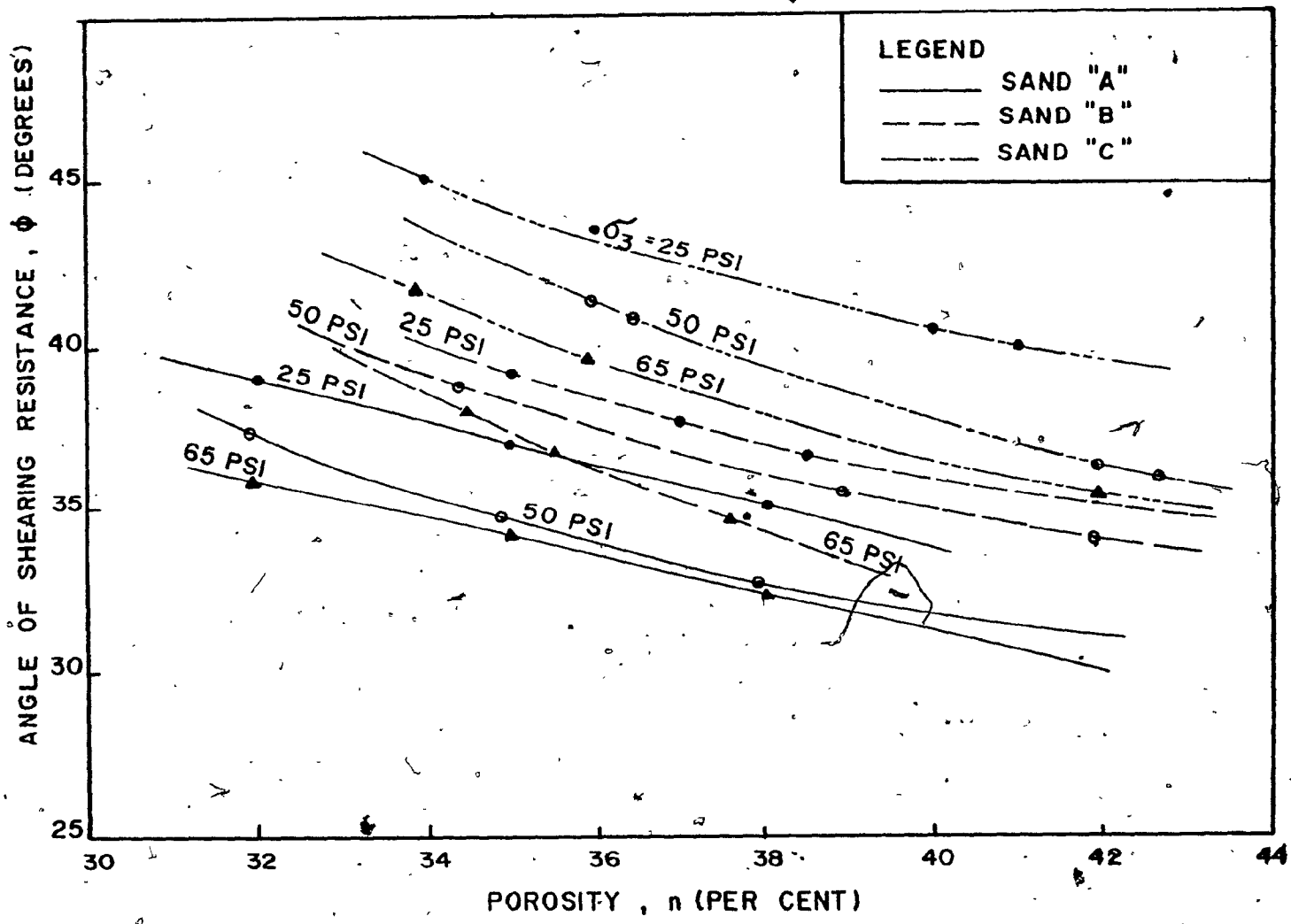

FIG. 5. 4 ANGLE OF SHEARING RESISTANCE VS POROSITY IN TRIAXIAL COMPRESSION TESTS

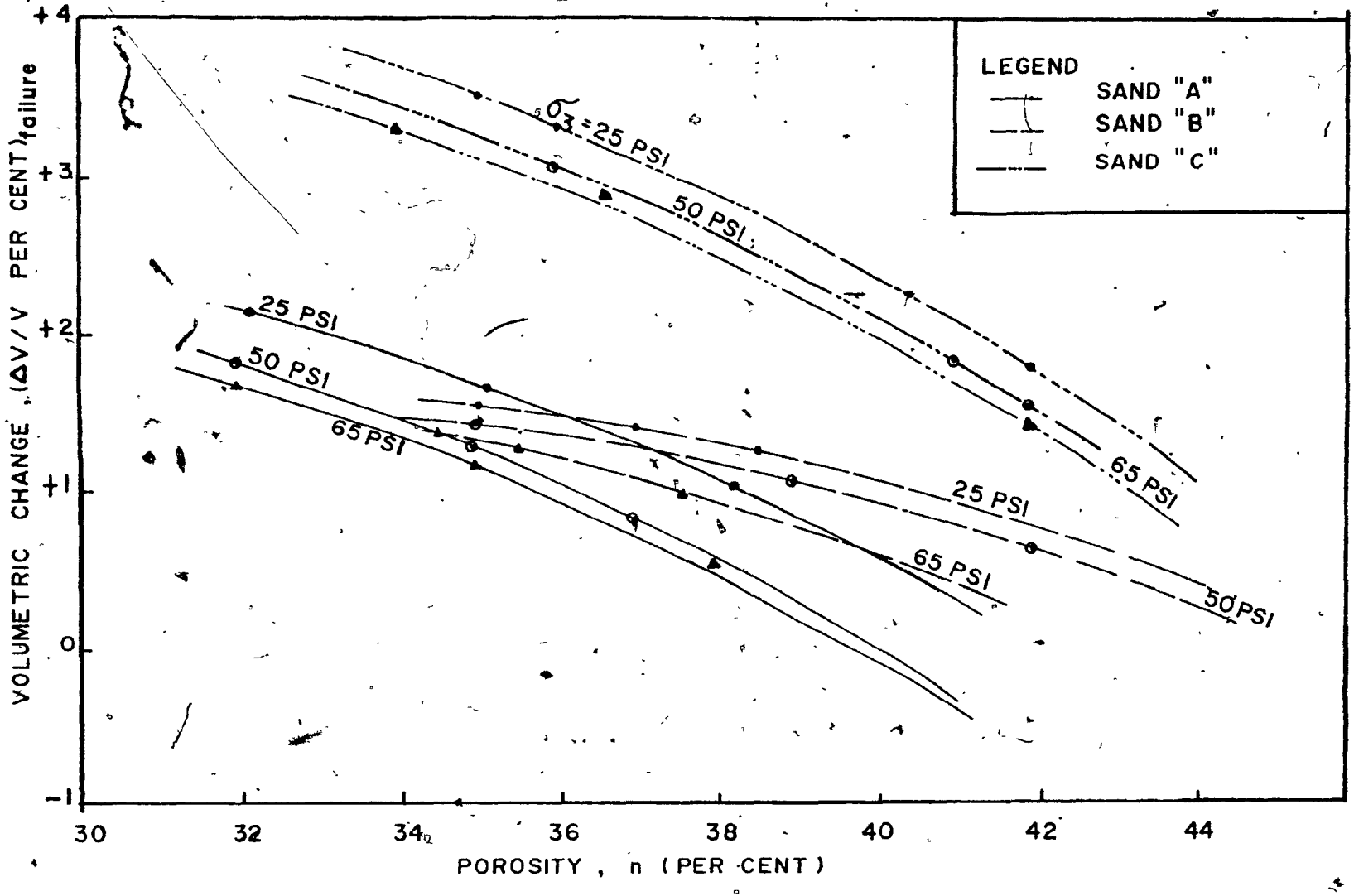

FIG. 5. 5 VOLUMETRIC STRAIN VS POROSITY IN TRIAXIAL COMPRESSION TESTS AT VARIOUS CONFINING PRESSURE AT FAILURE

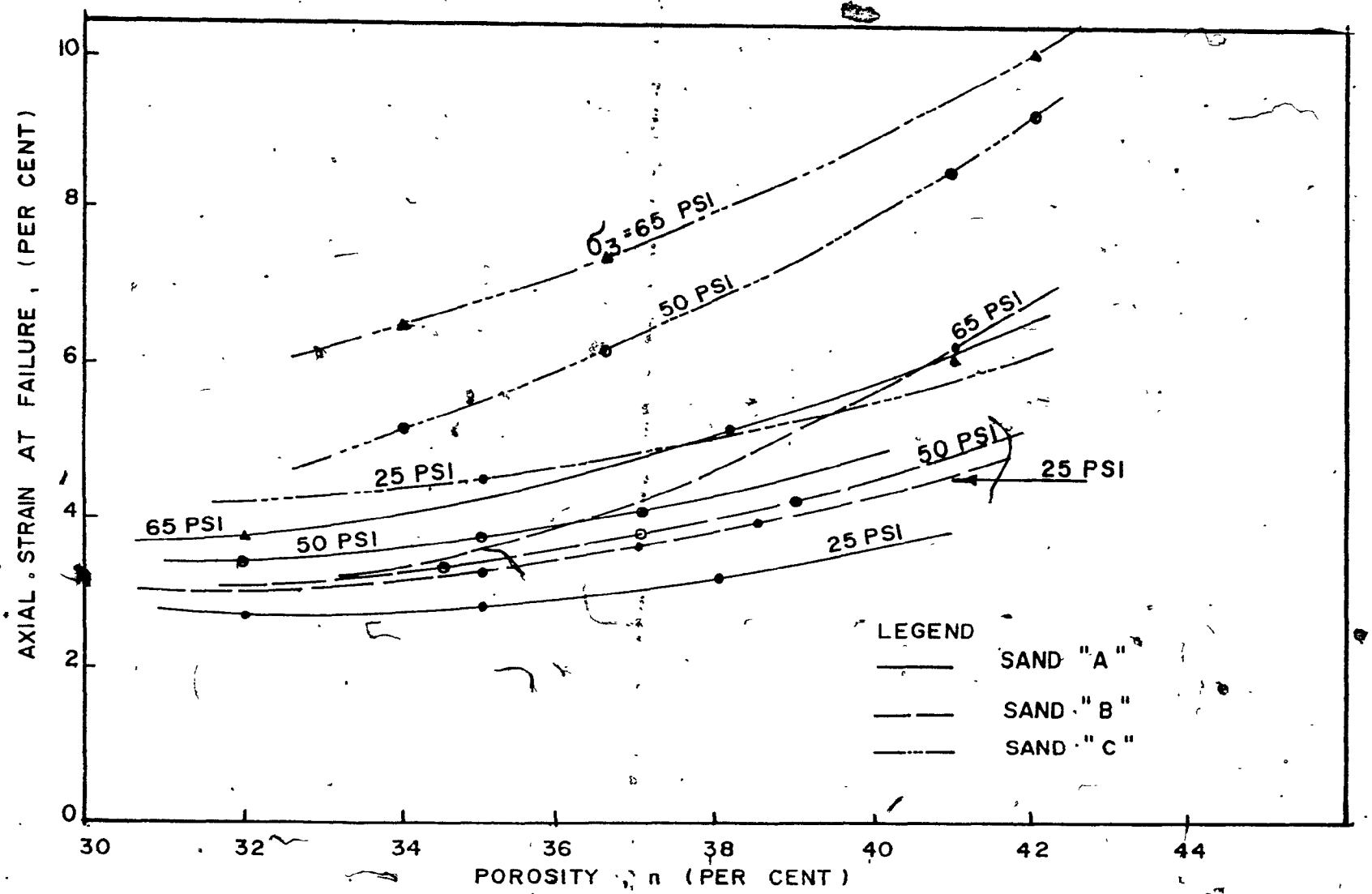

FIG. 5.6 AXIAL STRAIN IN TRIAXIAL COMPRESSION TESTS VS POROSITY

principal stress, as shown in figure 5.7.a. The shear displacement along this plane is obtained by dividing the vertical deformation by $\sin (45° + \frac{\phi}{2})$. The shear stress at failure (τ_f) along the failure plane can be obtained from the Mohr's Circle of stress, as shown in figure 5.7.b and given by the expression:

$$\tau = \frac{1}{2} (\sigma_1 - \sigma_3) \sin 2\theta \qquad (5.1)$$

where:

$\sigma_1 - \sigma_3$ is the deviator stress

and:

θ is the theoretical angle between the major principal plane and the plane of failure.

From the theory of elasticity:

$$\varepsilon_1 + \varepsilon_2 + \varepsilon_3 = \Delta V/v \qquad (5.2)$$

where ε_1, ε_2 and ε_3 are the major, intermediate and minor principal stresses respectively, and the volumetric strain is considered to be positive, if the sample expand against the confining pressure.

Since, $\varepsilon_2 = \varepsilon_3$ in triaxial compression test, then:

$$\varepsilon_1 + 2\varepsilon_3 = \Delta V/V \qquad (5.3)$$

The shear strain "γ_{xy}" can be obtained from the Mohr's circle of strain as shown in figure 5.7.C and given by the expression:

$$\sin 2\theta = \gamma_{xy}/(\varepsilon_1 + \varepsilon_3) \qquad (5.4)$$

then

$$\gamma_{xy} = (\varepsilon_1 + \varepsilon_3) . \sin (90° + \phi) \qquad (5.5)$$

The change of diagonal length (ΔL) is given by:

$$\Delta L = \frac{1}{\sqrt{2}} . \sin \gamma_{xy} \qquad (5.6)$$

where γ_{xy} is in radians, and has to be multilpied by $180/\pi$ to get the value in degrees.

The total deformation is given by the expression:

$$\text{Total deformation} = \Delta L \times (\text{length of failure plane})$$

$$= \frac{\text{Sin } \gamma_{xy}}{\sqrt{2}} \cdot \frac{D}{[\text{Sin } (45^{\circ} - \frac{\Phi}{2})]} \qquad (5.7)$$

where D is the sample diameter.

Sample calculations of the shear displacement deduced from the present investigation are summarized in tables 5.1 to 5.3 and also, the shear-displacement at failure are given in tables 5.4 to 5.6.

The experimental shear displacement at failure were calculated as follows (referring to figure 5.7,d):

$$\text{Shear Displacement} = \frac{\text{vertical deformation (measured)}}{\text{Sin } \theta}$$

It can be concluded that the theoretical values of shear-displacement were in good agreement with the experimental values deduced from the present test results.

The shear-displacement versus the shear stress for the sand samples, tested in triaxial compression tests is presented in graphical form in figures 5.8 and 5.9. From these figures, it may be noted that the shear-displacement and shear stress at failure increased as the confining pressure increased. At large confining pressure, the interlocking decreases, as a result of crushing the particles. Decrease in interlocking again means greater shear displacement. When the interlocking is negligible, the shear displacement is very high, and enough to let the particles slide up or down and over each other. The reverse is true for

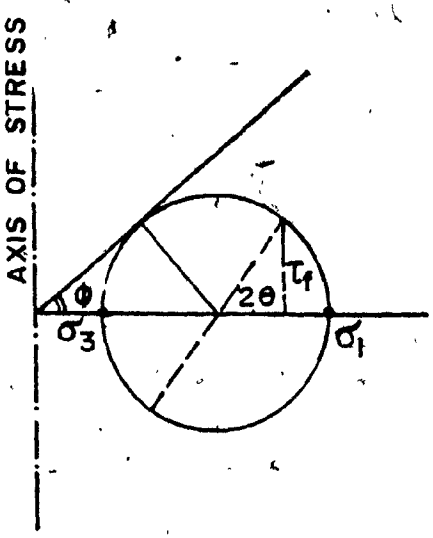

b- MOHR'S CIRCLE OF STRESS

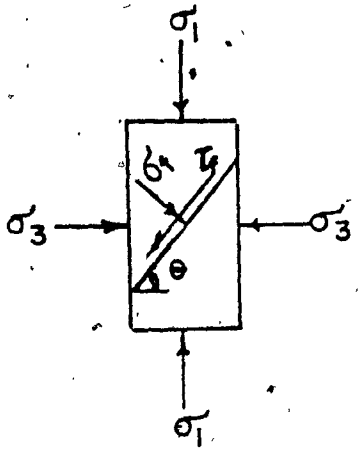

a- STRESSES ACTING ON TRIAXIAL SAMPLES

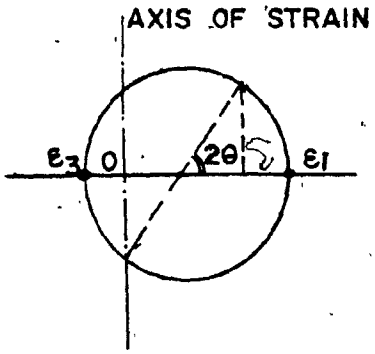

c - MOHR'S CIRCLE OF STRAIN

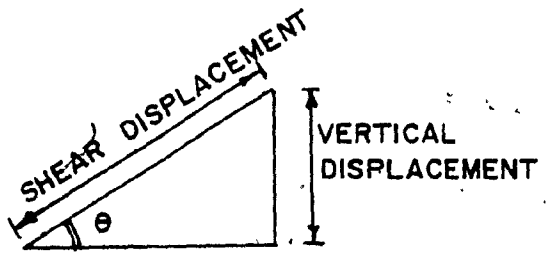

$\theta = 45^\circ - \phi/2$

(d)

FIG. 5.7

Table 5.1

Calculation of Shear Displacement in Triaxial Compression Test

$\phi = 39°$, $D_r = 80\%$, $\sigma_3 = 25$ psi , $\sin(90° + \phi) = 0.777$, $\sin(45° - \frac{\phi}{2}) = 0.43$,

Length of Failure Plane = $1.5/\sin(45 - \frac{\phi}{2}) = 3.49$"

Test : A-D-1

ε_1	$\Delta V/V$	Deformation $\times 10^{-3}$ (inch)	ε_3	$\varepsilon_1+\varepsilon_3$	$[\sin(90°+\phi) \times 57.3] \times (\varepsilon_1+\varepsilon_3) = \gamma_{xy}$	Change per unit length $= \frac{1}{\sqrt{2}} \sin \gamma_{xy}$ (inch)	$\tau = \frac{[\varepsilon_1-\varepsilon_3]}{2} \times$ Cos ϕ (lbs/in.^{2})	Shear Deformation $= 3.49 \times \frac{1}{\sqrt{2}} \cdot \sin \gamma_{xy}$ (inch)	Remark
0.008	0.000	24	.004	0.012	0.534	0.0066	22.10	0.023	difference in shear deformation at failure = -0.004"
0.012	.004	36	.008	0.020	0.890	0.011	23.50	0.038	
0.016	0.005	48	.010	0.025	1.158	0.014	25.26	0.049	
0.020	0.008	60	.014	0.034	1.514	0.018	27.2	0.063	
0.028	0.021	84	0.025	0.052	2.315	0.028	28	0.097	← Failure
.036	.014	108	.025	0.061	2.716	0.033	27.2	0.115	
.040	.015	120	.028	0.068	3.026	0.037	23.4	0.129	

Table 5.2

Calculation of Shear Displacement in Triaxial Compression Test

$\phi = 39°$, $D_r = 92.5\%$, $\sigma_3 = 25$ psi , $\sin(90° + \phi) = 0.777$, $\sin(45° - \frac{\phi}{2}) = 0.430$

Length of Failure Plane = $7.5/\sin(45° - \frac{\phi}{2}) = 3.49"$

Test: B-D-1

ε_1	$\Delta V/V$	Deformation $\times 10^{-3}$ (inch)	ε_3	$\varepsilon_1+\varepsilon_3$	$[\sin(90°+\phi) \times 57.3] \times (\varepsilon_1+\varepsilon_3) = \gamma_{xy}$	Change/ unit length $= \frac{1}{\sqrt{2}} \sin \gamma_{xy}$ (inch)	$\tau = \frac{[\sigma_1-\sigma_3]}{2} \cos \phi$ (lbs./in^2)	Shear Deformation $= 3.49 \times \frac{1}{\sqrt{2}} \sin \gamma_{xy}$ (inch)	Remarks
.0075	0.000	22.5	.0038	0.0113	0.490	0.006	13.65	0.0230	difference in shear deformation at failure = 0.007"
.0125	.003	37.5	.0075	0.0200	0.39	0.010	19.5	0.038	
.0175	.007	52.5	.0120	0.0295	1.29	0.016	21.45	0.061	
.0225	.008	67.5	.0150	0.0375	1.67	0.021	25.35	0.08	
.0325	0.013	97.5	.0230	0.0555	2.47	0.030	29.9	0.115	⇐ Failure
.035	.015	105	.025	0.060	2.67	0.033	27.3	0.127	
.040	0.016	120	.028	0.068	3.03	0.037	26.50	0.142	
.050	.019	150	.035	0.085	3.79	0.047	25.35	0.180	

Table 5.3

Calculation of Shear Displacement of Triaxial Compression Test

$\phi = 44°$, $D_r = 69\%$, $\sigma_3 = 25$ psi , $\text{Sin}(90° + \phi) = 0.719$, $\text{Sin}(45° - \frac{\phi}{2}) = 0.391$

Length of Failure Plane = $1.5/\text{Sin}(45° - \frac{\phi}{2}) = 3.84"$ or $3/\text{Cos}(45° + \frac{\phi}{2}) = 7.68"$

Test : C-D-1

ε_1	$\Delta V/V$	Deformation $\times 10^{-3}$ (inch)	ε_3	$\varepsilon_1+\varepsilon_3$	$[\text{Sin}(90°+\phi) \times 57.5] \times (\varepsilon_1+\varepsilon_3) = \gamma_{xy}$	Change/ unit length $= \frac{1}{\sqrt{2}} \text{Sin } \gamma_{xy}$ (inch)	$\tau = \frac{[\sigma_1-\sigma_3]}{2} \text{Cos } \phi$ (lbs./in.^{2})	Shear Deformation $= 3.84" \times \frac{1}{\sqrt{2}} \text{Sin } \gamma_{xy}$ (inch)	Remarks
0.015	0.000	45	.0075	.022	0.91	0.011	27	0.042	difference in shear deformation at failure = 0.006"
0.020	+ .008	60	.014	.034	1.40	0.017	32.4	0.065	
0.030	+ .017	90	.024	.054	2.22	0.027	36.9	0.104	
0.040	+ .025	120	.033	.073	3.0	0.037	39.6	0.142	
0.050	0.047	150	0.0485	.090	3.70	0.041	41	0.157	⇐ Failure
0.060	0.048	180	0.054	0.114	4.45	0.055	40.70	0.211	
.070	0.049	210	0.059	0.129	5.15	0.063	37.8	0.242	
.090	.050	270	0.070	0.160	6.59	0.081	30.60	0.311	

Table 5.4

Shear Deformation at Failure in Triaxial Compression Tests for Sand "A"

Test Number	ε_1	$\Delta V/V$	Deformation $\times 10^{-3}$ (inch)	ε_3	$\varepsilon_1+\varepsilon_3$	$[\sin(90°+\phi) \times 57.3] \times (\varepsilon_1+\varepsilon_3) = \gamma_{xy}$ (degrees)	Change per unit length $= \frac{1}{\sqrt{2}} \sin \gamma_{xy}$ (inch)	$\tau = \frac{(\sigma_1-\sigma_3)}{2} \times \cos\phi$ (Lbs./in.^{2})	Shear Deformation = length of failure plane $\times \frac{\sin \gamma_{xy}}{\sqrt{2}}$ (inch)	Difference between theoretical and experimental shear displacement (inch)
A-M-1	0.032	0.01	96	0.021	0.053	2.49	0.031	27.23	0.101	+ 0.007"
A-M-2	0.040	0.008	120	0.024	0.064	3.022	0.037	53.71	0.119	+ 0.017"
A-M-3	0.050	0.005	150	0.0275	0.078	3.73	0.0455	67.13	0.144	+ 0.026"
A-M-4	0.0295	0.016	90	0.023	0.053	2.46	0.030	28.80	0.099	+ 0.002"
A-M-5	0.0385	0.013	115.5	0.026	0.065	3.05	0.037	54.47	0.120	+ 0.010"
A-M-6	0.045	0.012	135	0.0285	0.074	3.536	0.043	66.29	0.091	+ 0.028"
A-D-1	0.028	0.021	84	0.0245	0.052	2.315	0.028	28	0.097	- 0.004"
A-D-2	0.032	0.0192	96	0.0255	0.058	2.654	0.032	59.90	0.072	+ 0.035"
A-D-2	0.038	0.0171	114	0.0275	0.0655	3.036	0.037	75.04	0.082	+ 0.046"

Table 5.5

Shear Deformation at Failure in Triaxial Compression Tests for Sand "B"

Test Number	ε_1	$\Delta V/V$	Deformation $\times .10^{-3}$ (inch)	ε_3	$\varepsilon_1+\varepsilon_3$	$[\sin(90°+\phi) \times 57.3] \times (\varepsilon_1+\varepsilon_3) = \gamma_{xy}$ (degrees)	Change per unit length $= \frac{1}{\sqrt{2}} . \sin \gamma_{xy}$ (inch)	$\tau = \frac{(\sigma_1-\sigma_3)}{2} \times \cos \phi$ (Lbs./in.^{2})	Shear Deformation = (Length of failure plane $\times \frac{\sin \gamma_{xy}}{\sqrt{2}}$ (inch)	Difference between theoretical and experimental shear displacement (inch)
B-M-1	0.037	0.012	.111	0.0245	0.061	2.77	0.034	33.12	0.077	+ 0.046
B-M-2	0.044	0.011	.132	0.0275	0.071	3.29	0.040	60.43	0.088	+ 0.05
B-M-3	0.048	0.010	144	0.029	0.077	3.658	0.045	76.69	0.096	+ 0.067
B-M-4	0.064	0.0065	192	0.035	0.099	4.54	0.055	40.04	0.122	+ 0.093
B-M-5	0.080	0.004	240	0.042	0.122	5.795	0.0707	52.64	0.151	+ 0.12
B-D-1	0.0325	0.015	99	0.0237	0.0562	2.47	0.030	29.90	0.115	- 0.007
B-D-2	0.035	0.013	108	0.024	0.059	2.657	0.032	63.79	0.073	+ 0.044
B-D-3	0.036	0.0125	103	0.0245	0.0605	2.75	0.033	79.59	0.075	+ 0.045
B-D-4	0.0295	0.012	90	0.0207	0.0502	2.43	0.03	60.0	0.067	+ 0.033
B-D-5	0.035	0.0135	105	0.0243	0.059	2.65	0.032	83	0.074	+ 0.02

Table 5.6

Shear Deformation at Failure in Triaxial Compression Tests for Sand "C"

Test Number	ε_1	$\Delta V/V$	Deformation $\times 10^{-3}$ (inch)	ε_3	$\varepsilon_1+\varepsilon_3$	$[\sin(90°+\phi) \times 57.3] \times (\varepsilon_1+\varepsilon_3) = \gamma_{xy}$ (degrees)	Change per unit length = $\frac{1}{\sqrt{2}} \cdot \sin \gamma_{xy}$ (inch)	$\tau = \frac{(\sigma_1-\sigma_3)}{2} \times \cos \phi$ (Lbs./in.^{2})	Shear deformation = (Length of failure plane) $\times \frac{\sin \gamma_{xy}}{\sqrt{2}}$ (inch)	Difference between theoretical and experimental shear displacement (inch)
C-M-1	0.060	0.018	180	0.039	0.099	4.346	0.053	27.92	0.188	0.010
C-M-2	0.090	0.016	270	0.053	0.143	6.63	0.081	54.78	0.268	0.035
C-M-3	0.100	0.014	300	0.057	0.157	7.37	0.09	72.49	0.292	0.046
C-M-4	0.055	0.0184	165	0.0365	0.091	3.96	0.048	35	0.115	0.067
C-M-5	0.084	0.017	252	0.101	0.185	8.47	0.103	61.90	0.230	0.056
C-M-6	0.086	0.0175	258	0.103	0.189	8.58	0.105	61.88	0.237	0.050
C-D-1	0.050	0.0325	150	0.041	0.091	3.75	0.046	41	0.124	0.039
C-D-2	0.055	0.030	165	0.0425	0.097	4.23	0.052	64.63	0.123	0.059
C-D-3	0.070	0.0295	210	0.0495	0.119	5.22	0.064	89.63	0.151	0.081
C-D-4	0.045	0.035	135	0.040	0.085	3.44	0.042	42.60	0.110	0.036
C-D-5	0.050	0.030	150	0.040	0.090	3.89	0.047	72.10	0.112	0.053
C-D-6	0.052	0.0494	156	0.050	0.102	4.40	0.054	94.57	0.13	0.041

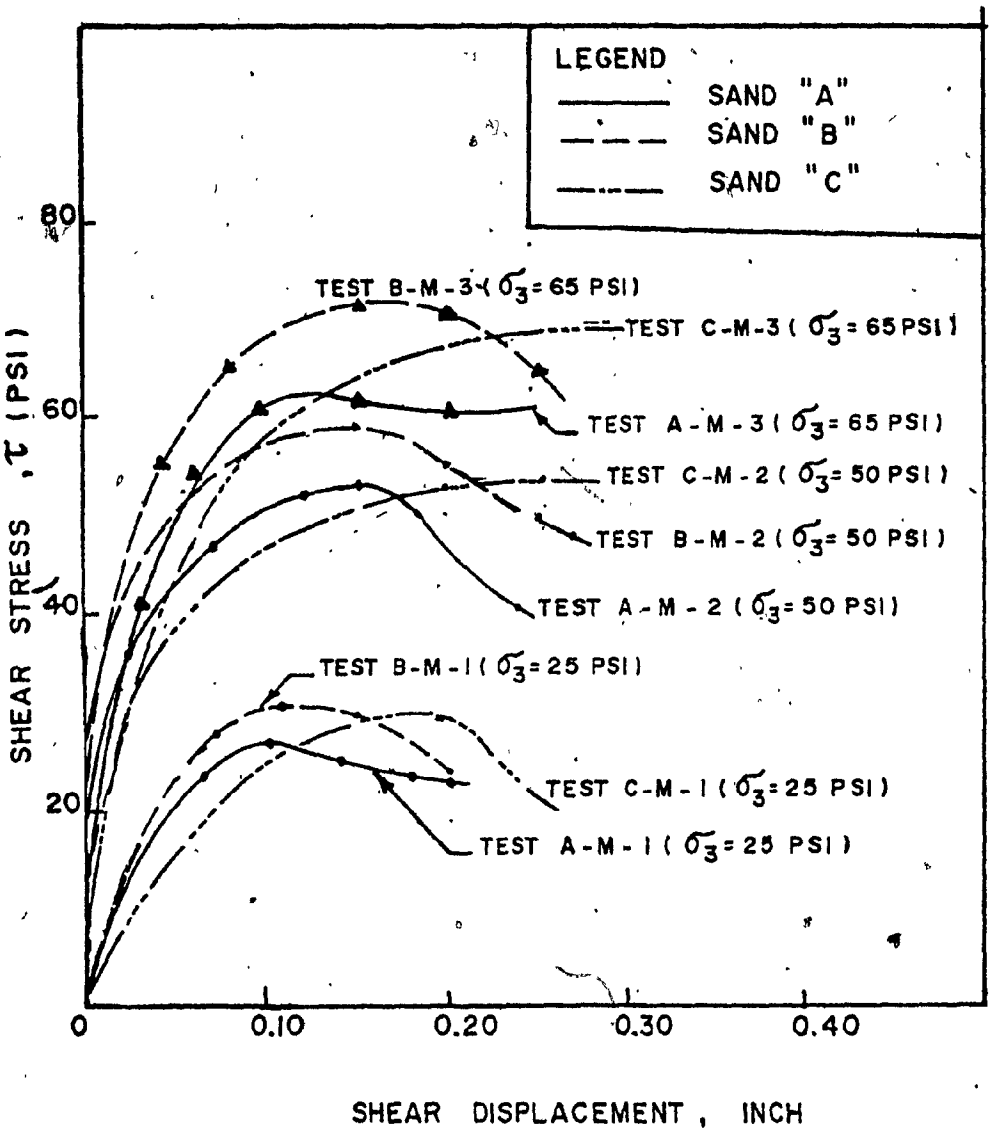

FIG. 5. 8 SHEAR DEFORMATION IN TRIAXIAL COMPRESSION TESTS FOR MEDIUM DENSE SANDS

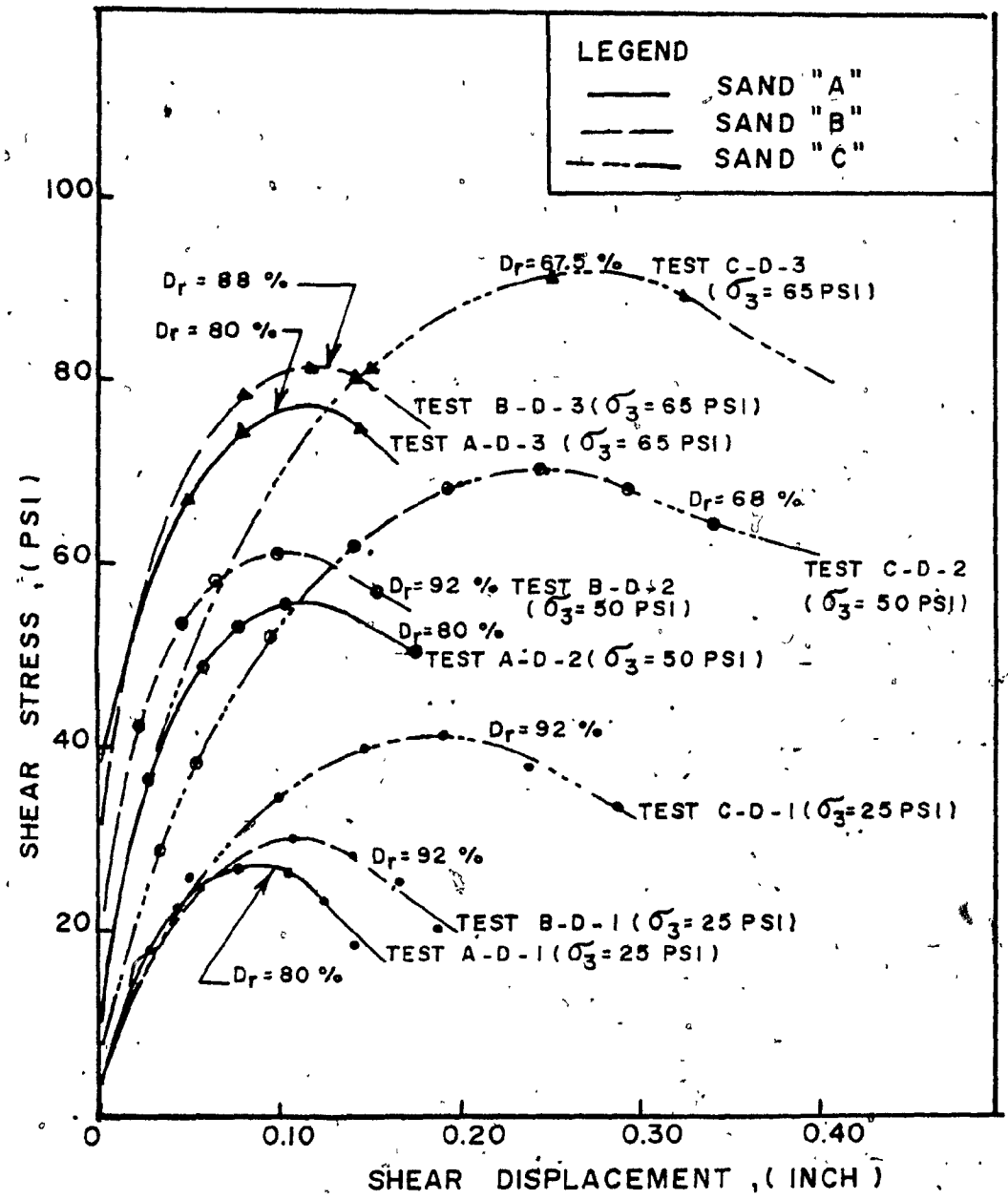

FIG. 5. 9 SHEAR DEFORMATION IN TRIAXIAL COMPRESSION TESTS FOR DENSE SAND

cases where interlocking increases.

5.1.2.2 Stress-Path and Strain Contours

The stress path and strain contours for the samples tested in triaxial compression tests are presented in figures 5.10 to 5.15. The strain contours were drawn by connecting the lines with the same strain. The failure line is presented by a line connecting the points that have the maximum stress at failure. It may be noted from these figures that the axial strain at failure increases as the relative density decreases and the confining pressure increases. The stress path and the strain contours can be used to predict the strains for a given relative density and stress range.

5.1.2.3 Interlocking

The interlocking between the particles, for the sand tested in triaxial compression tests, was determined from the expression given by Rowe, (1962) as:

$$\sigma_1/\sigma_3 = \tan\alpha \cdot \tan(45° + \phi_f/2)$$

and

$$\tan\alpha = \left|\frac{\sigma_1}{\sigma_3}\left(1 - \frac{dv}{d\varepsilon_1}\right)\right|^{1/2}$$

where:

dv = volumetric strain, and is negative for any dilation or expansion.

α = interlocking parameter.

$\frac{dv}{d\varepsilon_1}$ = the dilatancy rate.

$1 - \frac{dv}{d\varepsilon_1}$ = the dilatancy factor.

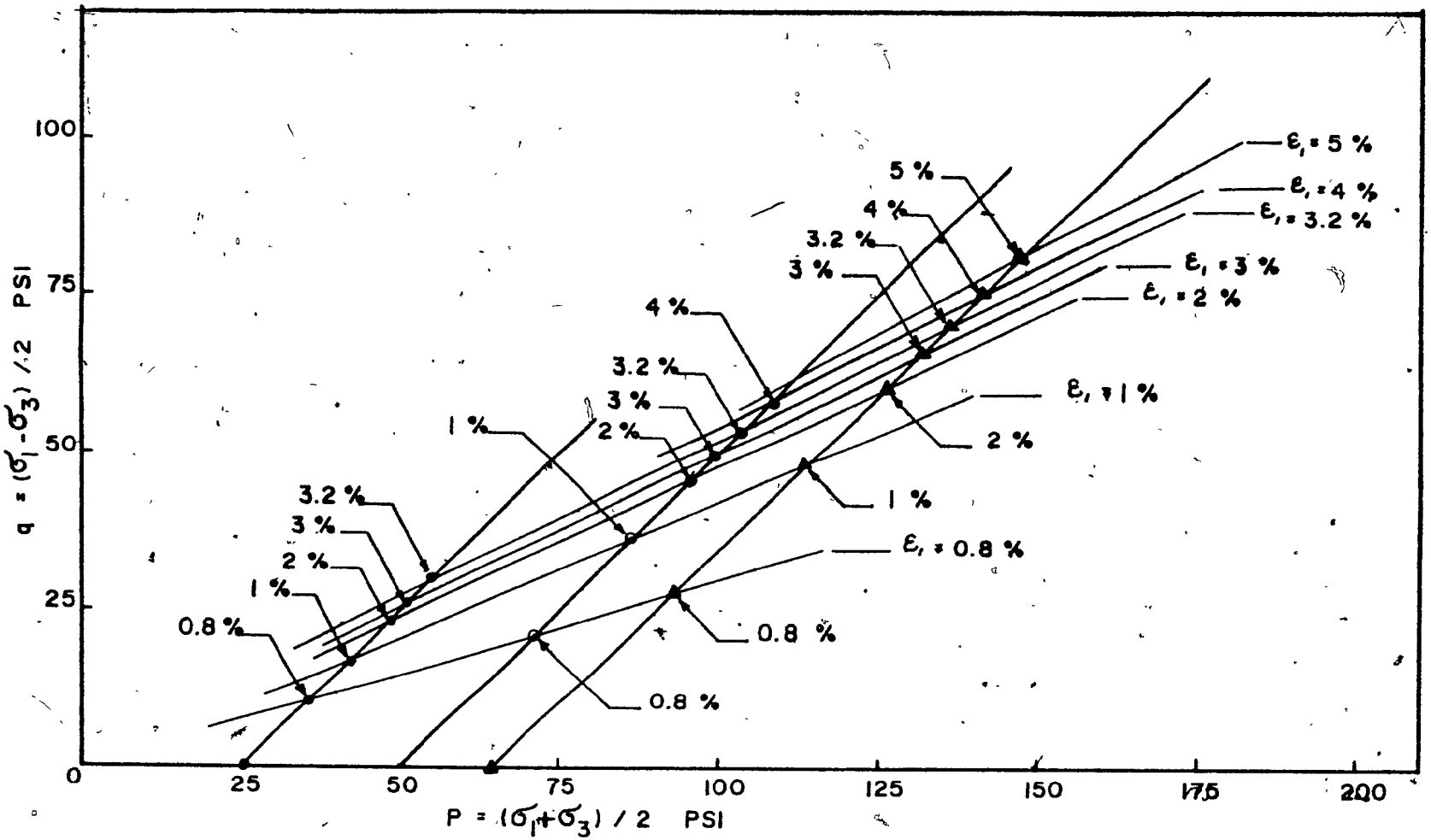

FIG. 5. 10 STRESS PATH & AXIAL STRAIN CONTOURS IN TRIAXIAL COMPRESSION TESTS FOR MEDIUM DENSE SAND (SAND "A")

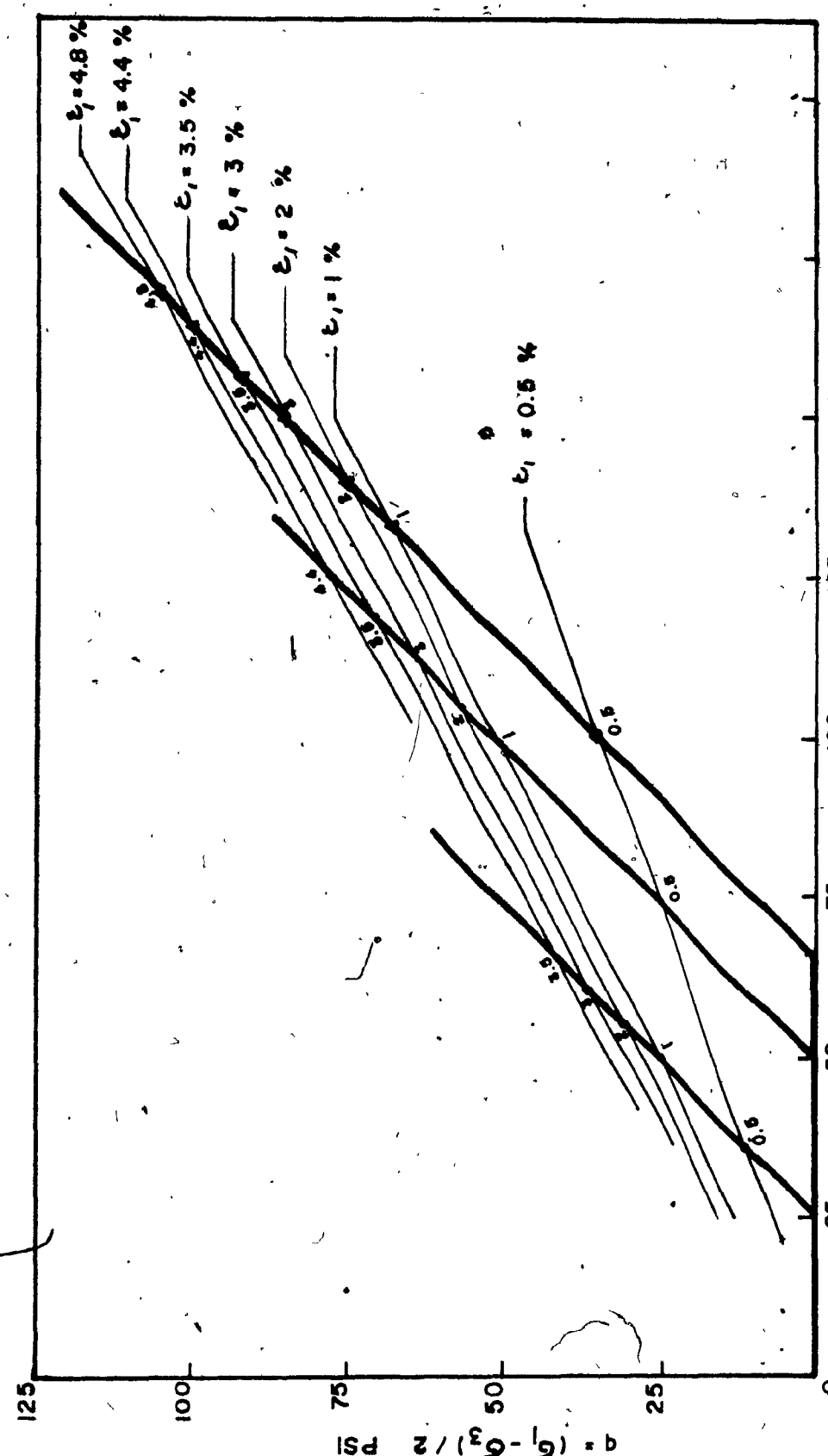

FIG. 5.11 STRESS PATH & AXIAL STRAIN CONTOURS IN TRIAXIAL COMPRESSION TEST FOR MEDIUM DENSE SAND ('SAND "B")

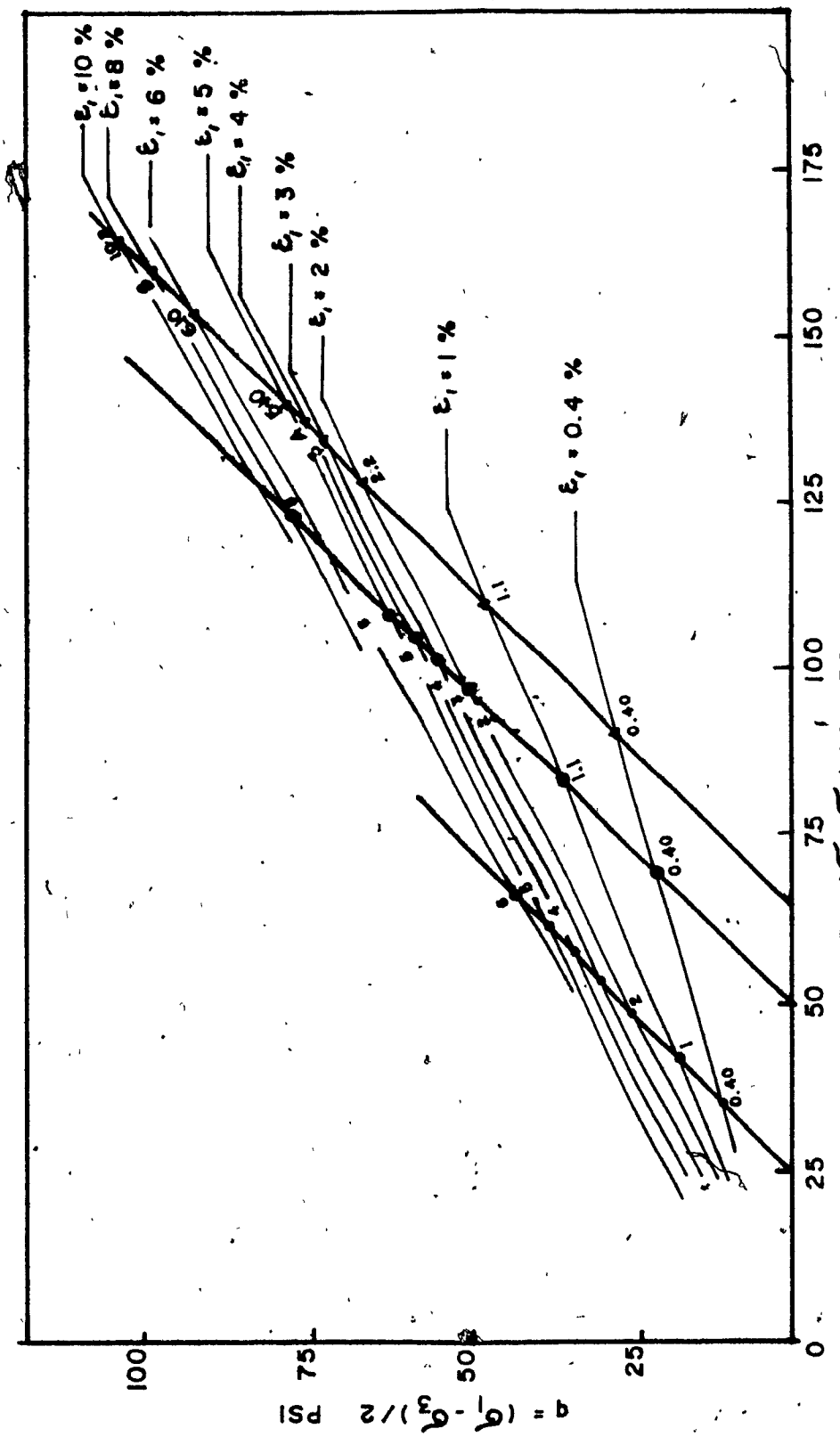

FIG. 5.12 STRESS PATH & AXIAL STRAIN CONTOURS IN TRIAXIAL COMPRESSION TEST FOR MEDIUM-DENSE (SAND "C")

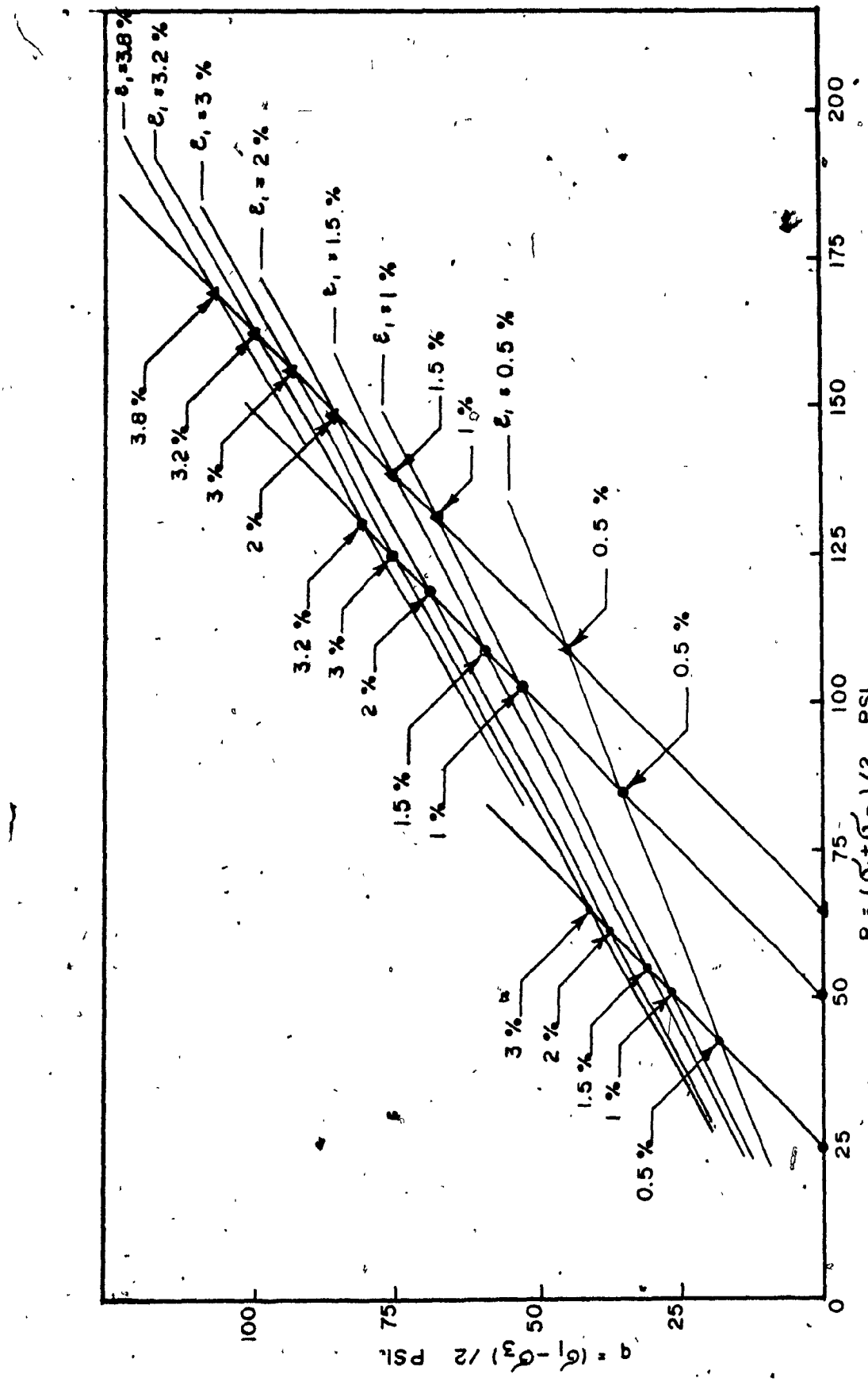

FIG. 5.13 STRESS - PATH & AXIAL STRAIN CONTOURS IN TRIAXIAL COMPRESSION TESTS FOR DENSE SAND (SAND "A")

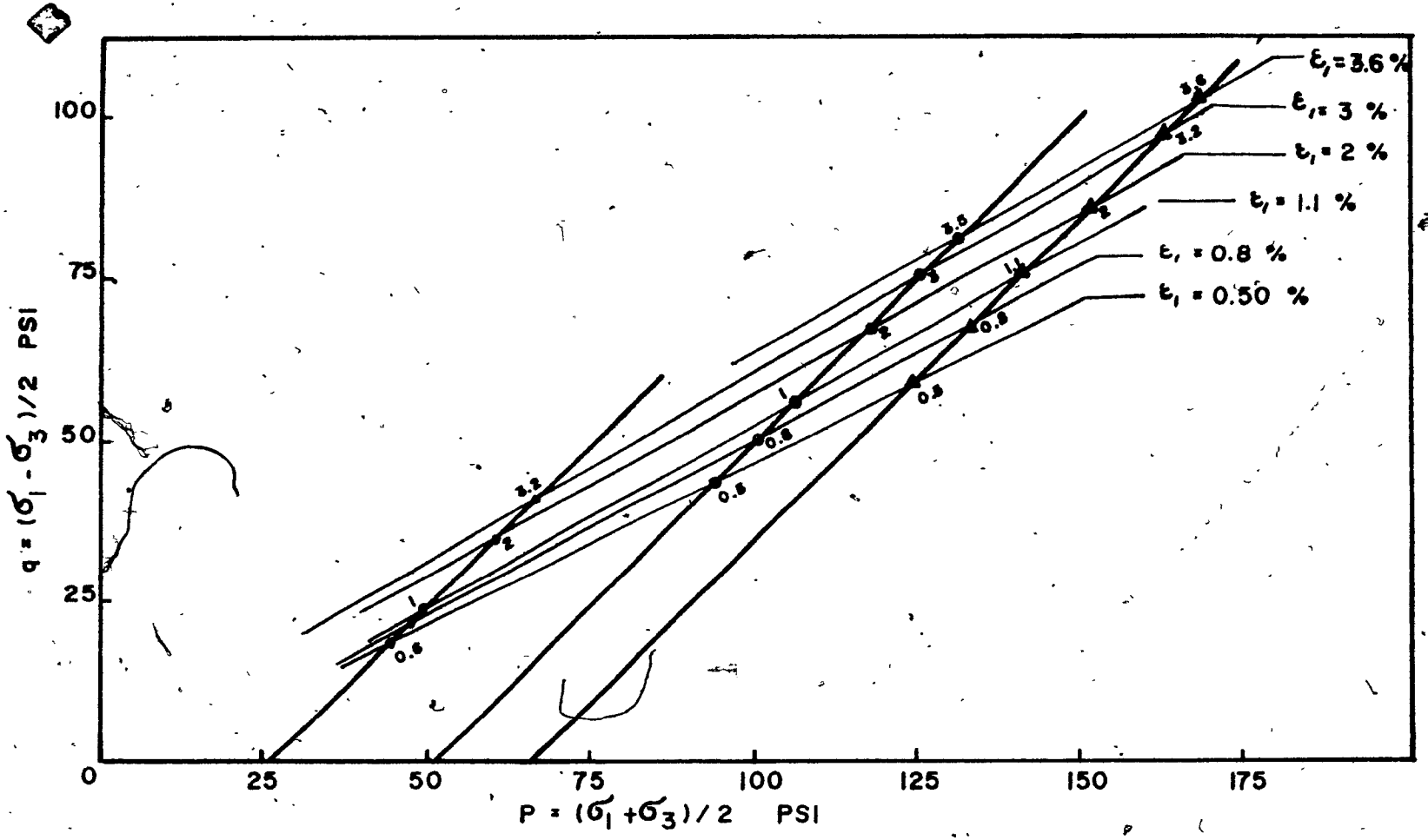

FIG. 5.14 STRESS PATH & AXIAL STRAIN CONTOURS IN TRIAXIAL COMPRESSION TEST FOR DENSE SAND (SAND "B")

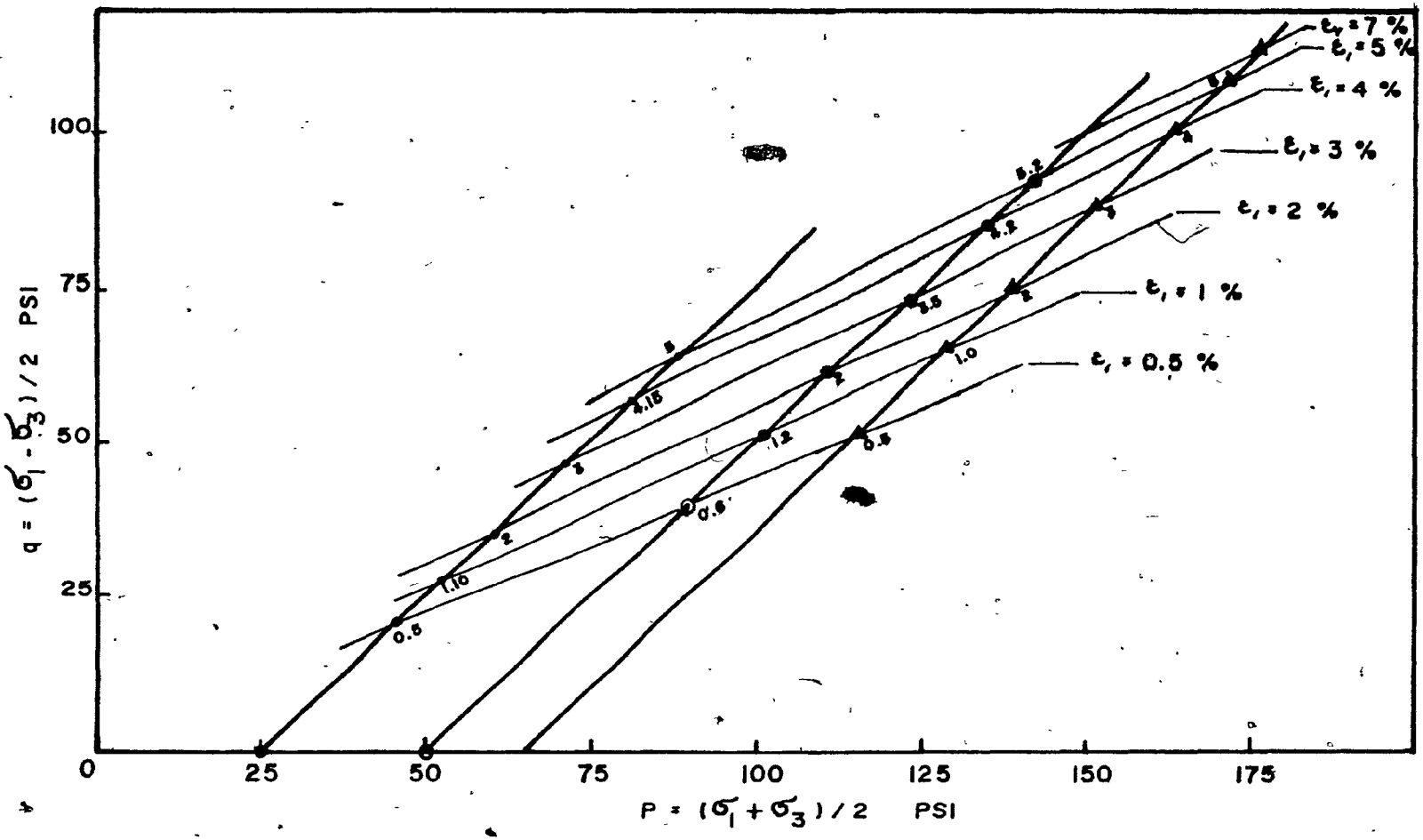

FIG. 5.15 STRESS PATH & AXIAL STRAIN CONTOURS IN TRIAXIAL COMPRESSION TEST FOR DENSE SAND (SAND "C")

ϕ_f = Rowe's friction angle.

σ_1/σ_3 = Stress-ratio.

The value of the interlocking paramter, α at failure, deduced from the present investigation are given below.

Referring to the test results given in figure 4.1:

At confining stress (σ_3) = 25 psi

$$\tan \alpha = [3.66 \ (1 + \frac{0.010}{0.032})]^{1/2}$$

$$= 2.192$$

therefore

$$\alpha = 65.48 \text{ degrees}$$

Similarly

At confining stress (σ_3) = 50 psi:

The interlocking parameter (α) = 64.30 degrees

and

At confining stress (σ_3) = 65 psi;

The interlocking parameter (α) = 62.93 degrees.

where, it can be noted that the interlocking between the particles increases with a decrease of the applied confining stress.

The interlocking parameter α, for the different types of sand tested in triaxial compression tests, is summaried in table 5.7 and presented in graphical form in figures 5.16 and 5.17.

Table 5.7

Interlocking Parameter α, in Triaxial Compression Tests At Failure

Test Number	Stress ratio σ_1/σ_3	Volumetric Strain $\frac{\Delta V}{V}$ %	Axial Strain ε_1 %	tan α	α (degrees)	Dilation Factor $(1 - \frac{dv}{d\varepsilon_1})$	Remarks
A-M-1	3.66	+1	3.2	2.190	65.48	1.313	Medium dense sand
A-M-2	3.60	+0.80	4	2.078	64.30	1.20	" "
A-M-3	3.48	+0.50	5	1.957	62.93	1.10	" "
A-M-4	3.88	+1.60	2.95	2.44	67.75	1.54	" "
A-M-5	3.66	+1.3	3.85	2.215	65.70	1.34	" "
A-M-6	3.45	+1.20	4.50	2.087	64.40	1.27	" "
A-D-1	4.40	+2.10	2.80	2.507	68.25	1.75	Dense sand
A-D-2	4	+1.92	3.20	2.29	66.42	1.60	" "
A-D-3	3.85	+0.90	3.80	2.18	65.40	1.45	" "
B-M-1	4.40	1.20	3.7	2.41	67.50	1.32	Medium Dense sand

Table 5.7

Interlocking Parameter α, in Triaxial Compression Tests at Failure

Test Number	Stress ratio σ_1/σ_3	Volumetric Strain $\frac{\Delta V}{V}$ %	Axial Strain ε_1 %	tan α	α (degrees)	Dilation Factor $(1 - \frac{dv}{d\varepsilon_1})$	Remarks
B-M-2	4.40	1.10	4.40	2.23	65.85	1.32	Medium dense sand
B-M-3	3.85	1.00	4.80	2.157	65.13	1.20	" "
B-M-4	5	0.65	6.50	2.34	66.90	1.10	" "
B-M-5	3.54	0.40	8	1.929	62.60	1.05	" "
B-D-1	4.07	+1.50	3.25	2.438	67.70	1.46	Dense sand
B-D-2	4.25	+1.30	3.50	2.41	67.50	1.37	" "
B-D-3	4.09	+1.25	3.60	2.356	67	1.35	" "
B-D-4	3.30	+1.20	2.95	2.145	65	1.40	" "
B-D-5	4.27	+1.35	3.50	2.445	67.75	1.40	" "
C-M-1	3.92	+1.80	6	2.246	66	1.30	Medium dense sand

Table 5-7

Interlocking Parameter α, in Triaxial Compression Tests at Failure

Test Number	Stress ratio σ_1/σ_3	Volumetric Strain $\frac{\Delta V}{V}$ %	Axial Strain ε_1 %	tan α	α (degrees)	Dilation Factor $(1 - \frac{dv}{d\varepsilon_1})$	Remarks
C-M-2	3.71	+1.60	9	2.087	64.40	1.18	" "
C-M-3	3.72	+1.40	10	2.059	64.10	1.14	" "
C-M-4	6.48	+2.75	5.50	2.078	64.30	1.50	" "
C-M-5	4.10	+1.70	8.40	2.22	65.75	1.20	" "
C-M-6	4.12	+1.75	8.65	2.225	65.80	1.20	" "
C-D-1	5.56	+3.25	5	3.024	1.70	1.65	Dense Sand
C-D-2	4.40	+3.00	5.50	2.76	70.10	1.55	" "
C-D-3	4.60	+2.95	7.00	2.63	69.16	1.42	" "
C-D-4	5.82	+3.50	4.50	3.21	72.70	1.78	" "
C-D-5	4.82	+3.00	5	2.777	70.10	1.60	" "
C-D-6	4.86	+4.94	5.20	3.078	72	1.95	" "

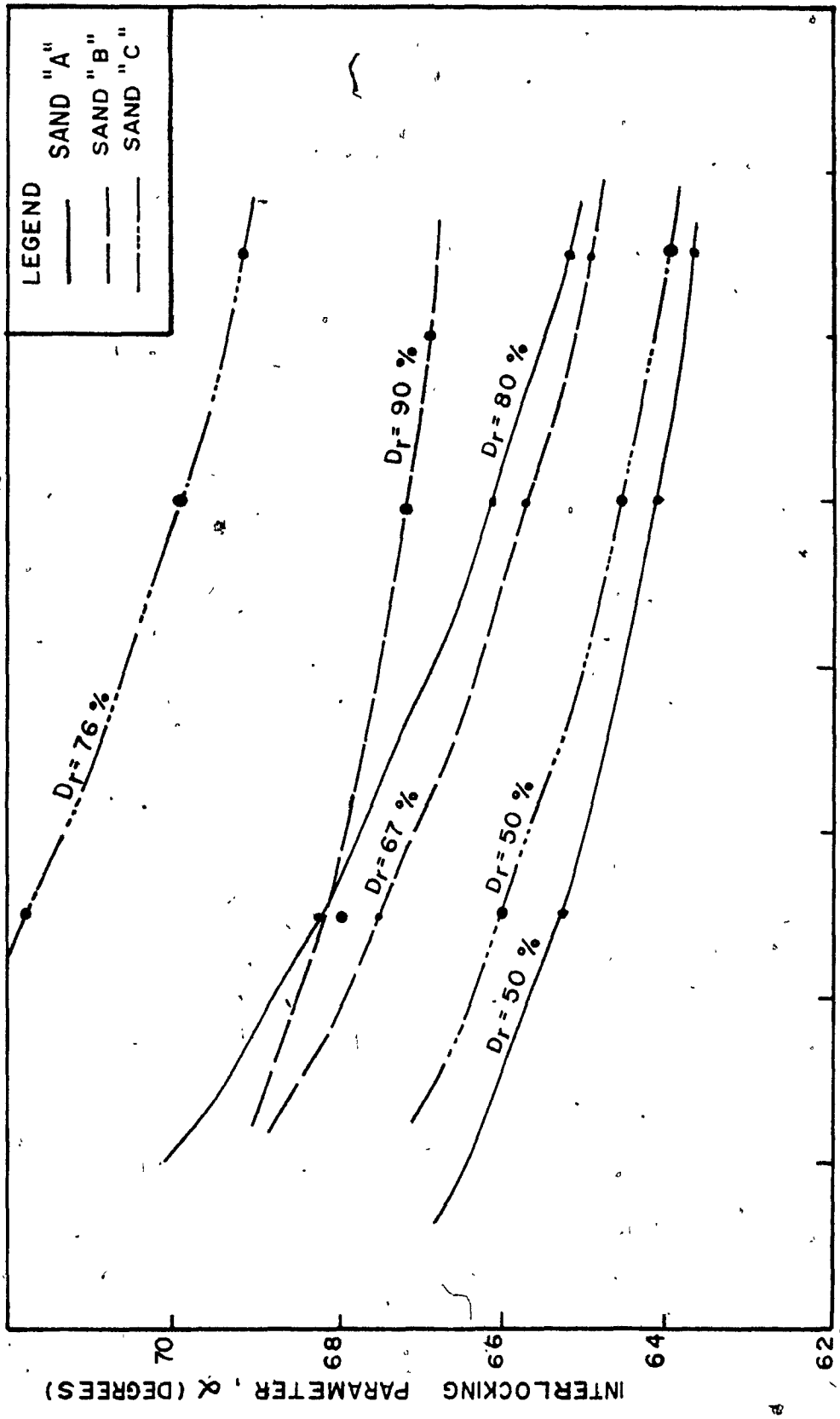

FIG. 5.16 INTERLOCKING IN TRIAXIAL COMPRESSION TESTS

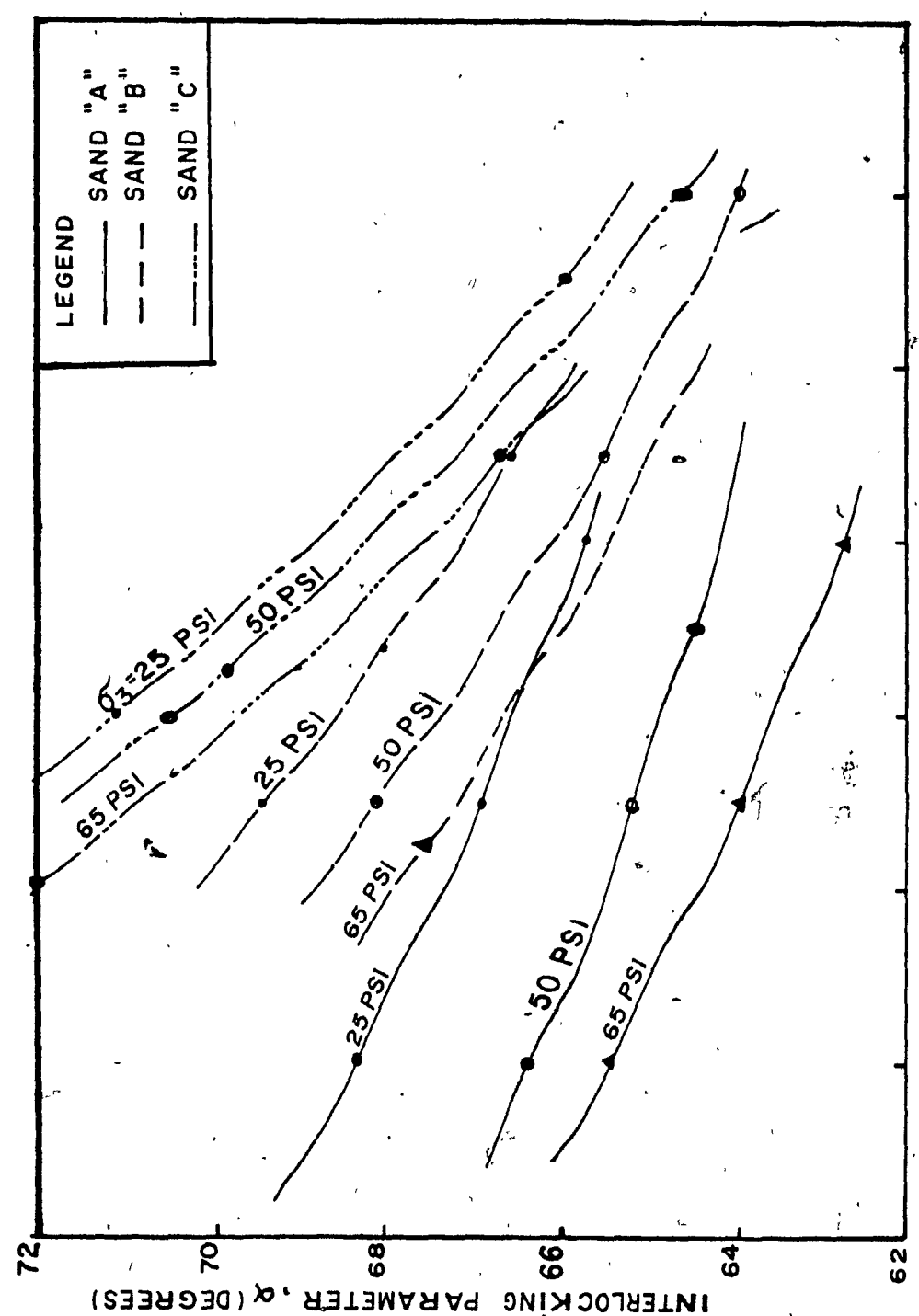

FIG. 5.17 INTERLOCKING IN TRIAXIAL COMPRESSION TESTS

From these figures, it may be noted that the interlocking parameter α, decreases with an increase the confining pressure, because the particles become flattened at the points of contact, sharp corners are crushed, and particles break. Also, an increase in the relative density increased the degree of interlocking. The interlocking between the particles of sand C was greater than those of sand A and B, which is related to the greatest effect of grading and angularity of the particles.

To examine the influence of the angularity, grading and grain size on the strength response, it has been shown, after Sowers and Sowers, 1951 and 1970, that the particle shape and grading has an effect on the angle of shearing resistance of cohesionless soils.

In the present investigation, the particle shape and grading were as follows: rounded and uniform for sand "A", angular and uniform for sand B, and angular and well graded for sand C. The values of the angle of shearing resistance (ϕ) obtained from the triaxial compression tests were in agreement with the values given in table 5.8.

Also, the effect of the grain size on the strength or the frictional angle "ϕ_u" has been examined by Rowe, (1962). His conclusion was indicated in figures 2.2. From this figure, it can be observed that, the value of "ϕ_u" increases with the decrease of the grain size, given a similar uniformity coefficient value.

The average grain size D_{50} for the sand used in this investigation was 0.30 mm for sand A and 0.60 mm for both sand B and C. The corresponding values of ϕ_u would be 25, 23 and 23 degrees respectively, according to Rowe (1962), as shown in figure 2.2. The values of ϕ_{cv} (Coulomb friction angle at constant volume), as found from the analysis of test

TABLE 5.8

Effect of Grading and Angularity
on the Angle of Shearing Resistance
(After Sowers and Sowers, 1951 and 1970)

Sand	Shape and Grading	Theoretical Value		Experimental Value
		Loose	Dense	Dense
A	Rounded, Uniform	30°	37°	39°
	Rounded, Well-Graded	34°	40°	-
B	Angular, Uniform	35°	43°	39.5°
C	Angular, Well-Graded	39°	45°	45°

results and shown in figure 5.18, for sand A, B and C, were 33, and 32.5 and 34.5 degrees, respectively.

By using the empirical formula derived by Bishop (1954),

$$\text{Sin } \phi_{cv} = \frac{15 \tan \phi_u}{10 + 3 \tan \phi_u} \qquad (2.54)$$

then, the frictional angle "ϕ_u", was 22.20, 22 and 23 degrees, in respect to sand A, B and C.

Hence, we can say that the value of "ϕ_u" for sand used in the test series was in agreement with Rowe (1962).

5.1.2.4 Strength and Energy Components

The strength components of the cohesionless soils, as proposed by Rowe (1962), are:

1. Strength component due to frictional resistance.
2. Strength component developed by the energy required to rearrange the soil particles.
3. Strength component developed by the energy required to cause expansion or dilation against the confining stress.

To analyse the strength components of the sand used during this investigation, the experimental results, are presented in graphical form in figures 5.19 to 5.21, in terms of the Coulomb friction angle, ϕ, and the Rowe friction angle, ϕ_f.

The values of Rowe friction angle "ϕ_f" at failure were obtained from the expression derived by Rowe (1962), as:

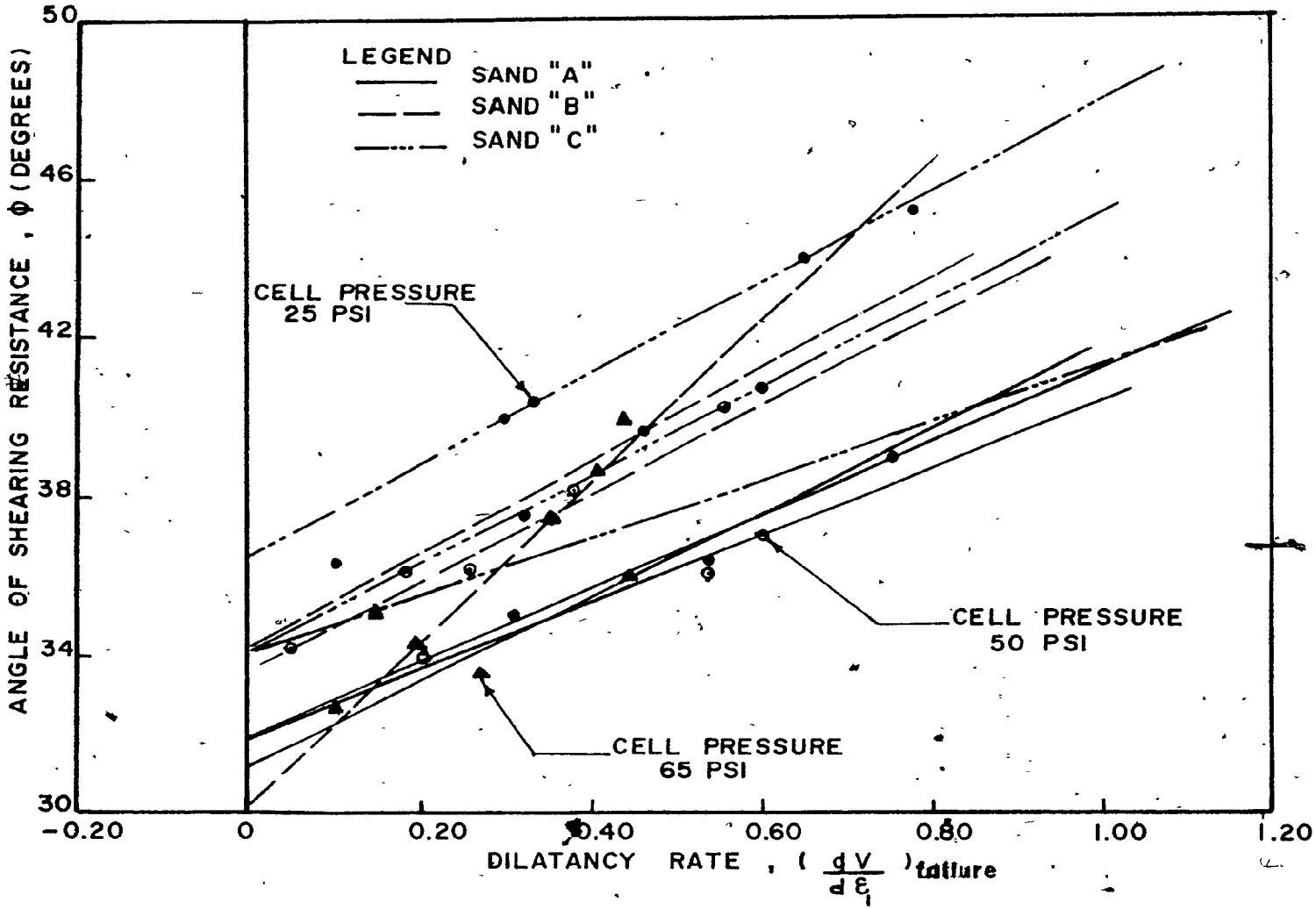

FIG. 5.18 ANGLE OF SHEARING RESISTANCE VS DILATANCY RATE AT FAILURE

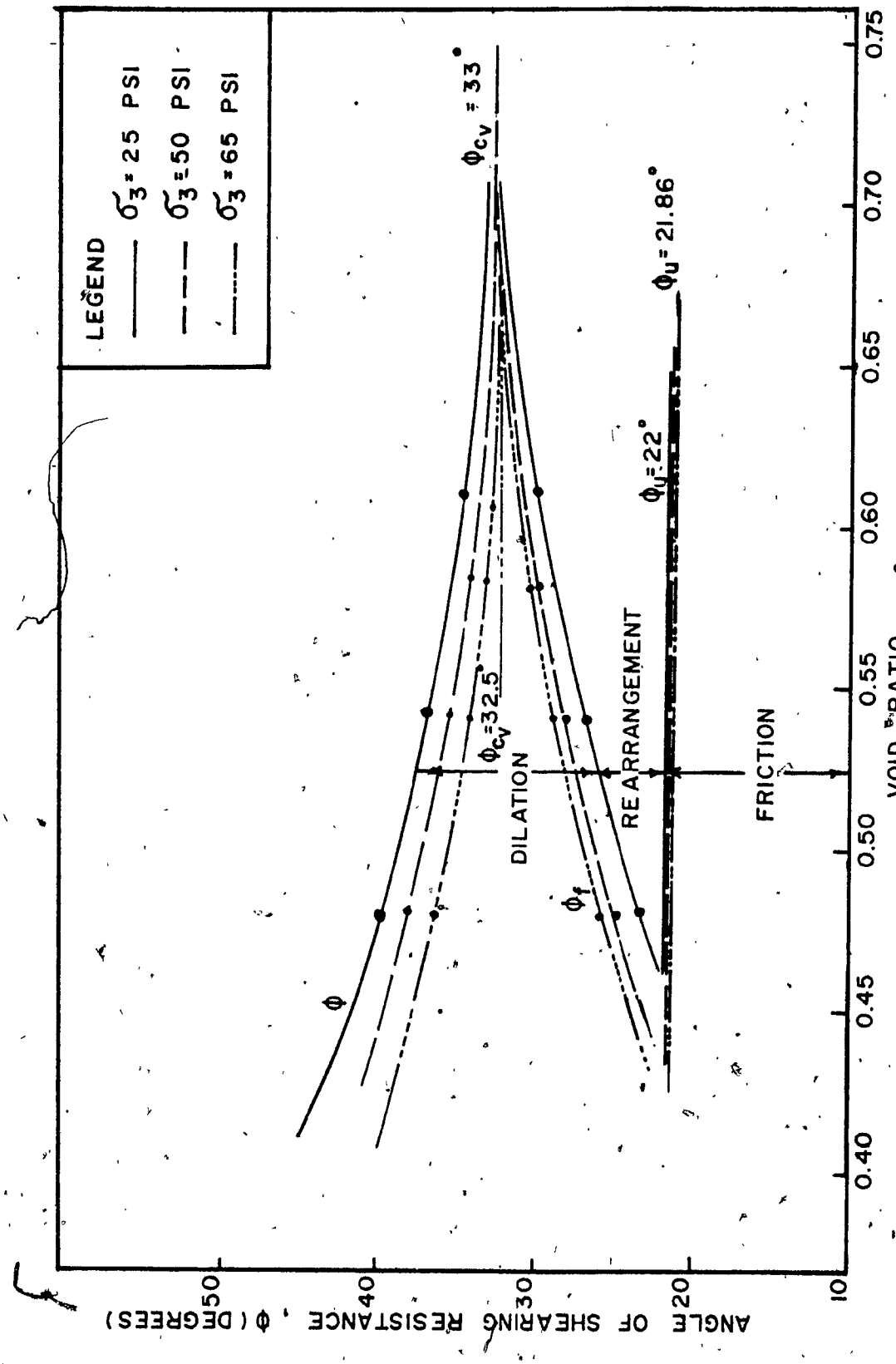

FIG. 5.19 RELATIONSHIP BETWEEN VARIOUS FRICTION ANGLES & VOID RATIO FOR SAND "A"

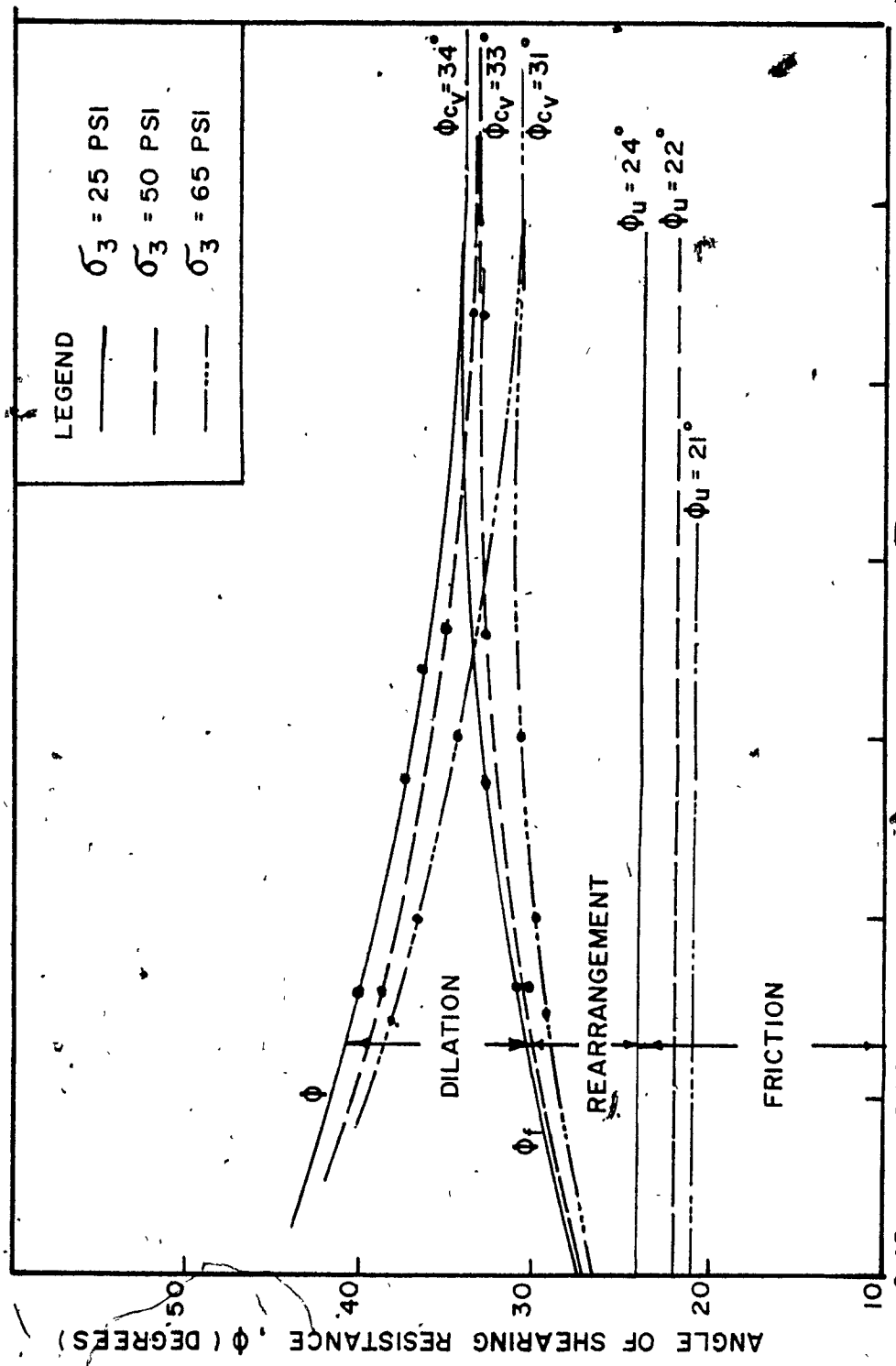

FIG. 5. 20 RELATIONSHIP BETWEEN VARIOUS FRICTION ANGLES & VOID RATIO FOR SAND "B"

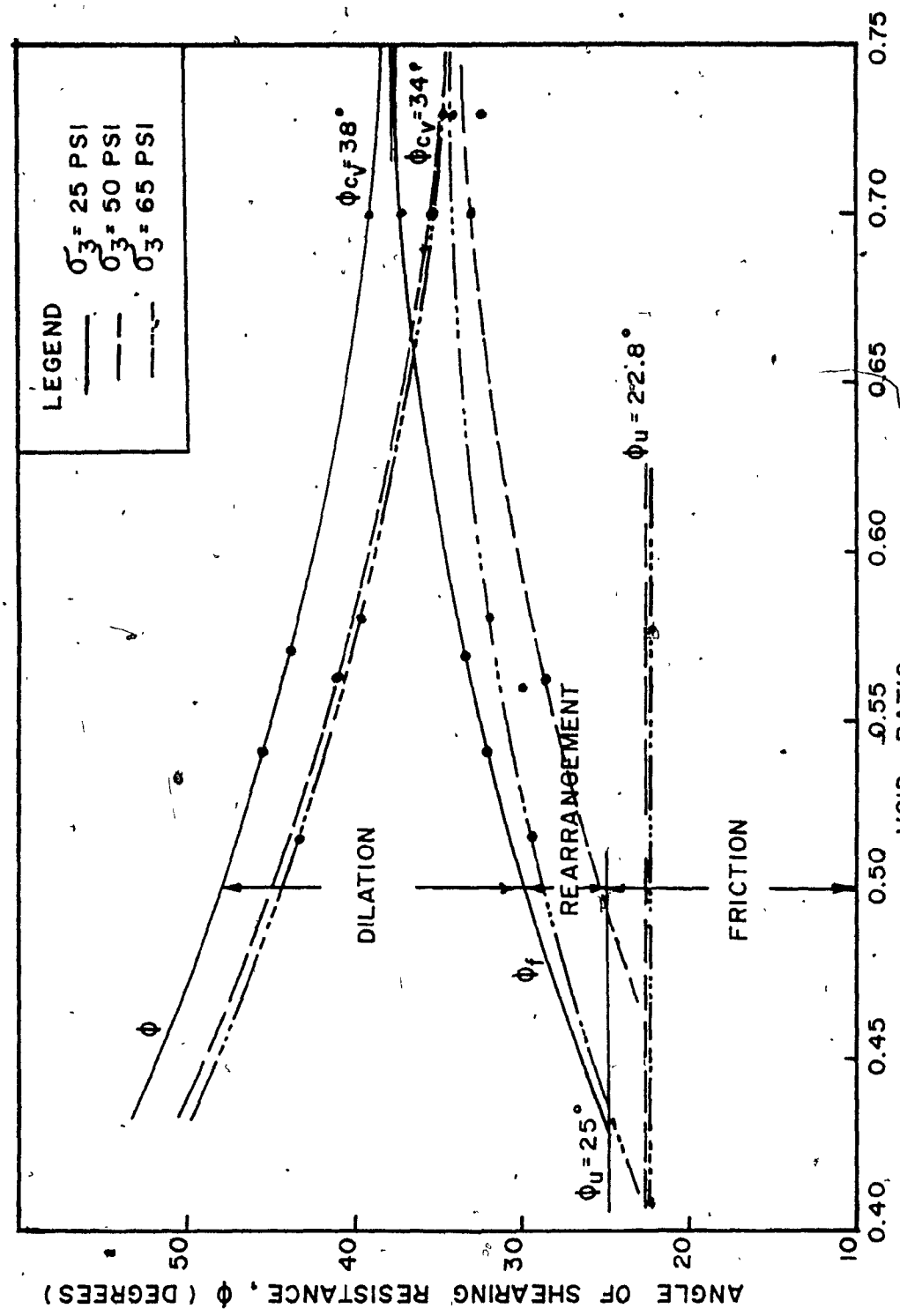

FIG. 5.21 RELATIONSHIP BETWEEN VARIOUS FRICTION ANGLES & VOID RATIO FOR SAND "9"

$$\tan^2 (45° + \frac{1}{2} \phi_f) = \frac{\sigma_1}{\sigma_3 [1 - (\frac{dV}{d\varepsilon_1})]} \qquad (2.21)$$

where

σ_1/σ_3 : the stress ratio

$1 - \frac{dv}{d\varepsilon_1}$: the dilatancy factor.

Sample calculations of Rowe's frictional angle "ϕ_f" at failure, for the tests conducted on sand "A", are given below:

1. Test No. A.M.1

$\sigma_1/\sigma_3 = 3.66$, e = 0.61 , $\frac{\Delta V}{V} = +1\%$ and

$\varepsilon_1 = 3.2\%$

then

$$\tan^2 (45° + \phi_f/2) = \frac{3.66}{[1 + (\frac{0.010}{0.032})]}$$

$$= 2.789$$

ϕ_f = 28.17 degrees

2. Test No. A.D.1

$\sigma_1/\sigma_3 = 4.40$, e = 0.48 , $\frac{\Delta V}{V} = +2.10\%$ and

$\varepsilon_1 = 2.80\%$

then

ϕ_f = 25.40 degrees.

where it can be noted the frictional angle "ϕ_f" increases with the decreasing of the density.

from the relationships plotted in figures 5.19 to 5.21, it can be seen

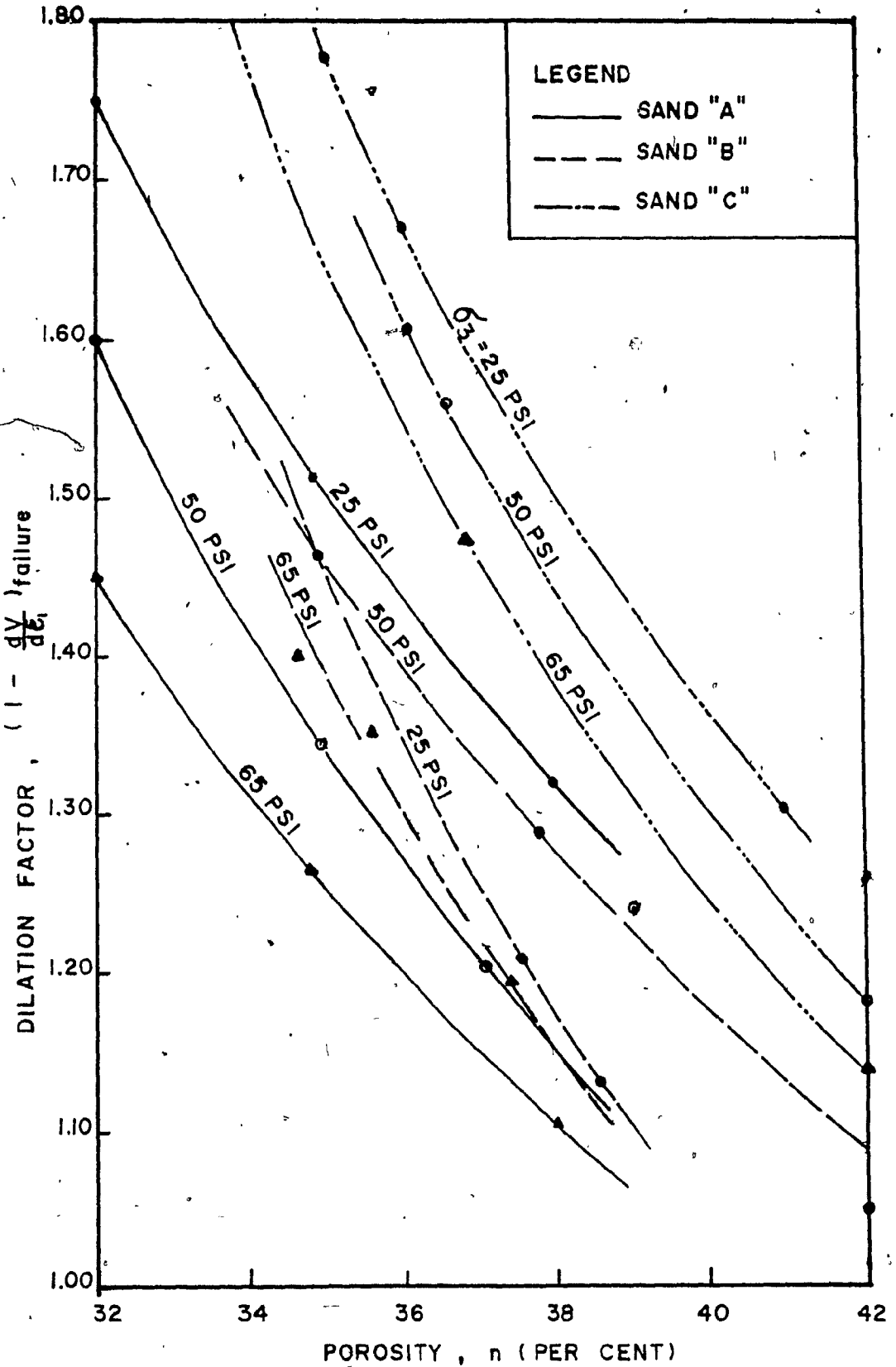

FIG. 5.22 DILATION FACTOR VS POROSITY IN TRIAXIAL COMPRESSION TESTS

that the strength parameter "ϕ" represents the sum of three contributions: ϕ_u, the frictional resistance at contacts; particle rearrangements; and finally, dilation. All friction angles approach ϕ_{cv} (ϕ at constant volume) at the maximum void ratio; Hence, ϕ_{cv} is an upper bound for ϕ_f and lower bound for ϕ. The value of ϕ_f decreases with increasing the dilatancy and has a minimum value equal to the friction angle, ϕ_u, between particle surfaces. The magnitude of difference between ϕ_f and ϕ_u increases with increasing void ratio and is considered as energy expended in the process of rearrangement.

Figure 5.22 shows the relationship between the dilation factor $(1 - \frac{dv}{d\varepsilon_1})$ and the porosity. From this figure, it can be observed that the dilation factor increases with decreasing the porosity and in turn increases the energy required for expansion against the confining stress.

The total work done during the application of the principal stresses to the sand samples tested in triaxial compression tests, can be divided into three main components, as shown from figure 5.23, after the analysis of test data:

1. Internal energy absorbed in friction if no volume change takes place, this is subdivided into two:
   (i) Energy due to interparticle friction angle (ϕ_u).
   (ii) Additional energy absorbed and required to rearrange soil particles.
2. Internal energy absorbed in friction as the mass dilate.

3. External work done during volume change.

The amounts of the rate of energy loss were determined from the expression derived by Rowe (1962), as:

$$K_p = \tan^2 (45° + \phi_f/2) = \frac{\sigma_1}{\sigma_3[1 - (\frac{dv}{d\varepsilon_1})]} \qquad (2.21)$$

and

$$\delta W = \sigma_1 . \Delta\varepsilon_1 + 2\sigma_3 . \Delta\varepsilon_3 \qquad (2.36)$$

Sample calculations of the rates of energy loss in triaxial compression are given below.

Referring to the test results given in figure 4.1:

At confining stress (σ_3) = 50 psi;

σ_1/σ_3 = 3.60; ε_1 = 4% and $\Delta V/V$ = 0.80%

a: $\delta(W_T)$ = the total increment of work applied by the deviator stress to the sample, without any energy corrections

$$= (\sigma_1 - \sigma_3)\Delta\varepsilon_1$$

$$= \sigma_3 . \Delta\varepsilon_1 [K_p(1 - \frac{\Delta V}{\Delta\varepsilon_1}) - 1]$$

then

$$\frac{\delta(W_T)}{\sigma_3 . \Delta\varepsilon_1} = \text{rate of total energy input by deviator stress}$$

$$= [K_p(1 - \frac{\Delta V}{\Delta\varepsilon_1}) - 1]$$

$$\frac{\delta(W_T)}{\sigma_3 . \Delta\varepsilon_1} = \frac{\sigma_1}{\sigma_3} - 1$$

$$= 3.60 - 1 = 2.60$$

b: $\delta(Wi.f.)$ = increment of internal work due to friction

with no dilation

$$\sigma_1 . \Delta\varepsilon_1 + 2\sigma_3 . \Delta\varepsilon_3$$

with no dilation

$$\sigma_1 = \sigma_3 . K_p \quad \text{and} \quad 2\Delta\varepsilon_3 = -\Delta\varepsilon_1$$

whence

$$\delta(W_{i.f.}) = \sigma_3 . \Delta\varepsilon_1 [K_p - 1]$$

then

$$\frac{\delta(W_{i.f.})}{\sigma_3 . \Delta\varepsilon_1} = \text{rate of energy loss due to friction}$$

without dilation

$$= K_p - 1 = \frac{\sigma_1}{\sigma_3[1 - (\frac{\delta V}{\Delta\varepsilon_1})]} - 1$$

$$= \frac{3.60}{1.2} - 1 = 2$$

c: $(W_{i.t.})$ = the total energy absorbed internally when dilation occurs

$$= \sigma_1 . \Delta\varepsilon_1 + 2\sigma_3 . \Delta\varepsilon_3$$

$$= \sigma_3 . \Delta\varepsilon_1 [1 - \frac{\delta V}{\Delta\varepsilon_1}] (K_p - 1)$$

$$= \sigma_3 . \Delta\varepsilon_1 [\frac{\sigma_1}{\sigma_3} - (1 - \frac{\delta V}{\Delta\varepsilon_1})]$$

then

$$\frac{\delta(W_{i.t.})}{\sigma_3 . \Delta\varepsilon_1} = \text{the rate of total energy absorbed internally when dilation occurs}$$

$$\frac{\delta(W_{i.t.})}{\sigma_3 \cdot \Delta\varepsilon_1} = \frac{\sigma_1}{\sigma_3} - (1 - \frac{\delta V}{\Delta\varepsilon_1})$$

$$= 3.60 - 1.2 = 2.40$$

d: $\frac{\delta(W_{i.t.}) - \delta(W_{i.f.})}{\sigma_3 \cdot \Delta\varepsilon_1}$ = additional rate of internal energy loss due to friction with dilation

$$= \frac{\delta V}{\Delta\varepsilon_1} [K_p - 1]$$

$$= 2.4 - 2 = 0.40$$

e: $\frac{\delta(W_T) - \delta(W_{i.t.})}{\sigma_3 \cdot \Delta\varepsilon_1}$ = rate of external energy spent in dilation

$$= - \frac{\delta V}{\Delta\varepsilon_1}$$

$$= + 0.20$$

The components of the rates of energy loss are summarized in table 5.9 and presented in graphical form in figure 5.23.

From this figure, the following comments can be given:

- The energy expended in the process of remolding or rearrangement of the particle assembly, is decreasing with a decrease of the porosity.
- The Coulomb friction angle ϕ corrected for external work only, ϕ_r, increases with decreasing the porosity because of the increasing work done internally due to dilation.

Table 5.9

Rates of Energy Losses in Triaxial Compression Tests

Test Number	Stress ratio (σ_1/σ_3)	Volumetric Strain $(\frac{\Delta V}{V}\ \%)_f$	Axial Strain $(\varepsilon_1\ \%)_f$	Dilation Factor $(1 - \frac{\delta V}{\Delta \varepsilon_1})_f$	$\frac{\delta(W_T)}{\sigma_3.\Delta\varepsilon_1} = (\frac{\sigma_1}{\sigma_3} - 1)$	$\frac{\delta(W_{i.f.})}{\sigma_3.\Delta\varepsilon_1} = \frac{\sigma_1}{\sigma_3[1-(\frac{\delta V}{\Delta\varepsilon_1})]} - 1$	$\frac{\delta(W_{i.t.})}{\sigma_3.\Delta\varepsilon_1} = (\sigma_1/\sigma_3) - (1 - \frac{\delta V}{\Delta\varepsilon_1})$	$\frac{\delta(W_{i.t.})-\delta(W_{i.f.})}{\sigma_3.\Delta\varepsilon_1}$	$\frac{\delta(W_T)-\delta(W_{i.t.})}{\sigma_3.\Delta\varepsilon_1}$
A-M-1	3.66	+1	3.2	1.313	2.66	1.788	2.35	0.562	0.35
A-M-2	3.60	+0.80	4	1.200	2.60	2	2.40	0.40	0.20
A-M-3	3.48	+0.50	5	1.100	2.48	2.165	2.38	0.215	0.10
A-M-4	3.88	+1.60	2.95	1.54	2.88	1.519	2.34	0.821	0.54
A-M-5	3.66	+1.30	3.85	1.34	2.66	1.73	2.32	0.59	0.34
A-M-6	3.45	+1.20	4.50	1.27	2.45	1.716	2.18	0.464	0.27
A-D-1	4.40	+2.10	2.80	1.75	3.40	1.514	2.65	1.14	0.75
A-D-2	4	+1.92	3.20	1.60	3.00	1.5	2.40	0.90	0.60
A-D-3	3.85	+0.90	3.80	1.45	2.85	1.655	2.40	0.745	0.45
B-M-1	4.40	+1.20	3.70	1.32	3.40	2.33	3.08	0.75	0.32
B-M-2	3.98	+1.10	4.40	1.25	2.98	2.18	2.73	0.55	0.25
B-M-3	3.85	+1.00	4.80	1.20	2.85	2.20	2.65	0.45	0.20

Table 5.9

Rates of Energy Losses in Triaxial Compression Tests

Test Number	Stress ratio (σ_1/σ_3)	Volumetric Strain $(\frac{\delta V}{V}\ \%)_f$	Axial Strain $(\varepsilon_1\ \%)_f$	Dilation Factor $(1 - \frac{\delta V}{\Delta \varepsilon_1})_f$	$\frac{\delta(W_T)}{\sigma_3 . \Delta\varepsilon_1} = (\frac{\sigma_1}{\sigma_3} - 1)$	$\frac{\delta(W_{i.f.})}{\sigma_3 . \Delta\varepsilon_1} = \frac{\sigma_1}{\sigma_3[1-(\frac{\delta V}{\Delta\varepsilon_1})]} - 1$	$\frac{\delta(W_{i.t})}{\sigma_3 . \Delta\varepsilon_1}$ $(\sigma_1/\sigma_3) - (1 - \frac{\delta V}{\Delta\varepsilon_1})$	$\frac{\delta(W_{i.t.}) - \delta(W_{i.f.})}{\sigma_3 . \Delta\varepsilon_1}$	$\frac{\delta(W_T) - \delta(W_{i.t.})}{\sigma_3 . \Delta\varepsilon_1}$
B-M-4	5	+0.65	6.50	1.10	4	3.545	3.90	0.355	0.10
B-M-5	3.54	+0.40	8	1.05	2.54	2.37	2.49	0.12	0.05
B-D-1	4.07	+1.50	3.25	1.46	3.07	1.788	2.61	0.82	0.46
B-D-2	4.25	+1.30	3.50	1.37	3.25	2.10	2.88	0.78	0.37
B-D-3	4.09	+1.25	3.60	1.35	3.09	2.03	2.74	0.71	0.35
B-D-4	3.30	+1.20	2.95	1.40	2.30	1.36	1.90	0.54	0.40
B-D-5	4.27	+1.35	3.50	1.40	3.27	2.05	2.87	0.82	0.40
C-M-1	3.92	+1.80	6	1.30	2.92	2.02	2.62	0.60	0.30
C-M-2	3.71	+1.60	9	1.18	2.71	2.14	2.53	0.39	0.18
C-M-3	3.72	+1.40	10	1.14	2.72	2.26	2.58	0.32	0.14
C-M-4	6.48	+2.75	5.50	1.50	5.48	2.32	4.98	2.66	0.50
C-M-5	4.10	+1.70	8.40	1.20	3.10	2.42	2.90	0.48	0.20
C-M-6	4.12	+1.75	8.65	1.20	3.12	2.43	2.90	0.47	0.22

Table 5.9

Rates of Energy Losses in Triaxial Compression Tests

Test Number	Stress ratio (σ_1/σ_3)	Volumetric Strain $(\frac{\delta V}{V}\ \%)_f$	Axial Strain $(\varepsilon_1\ \%)_f$	Dilation Factor $(1 - \frac{\delta V}{\Delta\varepsilon_1})_f$	$\frac{\delta(W_T)}{\sigma_3.\Delta\varepsilon_1} = \frac{\sigma_1}{\sigma_3}(\frac{\sigma_1}{\sigma_3} - 1)$	$\frac{\delta(W_{i.f.})}{\sigma_3.\Delta\varepsilon_1} = \frac{\sigma_1}{\sigma_3[1-(\frac{\delta V}{\Delta\varepsilon_1})]} - 1$	$\frac{\delta(W_{i.t.})}{\sigma_3.\Delta\varepsilon_1}$ $(\sigma_1/\sigma_3) - (1 - \frac{\delta V}{\Delta\varepsilon_1})$	$\frac{\delta(W_{i.t.})-\delta(W_{i.f.})}{\sigma_3.\Delta\varepsilon_1}$	$\frac{\delta(W_T)-\delta(W_{i.t.})}{\sigma_3.\Delta\varepsilon_1}$
C-D-1	5.56	+3.25	5.00	1.65	4.56	2.37	3.91	1.54	0.65
C-D-2	4.40	+3.00	5.50	1.55	3.40	1.84	2.85	1.01	0.55
C-D-3	4.60	+2.95	7.00	1.42	3.60	2.24	3.18	0.94	0.42
C-D-4	5.82	+3.50	4.50	1.78	4.82	2.27	4.04	1.77	0.78
C-D-5	4.82	+3.0	5	1.60	3.82	2.01	3.22	1.21	0.60
C-D-6	4.86	+4.94	5.20	1.95	3.86	1.49	2.91	1.42	0.95

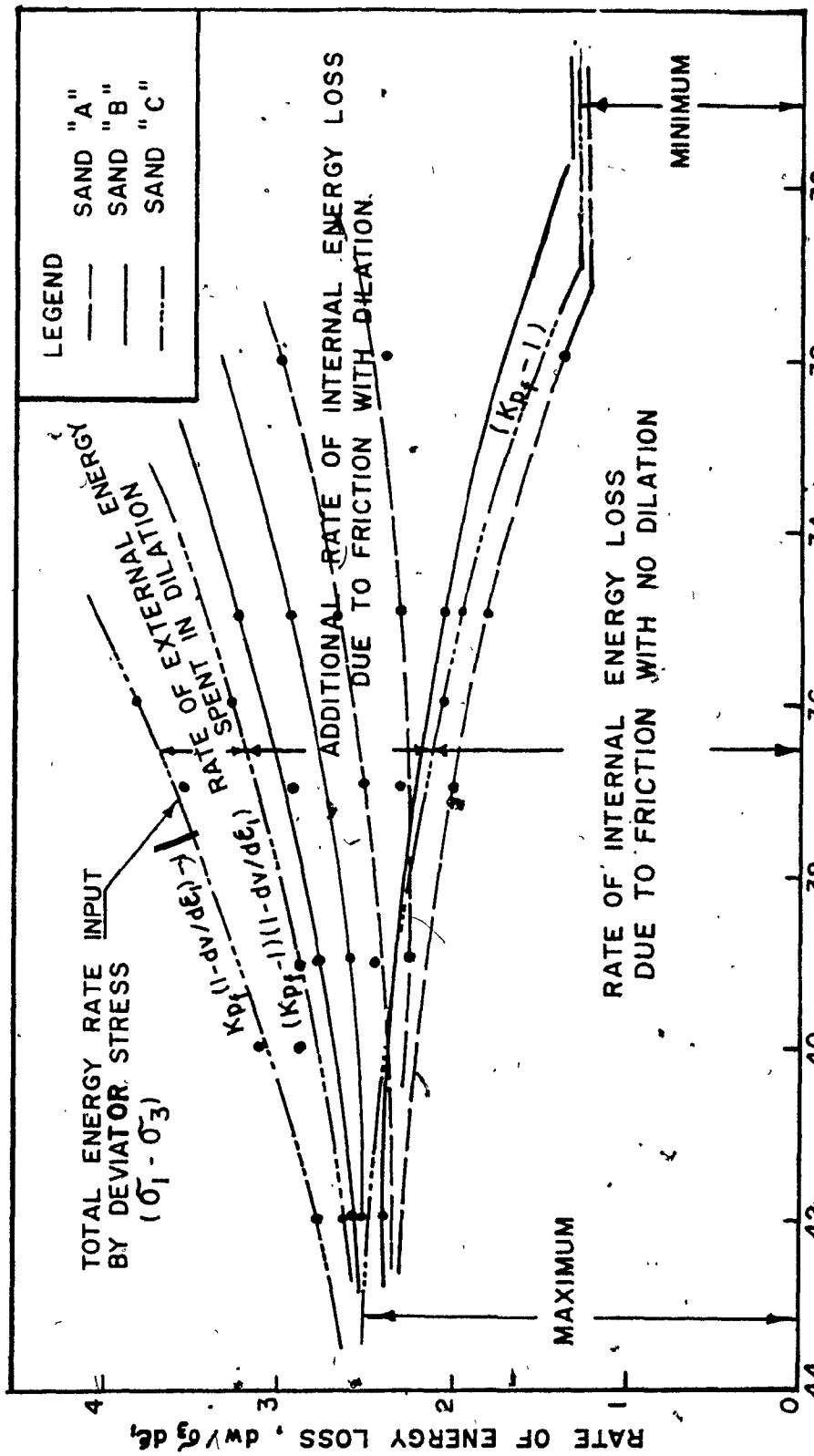

FIG. 5.23 COMPONENTS OF ENERGY LOSS IN TRIAXIAL COMPRESSION TESTS AT CELL PRESSURE OF 50 PSI

- The difference between the Coulomb friction angle, corrected for external work only, ϕ_r, and the one corrected for both external work and additional internal work due to dilatancy, ϕ_f, was increasing with a decrease of the porosity. The magnitude of the difference is negligible at the critical state where the dilation is nil. Also, the total energy rate input by the deviator stress for sand C is greater than those for sand A and B, due to the higher degree of interlocking.

5.2 Direct Shear Box Tests

5.2.1 General

The test results of this group are summarized in tables 4.4 to 4.6 and presented in graphical form in figures 4.10 to 4.16. In this chapter, these test results are also represented in graphical form in figure 5.24 to 5.27. Figure 5.24 shows a plot of the shear stress versus the normal stress at failure for the three types of the sand tested at different relative densities. From this figure, it may be noted that the shear stress at failure increases with an increase of the normal stress, and also, with an increase of the relative density of the samples tested at the same normal stress.

Figure 5.25 shows the relationship of the angle of shearing resistance against the normal stress at different relative densities. From this figure, it can be seen that the angle of shearing resistance (ϕ), decreases with an increase of the normal stress for the sand samples tested at the same density. An increase of the normal stress, decreases the degree of

interlocking, because the particles become flattened at the points of contact, sharp corners are crushed, and particles break.

The variation of the angle of shearing resistance (ϕ), is also presented against the porosity in figure 5.26. From this figure, it can be observed that the angle of shearing resistance was increasing with the decrease of the porosity of the sand samples tested at the same normal stress. That can be explained as: the energy that is put into a soil by the external load is expanded in two ways: to overcome the frictional resistance between the particles and to expand the soil against the normal stress. The denser the sand, the greater the expansion which tends to take place during shear. Hence, more energy (more force and a higher friction angle) must be expanded to shear the soil. Also, from the figure, it can be observed that the value of the strength paramter, ϕ, for sand C was greater than those for sand A and B, tested at the same conditions. The higher degree of angularity in sand C, increased the degree of interlocking between the particles and in its turn increased the angle of shearing resistance.

Figure 5.27, shows a plot of the horizontal displacement versus the porosity of the sand A, B and C tested at different normal stresses. From this figure, it can be seen that the shear displacement at failure increased with an increase of the porosity and the applied normal stress.

5.2.2 Strength Components

The strength components of the sand tested in direct shear tests, are given as follows:

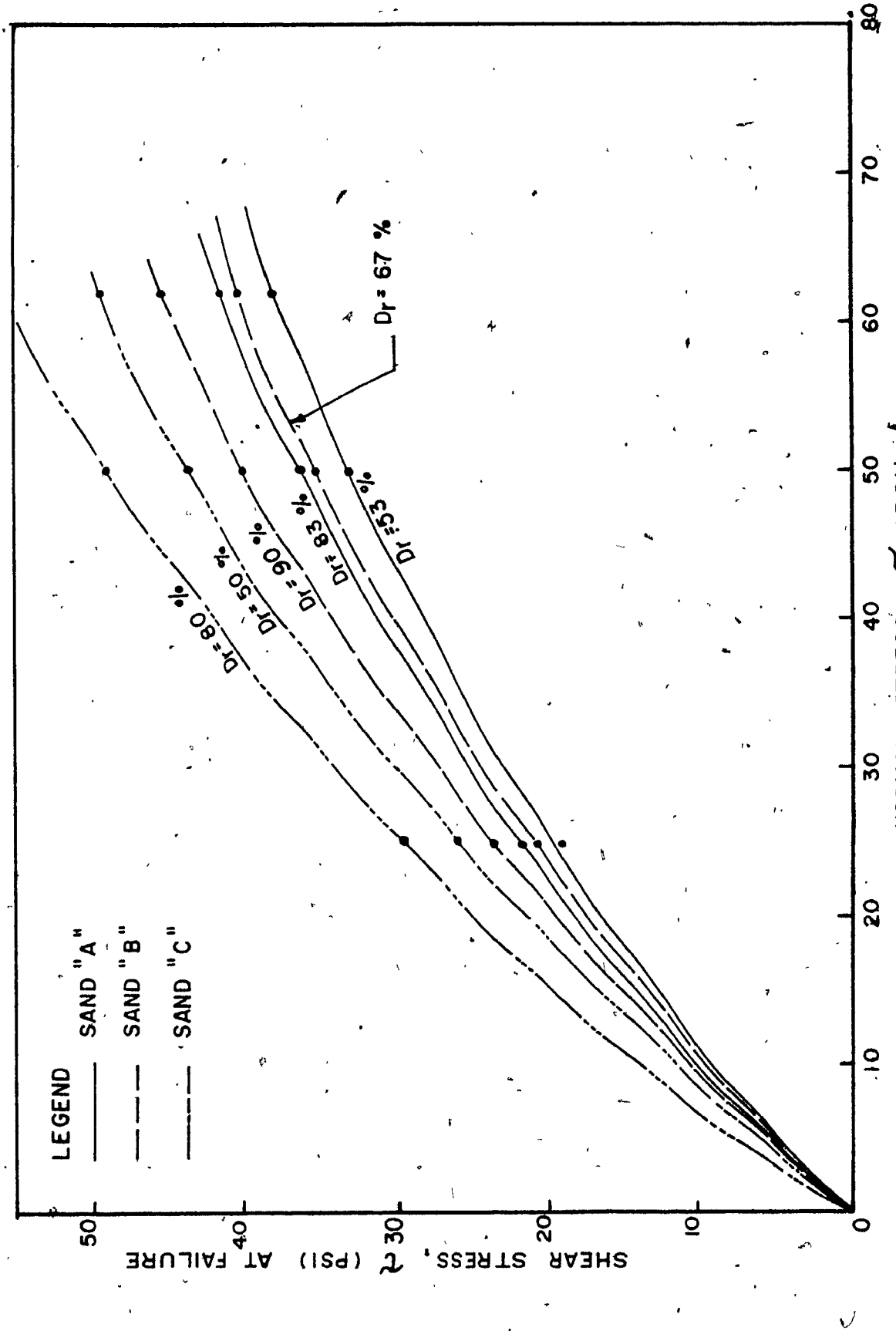

FIG. 5.24 NORMAL STRESS VS SHEAR STRESS IN DIRECT SHEAR TESTS

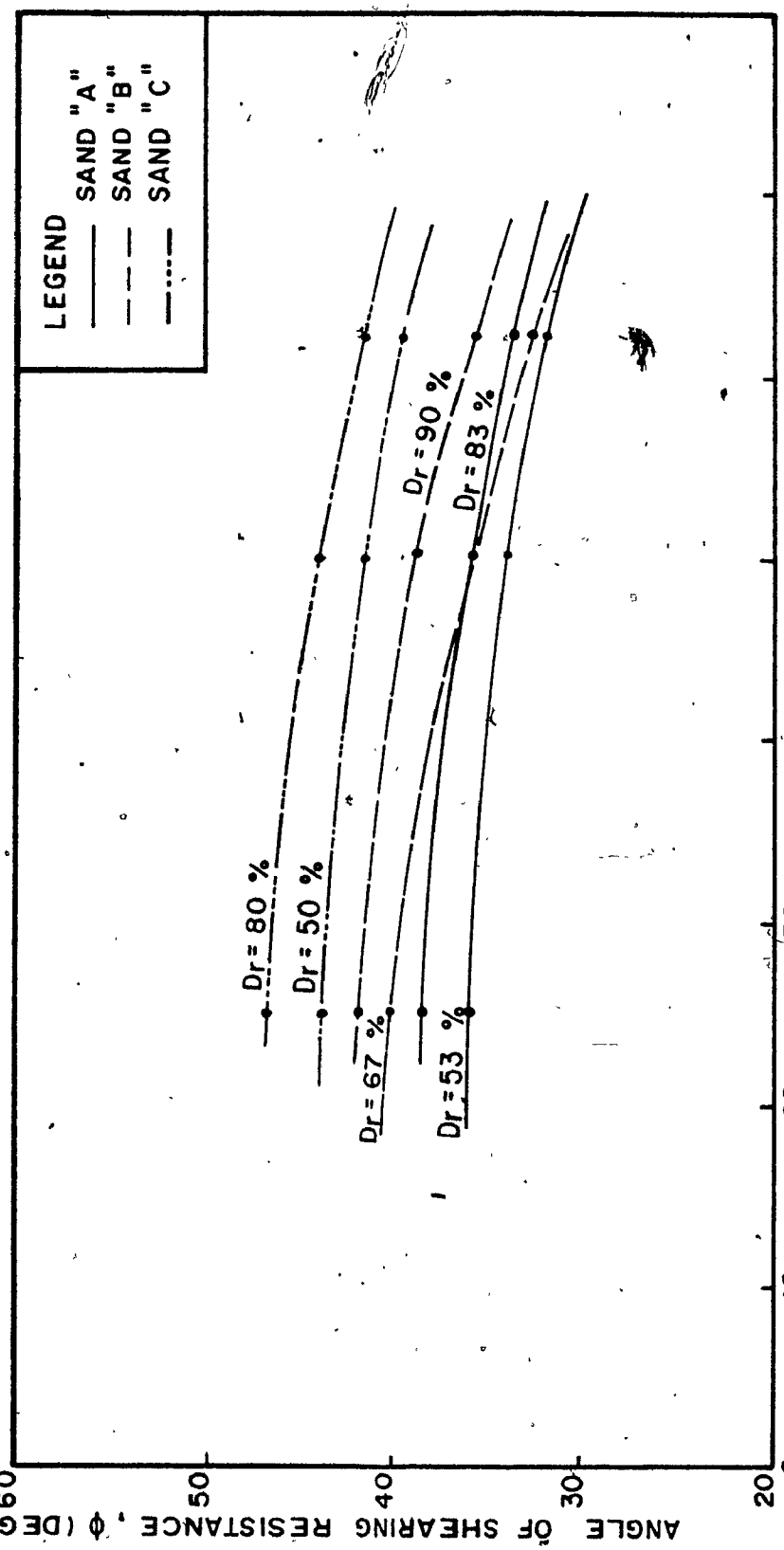

FIG. 5.25 ANGLE OF SHEARING RESISTANCE IN DIRECT SHEAR TESTS VS NORMAL STRESS

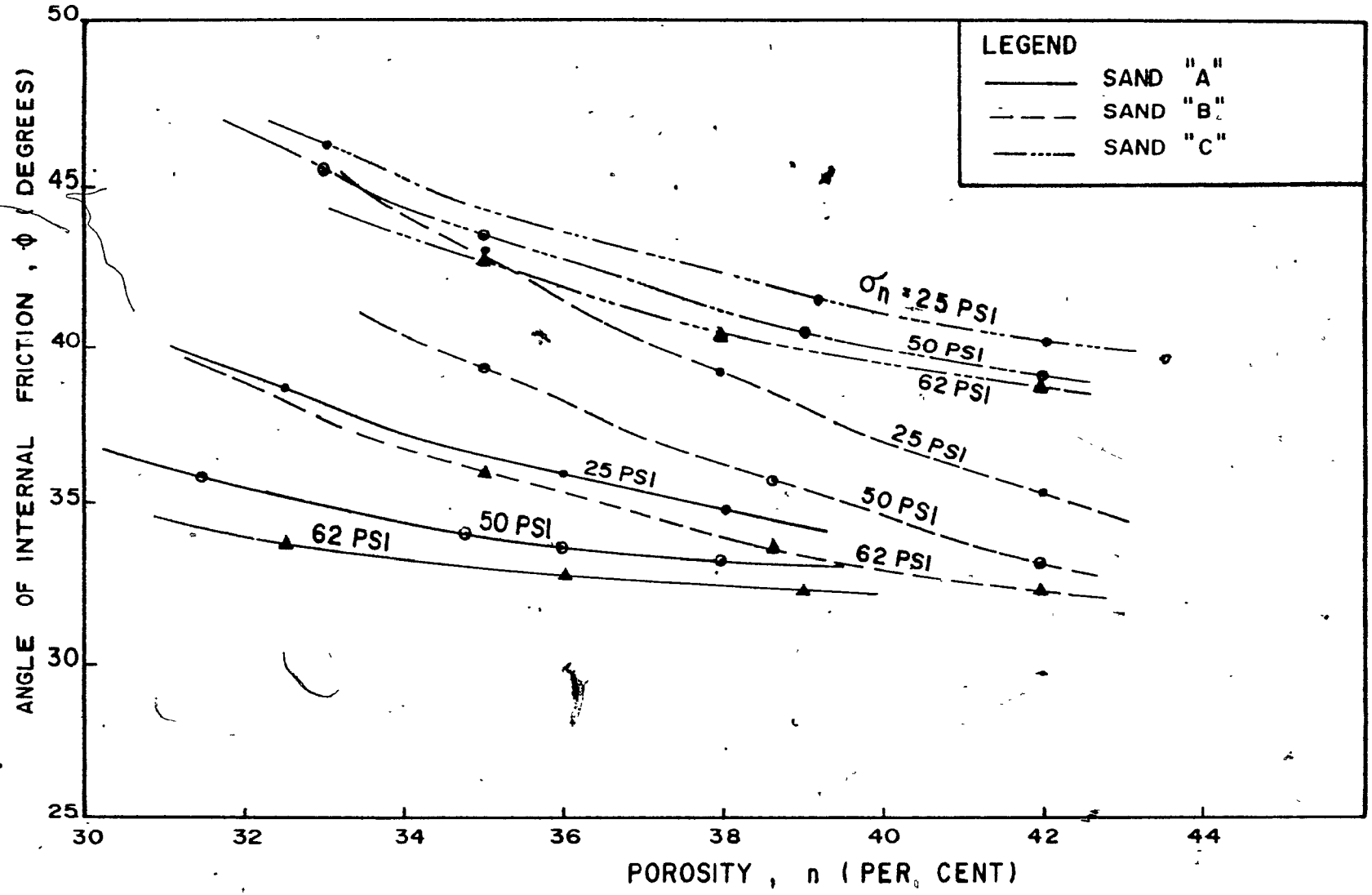

FIG. 5.26 ANGLE OF INTERNAL FRICTION AT VARIOUS NORMAL STRESSES IN DIRECT SHEAR TESTS VS POROSITY

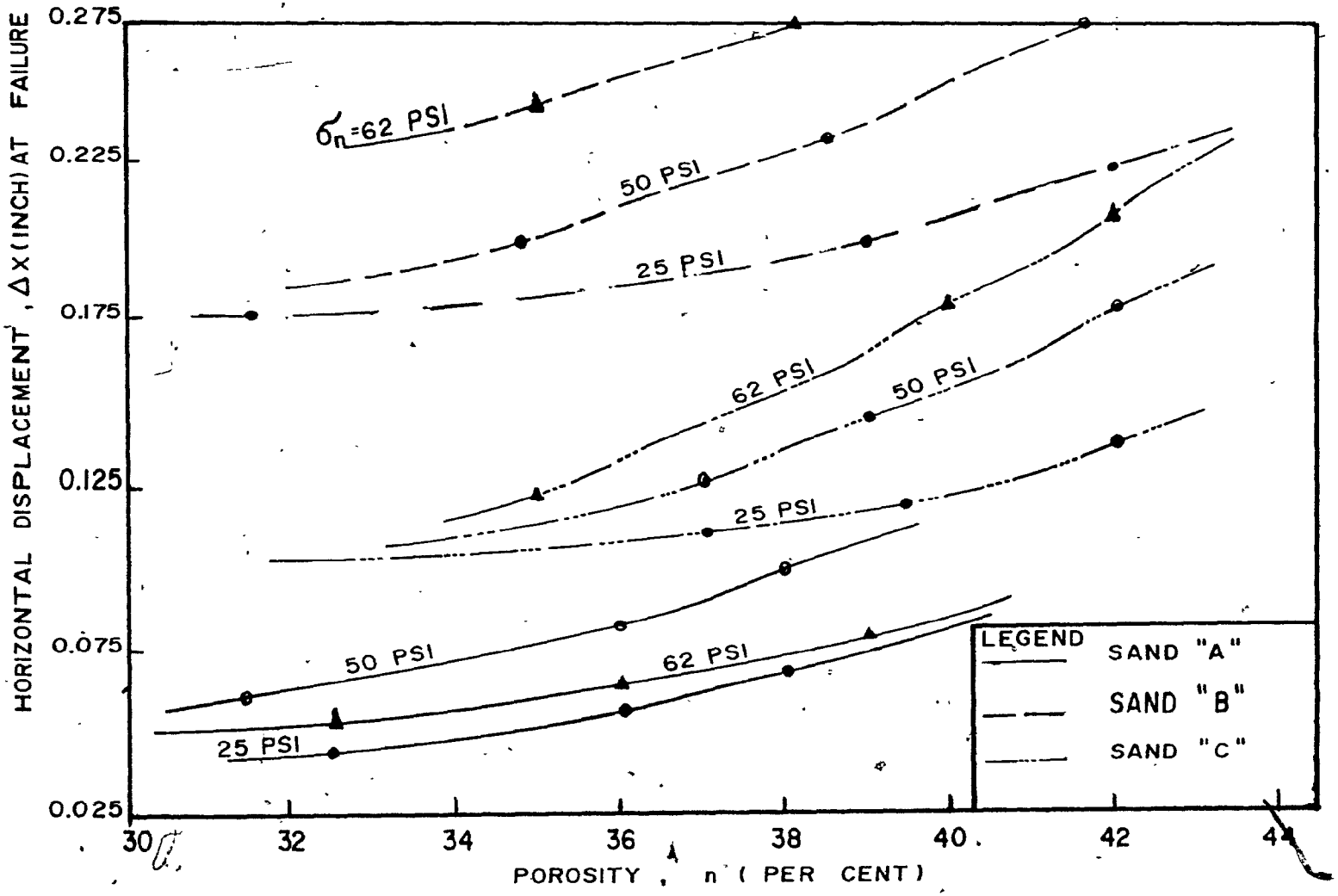

FIG. 5.27 HORIZONTAL DISPLACEMENT AT VARIOUS NORMAL STRESSES IN DIRECT SHEAR TESTS VS POROSITY

Referring to figure 2.8, previously presented in chapter II, the shear force S may be divided into three components S_1, S_2 and S_3 where:

S_1 : component due to external work done in dilating against the external force N.

then:

$$S_1 . \Delta X = N . \Delta Y$$

$$S_1 = N . \frac{\Delta Y}{\Delta X} \qquad (1)$$

where:

$S_1 . \Delta X$ is the gross work done through an incremental distance, ΔX.

$N . \Delta Y$ is the input energy used in raising or lowering the dead weight, N a distance, ΔY.

S_2 : components due to additional internal work in friction due to dilatancy.

then:

$$S_2 . \text{Cos } \theta = S . \sin \theta . \tan \phi_f$$

$S_2 . \text{Cos } \theta$ is the shear stress parallel to the plane of sliding between particles and $S . \sin \theta$ is the total normal force to this plane.

$$S_2 = S . \tan \theta . \tan \phi_f \qquad (2)$$

and

S_3 : component due to the work done in internal friction, if the sample did not change in volume during shearing.

then:

$$S_3 = N . \tan \phi_f \qquad (3)$$

Therefore:

$$\frac{S}{N} = \frac{\Delta Y}{\Delta X} + \frac{S}{N} \cdot \tan\theta \cdot \tan\phi_f + \tan\phi_f$$

$$\tan\phi_d = \frac{\Delta Y}{\Delta X} + \tan\phi_d \cdot \tan\phi_f \cdot \frac{\Delta Y}{\Delta X} + \tan\phi_f \qquad (4)$$

where

ϕ_d = angle of shearing resistance in drained tests.

ϕ_f = angle of friction at the residual condition.

ΔY = the incremental-displacement in direction of N.

ΔX = the incremental-displacement in direction of S.

Taking into account the external work done due to dilatancy, the corrected angle of shearing resistance, ϕ_r, is given by the expression:

$$\tan\phi_r = \tan\phi_d - \frac{\Delta Y}{\Delta X}$$

$$= \tan\phi_d \cdot \tan\phi_f \cdot \frac{\Delta Y}{\Delta X} + \tan\phi_f \qquad (5)$$

The strength components at failure for test number A.M.1, conducted on sand A and carried out at normal stress of 25 psi and relative density of 60%, are given below:

τ_{max} = 18.16 psi ; $\frac{\tau}{\sigma_n}$ = 0.726 and

ϕ_d = 36 degrees

At the peak point, the sample thickness increased from 0.0006 to 0.0016 in., during an incremental horizontal displacement of 0.006 in., which represents a rate of 0.0010 in., of shearing displacement.

τ_1 = the shear stress required to supply the sample with the energy to expand against the normal stress.

$= \sigma_n \cdot (\Delta Y/\Delta X)$

$= 25 \times (0.0010/0.006) = 4.17$ lbs. per sq. in.

which is 23 per cent of the total shearing stress at failure.

τ_2 = the shear stress component due to additional internal energy loss in friction with dilation.

$= \tau_{max} \cdot \tan \phi_f \cdot \frac{\Delta Y}{\Delta X}$

$\tan \phi_r = \tan \phi_d - \Delta Y/\Delta X$

$= 0.726 - 0.170 = 0.556$

then

$\phi_r = 29$ degrees

and

$$\tan \phi_f = \frac{\tan \phi_r}{1 + \tan \phi_d \cdot (\Delta Y/\Delta X)}$$

$$= \frac{0.556}{1 + 0.726 \times 0.17} = 0.495$$

then

$\phi_f = 26.33$ degrees

$$\tau_2 = 18.16 \times 0.495 \times \frac{0.0010}{0.006} = 1.5 \text{ lbs. per sq. in.}$$

and

τ_3 = shear stress component due to the internal energy loss in friction with no dilation.

$= \sigma_n \cdot \tan \phi_f$

= 12.48 lbs. per sq. in.

The sum of the shear stress components τ_1 and τ_2 is the portion contributed by the interlocking, or resistance to volume change.

The strength components of the sand tested in direct sand tests are summarized in table 5.10 and presented in graphical form in figures 5.28 and 5.29.

From these figures, it can be seen that the difference between the Coulomb friction angle, ϕ, and the one corrected for external work only, ϕ_r, is decreasing with an increase of the porosity. Also, the strength component contributed by the interlocking increases with a decrease of the porosity and the normal stress.

5.3 Plane-Strain Compression Tests

5.3.1 General

The test results are summarized in tables 4.7 to 4.9 and presented in graphical for in figures 4.17 to 4.22. In this chapter, these test results are represented in figures 5.30 to 5.33.

Figure 5.30 shows the variation of the angle of shearing resistance with the cell pressure. From this figure, it may be noted that the angle of shearing resistance increased with a decrease of the cell pressure applied to the samples and with an increase of the relative density. An increase of the cell pressure means a decrease of the degree of interlocking.

The variation of the volumetric strain and axial strain at failure, are presented in figures 5.31 and 5.32 respectively. From these figures, it can be observed the the volumetric strain at failure increased with a decrease of the porosity, and the cell pressure where the degree of

Table 5.10

Strength Components In Direct Shear Tests

Test Number	Normal Stress σ_n (Psi)	Shear stress τ_{max} (Psi) at failure	Stress ratio $(\tau/\sigma)_{max}$ at failure	$\frac{\Delta y}{\Delta x}$	Coulomb friction angle ϕ (deg.)	ϕ_r (deg.)	ϕ_f (deg.)	τ_1 (Psi)	τ_2 (Psi)	τ_3 (Psi)	Shear stress contributed by interlocking $= \tau_1 + \tau_2$ (Psi)
A-M-1	25	18.16	0.726	0.17	36	29	26.53	4.17	1.50	12.48	5.67
A-M-2	50	33.72	0.674	0.08	34	30.70	29.41	2	1.52	28.18	3.52
A-M-3	62	39.50	0.637	0.04	32.50	30.84	30.20	2.48	0.92	36.10	3.40
A-D-1	25	19.71	0.788	0.192	38.25	30.80	27.50	4.80	1.97	13	6.77
A-D-2	50	35.66	0.713	0.08	35.50	32.30	31	4	1.71	30	5.71
A-D-3	62	41.80	0.674	0.031	34	32.74	32	1.92	0.82	39	2.74
B-M-1	25	20.98	0.839	0.14	40	35	32	3.50	1.83	15.62	5.33
B-M-2	50	35.01	0.700	0.075	35	32	30.70	3.75	1.56	29.69	5.31
B-M-3	62	40.26	0.649	0.04	33	31.3	30.70	2.48	0.96	36.83	3.44
B-D-1	25	22.50	0.900	0.16	42	36	33	4	2.34	16.24	6.34
B-D-2	50	39.77	0.795	0.10	38.50	34.8	32.80	5	2.56	32.22	7.56
B-D-3	62	45	0.726	0.08	36	32.86	31.40	4.96	2.20	37.82	7.16

Table 5.10

Strength Components In Direct Shear Tests

Test number	Normal stress σ_n (Psi)	Shear stress τ_{max} (Psi) at failure	Stress ratio $(\tau/\sigma)_{max}$ at failure	$\frac{\Delta y}{\Delta x}$	Coulomb friction angle ϕ (deg.)	ϕ_r (deg.)	ϕ_f (deg.)	τ_1 (Psi)	τ_2 (Psi)	τ_3 (Psi)	Shear stress contributed by interlocking = $\tau_1 + \tau_2$ (Psi)
C-M-1	25	23.97	0.959	0.192	43.80	38	33	4.80	2.99	16.26	7.79
C-M-2	50	41.95	0.839	0.04	40	38.60	37.70	2	1.30	38.65	3.30
C-M-3	62	54.85	0.885	0.128	41.50	37	34	7.94	4.74	41.82	12.68
C-D-1	25	26.25	1.050	0.16	46.40	41.70	38	4	3.28	19.50	7.28
C-D-2	50	48.28	0.966	0.125	44	40	36.87	6.25	4.53	37.50	10.78
C-D-3	62	56.81	0.916	0.128	42.50	38	35.20	7.94	5.13	43.74	13.07

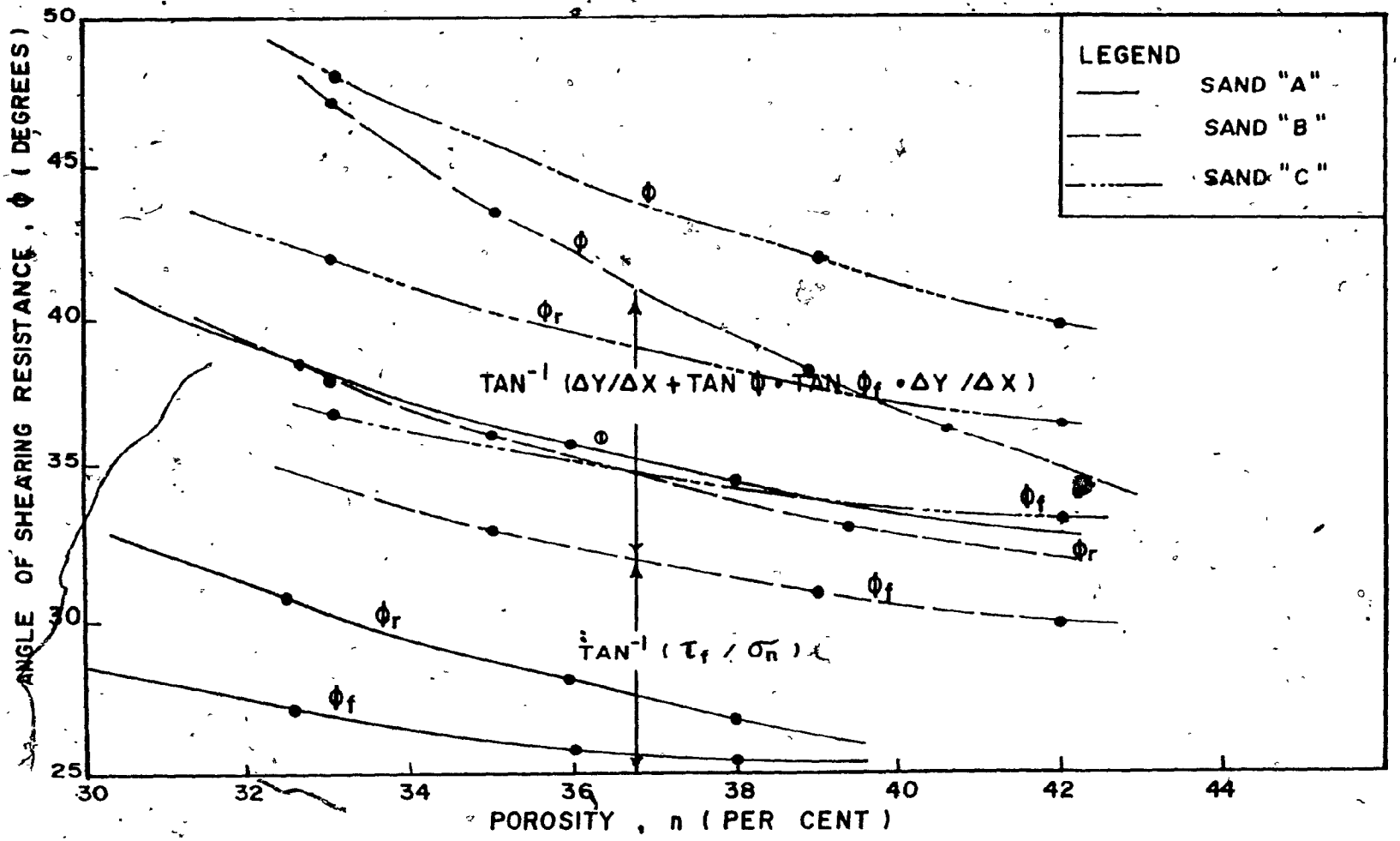

FIG. 5.28 RELATIONSHIP BETWEEN VARIOUS FRICTION ANGLES & POROSITY IN DIRECT SHEAR TESTS AT NORMAL STRESS = 25 PSI

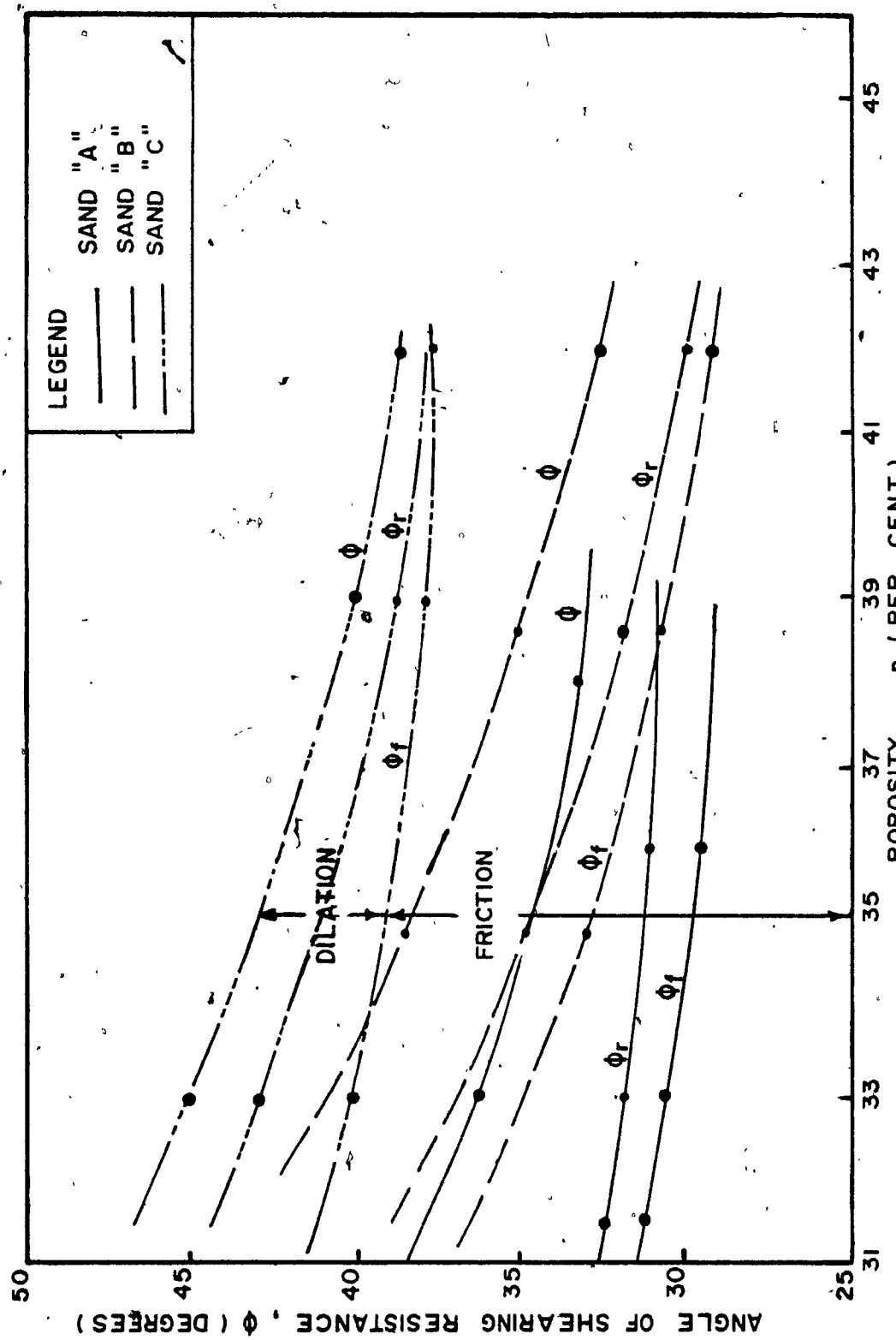

FIG. 5. 29 RELATIONSHIP BETWEEN VARIOUS FRICTION ANGLES & POROSITY IN DIRECT SHEAR TESTS AT NORMAL STRESS = 50 PSI.

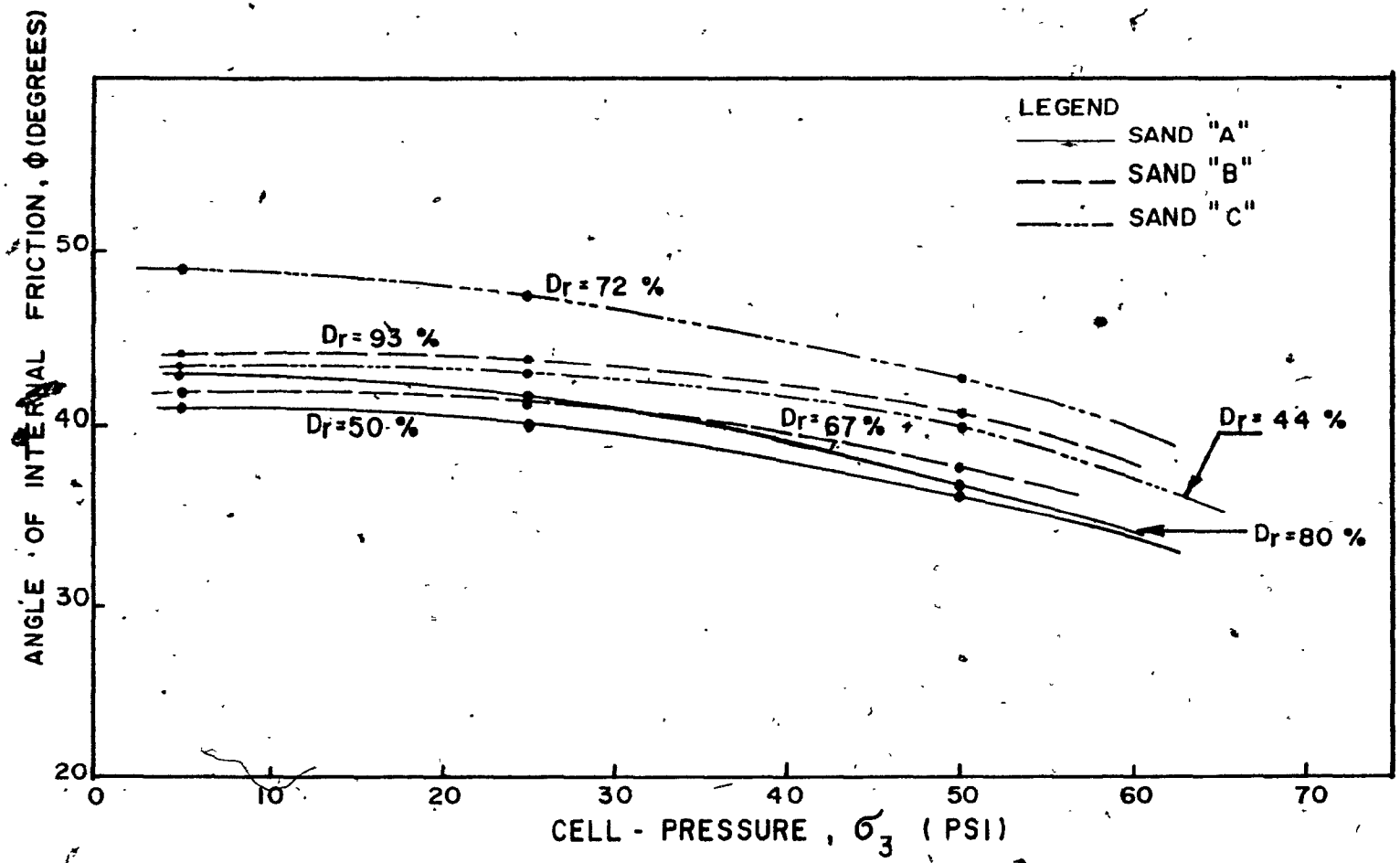

FIG. 5.30 ANGLE OF INTERNAL FRICTION VS CELL PRESSURE IN PLANE STRAIN TESTS

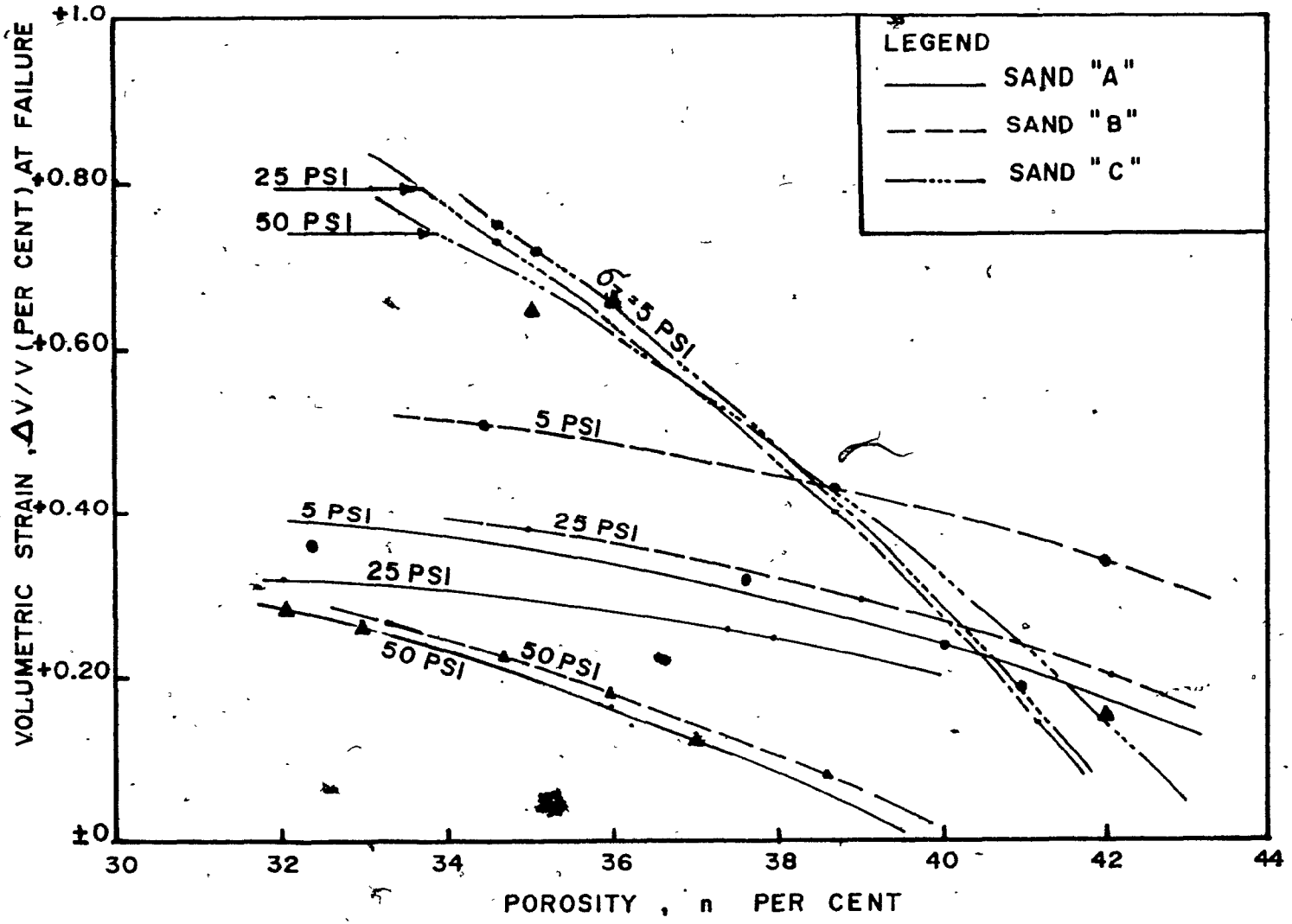

FIG. 5. 31 VOLUMETRIC STRAIN VS POROSITY IN PLANE - STRAIN TESTS

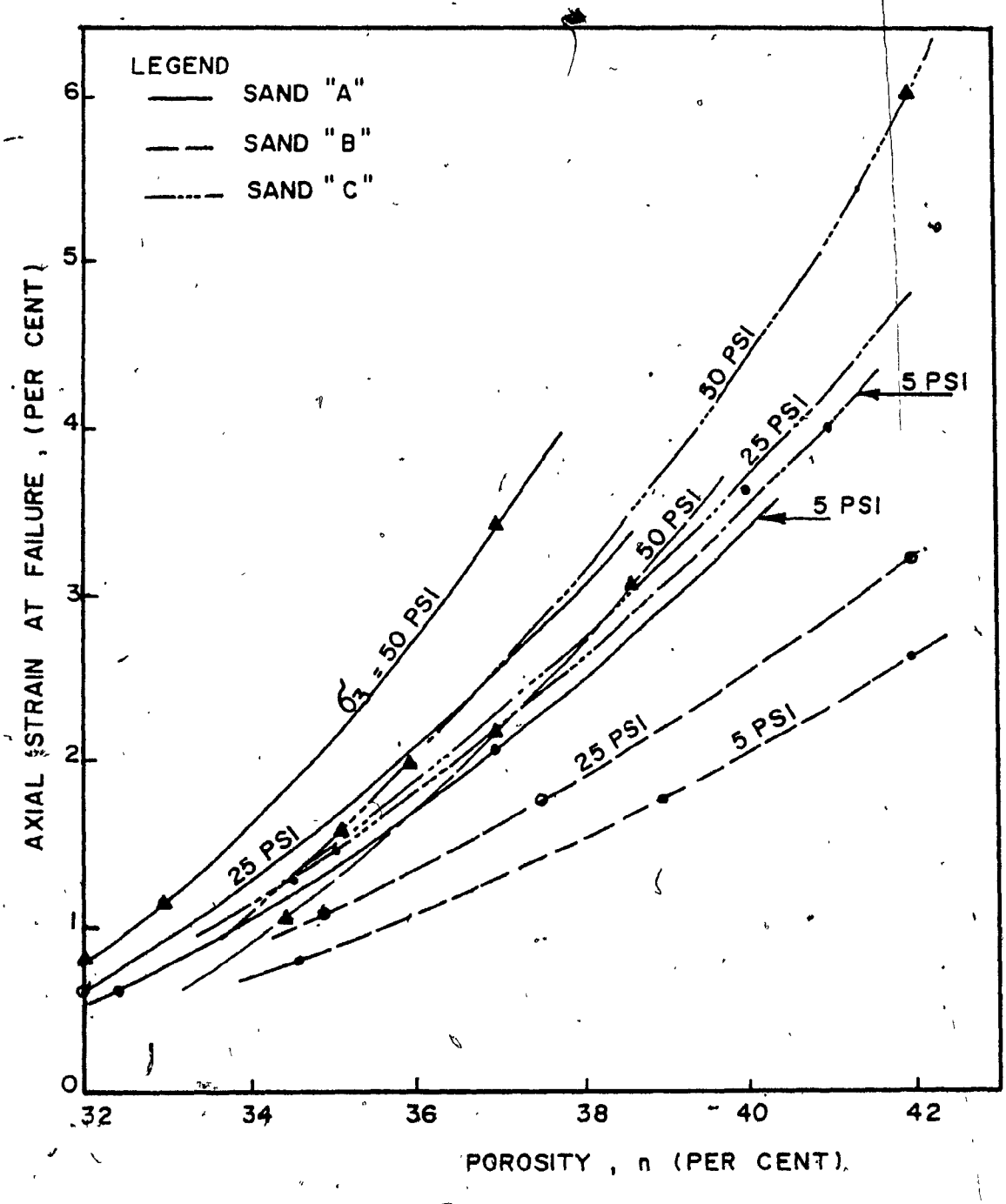

FIG. 5.32 AXIAL STRAIN VS POROSITY IN PLANE-STRAIN COMPRESSION TESTS

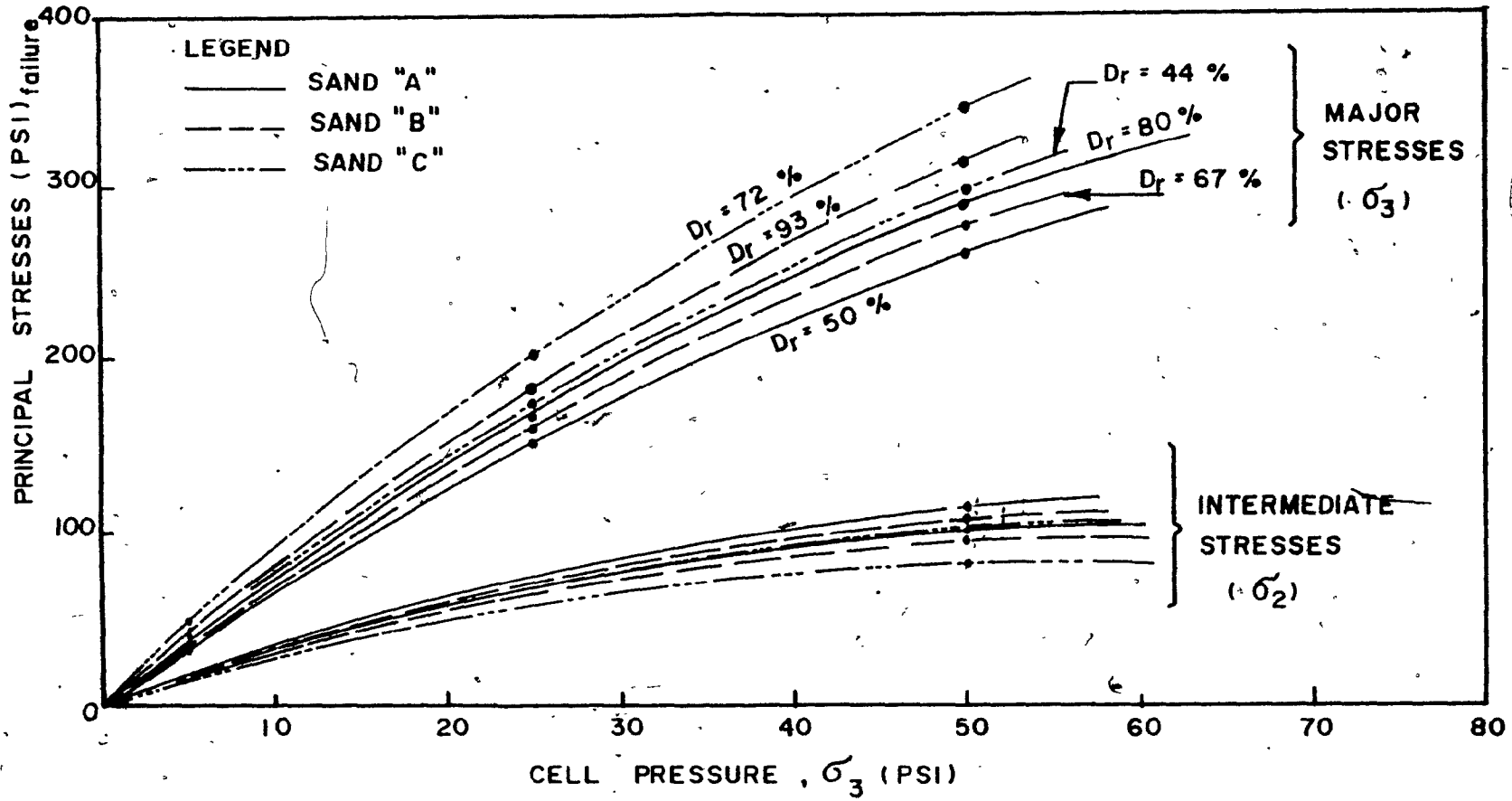

FIG. 5.33 CONDITION OF FAILURE FOR DENSE & MEDIUM DENSE SAND IN PLANE STRAIN TESTS (SANDS "A", "B" & "C")

interlocking is higher. Also, it can be seen that in case of sand C, the axial and volumetric strain at failure are greater than those in sand A and B, which is due to higher interlocking between the particles.

The principal stresses versus the cell pressure are also presented in figure 5.33. From this figure, it can be observed that the principal stresses at failure increased with an increase of the applied cell pressure.

5.3.2 Interlocking

The interlocking between the particles, for the sands tested in plane-strain compression tests, was determined from the expression derived by Rowe (1962) as:

$$\tan \alpha = \left(\frac{\sigma_1}{\sigma_3}\right)^{1/2} \cdot \left(1 - \frac{dv}{d\varepsilon_1}\right)^{1/2}$$

where

σ_1/σ_3 : stress ratio.

$\frac{dv}{d\varepsilon_1}$: dilatancy rate.

$1 - \frac{dv}{d\varepsilon_1}$: the dilatancy factor.

α : the interlocking parameter,

and is function to the stress ratio and the dilatancy factor.

Figure 5.34 shows the variation of the dilation rate $\frac{dv}{d\varepsilon_1}$ with the porosity of the sand tested. From this figure, it can be observed that the dilation rate at failure increases with an increase of the relative density, and a decrease of the applied cell pressure. The probable explanation for that can be given as: for dense sand, more energy is put into the samples by the external loads, then is expanded for the expansion

against the confining stress, which tends to take place during shearing. An increase of the energy is accompanied by an increase of the volume change.

Sample calculation of the interlocking parameter for the sand tested in plane-strain compression tests, is given below:

Referring to figure 4.17, (Test No. A.M.1):

$\sigma_1/\sigma_3 = 7.40$; $\left(\frac{\Delta V}{V}\right)_f = + 0.32\%$ and

$\varepsilon_1 = 2\%$

then

$$\tan \alpha = [7.40 \ (1 + \frac{0.0032}{0.02})]^{1/2}$$

$$= 2.93$$

$$\alpha = 71.16 \text{ degrees}$$

The interlocking paramter , for the sand tested in plane-strain compression tests are summarized in table 5.11 and presented in figure 5.35. From this figure, it can be seen that the interlocking increases with an increase of the relative density, and a decrease of the applied cell pressure.

5.4 Comparison of Test Results

Comparison of the strength results obtained from triaxial compression, direct shear and plane-strain compression tests, was conducted as follows:

1. Comparison of the resulted angle of shearing resistance against the porosity, as shown in figures 5.36 to 5.38.

This approach has been used by Cornforth (1964), for the comparison of

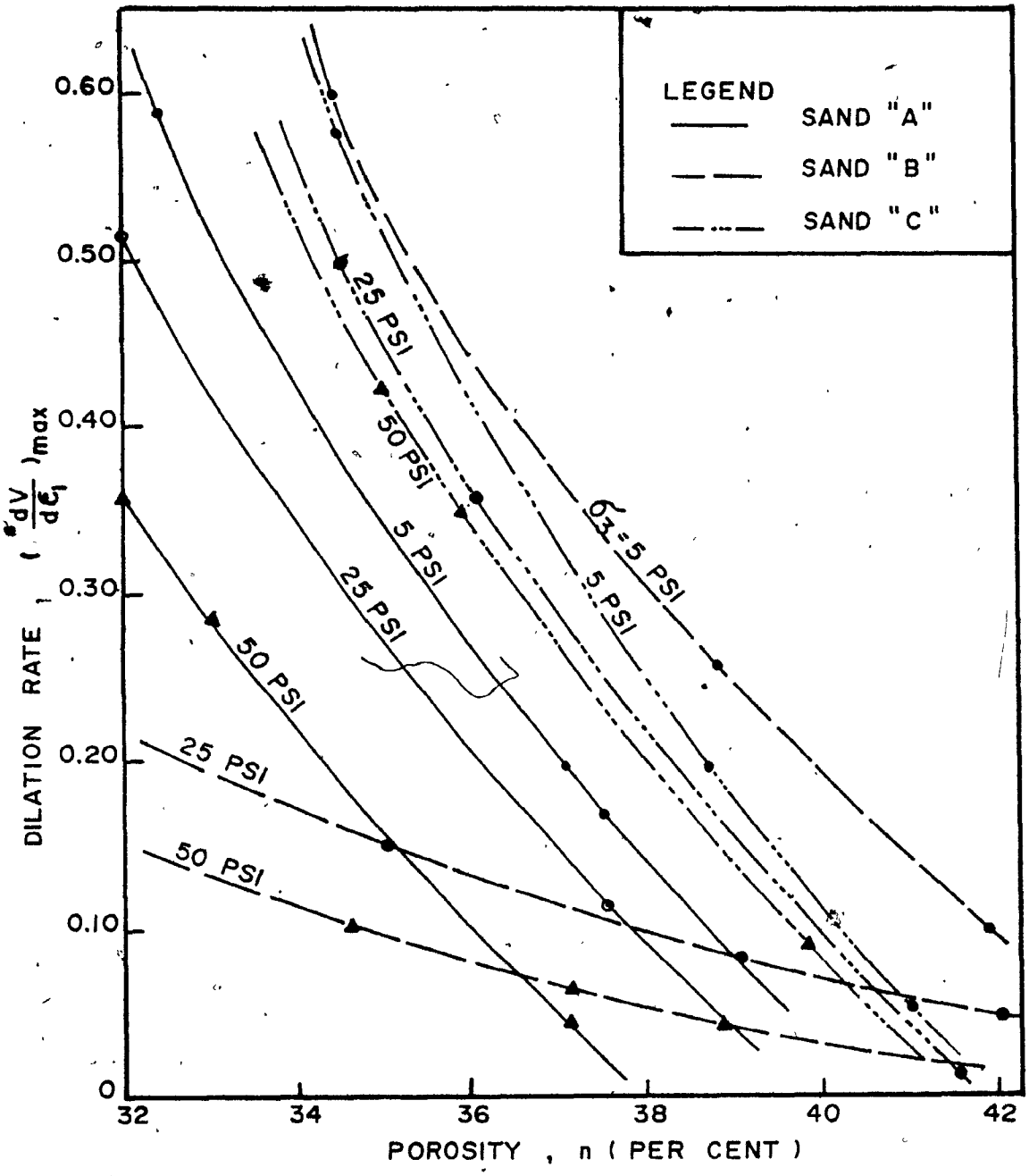

FIG. 5.34 MAXIMUM RATE OF DILATION IN PLANE STRAIN COMPRESSION TESTS

Table 5.11

Interlocking Parameter, α In Plane-Strain Compression Tests

Sand	Test Number	Stress Ratio σ_1/σ_3 at failure	Volumetric Strain $\Delta V/V$ % at failure	Axial Strain ε_1 % at failure	$t_{an}\ \alpha$	Value of α (degrees)	Dilation Factor $D = 1 - \frac{dv}{d\varepsilon_1}$ at failure	Remarks
A	A-M-1	7.40	+ 0.32	2	2.93	71.15	1.16	Medium dense sand
	A-M-2	5.50	+ 0.25	3	2.44	67.70	1.08	" " "
	A-M-3	5.24	+ 0.10	3.50	2.32	66.71	1.03	" " "
	A-M-4	6.30	+ 0.32	1.85	2.72	69.80	1.173	" " "
	A-M-5	6	+ 0.25	3.65	2.53	68.50	1.07	" " "
	A-M-6	5.76	+ 0.28	2.90	2.51	68.30	1.096	" " "
	A-D-1	9.14	+ 0.35	0.60	3.80	75.30	1.58	Dense sand
	A-D-2	6.73	+ 0.30	0.60	3.867	75.50	1.50	" "
	A-D-3	5.80	+ 0.27	1.60	2.60	69.0	1.17	" "
	A-D-4	6.14	+ 0.29	0.83	2.88	70.85	1.35	" "

Table 5.11

Sand	Test Number	Stress Ratio σ_1/σ_3 at failure	Volumetric Strain $\Delta V/V$ % at failure	Axial Strain ε_1 % at failure	$t_{an}\ \alpha$	Value of α (degrees)	Dialtion Factor $D = 1 - \frac{dv}{d\varepsilon_1}$ at failure	Remarks
	B-M-1	9.90	+ 0.54	2.40	3.49	74	1.225	Medium dense sand
	B-M-2	6.44	+ 0.28	2.75	2.66	69.40	1.10	" " "
	B-M-3	5.69	+ 0.10	3.25	2.43	67.60	1.03	" " "
	B-M-4	6.80	+ 0.415	2.60	2.81	70.40	1.16	" " "
B	B-M-5	5.32	+ 0.20	2.95	2.39	67.30	1.07	" " "
	B-M-6	7.24	+ 0.30	2.95	2.82	70.50	1.10	" " "
	B-D-1	10.20	+ 0.60	0.85	4.165	76.50	1.70	Dense sand
	B-D-2	7.08	+ 0.38	1.10	3.08	72	1.34	" "
	B-D-3	6.30	+ 0.22	1.00	2.77	70.17	1.22	" "
	B-D-4	6.02	+ 0.14	1.45	2.57	68.76	1.10	" "

Table 5.11

Sand	Test Number	Stress Ratio σ_1/σ_3 at failure	Volumetric Strain $\Delta V/V$ % at failure	Axial Strain ε_1 % at failure	$t_{an}\ \alpha$	Value of α (degrees)	Dilation Factor $D = 1 - \frac{dv}{d\varepsilon_1}$ at failure	Remarks
	C-M-1	8.50	+ 0.20	4	2.987	71.50	1.05	Medium dense sand
	C-M-2	6.39	+ 0.18	4.50	2.587	68.80	1.04	" " "
	C-M-3	5.78	+ 0.15	6	2.43	67.70	1.025	" " "
	C-D-1	12.40	+ 0.70	1.5	4.27	76.82	1.47	Dense sand
	C-D-2	7.68	+ 0.68	1.65	3.29	73.10	1.41	" "
C	C-D-3	6.92	+ 0.65	1.86	3.06	71.90	1.35	" "
	C-D-4	8.30	+ 0.75	1.30	3.62	74.60	1.58	" "
	C-D-5	8.44	+ 0.70	1.40	3.56	74.30	1.50	" "
	C-D-6	7.08	+ 0.62	1.48	3.17	72.50	1.42	" "
	C-D-7	7.32	+ 0.60	2.0	3.08	72	1.30	" "

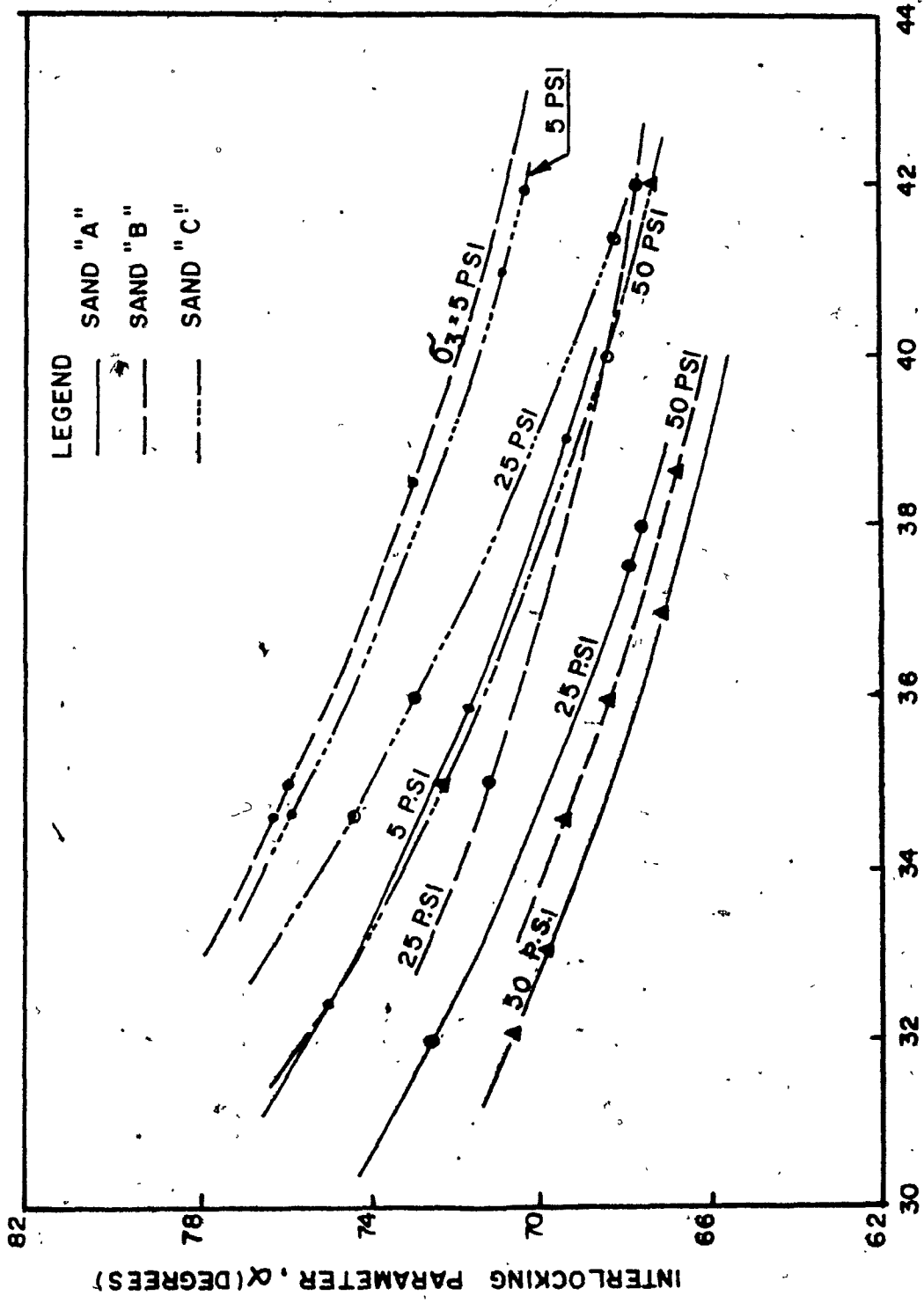

FIG. 5.35 INTERLOCKING IN PLANE STRAIN COMPRESSION TESTS

the strength values obtained from the triaxial and plane-strain compression tests conducted on brasted sand. Also, used by Nash (1953), for the comparison of the triaxial compression and direct shear strength tests.

From the strength-density curves for sand "A" plotted on figure 5.36, it can be observed that the shape of these curves are slightly concave upwards. The strength of the plane-strain specimens are always greater than the strength of the corresponding direct shear, and triaxial specimens at the same placement density. The difference in the strength values of plane-strain and triaxial tests, varies from 5% at the lowest density to more than 10% for the dense specimens. Also, at the lowest density, the strength values in triaxial tests are higher by about 2% than the strength of the corresponding direct shear tests and lower by 4% for the dense state.

From the strength-density curves, plotted on figure 5.37 and 5.38 for sand "B" and "C" respectively, the same comments given in case of sand "A" can be given here, where the strength values obtained from the plane-strain tests for dense sand samples are always greater by about 10% to 15%, than the values obtained from the triaxial compression tests, and 5% to 10% than the strength of the corresponding direct shear tests.

Also, at the lowest density the difference in the strength values of the plane-strain, and both the direct shear and triaxial compression tests are 2 - 3% and 1 - 2 % respectively. That is to say, that the strength results obtained from the triaxial compression, direct shear and plane-strain compression tests, during this investigation confirm the same conclusion given by Cornforth (1964) and Nash (1953).

2. Comparison of the strength results obtained from the triaxial compression, direct shear, and plane strain compression tests versus the normal stress, as shown in figures 5.39 to 5.41.

From these figures, it can be seen that at small normal stress, the strength values of the sand tested in plane-strain are greater than the strength values of the corresponding direct shear and triaxial compression tests. The difference increases with an increase of the normal stress.

Also, for the purpose of the comparison of the test results, the failure characteristics of the triaxial compression, direct shear and plane-strain compression test series are plotted on figures 5.42 to 5.46.

From figure 5.42, it can be observed that the strength values of sand C are greater than those of sand A and B, where the interlocking between the particles is less.

From figure 5.43, it is clear that the volumetric strain curves tend to converge at the lowest densities, and the triaxial specimens have a greater positive volume change at failure, than those of the corresponding plane-strain and direct shear tests. That can be explained, that in the case of triaxial tests the particles are given the freedom to move around each other, and the sample is free to expand against the confining stress, which results in an increase of the volumetric strain and a decrease of the interlocking.

Figure 5.44, shows a relationship between the dilatancy rate at failure and the porosity. From this figure it may be noted that the dilatancy seems to be much less widespread in plane-strain tests.

The interlocking in plane-strain and triaxial compression tests is given in figures 5.45. From this figure, it is clear that the interlocking in plane-strain tests is greater than the interlocking in triaxial compression tests under the same condition. The difference tends to be less at the lowest densities.

Figure 5.46, shows the variation of the axial strain at failure with the porosity. From this figure, it can be seen that the axial strain at failure for the sand samples tested in triaxial compression tests, is higher than that given by the plane-strain compression tests. The difference is increasing with an increase of the porosity.

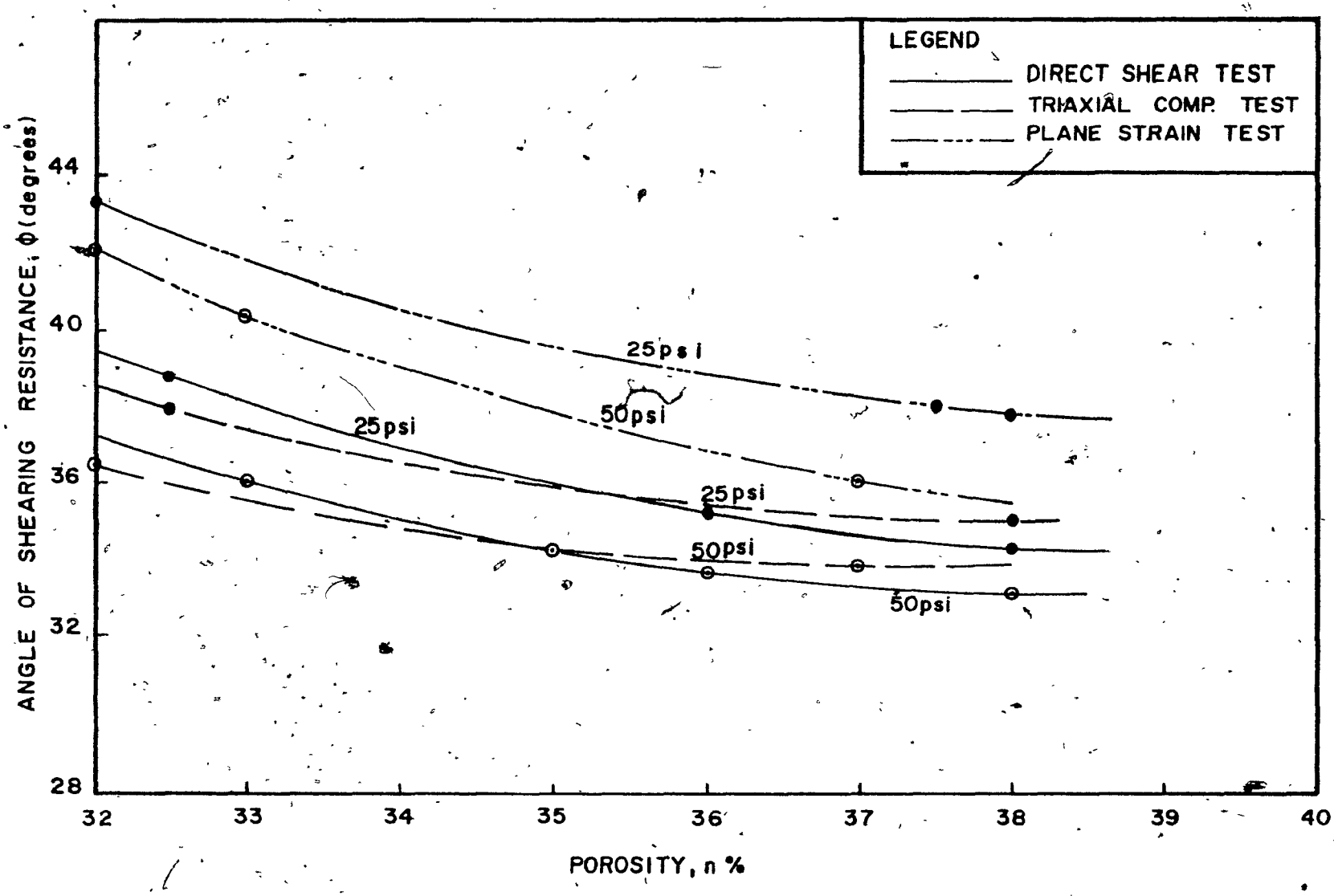

FIG. 5.36 ANGLE OF SHEARING RESISTANCE IN PLANE STRAIN, TRIAXIAL COMPRESSION & DIRECT SHEAR TESTS VS POROSITY (SAND "A")

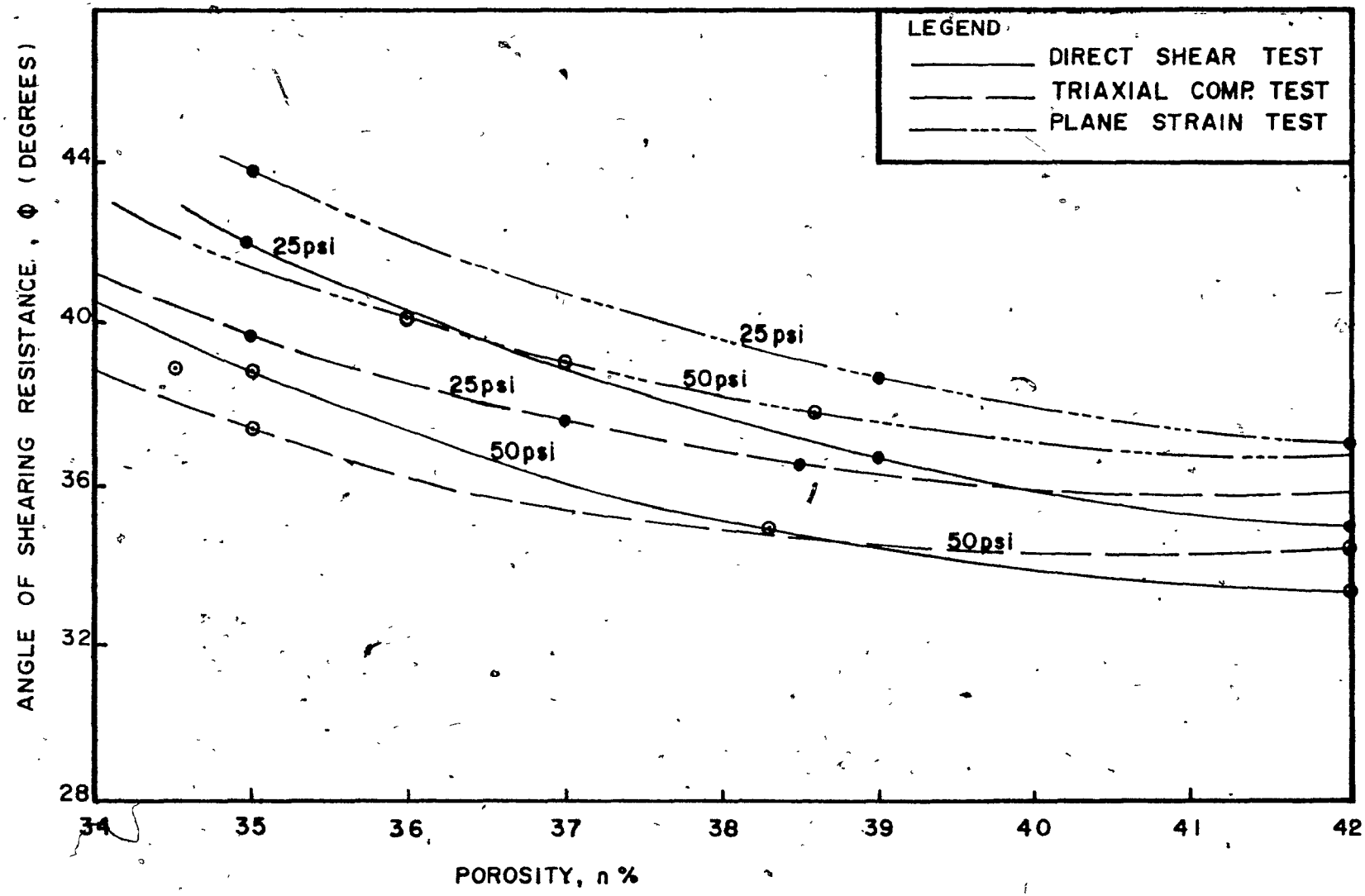

FIG. 5.37 ANGLE OF SHEARING RESISTANCE IN PLANE STRAIN, TRIAXIAL COMPRESSION & DIRECT SHEAR TESTS VS POROSITY (SAND "B")

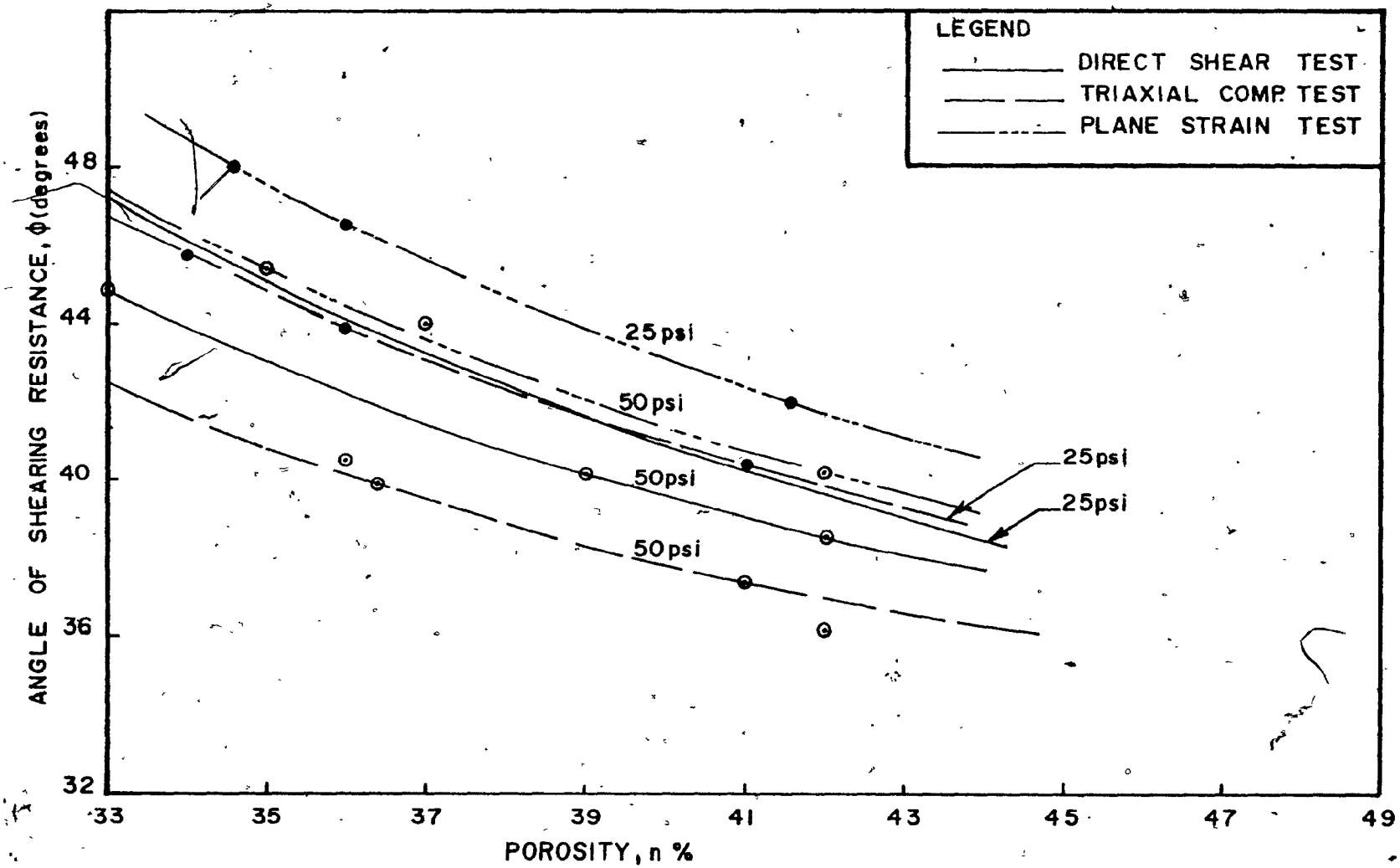

FIG. 5.38 ANGLE OF SHEARING RESISTANCE IN PLANE STRAIN, TRIAXIAL COMPRESSION & DIRECT SHEAR TESTS VS POROSITY (SAND "C")

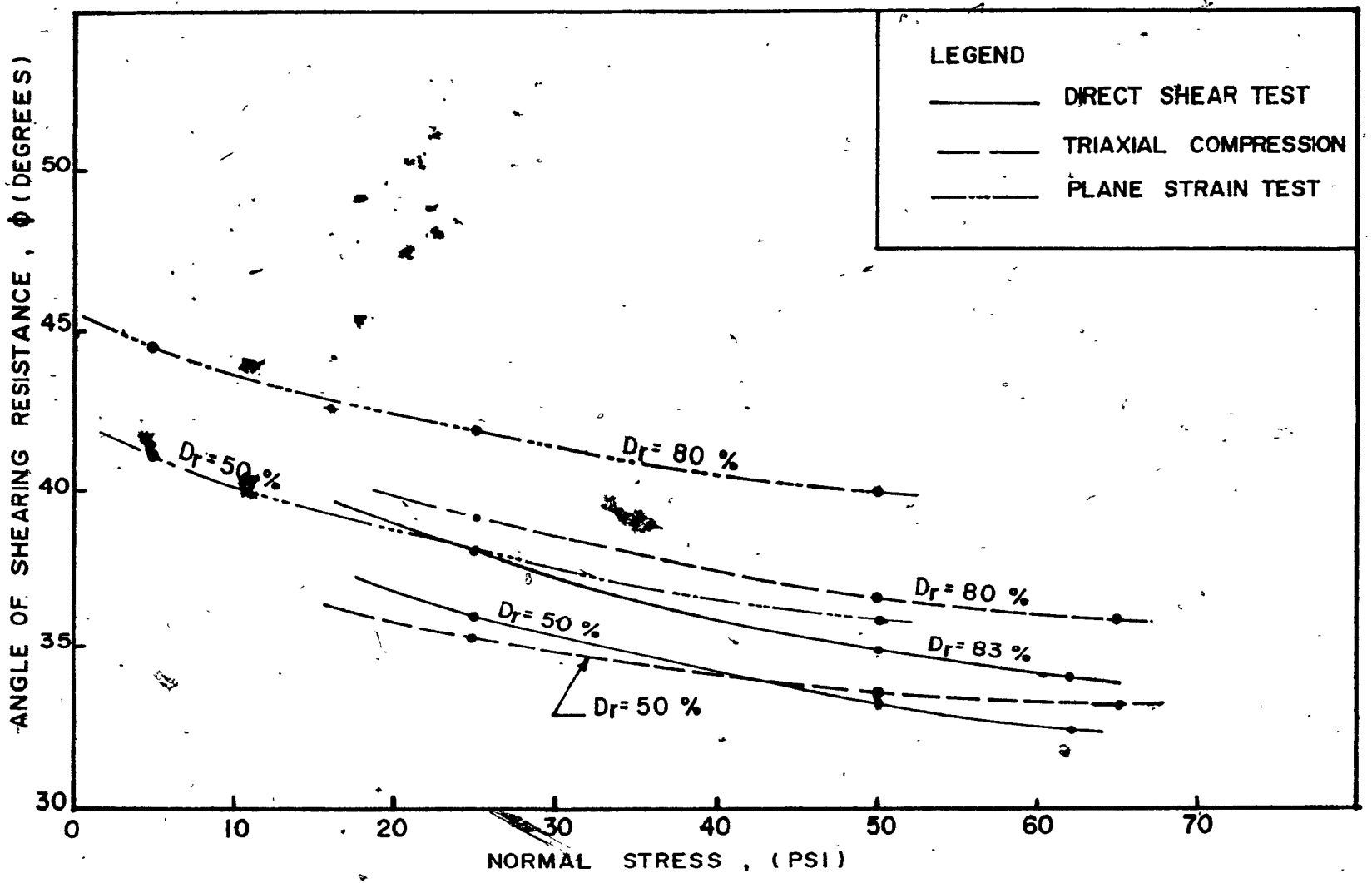

FIG. 5. 39 ANGLE OF SHEARING RESISTANCE FOR DIRECT SHEAR, TRIAXIAL COMPRESSION & PLANE STRAIN COMPRESSION TESTS VS NORMAL STRESS (SAND "A")

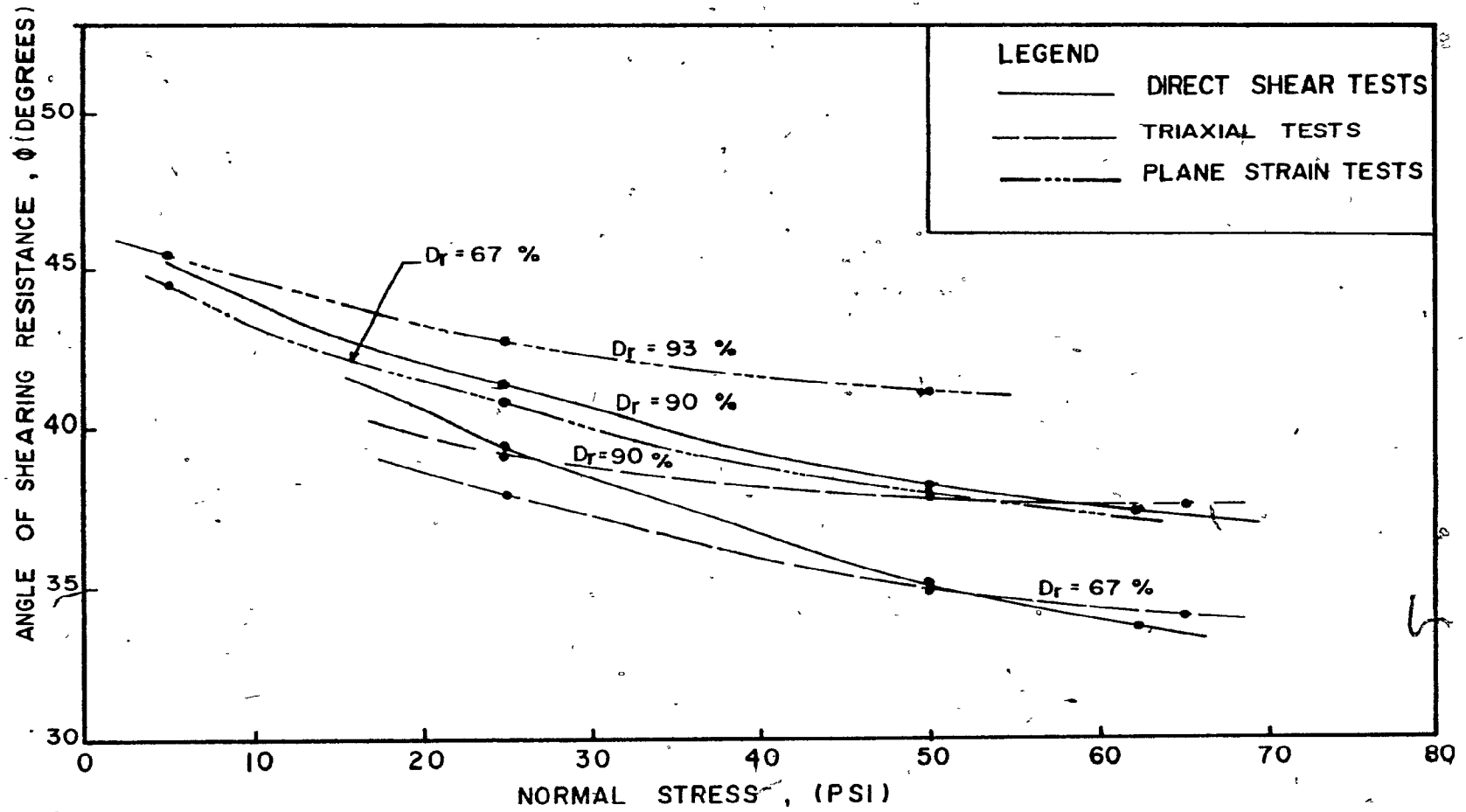

FIG. 5.40 ANGLE OF SHEARING RESISTANCE FOR DIRECT SHEAR, TRIAXIAL COMPRESSION & PLANE STRAIN COMPRESSION TESTS VS NORMAL STRESS (SAND "B")

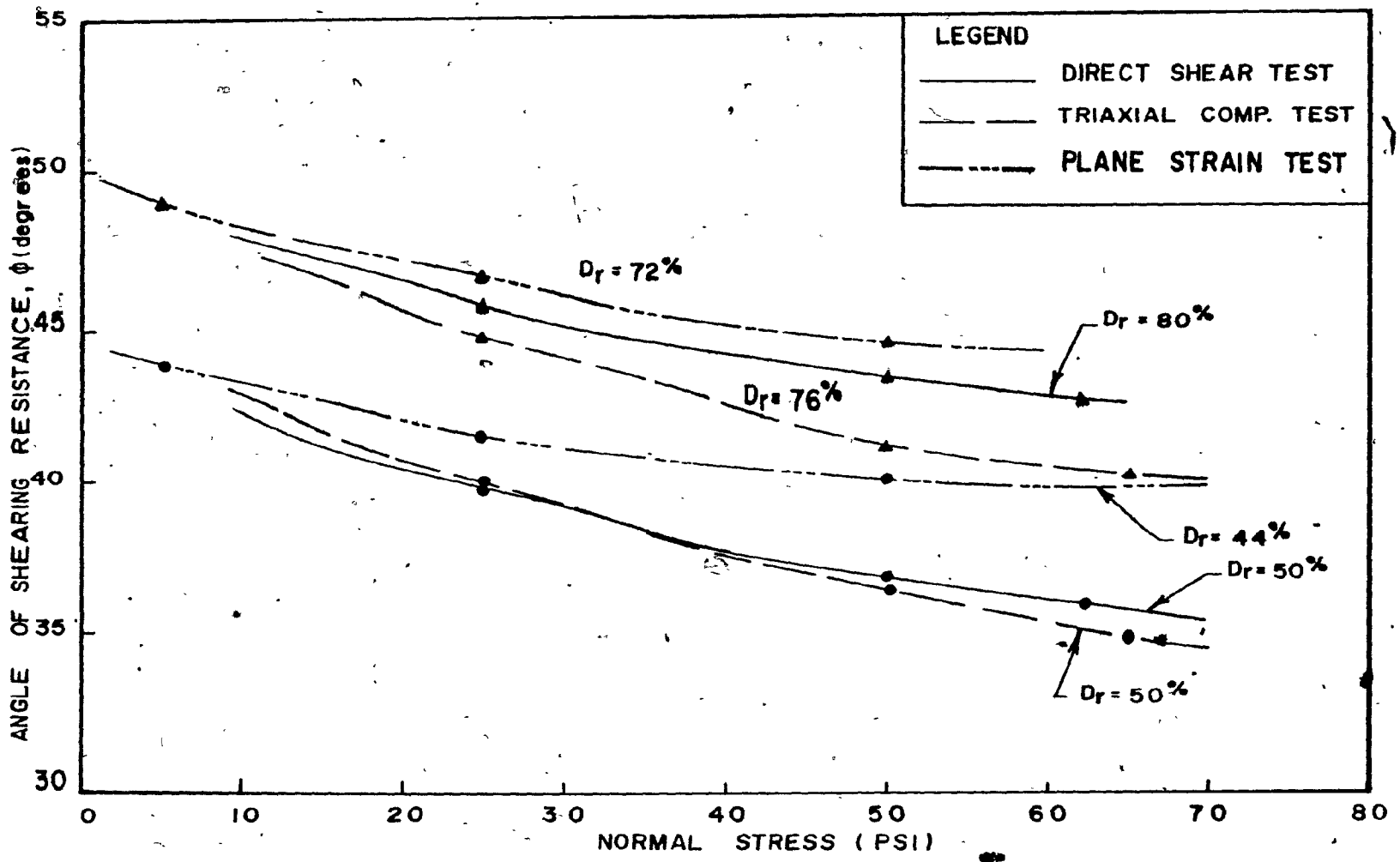

FIG. 5.41 ANGLE OF SHEARING RESISTANCE FOR DIRECT SHEAR, TRIAXIAL COMPRESSION & PLANE STRAIN COMPRESSION TESTS VS NORMAL STRESS (SAND "C")

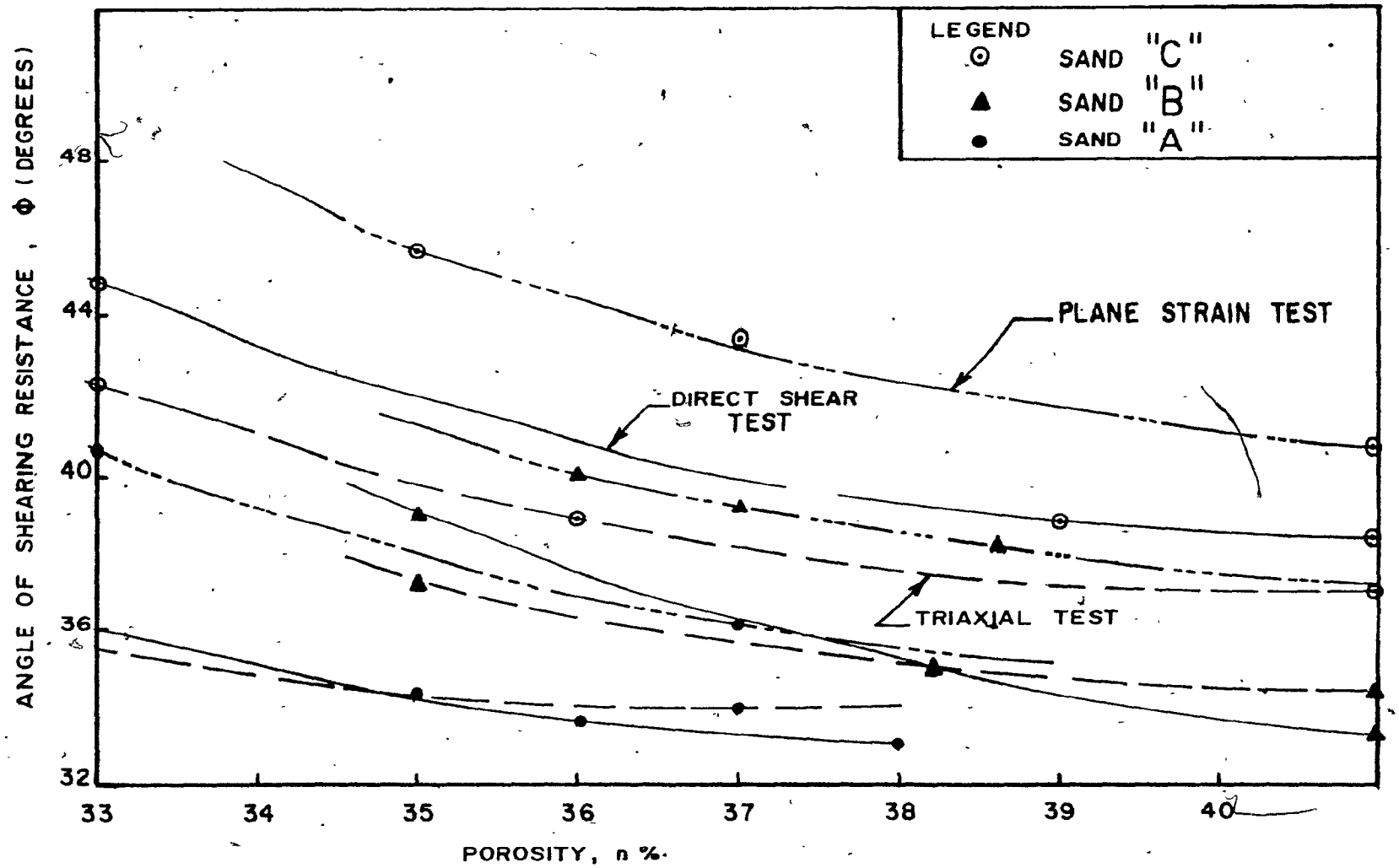

FIG. 5.42 ANGLE OF SHEARING RESISTANCE IN TRIAXIAL COMPRESSION, PLANE STRAIN & DIRECT SHEAR TESTS VS POROSITY
(ALL TESTS CARRIED OUT AT CELL PRESSURE OF 50 PSI)

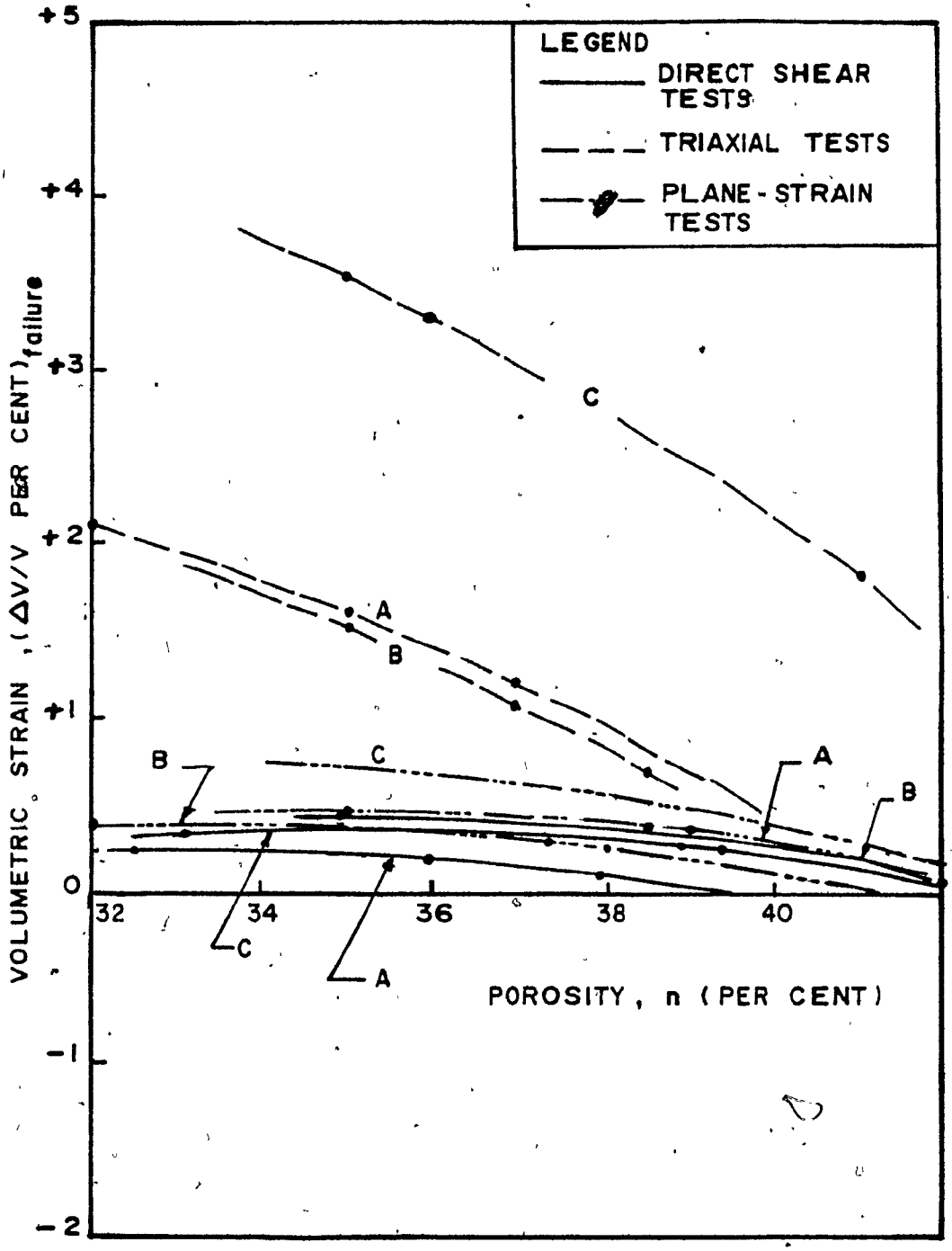

FIG. 5.43 VOLUMETRIC STRAIN AT FAILURE IN PLANE-STRAIN & TRIAXIAL COMPRESSION & DIRECT SHEAR TESTS AT NORMAL STRESSES OF 25 PSI

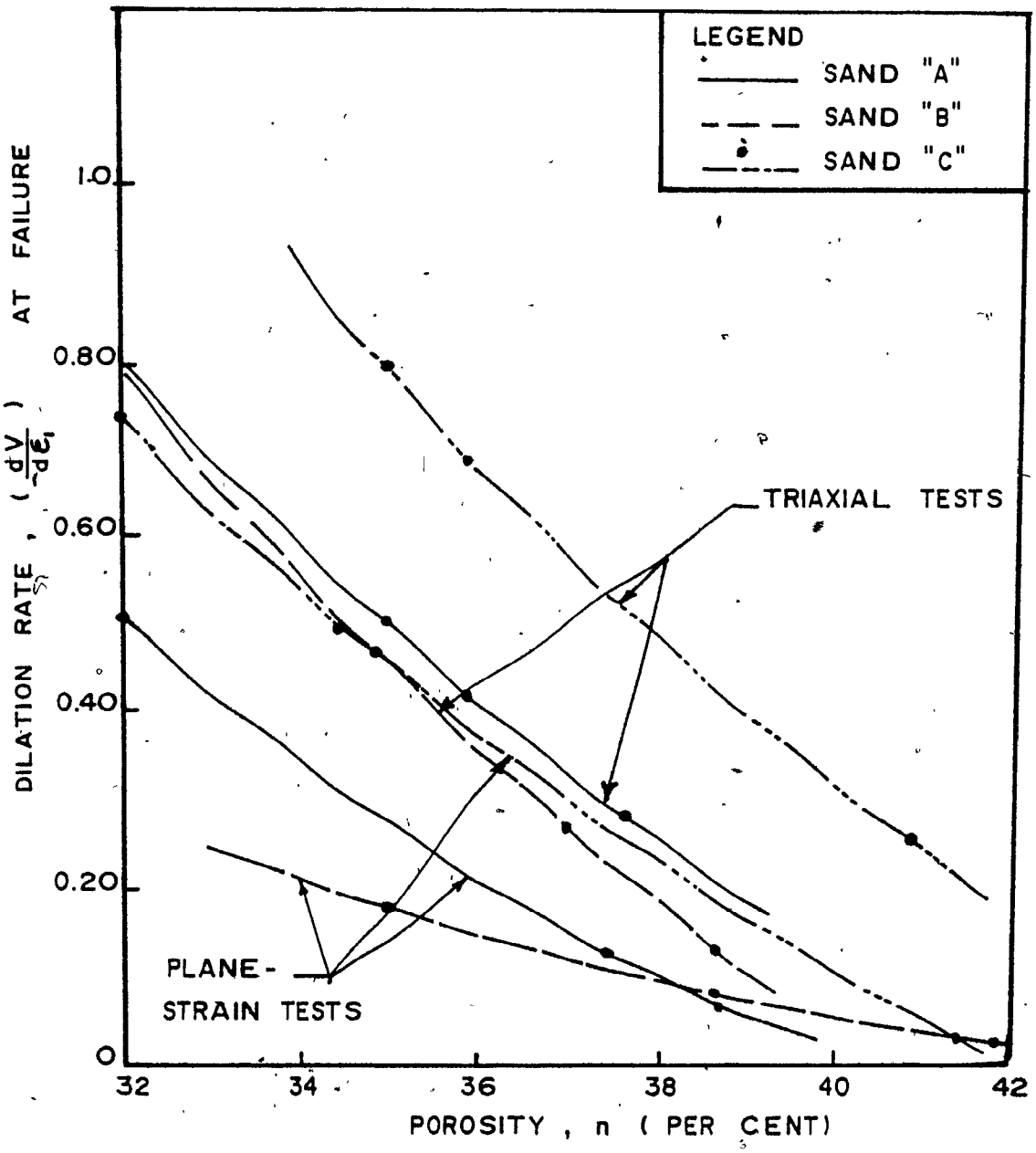

FIG. 5.44 DILATION RATE AT FAILURE IN PLANE STRAIN & TRIAXIAL COMPRESSION TESTS (CELL PRESSURE = 25 PSI)

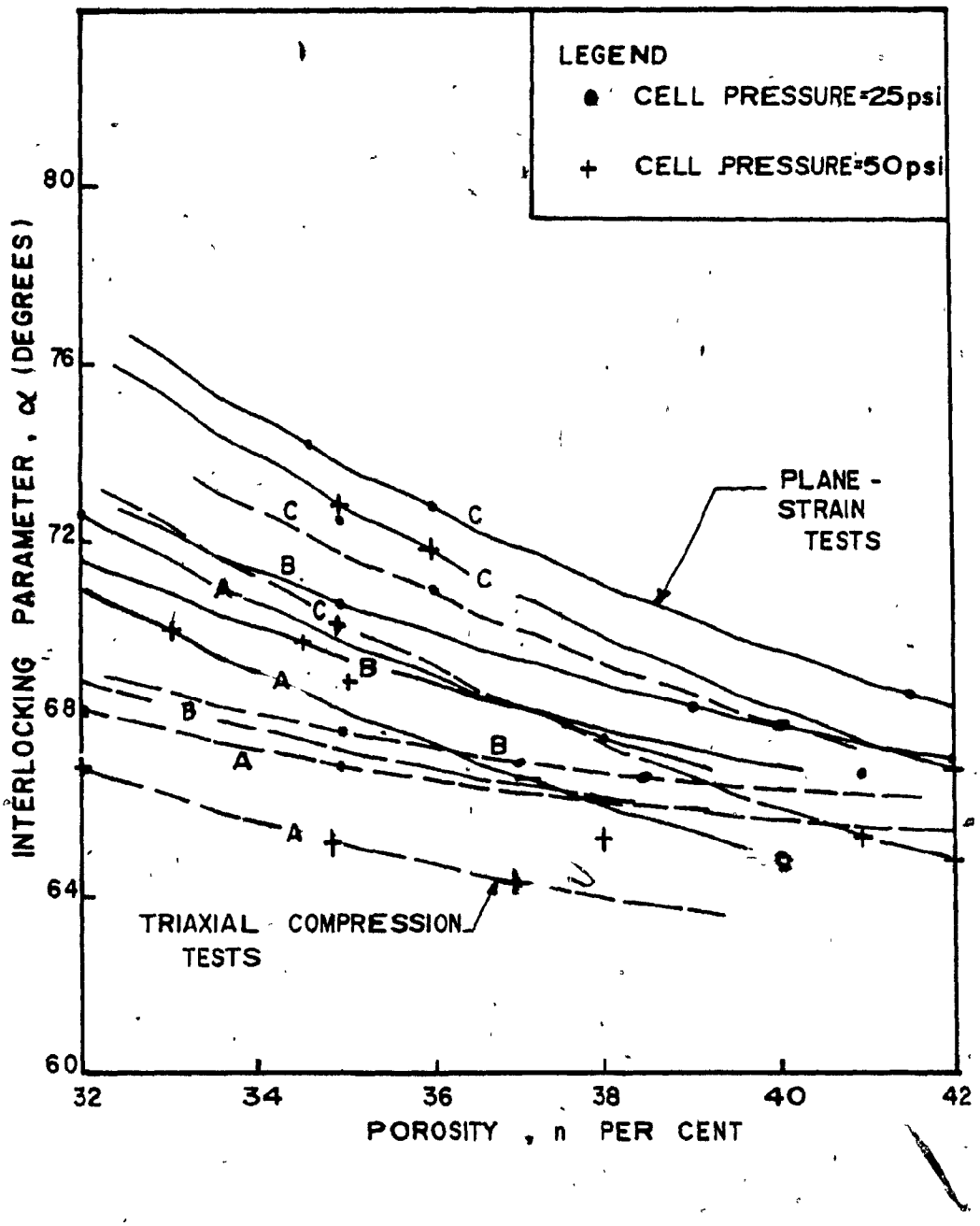

FIG. 5.45 INTERLOCKING IN PLANE - STRAIN & TRIAXIAL COMPRESSION TESTS

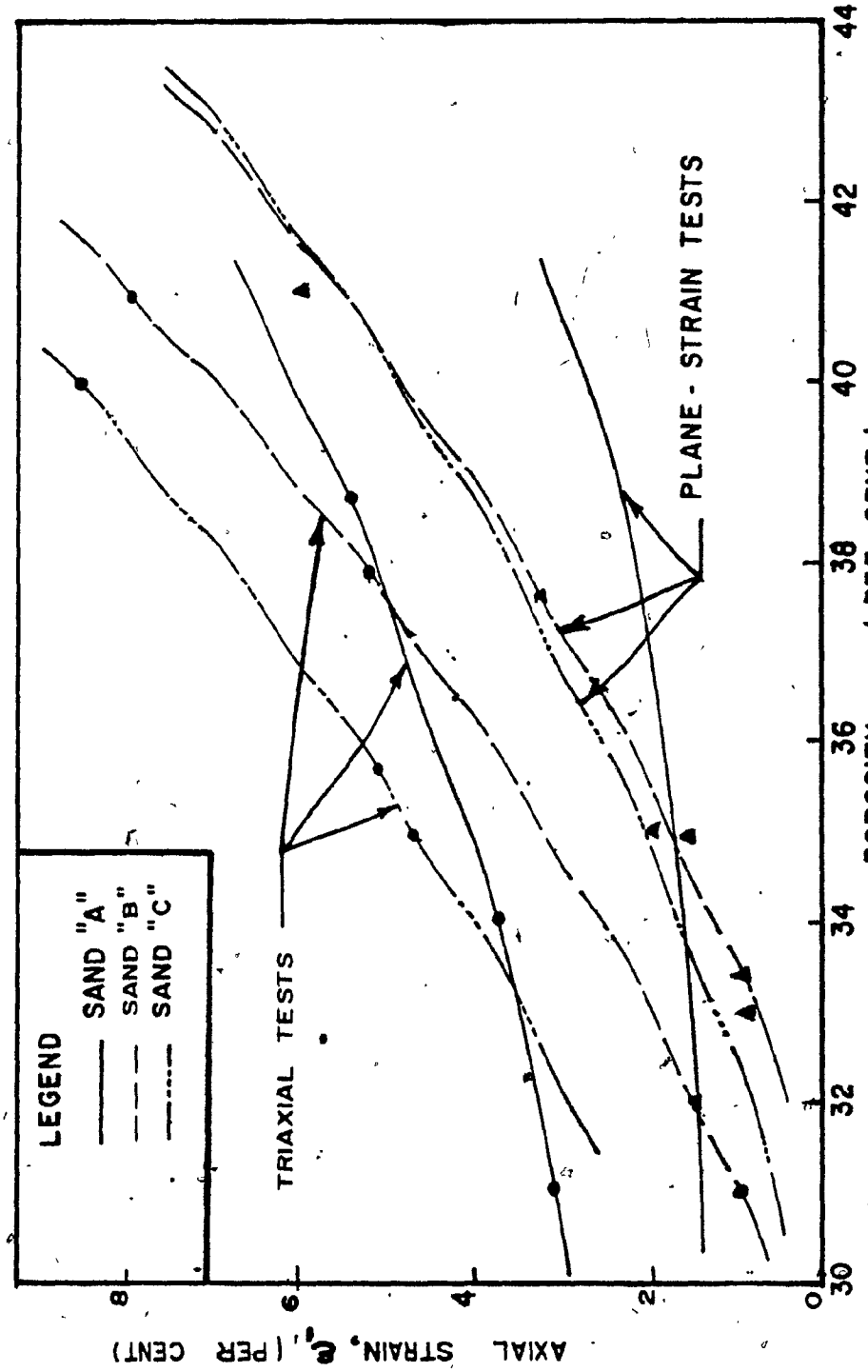

FIG. 5.46 AXIAL STRAIN, ε_1, (PER CENT) IN PLANE STRAIN & TRIAXIAL COMPRESSION TESTS AT 50 PSI CELL PRESSURE

CHAPTER VI

CONCLUSION

Base on the present experimental investigation, and the interpretation of the data presented, the following conclusion can be drawn.

1. The shear strength parameter (ϕ) increases with increasing density. This mainly due to a rise in interlocking.
2. The shear strength parameter (ϕ) increases with decreasing confining pressure for a sand at a given porosity. It appears that the effect of decreasing the confining pressure it to increases the interlock.
3. For the better graded and angular particles, the interlocking effect is greater than with the rounded and uniform particles.
4. The axial strain at failure in Triaxial tests is greater than the corresponding value in plane-strain tests at the same confining pressure and density.
5. From the comparison of plane-strain, triaxial compression and direct shear tests, the following conclusions can be given:
   a) The deduced angle of shearing resistance of plane-strain tests for the case of dense sand was about 15%, 10% and 15% higher than the corresponding values for the triaxial compression test for sand

A, B and C, respectively. At the same density, the angle of shearing resistance was also about 5%, 2.5% and 10% higher than the value obtained from the direct shear tests for the same sand.

b) The strength of the plane-strain specimens in the case of medium-dense sand is higher than the corresponding value in triaxial and direct shear tests, and lower than the one obtained in the case of dense sand samples.

6. The volumetric strain at failure in triaxial compression tests is greater than the corresponding value obtained from plane-strain and direct shear tests.

7. In direct shear tests a thin zone of the sample is subjected to shearing (probably to a simple shear) and hence, although the measured strains are small compared to the strains obtained from the triaxial or plane-strain, yet the measured strength is high.
This is because the strength is related to the rate of change of volumetric strain with respect to shearing strain and not related to other components directly.

8. In plane-strain tests, sand particles have less freedom to move around, which results in an increase of particle interlocking.

9. In triaxial tests, the particles possess the freedom to move around each other, and the sample is free to expand against the confining pressure, which results in an

increase of the volumetric strain and a decrease of interlocking.

BIBLIOGRAPHY

References

Bishop, A.W. and A.K.G. Eldin, 1953. "The effect of stress history on the relation between ϕ and porosity in sand". Proc. 3rd. Int. Conf. Soil Mech., 1: 100-105.

Bishop, A.W. and Henkel, B.J., 1962. "The measurement of soil properties in the triaxial test". Edward Arnold (Publishers) Ltd., reprinted 1969.

Bishop, A.W. and Green, G.E., 1965. "The influence of end restraint on the compression strength of cohesionless soils". Geotechnique XV, No. 3, pp. 243-266.

Bjerrum, L., 1954. "Theoretical and experimental investigations on the shear strength of soils", Norwegian Geotechnical Institute Publication No. 5, Oslo, p. 113.

Bjerrum, L. and O. Kummeneje, 1961. "The shear strength of fine sand", Proc. 5th Inter. Conf. Soil Mech. and Found. Eng. (London), Vol. 7, pp. 29-37.

Cornforth, D.H., 1961. "Plane-strain failure characteristics of a saturated sand", Ph.D., Thesis, Uni. of London. See also Geotechnique, Vol. 16, p. 95.

Cornforth, D.H., 1964. "Some experiments on the influence of strain conditions on the strength of sand", Geotechnique, Vol. XIV, pp. 143-166.

Casagrande, A., 1940. "Characteristics of cohesionless soils affecting the stability of slopes and earth fills", Contributions to Soil Mech., 1925-1940, Boston Society of Civil Engineers, October, 1940.

De Josselin De-Jong, G., 1976. "Rowe's stress dilatancy relation based on friction", Geotechnique Vol. 26, No. 3, 527-534.

Feda, J., 1969. "Effect of structure on the shearing strength of sand". 7th. Inter. Conf., Mexico, Vol. 1, pp. 121-126.

Hanna, A.M., Massoud N., (1981). "Interlocking of Granular Materials in Two and Three Dimensional Shear Failure", Proceedings of the 8th Canadian Conf. on Applied Mech., Vol. 2.

Kirkpatric, W.M., 1965. "Effects of grain size and grading on the strength behaviour of granular materials", Proc. 6th Inter. Conf. of Soil Mech. and Found. Eng., Vol. 1, p. 273.

Leussink, H. and Wittke, W., 1963. "Difference in triaxial and plane-strain shear strength", Symposium on Lab. Shear Testing of Soils, pp. 77-89.

Lee, K.L., 1970. "Comparison of plane strain and triaxial tests on sand", Jour. Soil Mech. and Found. Div., ASCE, Vol. 96, May, p. 901.

Lee, K.L. and Seed, H.B., 1967. "Drained strength characteristics of sand", Journal, Soil Mech. and Found. Eng., ASCE, SM6, Nov., pp. 117-141.

Lee, K.L., Rowe, P.W. and Barden, L., 1964. "Energy components in triaxial and direct shear tests", Geotechnique, Vol. XIV, No. 3, Spet., pp. 247-261.

Lambe, T.W., and Whitman, R.V., 1969. "Soil Mech.", John Wiley and Sons, Inc., New York.

Mitchell, R.J., 1973. "An apparatus for plane-strain and true triaxial testing of undisturbed soil samples", Canadian Geotechnical Journal, Vol. 10, No. 3, August, pp. 520-527.

Newland, P.L. and Allely, B.A., 1957. "Volume changes in drained triaxial tests on granular materials", Geotechnique 71, pp. 17-34.

Nash, K.L., 1953. "The shearing resistance of a fine, graded sand", 3rd. Inter. Conf. Soil Mech., Vol. 1, pp. 160-164.

Poorooshasp, H. and K.H. Roscoe, 1961. "The correlation of the results of shear tests with varying degrees of dilation", Proc. 5th Inter. Conf. Soil Mech., 1 : 297-304.

Rowe, P.W., Barden, L. and Lee, I.K., 1964. "Energy components in triaxial and direct shear tests", Geotechnique, Vol. XIV, No. 3, Sept., pp. 247-261.

Rowe, P.W., 1969. "The relation between the shear strengths of sand in triaxial compression, plane strain and direct shear tests", Geotechnique Vol. 19, No. 1, pp. 75-86.

Taylor, D.W., 1948. "Fundamental of Soil Mech.", John Wiley and Sons, Inc., New York, pp. 345-346.